



The author of the doctoral dissertation: mgr inż. Justyna Górską
Scientific discipline: Chemical Sciences

DOCTORAL DISSERTATION

Title of doctoral dissertation: Aromatic analogues of Amphotericin B – isolation and biological studies

Title of doctoral dissertation (in Polish): Aromatyczne analogi Amfoterycyny B – izolacja i badania biologiczne

Supervisor	Auxiliary supervisor
<i>signature</i>	<i>signature</i>
Piotr Szweda, PhD, DSc, Eng., associate prof.	Paweł Szczęblewski, PhD, Eng.

Gdańsk, year 2024



**GDAŃSK UNIVERSITY
OF TECHNOLOGY**

STATEMENT

The author of the doctoral dissertation: MSc Eng. Justyna Górską

I, the undersigned, declare that I am aware that in accordance with the provisions of Art. 27 (1) and (2) of the Act of 4th February 1994 on Copyright and Related Rights (Journal of Laws of 2021, item 1062), the university may use my doctoral dissertation entitled:

Aromatic analogues of Amphotericin B – isolation and biological studies
for scientific or didactic purposes.¹

Gdańsk,.....

.....
signature of the PhD student

Aware of criminal liability for violations of the Act of 4th February 1994 on Copyright and Related Rights and disciplinary actions set out in the Law on Higher Education and Science (Journal of Laws 2021, item 478), as well as civil liability, I declare, that the submitted doctoral dissertation is my own work.

I declare, that the submitted doctoral dissertation is my own work performed under and in cooperation with the supervision of PhD DSc Eng. Piotr Szveda, the auxiliary supervision of PhD Eng. Paweł Szczęblewski.

This submitted doctoral dissertation has never before been the basis of an official procedure associated with the awarding of a PhD degree.

All the information contained in the above thesis which is derived from written and electronic sources is documented in a list of relevant literature in accordance with Art. 34 of the Copyright and Related Rights Act.

I confirm that this doctoral dissertation is identical to the attached electronic version.

Gdańsk,.....

.....
signature of the PhD student

I, the undersigned, agree to include an electronic version of the above doctoral dissertation in the open, institutional, digital repository of Gdańsk University of Technology.

Gdańsk,.....

.....
signature of the PhD student

¹ Art 27. 1. Educational institutions and entities referred to in art. 7 sec. 1 points 1, 2 and 4–8 of the Act of 20 July 2018 – Law on Higher Education and Science, may use the disseminated works in the original and in translation for the purposes of illustrating the content provided for didactic purposes or in order to conduct research activities, and to reproduce for this purpose disseminated minor works or fragments of larger works.

2. If the works are made available to the public in such a way that everyone can have access to them at the place and time selected by them, as referred to in para. 1, is allowed only for a limited group of people learning, teaching or conducting research, identified by the entities listed in paragraph 1.



DESCRIPTION OF DOCTORAL DISSERTATION

The Author of the doctoral dissertation: Justyna Górka

Title of doctoral dissertation: Aromatic analogues of Amphotericin B – isolation and biological studies

Title of doctoral dissertation in Polish: Aromatyczne analogi Amfoterycyny B – izolacja i badania biologiczne

Language of doctoral dissertation: English

Supervisor: PhD DSc Eng. Piotr Szveda

Auxiliary supervisor: PhD Eng. Paweł Szczepkowski

Date of doctoral defense:

Keywords of doctoral dissertation in Polish: aromatyczne heptaeny makrolidowe, CPC, fotoizomeryzacja, hemoliza, cytotoksyczność, FLIM,

Keywords of doctoral dissertation in English: aromatic heptaene macrolides, CPC, photoisomerization, hemolysis, cytotoxicity, FLIM

Summary of doctoral dissertation in Polish:

Układowe infekcje grzybicze stanowią narastający problem, głównie ze względu na zdolność grzybów do rozwijania oporności na leki, których liczba jest ograniczona. W związku z tym poszukuje się nowych skutecznych chemoterapeutyków. Amfoterycyna B, makrolid heptaenowy, stosowany jako lek ostatniej szansy, wykazuje szerokie spektrum działania przeciwgrzybiczego, ale także wysoką toksyczność wobec organizmu człowieka. Aromatyczne makrolidy heptaenowe (AHM), będące jej analogami, charakteryzują się jeszcze wyższą aktywnością przeciwgrzybiczą i również wyższą toksycznością. Kilka lat temu w naszym zespole badawczym zaobserwowano, że AHM ulegają indukowanej światłem reakcji izomeryzacji, prowadzącej do zmiany geometrii chromoforu z *cis-trans* na *all-trans*. Takie izomery mogą wykazywać zmniejszoną toksyczność dzięki usztywnieniu pierścienia makrolaktonowego, co wpływa na interakcje ze sterolami. W ramach pracy doktorskiej opracowano metodę izolacji *cis-trans* AHM o wysokim stopniu czystości, a na drodze reakcji fotochemicznej otrzymano ich stabilne izomery *all-trans*, które następnie oczyszczono. Zbadano aktywność przeciwgrzybiczą, hemolityczną i cytotoksyczną tych związków oraz określono indeks selektywnej toksyczności. W ostatnim etapie - badaniach biofizycznych określono prawdopodobną orientację *cis-trans* i *all-trans* AHM w modelach błon biologicznych zawierających odpowiednie sterole.



Summary of doctoral dissertation in English:

Systemic fungal infections are an increasing concern, primarily due to the ability of fungi to develop resistance to a limited number of available antifungal drugs. Consequently, the search for new, effective chemotherapeutics is ongoing. Amphotericin B, a heptaene macrolide used as a last-resort drug, exhibits a broad spectrum of antifungal activity but also significant toxicity to human cells. Aromatic heptaene macrolides (AHMs), its analogs, demonstrate even higher antifungal activity but also greater toxicity. Several years ago, our research team observed that AHMs undergo light-induced isomerization, leading to a change in chromophore geometry from *cis-trans* to *all-trans*. These isomers may exhibit reduced toxicity due to the rigidification of the macrolactone ring, which could affect their interactions with sterols. As part of this doctoral project, a method for isolating highly pure *cis-trans* AHMs was developed, their stable *all-trans* isomers were obtained via photochemical reactions and then purified. The antifungal, hemolytic, and cytotoxic activities of these compounds were investigated, and their selective toxicity index was determined. In the final stage, biophysical studies were conducted to determine the probable orientation of *cis-trans* and *all-trans* AHMs in biological membrane models containing relevant sterols.

I would like to express my deepest gratitude to my supervisor, Dr hab. inż. Piotr Szweda, for his invaluable guidance and constant support throughout my journey as his PhD student.

I am also grateful to my auxiliary supervisor, Dr inż. Paweł Szczęblewski, for introducing me to the world of polyene macrolides, for imparting essential skills that significantly enriched my experience, and for his ongoing support.

I extend my sincere gratitude to Prof. Dr hab. inż. Sławomir Milewski for his valuable advice and support, which played an important role throughout my research.

I am grateful to Dr hab. inż. Tomasz Laskowski for his openness and guidance, which helped me overcome the challenges I faced during my doctoral project.

I am deeply thankful to Dr hab. Rafał Luchowski for introducing me to the FLIM technique and providing expert scientific insights.

I would like to thank Prof. Norbert Lange for giving me the opportunity to conduct part of my doctoral research under his supervision at the University of Geneva

I sincerely appreciate Julia Borzyszkowska-Bukowska for her invaluable expertise, kind words, and constant encouragement.

I am also deeply grateful for the scientific support provided by Dr inż. Katarzyna Kozłowska-Tylingo during the HPLC-DAD-ESI-MS analysis and invaluable support of Dr inż. Natalia Maciejewska during the biological part of my doctoral studies on human cell lines.

Finally, I would like to express my heartfelt thanks to my family and friends for their unwavering support during the journey of my doctoral studies. Your encouragement has been a constant source of strength.

TABLE OF CONTENTS

LIST OF SYMBOLS AND ABBREVIATIONS.....	12
1. INTRODUCTION.....	15
1.1. Invasive fungal diseases	15
1.2. Polyene macrolides	19
1.2.1. Heptaene macrolides	20
1.2.1.1. Discovery and formulation of Amphotericin B	21
1.2.1.2. Advantages of Amphotericin B as an antifungal drug.....	23
1.2.1.3. Disadvantages of AmB.....	25
1.3. Mechanism of action of AmB	26
1.3.1. Interaction of AmB with membrane sterols	26
1.3.2. Sterols interacting with AmB	27
1.3.3. (Half) Pore formation model.....	28
1.3.4. Surface adsorption model.....	30
1.3.5. Sponge model	30
1.3.6. Other proposed mechanisms of AmB action	31
1.3.7. Osmotic pressure	32
1.3.8. Oxidative damage model.....	32
1.3.9. Summary of the proposed mechanism of action.....	33
1.3.10. Cellular effect	34
1.4. Aromatic heptaene macrolides	36
1.4.1. Physicochemical properties of AHMs and characteristics of AHMs studied in this work 37	
1.4.2. AHMs studied in this work	39
1.4.2.1. Candididin complex.....	39
1.4.2.2. Aureofacin complex	41
1.4.3. Liquid-liquid separation techniques in the isolation of Aromatic Heptaene Macrolides	42
1.4.4. Mechanisms of action and cellular effects of aromatic heptaene macrolides: Insights into membrane permeability and ion channel formation	45
1.4.5. The role of the aromatic side chain	48
1.5. Light-induced isomerization of AHMs	49
1.5.1. Light-induced isomerization of AHM.....	50
2. RESEARCH OBJECTIVE AND DESCRIPTION OF THE RESEARCH PROBLEM	52
3. MATERIALS AND METHODS	54
3.1. Materials	54
3.1.1. Heptaene macrolide preparations	54
3.1.2. Isolated heptaene macrolides	54
3.1.3. Reagents and buffer preparations.....	55

3.1.4. Culture media.....	56
3.1.5. Human cell lines.....	57
3.1.6. Microorganisms.....	57
3.1.7. Laboratory equipment	57
3.1.8. Softwares.....	58
3.2. Methods.....	58
3.2.1. Determination of purity of antibiotic complexes	58
3.2.2. Preliminary isolation of heptaene macrolide complexes from crude preparations	59
3.2.3. Biphasic solvent system selection (shake-flask test) for the CPC purification process	60
3.2.4. Isolation of the antibiotics by CPC-DAD technique.....	61
3.2.5. Initial determination of purity by HPLC-DAD technique (analytical scale).....	62
3.2.6. Isolation of the antibiotics using Preparative HPLC	63
3.2.7. Photoisomerization of aromatic heptaene macrolides	64
3.2.8. Final identification and purity determination of the isolated antibiotics using LC-DAD-ESI-MS in positive ion mode	64
3.2.9. Determination of antifungal <i>in vitro</i> activity	65
3.2.10. Determination of hemolytic activity.....	65
3.2.11. Calculation of selective toxicity index (STI _{HEM}).....	66
3.2.12. Determination of cytotoxic activity	67
3.2.13. Imaging cell morphology using Confocal Microscopy	68
3.2.14. Calculation of selective toxicity index (STI _{CYT}).....	69
3.2.15. Determination of cell viability by flow cytometry.....	69
3.2.16. Investigation of the antibiotic behavior in the lipid bilayer using FLIM.....	69
4. RESULTS AND DISCUSSION.....	73
4.1. Selection of starting materials and determination of complex purity.....	74
4.2. Preliminary purification of the selected complexes.....	75
4.3. Separation and isolation of individual AHMs from complexes by CPC	77
4.3.1. Selection of the biphasic solvent system (shake-flask test)	78
4.4. Isolation of the antibiotics by preparative CPC with DAD detection	80
4.5. Isolation of <i>cis-trans</i> Candicidin D using preparative HPLC.....	86
4.6. Photoisomerization of AHMs and isolation of <i>all-trans</i> isomers.....	87
4.6.1. Isolation of <i>all-trans</i> AHMs by preparative HPLC.....	91
4.7. Final identification and purity determination of the isolated <i>cis-trans</i> and <i>all-trans</i> AHMs	94
4.8. Biological activity studies.....	99
4.8.1. Determination of antifungal activity (MIC assay)	99
4.8.2. Determination of hemolytic activity.....	102
4.8.3. Calculation of selective toxicity indexes values of AHMs isomers and AmB (STI _{HEM})	103
4.8.4. Determination of mammalian <i>in vitro</i> cytotoxicity.....	104
4.8.5. Calculation of selective toxicity indexes values of AHMs isomers and AmB (STI _{CYT})	106

4.8.6. Determination of cell viability by flow cytometry.....	109
4.9. Investigation of the antibiotic behavior in the lipid bilayer using FLIM	110
5. SUMMARY AND FINAL CONCLUSIONS	118
SCIENTIFIC ACHIEVEMENTS.....	120
BIBLIOGRAPHY	122
LIST OF FIGURES.....	135
LIST OF TABLES	139
LIST OF EQUATIONS	141

LIST OF SYMBOLS AND ABBREVIATIONS

$A_{540}^{0.1\% \text{ Triton X-100}}$	the absorbance of hemoglobin contained in the supernatant after centrifugation of erythrocytes suspension treated with 0.1% Triton X-100 measured at 540 nm, positive control
$A_{540}^{0.9\% \text{ NaCl}}$	the absorbance of hemoglobin contained in the supernatant after centrifugation of non-treated erythrocytes suspension measured at 540 nm, negative control
A_{540}^{DMSO}	the absorbance of hemoglobin contained in the supernatant after centrifugation of erythrocyte suspension treated with 1% DMSO measured at 540 nm
A_{540}^{sample}	the absorbance of hemoglobin contained in the supernatant after centrifugation of erythrocytes suspension treated with antibiotic measured at 540 nm
Abs_B	absorbance of the cell-free medium measured at 540 nm (MTT method) or at 450 nm and 690 nm (WST-1 method),
Abs_{DMSO}	absorbance of the viable cells treated with 0.5 - 1% DMSO, measured at 540 nm (MTT method) or at 450 nm and 690 nm (WST-1 method).
Abs_{sample}	absorbance of the viable cells treated with antibiotic, measured at 540 nm (MTT method) or at 450 nm and 690 nm (WST-1 method),
Å	angstrom
ACN	acetonitrile
AcOEt	ethyl acetate
AHM(s)	aromatic heptaene macrolide(s)
AmB	Amphotericin B
A_{mob}	sample absorbance in the mobile phase
Area_{mob}	peak area of the sample in the mobile phase measured by HPLC
$\text{Area}_{\text{stat}}$	peak area of the sample in the stationary phase measured by HPLC
ASC	ascending mode
A_{stat}	sample absorbance in the stationary phase
BSI	bloodstream infection
BuOH	butanol
c	concentration
CCC	Counter-Current Chromatography
CCD	Counter-Current Distribution
CH_2Cl_2	dichloromethane
CHCl_3	chloroform
CLSI	Clinical and Laboratory Standards Institute
C_{mob}	sample concentration in the mobile phase
CPC	Centrifugal Partition Chromatography
C_{stat}	sample concentration in the stationary phase
D-AmB	deoxycholate Amphotericin B, Fungizone
DAD	Diode Array Detector

DMA	dimethylacetamide
DMF	dimethylformamide
DMSO	dimethyl sulfoxide
DSC	descending mode
$E^{1\%}_{1\text{cm}}$	extinction coefficient
EH ₅₀	concentration at which 50% of erythrocytes released the hemoglobin [$\mu\text{g/mL}$]
EtOH	ethanol
F_{\perp}	fluorescence intensity polarized perpendicularly to the polarization of the excitation light
F_{\parallel}	fluorescence intensity polarized in parallel to the polarization of the excitation light
FDA	Food and Drug Administration
FLIM	fluorescence lifetime imaging microscopy
F_Y, F_Z	fluorescence signals recorded from two sides of membrane fragments spanned by the axes Y and Z
G	instrumental correction factor of the detector's sensitivity to the polarization direction of the recorded light, determined before each experiment
GUV(s)	giant unilamellar vesicle(s)
H ₂ O	water
HDL	high-density lipoproteins
HM(s)	heptaene macrolide(s)
HPLC-DAD	High-Performance Liquid Chromatography- Diode Array Detector
IA	invasive aspergillosis
IC ₅₀	concentration at which 50% of human cells are killed [$\mu\text{g/mL}$]
IC ₉₀	concentration at which 90% of human cells are killed [$\mu\text{g/mL}$]
ICU	intensive care units
IFDs	invasive fungal infections
InC	invasive candidosis
K_D	partition coefficient
LC-DAD-ESI-MS	Liquid Chromatography combined with Diode Array Detector, Electrospray Ionization mode, Mass Spectrometry
LC-MS	Liquid Chromatography-Mass Spectrometry
LDL	low-density lipoproteins
LFAB	lipid formulations of Amphotericin B
MDR	multi-drug resistance
MeOH	methanol
MHs	molecular harpoons
MIC	minimal inhibitory concentration [$\mu\text{g/mL}$]
MOA	mechanism of action
n_1, n_2	the number of GUVs tested in the two selected experimental systems

NMR	nuclear magnetic resonance
prep-HPLC	preparative High-Performance Liquid Chromatography
r	fluorescence anisotropy
RBCs	red blood cells
ROS	reactive oxygen species
RT	room temperature [°C]
S ₁ , S ₂	the sum of ranks assigned to the orientation angles obtained in the two selected experimental systems
SARS-CoV-2	severe acute respiratory syndrome coronavirus 2 (COVID-19)
STI _{CYT}	selective toxicity index calculated using IC ₅₀
STI _{HEM}	selective toxicity index calculated using EH ₅₀
U, U ₁ , U ₂	the value of the U-Mann Whitney test
v _i	injection volume [mL, µL]
WHO	World Health Organization
λ	wavelength of an electromagnetic wave [nm]
α	separatory factor (CPC) / orientation angle [°] (FLIM) / level of significance (statistic)
λ	detection wavelength [nm]
$\lambda_1^*/\lambda_2^*/\lambda_3^*$	wavelength of first/ second/ third absorbance maximum of <i>all-trans</i> AHMs [nm]
$\lambda_1/\lambda_2/\lambda_3$	wavelength of first/ second/ third absorbance maximum of <i>cis-trans</i> AHM [nm]
λ_{max}	absorbance maximum [nm]
ω	volumetric flow rate [mL/min]

1. INTRODUCTION

1.1. Invasive fungal diseases

For several decades, systemic mycoses (molds or yeast in deep-seated tissues) have become a significant and serious problem in clinical practice. According to established criteria, confirmation of a systemic or intensive fungal diseases (IFDs) includes [1]:

- identification of tissue damage, which is caused by fungal elements verified through histopathologic examination,
- isolation of the fungi from the culture of clinically sterile samples like blood, tissue, or cerebrospinal fluid.

Infection may begin through:

- the invasion of fungal microbiota into the mucosa,
- direct inoculation, leading to colonization and dissemination,
- inhalation of fungal spores from the environment.

IFDs mainly affect immunocompromised patients and it will be globally and “locally” (based on particular risk factors) discussed in this chapter. The global data gathered by Denning [2] highlighted the problem of invasive mycoses epidemiology. It indicates that the annual incidence of IFDs exceeds 6.55 million cases worldwide. The associated mortality is estimated at over 3.75 million deaths each year, with fungal infections identified as the direct cause of death (attributable mortality) in approximately 2.55 million cases. Among the most prevalent IFDs globally are invasive aspergillosis (IA; ca. 2,116,000 patients worldwide each year) and invasive candidiasis (InC; ca. 1,565,000 patients worldwide each year) [2]. In 2022, the World Health Organization (WHO) reported a list of 19 fungal priority pathogens [3]. Based on this report the main cause of serious invasive fungal diseases, that threaten public health, are certain fungi of the genus *Candida*, *Aspergillus*, and *Cryptococcus*. The most challenging fungal pathogens, prioritize to overcome include, among others, *Aspergillus fumigatus* and *Candida albicans* [4].

A. fumigatus is an omnipresent fungus. The exposure to its conidia (airborne) is constant and universal to the almost whole human population. *Aspergillus* genus affects mainly the lungs of immunocompromised patients and leads to IA. As mentioned it is responsible also for fungal allergies, such as allergic bronchopulmonary aspergillosis, and it is the particular agent present in patients with chronic pulmonary aspergillosis. Moreover, *A. fumigatus* can rarely affect patients after a solid organ transplant, mainly leading to death in such cases [5].

The second fungal pathogen mentioned above belongs to the *Candida* species, which are yeasts normally found on human skin and in the respiratory, digestive, and urinary tracts [6]. *C. albicans* is primarily responsible for causing the most common IFD - invasive candidiasis, specifically candidemia [7]. *Candida* spp. appears to be the third or fourth most frequent pathogens of bloodstream infection seen in ICU [7]. Candidiasis is associated with mucosal, cutaneous, and deep-seated organ infection in immunodeficiency patients [6]. The epidemiological characteristics of *Candida* bloodstream infection indicated that the blood flow infection rate of non-albicans *Candida* spp.

(*Candida parapsilosis*, *Candida tropicalis*, *Candida glabrata*, and *Candida krusei*) have also increased recently, which is another therapeutic challenge due to the different antibiotic susceptibility profiles among different *Candida* species [8]. Figure 1 presents the confirmed cases of fungal disease caused by *Candida* spp. The most interesting fact is that although *C. albicans* occurred most frequently among the sick, the total number of patients with non-*albicans Candida* is higher [9].

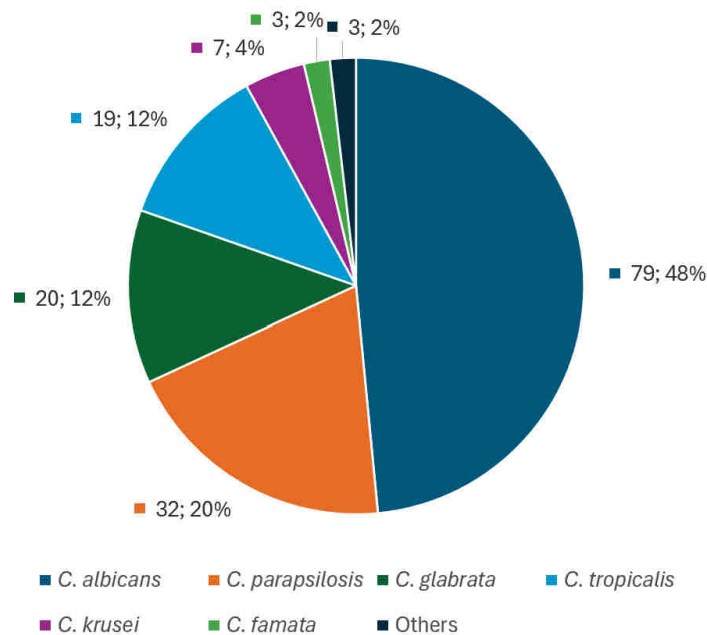


Figure 1. Percentage share of 163 cases of fungal bloodstream infection in *Candida* strains (%) based on [9]

In general, candidiasis accounts for up to 9–22% of all nosocomial infections [10]. The other statistical data [11][12] indicates that approximately 50% of patients had undergone surgery before developing candidemia, suggesting that prior surgery is one of the main triggers of candidemia. Furthermore, the collected data [13] concerning chemotherapy for acute leukemia shows that 2–49% of patients with this disease who were receiving chemotherapy suffered from IFDs. Invasive fungal diseases were an important cause of treatment failure, contributing to a mortality rate of around 20–30% [13].

The most significant increase in the incidence of invasive fungal diseases, which substantially highlight this worldwide problem, was observed during the severe acute respiratory syndrome coronavirus 2 (SARS-CoV-2, COVID-19) pandemic. SARS-CoV-2 is an enveloped and positive single-stranded RNA viruses belonging to the Coronaviridae family [14]. As of March 3, 2024, the total reported number of confirmed cases worldwide was 774,631,444, and 7,031,216 deaths [15]. Several studies have indicated that COVID-19 patients have a higher possibility of experiencing co-infection. In early 2020, Zhu et al. [16] reported the presence of fungal pathogens in 23.3% of patients with SARS-CoV-2. Furthermore, the patients who suffered from more severe illnesses were more vulnerable to fungal co-infections, including those caused by *Aspergillus* (23.3%), *Candida* (0.8%), and *Cryptococcus* (0.4%) [16]. Hospitalization data from the United States, collected from January 2020 to December 2021, highlighted a significant difference in

mortality between patients with COVID-19-associated IFDs (48.5%) and those with non-COVID-19-associated IFDs (12.3%) [17].

Since 1970, the prevalence of fungal infections and mortality caused by these diseases increased. It is associated with several changes in medical practice, including the frequent use of broad-spectrum antibiotics, the more widespread use of modern therapies, such as the application of indwelling intravenous devices [18]. As mentioned before, invasive fungal infections affect immunocompromised patients for example with Acquired Immunodeficiency Syndrome (AIDS), chronic obstructive pulmonary disease, and COVID-19. Furthermore, patients after surgery, solid organ transplantation, or chemotherapy are also in the group at risk for IFDs morbidity. Environmental exposure has a unique role in the prevalence of invasive mold infections. Tissue injuries such as deep skin trauma (rare) or surgery can be infected by fungi. It can lead to mucormycosis (black fungus), which is known as the most common fatal complication. The summary of major risk factors of IFDs occurrence is presented in Table 1 [1].

Table 1. Major risk factors associated with the occurrence of IFDs [1]. HIV – human immunodeficiency virus, COVID-19 – severe acute respiratory syndrome coronavirus 2.

Risk factor	Specific conditions	Most common pathogens
Medical intervention	intravascular / intracranial devices	<i>C. albicans</i> and other <i>Candida</i> spp.
	Broad-spectrum antibiotics use	<i>C. albicans</i> and other <i>Candida</i> spp.
	contaminated devices, neurosurgical procedures, drug preparations	<i>Candida</i> spp., <i>Saprophyte fungi</i>
Treatment-induced immunosuppression	Solid organ transplant	<i>C. albicans</i> and other <i>Candida</i> spp., <i>A. fumigatus</i> , <i>Cryptococcus neoformans</i>
	Haemopatic stem cell transplantation	<i>A. fumigatus</i> , <i>C. albicans</i> and other <i>Candida</i> spp., <i>Pneumocystis jirovecii</i> , <i>Mucormycetes</i>
Disease-induced immunosuppression	HIV infection	<i>P. jirovecii</i> , <i>C. neoformans</i> , <i>Histoplasma capsulatum</i> , <i>Talaromyces marneffeii</i>
	Chronic obstructive pulmonary disease	<i>A. fumigatus</i>
Co-infection	Tuberculosis	<i>A. fumigatus</i> , <i>Aspergillus niger</i> , <i>H. capsulatum</i> , <i>C. neoformans</i> , <i>C. albicans</i>
	COVID-19 infection	<i>A. fumigatus</i>
Environmental exposure	Trauma	<i>R. oryzae</i> , <i>Mucormycetes</i>

Recently, invasive fungal diseases have become an increasingly significant concern that is difficult to overcome, with many of these infections posing life-threatening risks. Furthermore, the arsenal of antifungal drugs is limited. This limitation stems from the apparent similarity between fungal and mammalian cells at the molecular level. Both are phylogenetically closely related as eukaryotic organisms. The current arsenal of antifungal drugs consists of azole and triazole derivatives, commonly known as “azoles”, echinocandins, 5-fluorocytosine, and polyene macrolide antibiotics, mainly Amphotericin B (AmB) (Figure 2).

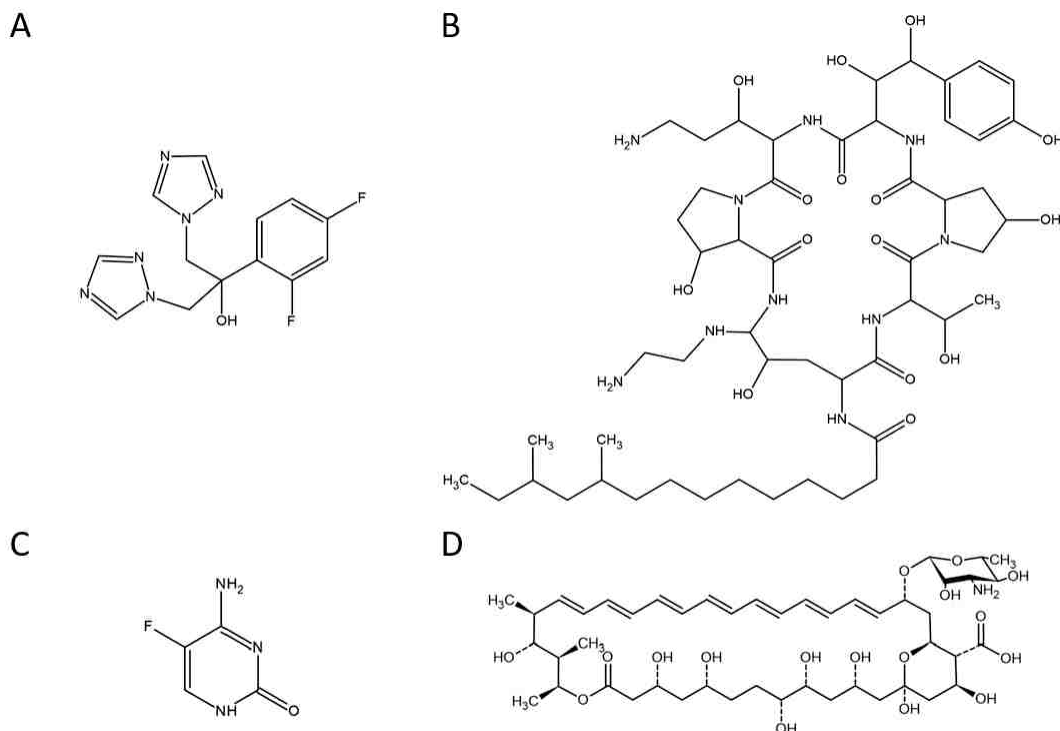


Figure 2. Compounds used against systemic mycoses belonging to A) the azole group - on the example of Fluconazole, B) the echinocandin group - on the example of caspofungin, C) 5-fluorocytosine, D) polyene macrolides on the example of Amphotericin B

The mentioned antifungal agents target different components of the fungal cell [19]. Azoles target the cytochrome P₄₅₀-dependent lanosterol demethylase and in consequence inhibit the synthesis of ergosterol, a key component of fungal cell membranes. Echinocandins are inhibitors of $\beta(1\rightarrow3)$ glucan synthase, which results in blocking the production of 1,3- β -D-glucan, an essential component of the fungal cell wall. 5-Fluorocytosine, after intracellular conversion in fungal cells to 5-fluorouracil, affects DNA and RNA biosynthesis. Amphotericin B binds to ergosterol, extracting these molecules from the cytoplasmic membrane (the sterol sponge concept) and/or assembling into pore-like transmembrane pores (the transmembrane channel concept).

The use of such a limited group of antifungal agents results in the emerging challenge of fungal resistance, which is another significant subject of concern. Fungi employ four primary mechanisms to resist antifungal treatments [19];

- overexpression of target proteins (azoles);
- mutations occurring in target proteins (azoles and echinocandins, 5-fluorocytosine);
- increased production of efflux pumps and/or greater incorporation of these pumps into cell membranes (azoles);
- reduced accessibility to the target, such as ergosterol sequestration or possession of thicker cell walls (polyene macrolides).

Additionally, the global enhancement of multi-drug resistant fungal species, which exacerbates treatment outcomes, increases mortality rates. The membrane proteins exporting

chemotherapeutics from the fungal cells are overexpressed and the therapeutic concentration of the medicament cannot be achieved. Some fungi exhibit intrinsic resistance (e.g. fluconazole-resistant *C.krusei*), however numerous fungal species have developed significant resistance to currently used antifungal drugs as a consequence of prolonged medical treatment [20][21]. *Candida auris* (also responsible for bloodstream infection, otitis, wound infection) is the perfect representative of a multi-drug resistant fungus. It possesses high resistance to almost all used drugs, with resistance to Fluconazole occurring in as many as 90% of clinical isolates. However, what is worth marking, based on Saris et al. [21] review ONLY 23% of 56 isolates and in larger studies, 8% of 350 isolates were resistant to non-aromatic heptaene macrolide, Amphotericin B. Resistance to macrolide polyene antifungals is less common compared to resistance to azole antifungals [22].

The new possibilities for therapy treatment are still being searched. There hasn't been created or found any drug candidate that is characterized simultaneously by high antifungal activity and very low toxicity to patients.¹ Historically, polyene macrolides are the first antibiotics used in antifungal therapy and still the most promising group of compounds, exhibiting the greatest number of traits of the non-existing "ideal" fungicide. Heptaene macrolides are characterized by a broad spectrum of antifungal activity, higher than other antifungal drugs (azoles or echinocandins) [19]. This group is represented by the mentioned AmB, a drug that is currently considered life-saving in the treatment of systemic mycoses [23]. It is used as a last-chance antifungal agent due to the typical heptaene macrolides' high toxicity against humans [24].

In the light of mentioned facts, fungal resistance threatens public health. Therefore, the search for new solutions - such as new drugs and rational chemical modifications of molecules with high therapeutic potential - is crucial for the effective treatment of fungal infections. The expected features of novel antifungals to be applied in chemotherapy of disseminated fungal infections include:

- high antifungal activity,
- broad spectrum of antifungal action,
- very low, if any, toxicity to patients,
- ability to overcome multidrug resistance.

The literature data [25] suggested that aromatic heptaene macrolides (AHMs) exhibit two to three orders of magnitude higher *in vitro* antifungal activity than Amphotericin B [25]. Moreover, AHMs could have the same potential as AmB to overcome fungal multidrug resistance. These features give them a promising role in the search for new agents in antifungal therapy.

1.2. Polyene macrolides

As mentioned in the introduction, polyene macrolides historically belong to the first group of agents targeting fungal diseases [24]. They form a large group of natural compounds

¹ In November 2023, researchers from the University of Illinois at Urbana-Champaign reported the synthesis and biological properties of a novel AmB derivative with low mammalian toxicity and high antifungal activity [98]. However, the potential of this compound as a drug candidate needs to be confirmed.

biosynthesized through polyketide pathway by various bacteria (mainly from *Streptomyces* species [26] and some fungi) [24]. The unique structural feature of all polyene macrolides is a different-size macrocyclic ring (macrolactone) composed of carbon atoms closed by lactonization [27]. Besides, numerous factors contribute to the categorization of macrolides, among which polyene macrolides can be distinguished.

Polyene macrolides exhibit a broad spectrum of biological properties including first of all antifungal but also immunosuppressive, antiparasitic, and antibacterial potential. Polyene macrolides are named for their alternating conjugated double bonds in the structure: trienes (Trienine), tetraenes (Pimaricin), pentaenes (Filipin), hexaenes (Endomycin B), and heptaenes (Amphotericin B) [27][28]. Among them, heptaenes (heptaene macrolides - HMs, containing 7 conjugated double bonds) deserve special attention, as they are the most promising and active group of polyene macrolides, characterized by their high antifungal potential and, unfortunately, significant toxic effects on humans [27][29]. However, when comparing heptaene macrolides' toxicity with their simultaneous ability to overcome the resistance to pathogens and their broad spectrum of activity against fungi, polyene macrolides remain the strong contender in the battle with life-threatening systemic fungal infections [24][30].

According to the literature [25][31], among heptaene macrolides, there is a promising subgroup – aromatic heptaene macrolides (AHMs). These compounds have been suggested to exhibit enhanced antifungal activity when compared to AmB, which remains the "life-saving" drug in antifungal therapy. Moreover, besides Amphotericin B and its derivatives, Candicidin, Trichomycin, and methyl ester of Partricin are used in medicine [24][27][32]. Recent structural studies on Candicidin D [33], one of the representatives of AHMs, have revealed the formation of a stable isomer with an altered chromophore geometry, additionally adapting its structural characteristics with those of AmB.

1.2.1. Heptaene macrolides

In general, heptaene macrolides are characterized by the two main structural segments; a 20-44 membered macrolactone ring and an aminosugar (except e.g. Filipin, which lacks sugar) [28]. AHMs possess an additional, distinct segment – alkyl-aromatic side chain [28][34][35].

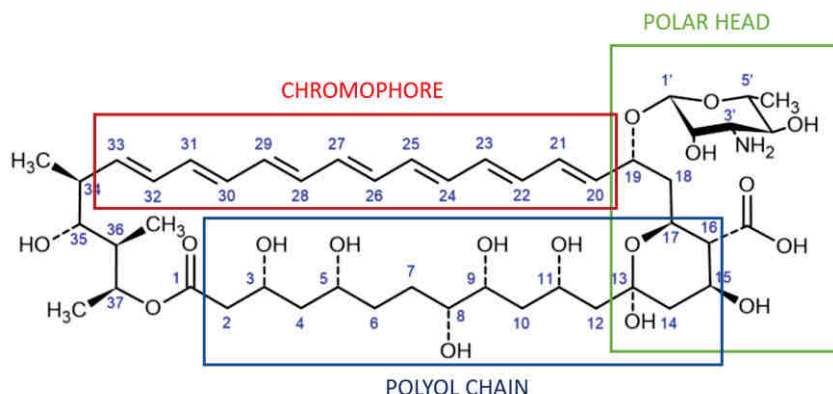


Figure 3. The elements of HM structure based on the stereostructure of Amphotericin B. Red box- chromophore (seven conjugated double bonds); green box – polar head consisting of a hemiketal ring with the carboxylic group and sugar (mycosamine); blue box – polyol chain containing “system of oxygen functions”

Heptaene macrolides are amphipathic molecules categorized as antibiotic ionophores [36]. Their macrolide ring (Figure 3) comprises a flexible hydrophilic region (polyol chain), containing numerous polar groups, commonly referred to 'system of oxygen functions' - hydroxyls, carbonyls, and epoxides [24][37]. It was observed, based on the Candidicin complex, that the higher the polarity of the compound (due to more oxygen functions present in the polyol fragment), the greater its antifungal activity [38]. The unsaturated planar part (seven conjugated double bonds) constitutes the rigid chromophore located directly opposite the polyol chain [30][37], determining the specific shape of the molecule's UV absorption spectra [27][39]. Moreover, this region is supposed to participate in the interactions with sterols, contributing to the formation of the transmembrane pores in one of the proposed models for the mechanism of action studies of heptaene macrolides [30] (for more details see section 1.3.).

The hydrophobic part differs in non-aromatic and aromatic heptaene macrolides. In the former, the chromophore geometry is consistently *all-trans*, whereas in native AHMs, it adopts the *cis-trans* geometry. Table 2 lists the *cis-trans* bond location, indicating the position of the two Z-geometry double bonds found in the chromophore of AHMs [33][38].

Table 2. *Cis-trans* bond location with the position of Z-geometry double bonds which is found in the chromophore of HM (E means E-geometry) – own work based on [38][40]

Antibiotic	Location/position of <i>cis-trans</i> bonds	Chromophore geometry
AmB	-	19E, 21E, 23E, 25E, 27E, 29E, 31E
Candidin D	26Z, 28Z	22E, 24E, 26Z, 28Z, 30E, 32E, 34E
Partricin A	28Z, 30Z	22E, 24E, 26E, 28Z, 30Z, 32E, 34E
Partricin B	28Z, 30Z	22E, 24E, 26E, 28Z, 30Z, 32E, 34E

The particular structure-property feature for HMs is a „polar hydrophilic head” (or C8 region) composed of eight carbon atoms within the macrolide ring linked by one side to the chromophore and the other side to the polyol chain, forming a hemiketal ring (atom numbers C13-C17 in AmB structure). This region is also specified by the attached chemical groups. The macrolactone is β -glycosylated to an aminosugar moiety, which bounds to the first carbon atom located after the conjugated double bonds (counter-clockwise direction from the chromophore) [24]. Most aromatic polyene macrolides contain mainly mycosamine (3-amino-3,6-dideoxy-D-mannose), with only a few containing perosamine (4-amino-4,6-dideoxy-D-mannose) in their sugar segment [30][37]. Additionally, there is another noteworthy functional group concerning HMs (not applicable for Perimicin) [27] - exocyclic carboxyl, invariably located on the fourth carbon atom after the chromophore (at C16 or C18 of macrolactone ring for AmB and AHMs, respectively) [24][37]. Therefore, the „polar head” is formed by both the amino group from the aminosugar moiety and the carboxyl group located in the hemiketal ring, allowing for inter- and intramolecular interactions when considering the mode of action of HMs [36][41].

1.2.1.1. Discovery and formulation of Amphotericin B

The discovery of Amphotericin B in 1953 was a milestone of the XXth century in antifungal treatment. This antibiotic, together with its analogue Amphotericin A (AmA, a dieno-tetraene macrolide), was named after its amphoteric properties. AmB is produced by *Streptomyces*

nodosus, which was isolated from a soil sample taken from the Orinoco River (Venezuela) [42][43][44]. Although both Amphotericins exhibit a broad antifungal spectrum [42][45], the activity of AmB is substantially higher [46]. This amphipathic molecule is characterized by poor solubility in water, posing a notable disadvantage for drug delivery. It cannot be administered orally or intramuscularly [23][47]. Moreover, AmB causes intrinsic host toxicity [48], in most cases nephrotoxicity and hepatotoxicity [49]. Despite its harmful effects, the broad spectrum of activity of Amphotericin B held promise for the antifungal treatment. Therefore, there were trials to find a new useful drug formulation to reduce its toxic effects and facilitate the administration pathway.

The first formula of AmB, known as Fungizone (D-AmB) was swiftly approved as a therapeutic antifungal drug by the Food and Drug Administration (FDA) in 1959. Interestingly, its structure remained unknown at that time [43][50]. Fungizone is an intravenous solution for injection, containing a micellar form of AmB solubilized with detergent, sodium deoxycholate (responsible for AmB micellar dispersion), and sodium phosphate (buffer) [51][52]. When approved for clinical use, AmB was the sole agent capable of preventing systemic fungal infections, before the implementation of flucytosine in clinical practice. After sixty years, Fungizone is still being prescribed for the treatment of life-threatening IFDs such as invasive candidiasis, aspergillosis, histoplasmosis, mucormycosis, and blastomycosis [50][53]. Fungizone is used up to date and considered as a reference conventional formulation in the antifungal treatment [51][54]. Additionally, it remains the antifungal agent with the broadest activity spectrum, exhibiting the lowest potential for resistance among all known antifungal drugs [50]. However, it is important to note that patients treated with Fungizone may experience decreased renal function and kidney abnormalities (nephrotoxicity) [52][55].

The next developed drug formulation aimed at alleviating the side effects of AmB was its encapsulation in liposomes or complexation with different lipid carriers [56]. The lipid coating's purpose was to alter *in vivo* administration, rather than to facilitate the optimal condition for *in vitro* drug release [50]. In comparison to Fungizone, such combinations significantly reduced acute toxic activity (adverse effects) associated with the drug delivery [57][58], showing a greater efficacy-to-toxicity ratio [51][50] [56]. The development of lipid formulation of AmB (LFAB) resulted in three intravenous formulas approved by the FDA [50][49]:

- Unilamellar Liposomal AmB (L-AmB) - AmBisome,
- AmB Lipid Complex (ABLC) – Abelcet,
- AmB Colloidal Dispersion (ABCD) - Amphotec or Amphocil.

As mentioned, lipid-based agents serve as a viable alternative to Fungizone in the therapy of IFDs, particularly in patients who are intolerant to or have experienced treatment failure with non-lipid formulations of Amphotericin B [50][56]. Table 3 presents the comparison of the formulation approved by the FDA.

Table 3. Characteristic of LFAB and Fungizone – own work based on [23][59][60]. FDA - Food and Drug Administration; AmB – Amphotericin B; DMPC - 1,2-Dimyristoyl-sn-glycero-3-phosphocholine; DMPG - 1,2-Dimyristoyl-sn-glycero-3-phosphoglycerol; HSPC - Hydrogenated Soybean Phosphatidylcholine; DSPG - 1,2-Distearoyl-sn-glycero-3-phosphoglycerol.

Brand name	Fungizone	Amphotec	Abelcet	AmBisome
Class	Emulsion (micelle)	Colloidal lipid dispersion (lipid disc)	Lipid complex (ribbons)	Unilammellar liposome
Formulation	sodium deoxycholate	Disc-shaped AmB cholesteryl sulfate complex	DMPC, DMPG	HSPC, Cholesterol, DSPG
Year of FDA approval	1959	1996	1995	1997
Recommended dose	0.25 to 1.0 mg/kg/day	3 to 4 mg/kg/day at the beginning; up to 6 mg/kg/day if needed	5 mg/kg/day	3 to 5 mg/kg/day
Approved indications	Potentially fatal fungal infections	Invasive aspergillosis (if the use of conventional AmB therapy is not successful)	Aspergillosis (patients with refractory infection/intolerance to standard AmB)	If renal dysfunction or toxicity precludes the use of conventional AmB; leishmaniasis; neutropenic patients

Lipid formulation of AmB exhibits reduced acute systemic and renal toxicity compared to micellar form, leading to significantly fewer therapy-limiting adverse effects. However, the main limitation of liposomal AmB lies not in its adverse effects, but rather in its cost and accessibility (the most expensive based on daily dose) [51]. Encapsulation into liposomes is the most broadly studied AmB administration due to the most efficient and safe approach to date [58]. There are also promising studies concerning nanoparticles and other alternatives for lipid formulation (e.g. emulsion) [61][63][62][63]. Nanoparticles demonstrate significant advantages over liposomes due to their longer shelf-life and lower production cost [51].

1.2.1.2. Advantages of Amphotericin B as an antifungal drug

Amphotericin B earns its reputation as a life-saving drug primarily due to its broad-spectrum activity against human pathogenic fungi responsible for IFDs, with only a limited number of reported cases of fungal resistance. [64]. AmB is used against most fungal pathogens in humans, including *Cryptococcus* spp., *Candida* spp., *Fusarium* spp., *Aspergillus* spp., endemic mycoses like *Histoplasma* spp., and *Mucorales* such as *Rhizopus* spp. [48][65]. Furthermore, LFAB is also used in the therapy against the parasite, *Leishmania* spp., causing visceral leishmaniasis [23]. Amphotericin B exhibits either fungistatic or fungicidal properties, depending on the concentration achieved in body fluids and the fungal susceptibility [66]. For example, D-AmB MIC₅₀ could range from 0.1 to 0.5 µg/mL according to Lovary et al. [67] or 0.25 to 1.00 µg/mL according to Montagna et al. [68]. Among *Candida* spp., *C.albicans*, *C.tropicalis*, *C.parapsilosis*, *C.krusei*, *C.kefyr*, *C.famata*, *C.glabrata*, *C.guilliermondii* are regarded as susceptible to AmB [48][64][69]. Some occasional instances of resistance were reported for strains of the first four mentioned species [64]. Additionally, a greater proportion of resistant strains is observed among species against *C. auris*, *C. lusitanae*, *C. haemulonii*, *Aspergillus*

terreus, and *Scedosporium* spp. [23][48]. The occurrence of fungal resistance to AmB (however rarely observed) might be attributed to various following factors [23][65][69]:

- modification of the cell membrane permeability (e.g. increased membrane fluidity through the alteration of fatty acids content, which may disrupt the interaction with AmB),
- modification in the content of ergosterol (e.g. through mutation in genes implicated with ergosterol biosynthesis). The mechanism of AmB action is connected with the AmB-ergosterol affinity and it could result in the decrease of binding sites, sensitivity to polyene macrolides,
- modification of cell wall constituents (e.g. chitin or/and glucans, due to their initial involvement in polyene kinetics),
- alteration in the sphingolipids (ergosterol tends to be closely linked with sphingolipids in lipid rafts, and a reduction in sphingolipids might increase ergosterol's susceptibility to AmB binding, potentially enhancing cellular sensitivity to the drug) [70],
- decreased oxidative stress (through enhanced catalase activity and exposure to hypoxic conditions).

It is essential to choose the most suitable agent for treating fungal infections. The primary considered factor is its antifungal effectiveness. As mentioned before, the arsenal of antifungals (azoles, echinocandins, pyrimidine analogues, polyene macrolides) is very limited and threatened by the occurrence of drug-resistant strains in medical practice. The complexity of AmB and its interaction with the fungal plasma membrane demand multiple modifications to avoid cell membrane disruption. Therefore, there is little tendency for fungi to develop secondary resistance during the AmB administration, which is a highly desired property for chemotherapy. In general, the emergence of resistant strains is not proportional to the duration of AmB usage [65][71][72]. It is worth adding that although there are medicaments such as azoles (e.g. fluconazole), pyrimidine analogues (e.g. fluorocytosine), and echinocandins (e.g. caspofungin), AmB remains the drug with the broadest spectrum of activity characterized by a low resistance rate of fungi to date. In the context of clinical treatment, AmB also becomes an exceptional chemotherapeutic as it is active against most multidrug resistance (MDR) fungal species.

Chemotherapy involving AmB also includes methods that administer this antibiotic in combination with other antifungal agents. The example of antifungal medicaments combination with AmB is presented in Table 4 [23].

Table 4. Combined antifungal treatment for certain IFDs – own work based on [23]. AmB – Amphotericin B, AIDS - Acquired Immunodeficiency Syndrome,

Fungal disease	Combination of antifungals	Recommendation
Invasive aspergillosis	AmB + echinocandin	<ul style="list-style-type: none"> • Hematological malignancies • An elevated galactomannan level • Salvage therapy (patient of high-risk)

Fungal disease	Combination of antifungals	Recommendation
Candidiasis	AmB + flucytosine AmB + fluconazole	<ul style="list-style-type: none"> • Native valve endocarditis • Candida central nervous system infection • Azole-resistant <i>C. glabrata</i> • Ascending pyelonephritis • Fluconazole-resistant candida endophthalmitis
Cryptococcosis	AmB + flucytosine AmB + fluconazole	<ul style="list-style-type: none"> • Central nervous system cryptococcal infections (particularly patients with AIDS) • Organ transplantations
Mucormycosis	AmB + echinocandin AmB + azoles	<ul style="list-style-type: none"> • Refractory diseases

To briefly summarize this chapter, from the perspective of chemotherapy criteria, AmB, despite its harmful effects on health, possesses highly valuable biological properties, such as [72]:

- broad spectrum of activity,
- high antifungal activity,
- fungicidal effect,
- low tendency to induce secondary resistance,
- activity against fungal species with MDR,
- almost a lack of unfavorable interaction with other drugs.

1.2.1.3. Disadvantages of AmB

The chemotherapy of IFDs is significantly hindered by the mammalian toxicity of AmB. According to Bonner et al. [73], this toxicity is partially attributed to its poor solubility in water and body fluids. The solubility in water is associated with the AmB aggregation state. Based on the human erythrocytes membrane model and investigation of the K⁺ leakage (referring to the toxicity of AmB), Legrand et al. [74] discovered that the harmful effects on cholesterol-containing membranes are related to water-soluble self-associated oligomers of AmB. Additionally, AmB in water insoluble form (aggregates of oligomers) was less toxic or even non-toxic. In turn, the investigation of activity against ergosterol-containing membranes showed that the toxicity is attributed to both water-soluble aggregates and the AmB monomeric form [74][75]. In Fungizone formulation, AmB takes the form of an oligomer, exhibiting the highest toxicity, while LFAB exhibits a less toxic aggregation form [76]. It is believed that AmB's high tendency to self-association plays a significant role in its mechanism of action, which will be discussed later.

One of the main side effects of AmB is nephrotoxicity, indicated by increased serum creatinine levels [77]. Conventional D-AmB treatment results in nephrotoxicity in about 60.8% of cases, with 50% of patients experiencing acute kidney injury and 10.8% requiring dialysis [62]. Among patients who switched to Abelcet after renal dysfunction, 84% did not show renal impairment, 13% developed acute kidney injury, and 3% required dialysis. Other studies report [78] [79] that 76.4% and 46.2% of patients on D-AmB developed acute kidney injury, while LFAB generally leads to fewer kidney-related side effects [80]. AmBisome and Abelcet have lower nephrotoxicity rates (10.6% and 22.2%, respectively) compared to D-AmB [81]. Liposomal AmB

formulations are less nephrotoxic but are significantly more expensive. Additional AmB side effects include infusion-related reactions, hepatotoxicity, and anemia.

1.3. Mechanism of action of AmB

Although Amphotericin B has been used for decades, its detailed mechanism of action (MOA) is still being discussed, as well as for aromatic heptaene macrolides. Polyene macrolides, including AmB, are mainly supposed to interact with the cells at the membrane level. However, certain researchers also suggested their intracellular activity, leading to cell death without involving the cell membrane [30].

According to data collected by Mesa et al. [82], the biological impact of AmB is highly intricate and contingent upon various factors, such as the fungal growth phase and oxygen presence. These findings imply that the action of AmB may also rely on metabolic factors, indicating that the MOA is more complex than just binding to ergosterol and pore formation. Therefore, some additional 'mechanisms' were also distinguished and experimentally verified:

- Osmotic pressure,
- Oxidative damage.

All mentioned mechanisms of action will be discussed in this section.

1.3.1. Interaction of AmB with membrane sterols

AmB can form complexes with sterols having a 3β -OH group, a hydrophobic side chain in a C₁₇ position, and a system of planar rings [83]. The degree of interaction is also affected by the sterol type and quantity [65]. According to literature data, a few models of molecular assemblies of AmB: sterol complexes have been proposed:

- (half) pore formation model (1,2)
- Surface adsorption (3)
- Sponge model (4)

The models are presented in Figure 4 [48].

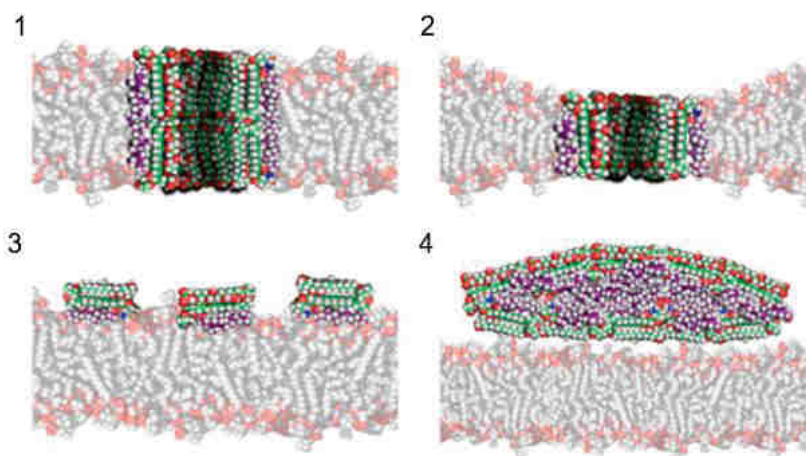


Figure 4. Models of molecular assemblies of AmB: sterol complexes. 1 – pore formation model, 2- half-pore model; 3 – surface adsorption model; 4- sterol sponge model. Based on [48]

1.3.2. Sterols interacting with AmB

According to the model presented in Figure 4, binding to sterols likely contributes to the AmB mechanism of action [84]. As a target of this antibiotic, sterols may be involved in forming specific complexes that impact cell decomposition, dysfunction, and damage. The most crucial sterols in this respect are ergosterol in fungal cells and cholesterol in mammalian cells.

Sterols are present in the cell membrane of all eukaryotic microorganisms susceptible to polyene macrolides (fungi, protists, algae), as well as in mammalian cells. In contrast, prokaryotic micro-organisms, such as bacteria, exhibit resistance to polyene macrolides due to the lack of membrane sterols [85]. The sterol components of eukaryotic membranes are believed to contribute to pore stability and, hence, play an important function in cell physiology (e.g. vacuole fusion, membrane fluidity, endocytosis) [48][82]. Among them, ergosterol, demonstrates a better capability to stabilize channels, providing its larger size and longer time for its open state. Moreover, it has been suggested that the membrane selectivity of polyene macrolides is due to the structural alterations induced by the sterols in the membrane [30]. This selectivity is thought to arise from sterol-driven modifications in membrane architecture, rather than a direct interaction between macrolide polyenes and the sterols themselves [30].

The cholesterol molecule adopts a sigmoidal conformation, while that of the ergosterol molecule, is cylindrical. This structural disparity likely accounts for the polyene macrolide's stronger binding affinity to the mentioned fungal sterol compared to human sterol (in the heptaene macrolides hydrophobic "pocket", see Figure 5) [48].

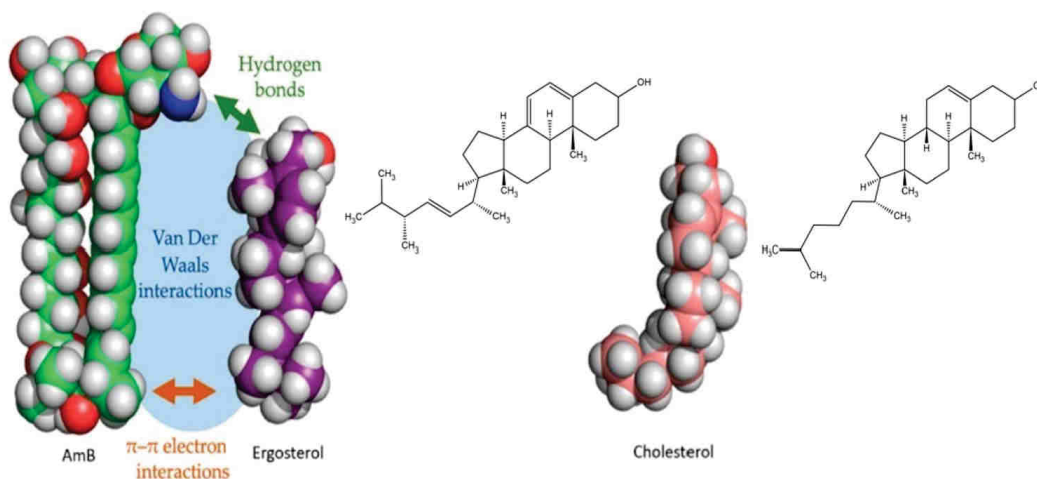


Figure 5. 3D model of AmB, ergosterol, and cholesterol with the marked non-covalent interaction of AmB-ergosterol complex, modified based on [48]

Three interactive forces contribute to the binding of polyene macrolides to ergosterol: Van der Waals forces (the strongest when those molecules are oriented parallel and co-planar); a hydrogen bond network (between the sterol 3β -OH group and the AmB mycosamine group, see Figure 6); π - π electron interactions between the chromophore and the side chain of ergosterol. In comparison, this crucial "attachment point" is absent in the AmB-cholesterol interaction [48].

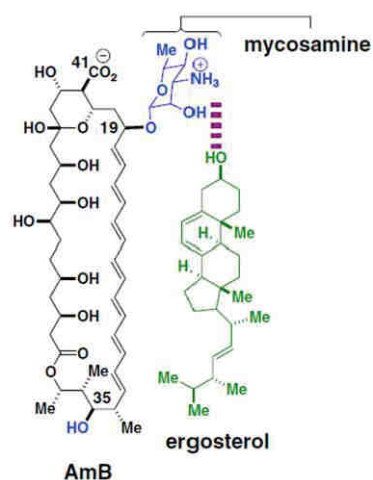


Figure 6. The structural interaction between AmB and ergosterol based on [86]

Additionally, in the AmB-cholesterol complex, the sigmoidal conformation exhibited by the sterol side chain makes the Van der Waals interactions weaker [48][87]. Furthermore, the stronger binding between polyene macrolide and ergosterol is also due to the higher number of double bonds in ergosterol than cholesterol, rendering it more rigid and planar. This, in turn, enhances the stabilization of π - π electron interactions [85]. Additionally, the selectivity of most polyene macrolides for fungal cells can be attributed to their specific binding and the higher ergosterol-to-phospholipid ratio in fungal cell membranes, compared to the cholesterol-to-phospholipid ratio found in mammalian cells [48]. However, this mentioned selectivity is low and could contribute to the probable toxicity of AmB for mammalian cells [88]. To summarize, the differential binding affinity of polyene macrolides for the two sterols is widely regarded as the primary basis for their selective toxicity in the fungi-mammal system [86][89].

1.3.3. (Half) Pore formation model

The oldest and the most widely accepted model of molecular assembly of AmB: sterol complexes, and possibly other heptaene macrolides is the pore (or channel) formation model proposed by Finkelstein and Holz [89]. This classic model is also supported by most of the available literature data concerning AHMs (e.g. [25][90][91][92]). In brief, the interaction between AmB-sterol molecules results in the mentioned channel formation and causes an electrolyte imbalance leading to cell death. In order to verify the validity of the pore formation mechanism, most studies were conducted on ion leakage from human cells, artificially created lipid vesicles, as well as computer simulations. Since this model is the most prominent, most probable, and most extensively studied in the context of the mechanism of action of the compounds tested in this doctoral studies, it will be described in more detail in this chapter.

According to the pore formation model, polyene macrolide molecules incorporate into the membrane through the hydrophobic part and bind to sterol [82]. The created pore consists of heptaene macrolide and sterol molecules arranged in a circular form, a so-called barrel-like structure, comprising 4 to 12 HMs' molecules interspersed with sterol in 1:1 stoichiometry [83]. Several studies specify the number of AmB and ergosterol molecules to 8 [65][83]. Its inner hydrophilic part contains the hydroxyl groups from the polyene macrolides' polyol region, whereas

the outer hydrophobic part consists of the non-polar polyene fragment (chromophore) and sterol aligned parallel to the phospholipid's hydrophobic tail (fatty acid chains), see Figure 7 [24][30][83]. The intermolecular hydrogen bonds between the carboxyl and amino groups of the polyene macrolides enhance the stability of the pore-forming complexes [85].

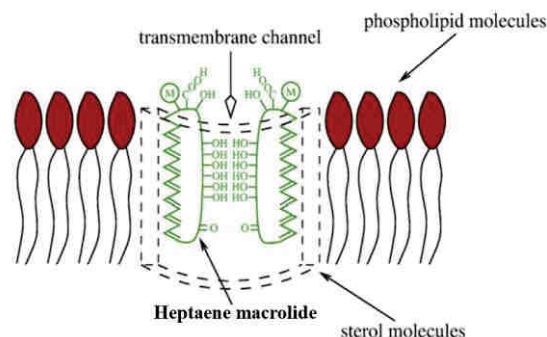


Figure 7. The scheme of the pore formed in the lipid layer. Based on [85]

An ion channel may form through two mechanisms. One theory proposes that a barrel complex exists as a singular half-pore (or single-length channel) traversing the lipid bilayer. The other one is that creating a full ion-conducting channel requires the fusion of two half-pores (double-length channel) within each layer of the lipid bilayer. Additionally, the transmembrane channel may arise through a conformational thinning of the membrane, extending across the entire bilayer. This conclusion was drawn from experiments [87] using large unilamellar vesicles composed of DMPC and egg phosphatidylcholine, with or without cholesterol or ergosterol. Evidence indicates that both structures, single-length and double-length channels, coexist and display different levels of ion selectivity [30]. The channel size is mainly determined by the polyene macrolide's structure, the monomers' number, and sterols [84][85]. Furthermore, the diameter of the channel is responsible for the leakage from the cell and the transport selectivity [48]. Additionally, literature data indicates [30] that the pore properties depend also on the concentration and type of the salt present in the cell's external environment. At high concentrations of the salts (e.g. KCl), the presence of a singular half-pore may become evident [84], as it undergoes numerous shifts between open and closed states [30][84].

Pores are formed once a specific concentration of polyene macrolide molecules is attained in the membrane. Until this threshold is reached, aggregate complexes known as "non-aqueous pores" or "cation-selective pores" can enhance membrane permeability to monovalent cations (with a lower permeability to monovalent anions). Interestingly, certain research found that ion transport in AmB channels had a shorter dwell time (was faster) in membranes containing ergosterol than cholesterol, suggesting the explanation for antifungal specificity [48][82]. Subsequently, the further formation of aqueous pores allows the transfer of monovalent and divalent ions, as well as large electrolytes (e.g. glucose) [82][85]. The formed channel of the polyene macrolide-sterol complex induces the fungal glycolysis inhibition, an increase of lipid membrane cell permeability, and the leakage of its components such as water, non-electrolytes, small organic particles (important for cell function), and ions (predominantly K^+) [65] [92].

The rapid potassium ions (cations) loss is compensated by the further influx of hydrogen and magnesium ions from the environment (at pH < 7.0), leading to internal acidification [93]. Furthermore, the pH change results in cytoplasm damage and possible cell killing. Interestingly, K⁺ ion leakage does not always lead to the death of fungal cells. The AmB doses causing cell death due to the ion leakage are higher than those causing a simple ion efflux [65]. In the case of Candididin (20 µg/mL known as a lethal dose), researchers noticed internal acidification in the fungal cell [92].

1.3.4. Surface adsorption model

The surface adsorption model hypothesizes that heptaene macrolides sequester ergosterol and adsorb it to the membrane surface (both oriented parallel to the lipid bilayer). Polyene macrolide hydrophilic fragment is at the membrane surface. Such complexes are not prone to aggregation. Although the surface adsorption model is formed differently, it has the same consequences as the sponge model [83][94]. Therefore, it will not be discussed here. The description is presented in the next section ("Sponge model").

1.3.5. Sponge model

The next model, gaining recently a lot of attention, is the sponge model proposed by Anderson et al. [94]. The model assumes that Amphotericin B molecules form large aggregates on the fungal membrane surface in a perpendicular (orthogonal) orientation to the phospholipids bilayer. Due to its high affinity for sterols, AmB aggregates extract ergosterol from the membranes of fungal cells, retaining it within the complex (sponge). This establishes a sterol sponge that destabilizes the membrane and disrupts crucial cellular processes reliant on ergosterol including cell division, endocytosis, or membrane protein function [30][48][94]. The described mechanism may explain the rare occurrence of resistance to heptaene macrolides in certain fungal strains that are generally sensitive to these antibiotics. Resistant fungal strains have developed various strategies to counteract the effects of HMs, such as altering sterol biosynthesis pathways, which can affect membrane fluidity [19]. Since ergosterol is the primary target of HMs, fungal species like *C. albicans* and *C. glabrata* can reduce or eliminate ergosterol from their membranes [95]. In these cases, the antibiotic, which acts according to the sponge model by sequestering ergosterol from the membrane, cannot bind effectively, preventing fungal cell death. In contrast, *Cryptococcus neoformans* has been shown to overproduce ergosterol, as reported by Choy et al. [96]. The excess sterol is subsequently removed from the cell membrane to maintain homeostasis. This surplus ergosterol can be captured by HMs without disrupting membrane integrity, allowing the fungal cell to survive. Moreover, studies by Anderson et al. [94] suggest that increasing concentrations of Amphotericin B lead to a greater accumulation of ergosterol outside the membrane, further supporting this mechanism of resistance.

However, Kamiński [89] pointed out several critical remarks concerning the sponge model proposed by Anderson et al. [94]. First, the ratio of ergosterol-to-lipid (phosphatidylcholine) in performed experiments does not align with the natural cell composition, which is a key factor in determining susceptibility to heptaene macrolides. Additionally, in the host (mammalian)

environment where fungal infections occur, cholesterol is more abundant than ergosterol. This suggests that the competition between ergosterol-AmB and cholesterol-AmB interactions would favor cholesterol, implying that the sterol sponge would be filled with the cholesterol inside not ergosterol. Furthermore, the hydrophilic nature of the fungal cell wall, which contains chitin, could impede the transport of hydrophobic ergosterol, potentially inhibiting the formation of the sterol sponge [48][89]. Based on these concerns, Kamiński [89] argued that the pore model does not encounter these limitations and may represent a more compelling explanation for the mechanism of action of heptaene macrolides.

The combined results from solid-state nuclear magnetic resonance (NMR), transmission electron microscopy, and cellular assays performed by Anderson et al. [94] provide evidence supporting the sterol sponge model, in which extramembranous AmB aggregates extract ergosterol from phospholipid bilayers, leading to yeast cell death. Further analysis by Lewandowska et al. [97] showed that the AmB sterol sponge clathrate structure contains large voids sized for 1 to 2 ergosterol molecules. This could indicate a binding ratio of AmB molecules to ergosterol molecules of 1:1 or 1:2. As they also observed an excess of AmB compared to ergosterol at its minimal inhibitory concentration (MIC), it could be suggested that there is an additional capacity for ergosterol binding under fungicidal conditions.

Furthermore, based on the sterol sponge model, Maji et al. [98] sought new derivatives of AmB with reduced toxicity to humans. The authors considered observed correlations between the C2'OH group of AmB and the 3 β -OH group of both sterols, as well as the additional π -interaction of the B-ring of ergosterol with the chromophore of AmB, being responsible for the antibiotic-sterol interactions. According to literature data, Maji et al [98] performed epimerization of the C2' group of AmB, which, as reported in the experiments, disrupted hydrogen bonds with the 3 β -OH group of the sterol, preventing the antibiotic from interacting with cholesterol. They also carried out amidation (serinol side chain) of the COOH group at position C16 of AmB, thereby increasing ergosterol extraction from the membrane. The *in vitro* results suggest that the resulting derivative was toxic to fungal cells but not to mammalian cells, including renal human cells. Moreover, *in vivo* studies in mouse models showed strong antifungal activity and renal sparing. The derivative created is a promising chemotherapeutic agent that could be used to treat systemic fungal infections.

1.3.6. Other proposed mechanisms of AmB action

The experimental evidence supporting the notion that sterols are not an absolute prerequisite for pore formation is provided by the observations of AmB channel formation in lipid bilayers lacking sterols. However, this requires higher concentrations of AmB. Several research have proposed that channels without sterols represent non-aqueous pores (lacking pharmacological relevance) and would not transit into aqueous ones. Furthermore, the molecular characteristics of these sterol-free single channels are closely similar to supramolecular structures akin to those observed in polyene macrolide-sterol complex [30].

1.3.7.Osmotic pressure

In the investigation of pore formation by Nystatin² in giant unilamellar vesicles (GUVs), osmotic pressure phenomena were also observed [99]. As a result, a theoretical model based on osmotic lysis induced by polyene macrolides was developed. The model suggests that the formation of transmembrane pores increases membrane permeability to major ions (Na^+ , K^+ , Cl^-), while remaining impermeable to proteins and other macromolecules. This results in a net concentration of ions with higher permeabilities outside the vesicle. Once pores form, the concentrations of Na^+ and Cl^- rise inside the cell, while K^+ decreases due to the rapid ion exchange driven by large transmembrane electrolyte gradients. Consequently, changes in cytosolic osmolality occur, causing water influx and cell swelling. When the membrane reaches a critical tension, a tension pore forms, allowing non-selective extrusion of cell contents, reducing cell volume, and restoring osmotic balance by enabling macromolecule exit [85].

There was also an observation made on AmB activity in large unilamellar vesicles [100]. It supported the idea that polyene macrolides can form ion channels induced by osmotic pressure in sterol-absent conditions. The researchers observed AmB activity and enhanced membrane permeability in the vesicles without sterols under hypoosmotic conditions. A correlation between activity and changes in osmotic pressure was seen. However, it is important to note, that the study did not ascertain whether mentioned activity was assigned to channel formation or disruption of the membrane [30][100][100]. It suggested that polyene macrolides may act as Molecular Harpoons corresponding to the amphipathic molecules that detect osmotic stress within lipid bilayers due to their hydrophobic part. The oligomerization state of the antibiotic facilitates insertion into the sterol-free membrane. Molecular Harpoons once embedded into the membrane, induce instability, facilitating ion permeation without necessarily causing membrane rupture. Permeation induced by polyene macrolide antibiotics is significantly enhanced when the lipid bilayer is subjected to osmotic stress. The hypothesis proposed that the increased ease of insertion is attributed to the formation of crevices in the outer monolayer, which expose the hydrophobic core of the membrane [30][100].

1.3.8.Oxidative damage model

The mechanisms mentioned above relate to changes in membrane permeability and disruptions caused by the use of heptaene macrolide antibiotics. Certain literature data [101][102][103] suggest that the previously presented mechanisms of action could elucidate the fungistatic effect or would not be the one responsible for cell death. Anderson et al. [101][102] reported that oxidative damage is involved in the process by which AmB kills fungal cells, however, its correlation with the K^+ leakage was not found. Such a conclusion was based on studies involving cell killing and catalase activity assays, supported by the measurements of K^+ leakage induced by AmB. In particular, higher concentrations of intracellular or extracellular catalase, along with exposure to low-oxygen environments, were found to decrease the toxic effects of AmB on *C. albicans* cells and protoplasts. Furthermore, Sangalli-Leite et al. [103]

² Diene-tetraene polyene macrolide, exhibiting antifungal activity

observed that in *C. neoformans*, Amphotericin B induces intracellular damage through the generation of free radicals, occurring before cell membrane damage, as indicated by the uptake of propidium iodide. Therefore, another proposed mechanism involves the induction of oxidative stress in the cell by AmB.

The mechanism of oxidative damage and its role have not yet been completely elucidated. However, it has been supported by numerous studies [49][65][82][101]. It is suggested that AmB may autooxidize, thereby inducing oxidative stress within the cell. The assumption is that AmB directly contributes to the production of reactive oxygen species (ROS), e.g. hydrogen peroxide, peroxyxynitrite anions, superoxide, and hydroxyl radicals. This induced oxidative stress can be responsible for disruption of cellular pathways, DNA damage, lipid peroxidation, and protein carbonylation [48][82][85]. According to Mesa et al. [82], AmB's biological activity is highly intricate and contingent upon various factors, including the fungal growth phase and the presence of oxygen.

1.3.9. Summary of the proposed mechanism of action

For the summary of mechanisms; (half) pore formation model, sponge model, and intracellular oxidative damage model discussed above are compiled together and shown in Figure 8. Additionally, Figure 8 presents membrane effects that refer to the AmB binding to ergosterol (1) and either forming pores or causing ergosterol sequestration (2). These mechanisms lead to membrane destabilization. Thus, in addition to the tension-pore effects caused by heptaene macrolides (which act as pore-forming agents), the cell can actively regulate its volume through the gain or loss of osmotically active solutes such as inorganic ions (Na^+ , K^+ , and Cl^-) or osmolytes like polyols, amino acids, and methylamines. Alongside changes in cell shape and the volume-regulatory loss of electrolytes is facilitated by membrane transport processes [85]. Additionally, AmB can act through the Molecular Harpoons. Within the cell, AmB also triggers an oxidative burst. The exact mechanism behind this, as mentioned, remains unclear, but several possibilities exist (Figure 8, no. 3-5). Certain researchers postulate a possibility that all the mechanisms described above may occur simultaneously [30].

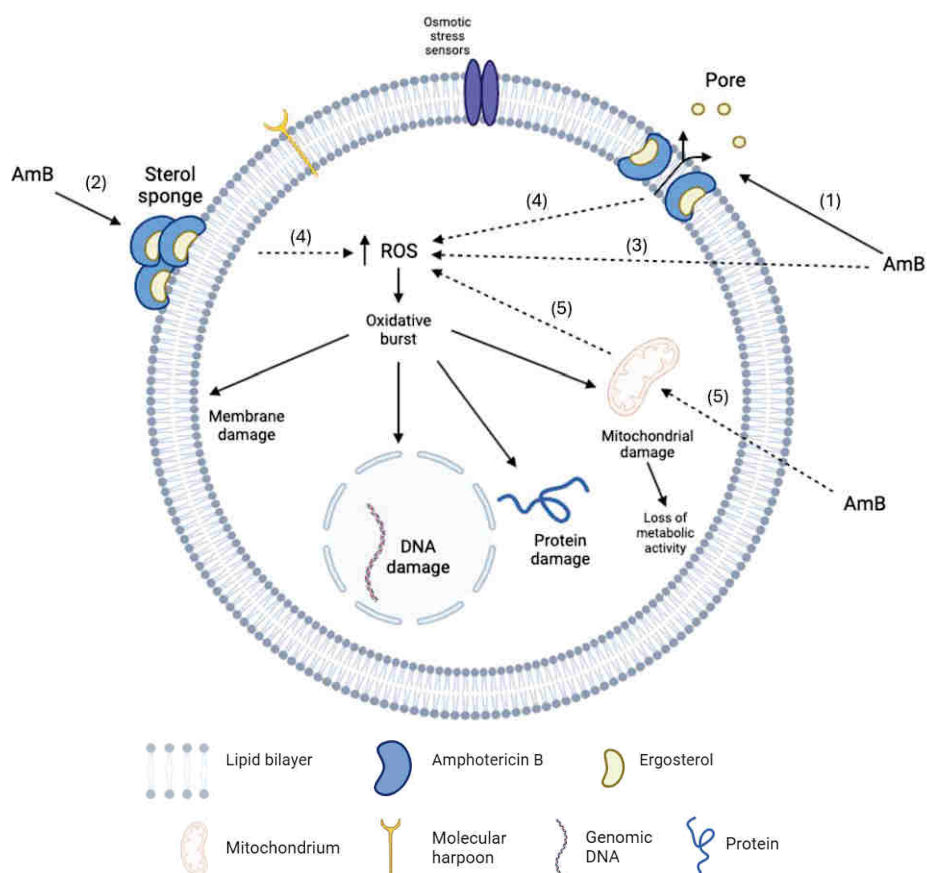


Figure 8. Schema of the AmB mechanism of action.

AmB – Amphotericin B, ROS – reactive oxygen species, 1- ion channel model formation, 2 – sponge model formation, 3, 4, 5 – oxidative damage model formation. The increase of ROS causes oxidative burst, leading to DNA, membrane, DNA, membrane, and mitochondrial damage. The molecular harpoon and the osmotic stress sensor are associated with the osmotic pressure model.

1.3.10. Cellular effect

It is postulated that AmB, along with other heptaene macrolides, exerts a rather complex influence on cell function, a property often referred to as “pleiotropic” nature. This *in vitro* effect depends on many factors, including the antibiotic formulation, the concentration of the compound, its administration pathway, the fungal growth phase, and the cultivation medium [82]. Among the effector action of HMs on cells, the stimulatory effects, the increased membrane permeability, and the lytic action can be distinguished [104].

Certain sources indicate that AmB, at low concentrations - below the threshold for membrane permeabilization, exerts a stimulatory effect, including enhanced synthesis of DNA, RNA, and proteins, in various cell types e.g. in host cells. This stimulation is particularly noticeable in immune system cells and the production of its intermediary mediators [49][72][104]. On the other hand, reaching a certain threshold concentration of the antibiotic in the membrane environment, as mentioned earlier, leads to increased permeability and the uncontrolled efflux of ions into and out of the cell. However, this effect does not always result in cell death, which has led to the recognition of AmB's fungistatic action, inhibiting cell growth. This has been observed in studies conducted on polyene-resistant strains [23]. Additionally, as mentioned earlier, AmB contributes to the generation of ROS, leading to cell death. However, in the yeast resistant to

AmB, the enhanced catalase activity can reduce the formed oxidative damage [105]. A sufficiently high concentration of the polyene macrolide leads to a lethal effect, but doubts the precise relationship between membrane permeabilization and cell death remains unclear. Therefore, several studies have been conducted indicating that the cell membrane becomes susceptible to the flow of water molecules, which may result in osmotic lysis [85].

The fungicidal effect can be attributed to, for example, the acidification of the cytoplasm caused by the influx of protons into the cell enhanced through the AmB pore formation. The direct impact of the pH gradient is termed “proton-induced endocytosis”. This proposed mechanism can be initiated when cells are exposed to external pH below 6. This effect is thought to arise from the protonation of negatively charged lipids in the outer leaflet of the plasma membrane, which decreases electrostatic repulsion and allows for a reduction in the area occupied by each lipid molecule. Consequently, this mechanical imbalance across the plasma membrane is compensated for by an increase in local membrane curvature. It is hypothesized that invaginations in the membrane occur at sites of pre-existing line tension, such as membrane microdomains. Furthermore, changes in lipid packing are believed to influence endocytic activity by altering this line tension [106]. The disruption of the electrochemical gradient of protons generated by membrane pumps is associated with impaired active transport of essential nutrients, such as amino acids and oligosaccharides (symport transport with protons). The H^+ influx is preceded by rapid K^+ efflux and would probably lead to the diminished action of cellular metabolism [72]. The loss of intracellular potassium ions is partially counterbalanced by the influx of potassium ions through the activation of potassium transport mechanisms like Na^+/K^+ -ATPase³ or Na^+ , K^+ , $2Cl^-$ cotransport. Apoptosis, resulting in decreased cell volume, is amplified when the intracellular potassium concentration is reduced. Apoptosis-associated processes, including DNA fragmentation and caspase-3-like activity elevation, are observed primarily in shrunken cells with decreased intracellular K^+ concentration. The efflux-induced cell shrinkage is counteracted by enhanced inward pumping of not only K^+ but also by other solutes. Additionally, the modulation of potassium pumps can either decrease or increase apoptosis, depending on how cellular potassium homeostasis is disrupted [107]. AmB initiates apoptosis-like responses, including a decrease in mitochondrial membrane potential, an enhancement of intracellular Ca^{2+} levels, and the cleavage of caspase-like proteins in both leishmanial and fungal cells [85].

Furthermore, as mentioned partially above, AmB can modulate certain membrane enzymes involved in ion leakage [108]. For example, it was proven that it can inhibit Na^+/K^+ ATPase presented in the erythrocyte membrane [108]. The results obtained from Vertut-Doi [108] showed that the Na^+ pump was wholly inhibited by AmB in red blood cells at a concentration of 5 μM . Additionally, it was indicated that AmB binds to lipoproteins and serum albumin. The conducted research on the inactivation of ATPase indicated that possible inhibition of its activity may result from the direct binding of AmB to the enzyme and altering its conformation (which was supported by circular dichroism studies). The Na^+ pump inhibition can also result from

³ adenosine triphosphatase, ATPases are enzymes that link the hydrolysis or synthesis of ATP to the movement of ions across membranes [177]

the membrane disorganization induced by the AmB. It may affect membrane fluidity, as observed for lymphocytes using fluorescent probes, or reduce pump activity demonstrated in erythrocytes. Phosphatidylethanolamine in red blood cells rapidly loses its asymmetric orientation, and ATPase activity, which likely requires a charged phospholipid, is deactivated. Additionally, oxidative stress, as mentioned earlier, may also play a significant role. Endogenous inhibitors selectively inactivate Na^+/K^+ ATPase, which is probably associated with the radical damage of unsaturated membrane phospholipids induced by the mentioned ROS [108].

The AmB formulations used in medicine are administered intravenously, therefore, their interaction with blood serum is interesting. Furthermore, AmB binds particularly to lipoproteins [109]. Lipoproteins associated with a drug may have a significant effect on its pharmacology and relative toxicity, as they participate in the nutrients' transport to peripheral tissue and other biological processes, such as tissue repair and immune system reaction [110]. Free AmB in the serum exhibits a high affinity to low-density lipoproteins (LDL), therefore it can be easily recognized by receptor-mediated endocytosis and transferred into the host cells (renal tubular cells). In effect, the LDL-AmB complex results in increased toxicity [109][111][112]. Wasan et al. [110] marked that higher LDL cholesterol concentrations exacerbate the AmB renal toxicity, whereas elevated serum triglyceride levels mitigate it. In comparison, antibiotic binding with high-density lipoproteins (HDL) is less toxic to kidneys probably due to the lower amount of expressed HDL receptors on the cells. Interestingly, the antifungal activity of AmB associated with LDL or HDL remains unaltered [113]. It is worth noting that the drug formulation also bears great importance in the lipoprotein-polyene macrolide interaction. Increased stability of lipid formulations of AmB leads to reduced amounts of AmB bound to LDL resulting in lower toxicity compared to Fungizone. Moreover, Abelcet shows preferential binding to HDL, while Amphotec does not exhibit any binding affinity towards lipoproteins [109].

1.4. Aromatic heptaene macrolides

The particular regions of AHMs, except for the alkyl-aromatic side chain, are similar to the highlighted regions of AmB (Figure 3) discussed above. These regions are also presented in the example of the stereostructure of AHMs based on Candicidin D in Figure 9.

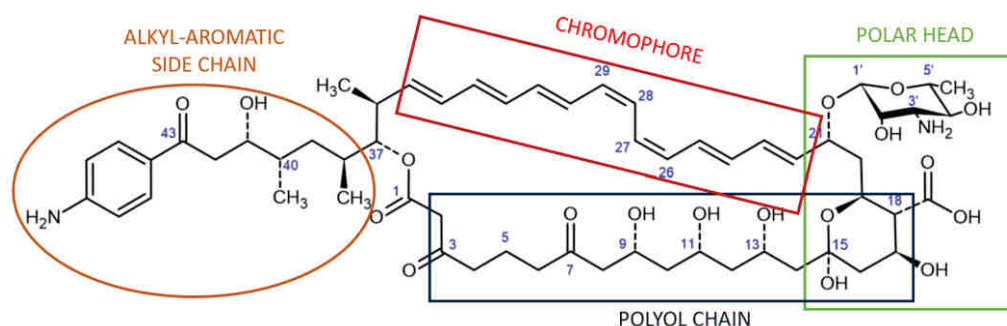


Figure 9. The elements of AHM structure based on the stereostructure of Candicidin D. Orange box – alkyl-aromatic side chain; red box – chromophore (seven conjugated double bonds); green box - polar head consisting of hemiketal ring with the carboxylic group, and sugar (mycosamine); blue box – polyol chain consisting of a system of oxygen functions

In AHMs, a hydrophobic “tail”, i.e. an aliphatic chain ending with the aromatic moiety which can be represented by *p*-aminoacetophenone or *N*-methyl-*p*-aminoacetophenone [24][27], is linked to the macrocyclic ring, vis-a-vis the C8 region (Figure 9). The alkyl-aromatic side chain's role is not yet known. However, there are a few models of the AHMs mechanism of action that allow to suggest its role in their biological activity [90]. Interestingly, this part of an antibiotic molecule is not a product of polyketide biosynthesis but is formed from precursors derived from the shikimate pathway [34].

All these structural features of heptaene macrolides can be responsible for their biological activity and also for their mechanism of action. Aromatic and non-aromatic heptaenes, as mentioned previously, apart from the aromatic moiety and geometry of the chromophore, are structurally very similar, especially when comparing Candicidin D, Gedamycin, and Vacidin (studied compounds, AHMs) with Amphotericin B (representative of non-aromatic HMs). In Figure 10, the stereostructures of the mentioned antibiotics were compiled together.

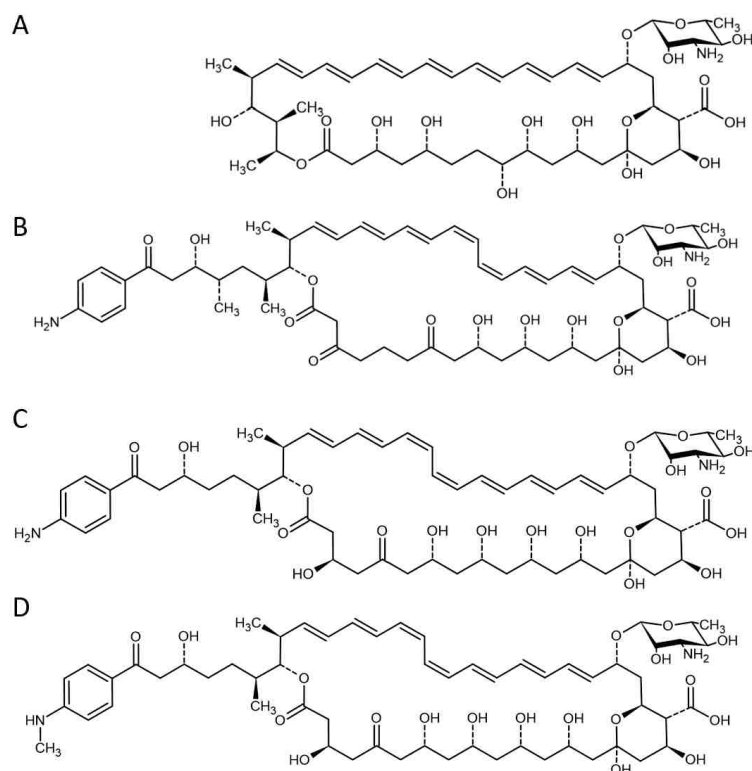


Figure 10. The stereostructures of A) Amphotericin B, B) Candicidin D, C) Vacidin, and D) Gedamycin

1.4.1. Physicochemical properties of AHMs and characteristics of AHMs studied in this work

Aromatic heptaene macrolides are synthesized by bacteria, particularly by certain *Streptomyces* species. Usually, the result of biosynthesis is a mixture of antibiotics with very similar structures (described as “sister-structures”). Due to their close structural relationship, they are commonly referred to as a “complex” of AHMs (Figure 13,14)⁴. These antibiotics can vary, for example, by the presence of a single hydroxyl group in the polyol fragment within the same

⁴ The stereostructures of the components of the Candicidin complex and the Aureofacin complex are presented in Figures 13 and 14, respectively. These components are described in section 1.4.2.

complex, or, as seen in the Aureofacin complex, by a methyl group in the aromatic part of the side chain. Such structural changes are relatively minor considering the large size of the compounds, however, these “small” differences in structure can importantly affect biological activity. Isolation and purification of pure compounds from such complexes obtained as a result of the cultivation of producing strains is very difficult. Moreover, both the isolation and purification of AHMs are hindered by their inherent chemical instability. These antifungal antibiotics are highly sensitive to light, oxygen, humidity, heat, and ultrasonication [27].

In general, aromatic polyene macrolides exhibit hues ranging from pale yellow to orange⁵ [27] (Figure 11B) and occur in the form of an amorphous powder. Exposure of the antibiotics to the indicated factors e.g. high-temperature results in their degradation, which is also associated with a color change (to a darker shade) and a worsening of their biological activity. Additionally, after exposure to light and prolonged contact with air, their color may change to a “dirty” orange or brown.

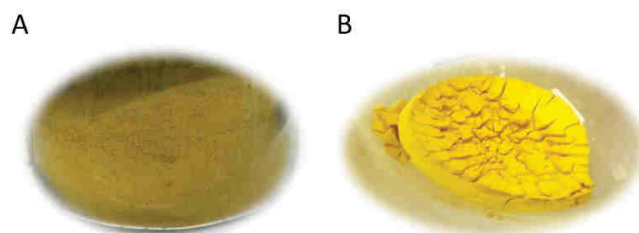


Figure 11. The color comparison of A) long-term stored antibiotic (before purification) and B) pure (freshly purified) antibiotic

The compound's color is the result of the presence of seven conjugated double bonds in the chromophore. Moreover, the hydrophobic part contributes to several distinct physical and chemical characteristics. Notably, its capacity for strong light absorption (UV-Vis) is characterized by three specific absorbance maxima, at 360 nm, 380 nm, and 401 nm as depicted in Figure 12 [36][40].

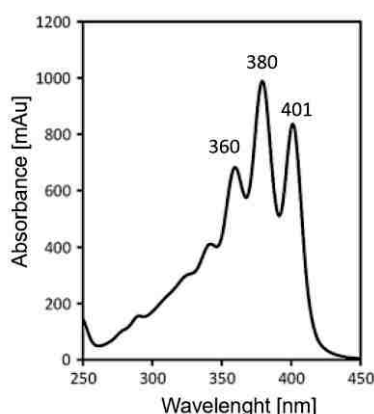


Figure 12. The absorption spectrum of 3'-N-acetylcandidin D methyl ester in MeOH [40]

As can be seen in Figure 12, the absorbance maximum at 380 nm is the strongest. Such a specific spectrum is assigned to the *cis-trans* chromophore geometry of AHMs. However,

⁵ In my doctoral research, as a result of the purification process employed, none of the purified compounds exhibited an orange color.

it changes when the antibiotics are exposed to the light. In that case, the bathochromic shifts can be observed in the spectrum compared to *cis-trans*, and the absorbance maxima change with the highest at 407 nm. More details are presented in the section 1.5.

As has been mentioned, AHMs are amphoteric compounds due to the presence of carboxyl, amino, and aromatic amino groups in the structure [24]. Their hydrophobic and hydrophilic parts are responsible for particular physicochemical properties such as poor solubility in water and most organic solvents (except DMSO, DMF, DMA, and hydroalcoholic solutions such as MeOH/water) [36][114][115]. The positive and negative charge ($-\text{NH}_3^+$, COO^-) might influence the formation of insoluble polyaggregates (by self-association of the antibiotic). AHMs tend to aggregate in an aqueous solution such as water or PBS, similarly to AmB. Moreover, the pH of the solution influences their solubility; in the basic and acidic environment, the ionized antibiotics dissolve better but on the other hand, are more prone to degradation due to hydrolysis [114][116]. In organic solvents, AHMs are present as monomers, while in aqueous solution they may form oligomeric structures [114]. The pH of a solution, antibiotic concentration, and the presence of additional solutes are responsible for a particular oligomerization status. The aggregation state depends on antibiotic concentration, with a lower tendency to aggregate at lower concentrations. From the pharmacological perspective, it is postulated, that the aggregation state of AHMs may be significant for their interaction with cellular membranes and pharmacological activity, potentially contributing to mammalian toxicity [30]. According to the literature data, AHMs may appear in one of three forms; positively charged, zwitterionic, or negatively charged, depending on environmental conditions [25]. A positive net charge is presumed to be the most favorable for optimal selective toxicity of these antibiotics. Both the hemolytic and antifungal properties of AHMs seem to be largely influenced by the ionization state of their polar head groups, specifically the carboxyl group at C18 and the amino sugar.

1.4.2. AHMs studied in this work

My studies, the results of which are described in this dissertation, focused on two aromatic heptaene macrolides complexes as representatives of this subgroup of antibiotics – Candididin (Figure 13) and Aureofacin (Figure 14). Their molecular masses and formulas compared with those of AmB are presented in Table 5.

Table 5. The molecular mass and molecular formula of the tested antibiotics in comparison to AmB.

Antibiotic	Molecular Mass [g/mol]	Molecular formula
Amphotericin B	924.1	$\text{C}_{47}\text{H}_{73}\text{NO}_{17}$
Candididin D (Candididin A2)	1109.3	$\text{C}_{59}\text{H}_{84}\text{N}_2\text{O}_{18}$
Gedamycin	1127.3	$\text{C}_{59}\text{H}_{86}\text{N}_2\text{O}_{19}$
Vacidin	1113.3	$\text{C}_{58}\text{H}_{84}\text{N}_2\text{O}_{19}$

1.4.2.1. Candididin complex

The Candididin complex was first isolated in 1948 but named in 1953 by Lechevalier [117]. Its main producer is *Streptomyces griseus* IMRU 3570, although it is also biosynthesized

by *Actinomyces levoris*. The complex consists of three main antibiotics – Candididin A1, Candididin A2 (D), and Candididin A3 (stereostructures are shown in Figure 13).

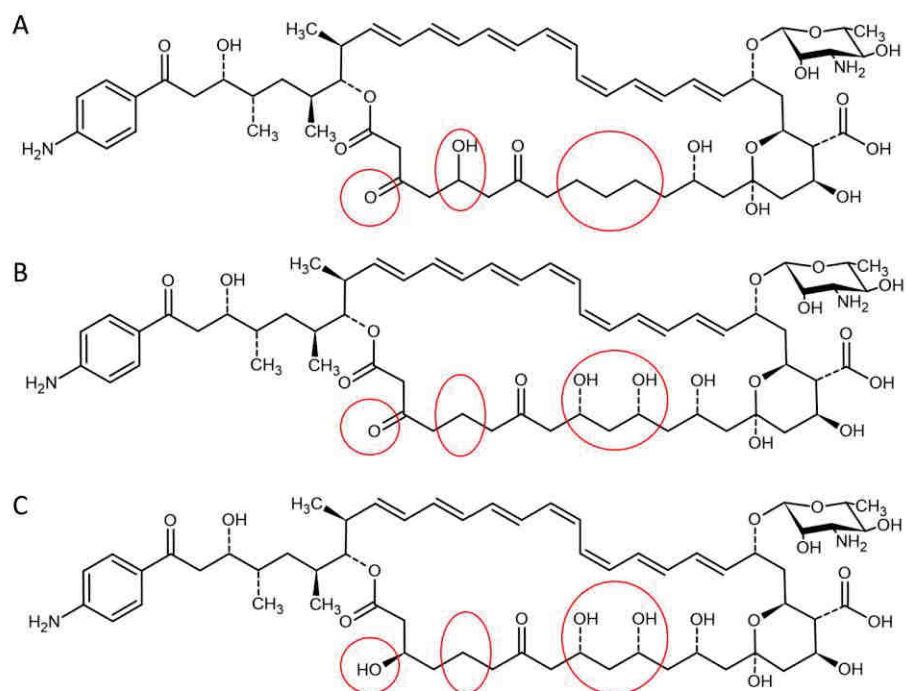


Figure 13. The stereostructures of A) Candididin A1, B) Candididin A2 (D), C) Candididin A3 – own work based on [118]

Structural differences between components of the Candididin complex are noted solely in the polyol chain (Figure 13, highlighted by red circles). The hydrophobic side chain is terminated by *p*-aminoacetophenone, and the mycosamine (aminosugar moiety) is attached to the macrolactone ring [118][119]. According to the previously mentioned literature [38], a higher number of oxygen functions in this hydrophilic region correlates with increased compound activity. Consequently, within the Candididin complex, Candididin A3 is identified as the most active, while Candididin A1 exhibits the lowest activity. The most well-known component of this antibiotic mixture, and the one present in the highest amount is Candididin D. However, depending on the producer strain, the relative content of these three main components may vary.

According to the literature, aromatic heptaene macrolides, such as Candididin D, like AmB, exhibit high antifungal activity and also show significant toxicity in humans. The research showed that the hemolytic activity of Candididin D is slightly lower than that of Amphotericin B and ten times lower than that of Vacidin and Gedamycin (described in this section). It was assumed then, that the hemolytic effect is thought to result from the hydrophilic region of the macrolide ring and the presence of an aromatic side chain [25][120]. This toxicity limits their clinical use for treating systemic fungal infections. However, topical applications of the Candididin and Aureofacin complexes are still utilized [40].

Heptaene macrolides are not orally administrated as they are not resorbed from the gastrointestinal tract. However, research on Candididin oral administration was performed. Oral Candididin was significantly less toxic than in parental routes, allowing for a reduction

in androgen activity and the plasma cholesterol content in cases of benign prostatic hyperplasia or prostate gland [40][121][122]. This was followed by Candicidin's cholesterol-binding affinity in the gastrointestinal tract [123]. Moreover, Candicidin in the vaginal tablet form was used against candidal vaginitis due to its high antifungal activity against *Candida* spp. strains [124][125][119].

1.4.2.2. Aureofacin complex

Aureofacin complex (syn. Partricin) is produced by *Streptomyces aureofaciens* [126][127]. This complex is composed of two major antibiotics – Gedamycin (syn. Partricin A) and Vacidin (syn. Partricin B). The difference between these components is very subtle and lies in the aromatic moiety linked to the aliphatic chain. The side chain of Vacidin is ended by *p*-aminoacetophenone, while in Gedamycin, the aromatic amino group is *N*-methylated (stereostructure shown in Figure 14). Both antibiotics contain mycosamine glycosidically bound to the 38-membered macrolactone ring [126][128][129].

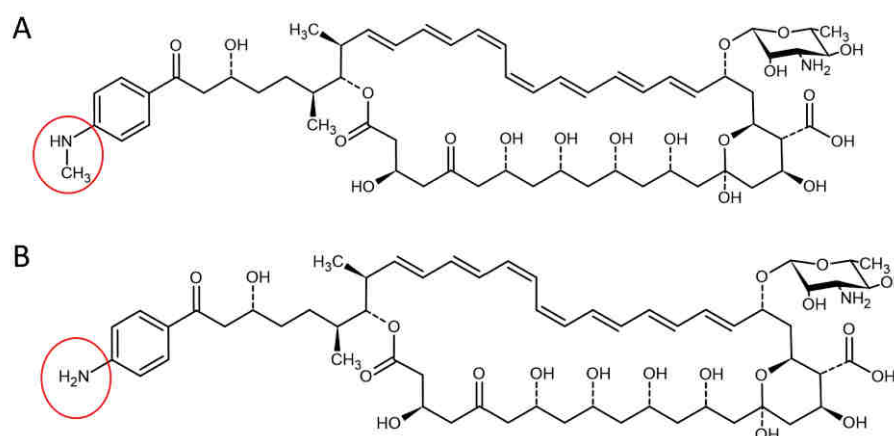


Figure 14. The stereostructures of A) Gedamycin and B) Vacidin – own work based on [126][128][129]

The derivatives of Aureofacin are used in medicine. Under the form of methyl ester, the complex of Aureofacin derivatives (Mepartricin) is utilized as an active substance in drugs like Ipertrofan and Tricandil. This semi-synthetic derivative is administered in tablet or ointment form for the treatment of benign prostatic hyperplasia, chronic pelvic pain, and vaginal candidiasis [130][131]. Moreover, for several years, a new derivative of Gedamycin, known as Amcipartricin (N-dimethylaminoacetylpartricin A 2-dimethylaminoethylamide) has been under development. The mentioned water-soluble semi-synthetic salt exhibits high effectiveness (*in vitro*) against *C. neoformans*, *Candida* spp., and *Aspergillus* spp. Its activity rivals or surpasses that of Amphotericin B [132][133]. Amcipartricin entered the II phase of clinical trials in 2004 but for unknown reasons, it was abandoned for further development.

It should be noted that none of the forms of the aforementioned AHMs are used in the antifungal treatment of systemic mycoses.

1.4.3.Liquid-liquid separation techniques in the isolation of Aromatic Heptaene Macrolides

As previously mentioned, polyene macrolides are generally produced as a mixture of structurally similar compounds, making their separation challenging. One of the techniques used to isolate the heptaene macrolides was counter-current extraction with a Craig apparatus. This approach was commonly applied in the 1950s for purifying natural compounds. The Craig apparatus itself represents an advanced design, consisting of hundreds of intricate glass partition units linked in series to enhance separation efficiency [134]. Counter-current distribution (CCD) in the Craig apparatus was the first method for the separation of heptaene macrolides such as AmB and Candididin [135][136]. However, this process required 48–64 hours, resulting in irreversible structural modifications of the antibiotic molecules and their partial degradation.

Based on the CCD technique, in the early 1970s, Counter-Current Chromatography (CCC) emerged as a novel separation method. In the Craig apparatus, both liquids were in counter-current move, while in CCC one of the liquids remains stationary – this is the reason why “CCC” is called chromatography. In the CCC technique, two main equipment constructions can be distinguished – hydrodynamic, High-Speed Counter-Current Chromatography (HSCCC), and hydrostatic, Centrifugal Partition Chromatography (CPC). CPC is a relatively new technique representing the technologically advanced version of liquid-liquid extraction and it is commonly used to separate natural products such as flavonoids, alkaloids, and many others [137].

Given the physicochemical foundations of both processes, CPC and CCD, it is highly probable that adapting systems previously used for AHM separation (in CCD) to CPC chromatography, along with optimizing chromatographic parameters, could result in the development of an efficient isolation method. While such an approach is scientifically justified and has been validated for the isolation of various plant metabolites, there are no existing reports in the literature regarding the application of CPC for the isolation of AHM. Unlike traditional column chromatography, the mentioned technique eliminates the need for solid support, which limits the stationary phase and the risk of irreversible adsorption to the support material. This innovation represented a significant advancement in chromatographic methods.

CPC is a liquid-liquid chromatographic technique and it is considered as one of the CCC variants. In general, its action relies on the analyte separation between two immiscible liquids of different polarities in a biphasic solvent system, which are regarded as mobile and stationary phases [138]. In such solvent systems, the phases, which differ in density, can be considered as lower (heavier) or upper (lighter) phases, respectively. These phases are mixed and separated multiple times in a rotor (Figure 15) to form theoretical plates, allowing the exchange of molecules between the two phases.

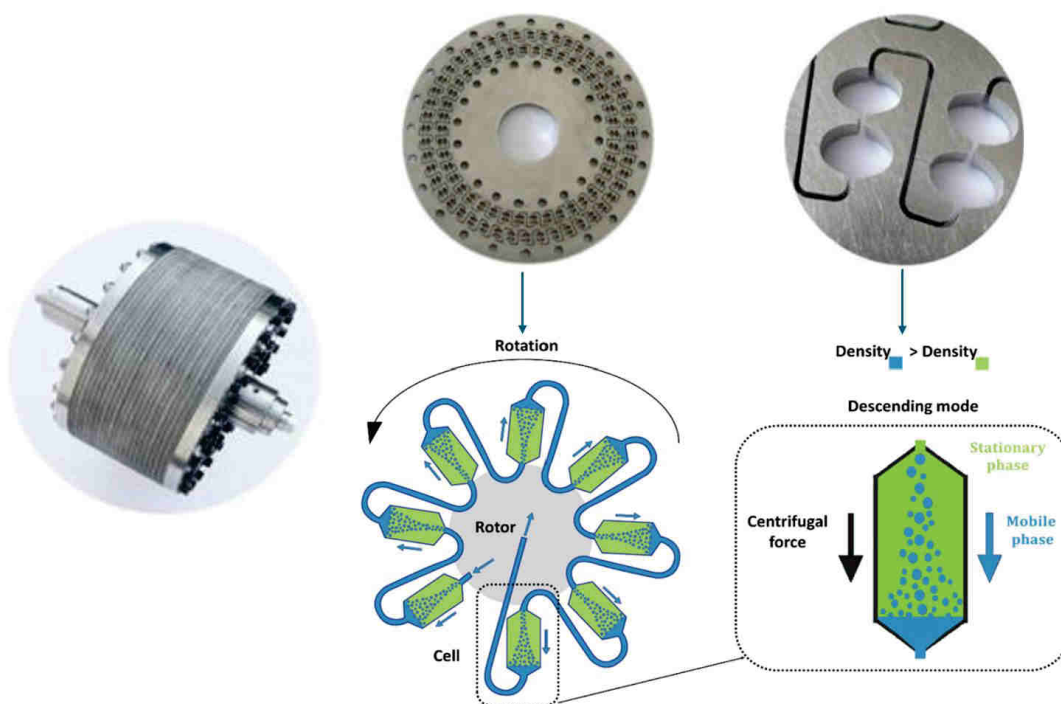


Figure 15. CPC's rotor construction images (up) [139] and schema of the CPC operation principles (down). Schema illustrating a CPC rotor and a CPC cell operating in descending mode. The upper, lighter phase (green color), the lower, heavier phase (blue color) [140]

Figure 15 illustrates the schemas of the CPC rotor and a single CPC cell functioning in one of the two main modes of action - descending mode. In this mode, the upper, lighter phase (green color) is immobilized within the cell by centrifugal force, serving as the stationary phase, while the lower, heavier phase (blue color) is pumped through it, moving along with the centrifugal field. In the second mode of action - in ascending mode, the phases undergo a role reversal, with the flow direction being inverted [140].

The crucial step for the CPC analysis is selecting an appropriate solvent system, which is usually done using the shake-flask method. The composition and proportions of the mentioned solvent systems play a critical role in the separation of compound mixtures in CPC. Solvents and their ratios are carefully selected to form a biphasic system of immiscible liquids, corresponding to the stationary and mobile phases. Once introduced into the CPC rotor, these phases create a chromatographic column where the separation of the target substance occurs. For more demanding compounds, ternary or quaternary solvent systems are typically employed to achieve optimal-separation.

In a CPC chromatographic process, four main stages can be distinguished: initiation, equilibration, elution, and extrusion. Their characteristic is presented in Table 6.

Table 6. Characteristic steps of a single run during the CPC chromatographic process.

Step of CPC chromatographic analysis	Characteristic
Initiation	The stationary phase fulfills 100% of the rotor interior volume and it is retained by centrifugal force.

Step of CPC chromatographic analysis	Characteristic
Equilibration	The mobile phase is pumped through the rotor. Consequently, part of the stationary phase is eluted until phase equilibrium is reached (a point at which no further phase displacement occurs).
Elution	The mobile phase with the solute to be extracted passes through the stationary phase after sample injection and the separation process occurs. Components with higher affinity for mobile phase elute first.
Extrusion	The stationary phase is pumped again to the rotor. The mobile phase with the residuals of solute is removed from the column. A new, "fresh" stationary phase replaces the previous stationary phase that remained in the rotor.

Extrusion can be used as the initiation stage of the next isolation process. Analyte separation in a two-phase solvent system is highly correlated with the Nernst partition coefficient (K_D), an important parameter in CCC, expressed as a ratio of the sample concentration in the stationary phase to its concentration in the mobile phase (equation 1.4.3.1). "A" and "Area" are sometimes used interchangeably as parameters representing concentration function. The partition coefficient is experimentally determined by measuring the sample concentration in either the lighter or heavier phase of the biphasic solvent system, using the shake-flask test [141]. K_D was calculated according to equation 1.4.3.1.

$$K_D = \frac{A_{stat}}{A_{mob}} \text{ or } K_D = \frac{C_{stat}}{C_{mob}} \text{ or } K_D = \frac{Area_{stat}}{Area_{mob}} \quad (\text{equation 1.4.3.1})$$

where,

C_{stat} – sample concentration in the stationary phase

A_{stat} – sample absorbance in the stationary phase

$Area_{stat}$ – peak area of the sample in the stationary phase measured by HPLC

C_{mob} - sample concentration in the mobile phase

A_{mob} - sample absorbance in the mobile phase

$Area_{mob}$ – peak area of the sample in the mobile phase measured by HPLC

The separation of individual solutes is achieved based on the different partition coefficients (K_D) of each compound in this two-phase system [142]. The K_D value indicates the affinity of component partitioning in a two-phase solvent system (at equilibrium) and enables the separation of the solute (Figure 16).

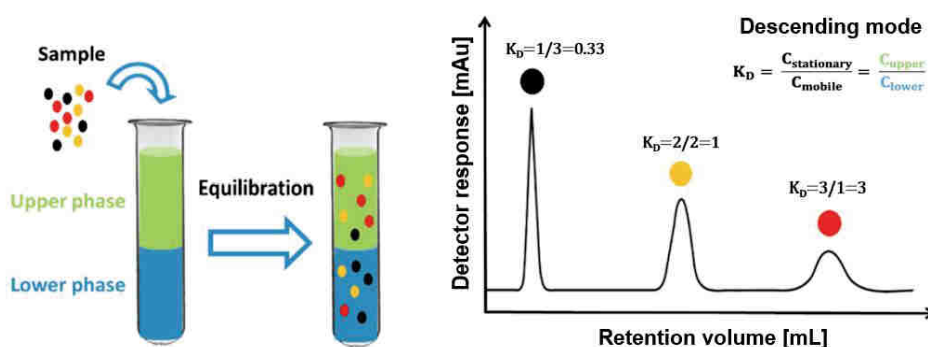


Figure 16. K_D determination by the shake-flask test, and the obtained chromatographic elution profile of a mixture with three components [140]

The partitioning of the three-component solute mixture in the CPC system is depicted in Figure 16. The K_D influences the separation process, as it governs how each compound interacts with the stationary and mobile phases. When $K_D \approx 1$, the compound is evenly distributed between the two phases. $K_D < 1$ indicates a preference for the mobile phase, while $K_D > 1$ suggests a higher affinity for the stationary phase. Low K_D values improve peak resolution and reduce broadening, whereas high K_D values increase peak broadening and run times [143][144].

The unique feature of CCC is the liquid-liquid stationary phase without any solid support, which distinguishes it from all other techniques. Aromatic heptaene macrolides tend to irreversibly bind with the bed of common chromatographic columns or form aggregates (micelles). Both contribute to the destructive effect on the column and thus, to the loss of valuable antibiotics. Therefore, CPC can be a better alternative to HPLC for purification of AHMs.

1.4.4. Mechanisms of action and cellular effects of aromatic heptaene macrolides: Insights into membrane permeability and ion channel formation

The literature data concerning the mechanism of action of aromatic heptaene macrolides provide limited insights into their cellular effects. This section aims to compile and present the existing knowledge on the mechanisms through which these antibiotics exert their effects at the cellular level. Understanding these mechanisms is further complicated by the challenges associated with the limited availability and low purity of heptaene macrolides, which hinder comprehensive characterization studies [145]. It should also be noted that AHMs are produced as complexes of antibiotics with similar structures. It is known that they affect the permeability of membranes containing sterols similarly to other heptaene macrolides. Studies by Cybulska et al. [31] on cation permeability indicated that Vacidin and Candicidin D induce intercationic selective pathways [28][31]. Therefore, it is reasonable to propose that the mechanism of action of AHMs is similar to that of the widely studied heptaene macrolide, Amphotericin B. Most of the available literature on aromatic heptaene macrolides refers to the oldest proposed molecular action of AmB – the channel formation model [31].

Furthermore, the performed studies on egg yolk phosphatidylcholine single unilamellar vesicle [31] highly support the pore formation model. The experiment confirmed the cation permeability of AHMs (Vacidin and Candicidin D). Notably, sterol-free vesicles exhibited insensitivity to the tested AHMs, in contrast to vesicles containing incorporated sterols (cholesterol or ergosterol). Moreover, when the concentration of Vacidin and Candicidin D was increased the percentage of proton efflux also increased [31]. Based on the results of Mazerski et al. [114], it can be concluded that aromatic heptaene macrolides may exist in two complexes within lipid vesicles of AHM: AHM-phospholipid and AHM-sterol. The AHM-sterol interaction is responsible for triggering membrane permeability. Moreover, it was shown that AHMs form cation-selective channels in black lipid⁶ membranes [28].

⁶ Model of syntetic planar phospholipid bilayer, made of phospholipid molecules painted across a 1 mm hole between two solution chambers [178]

Subsequent research by Cybulska et al. [25] indicated a relationship between the charge of the aromatic heptaene macrolides and its activity in the membrane containing ergosterol. Candicidin D, Gedamycin, and Vacidin, at neutral pH, adopt the form of a zwitterion and exhibit the highest biological activity (hemolytic and antifungal). As mentioned in the previous section (1.4.2.), the structure of Vacidin and Gedamycin (components of Aureofacin complex) differs in the substituent attached to the aromatic ring, -NH_2 and -NHCH_3 , respectively. This likely resulted in a slight difference in the antifungal activity of these compounds. Candicidin D contains fewer hydroxyl groups in the polyol fragment compared to the components of the Aureofacin complex. This difference probably accounted for the 10-fold lower hemolytic activity of Candicidin D in the research. Additionally, the observed hemolytic and antifungal effects were connected to the polar structure of the polyene macrolide head, as the absence of a carboxyl group resulted in a significant reduction in hemolytic activity while maintaining an almost unchanged antifungal effect. In turn, the substitution of an amino group in the sugar moiety resulted in lower antifungal activity [25][91]. The inhibition of fungal growth occurs due to a metabolic imbalance caused by a reduction in intracellular K^+ concentration [25].

As mentioned in a previous chapter, literature data overall indicate that AHMs exhibit around two or three orders of magnitude higher activity compared to Amphotericin B. The pharmacological action of heptaene macrolides and promising analogs in antifungal therapy is mainly attributed to the higher affinity of the antibiotic for ergosterol than for cholesterol present in the biological membranes of fungal and human cells, respectively [28]. One of the most commonly used models for studying the mechanism of action of polyene macrolides and their toxic properties in mammalian cells are erythrocytes, which contain cholesterol in their membrane (approximately 30%) [31][91]. Aromatic heptaenes, as studies show [25][31], lead to increased membrane permeability by channel formation and uncontrolled flow of ions, mainly monovalent cations. Taking into account the structure of the polyene macrolide, membrane permeability is primarily associated with the carboxyl group, amino groups of sugar, and the aromatic moiety of AHMs (see Figure 9, section 1.2.1.). The resulting osmotic imbalance causes a hemolytic effect.

In studies [91][146][147], different iso-osmotic solutions (such as those of potassium chloride, choline chloride, and sodium chloride) were used to determine the pore selectivity during hemolytic tests. The results showed that Vacidin induces slightly higher membrane permeability to K^+ than Na^+ . Furthermore, the zwitterionic form of Vacidin and Gedamycin likely forms narrow channels (permeable to K^+ and slightly permeable to choline), which are more selective than those formed by their positively or negatively charged derivatives. This indicates the importance of the charge of the macrolide heptaene's polar head. Hemolytic activity largely depends on the medium composition in which the study is conducted [91][147]. Cybulska et al. [146] demonstrated that while both polyene macrolides significantly increased permeability to K^+ , the subsequent volume change of the red blood cell in isotonic KCl medium relied on the macrolide heptaene's capacity to induce H^+ permeability. The mentioned volume change, resulting from the alteration of the salt concentration in the medium, could lead to cell lysis. Moreover, it is proportional to ion exchange (influx and efflux) through the pore formed by

the macrolide heptaene antibiotic. The diverse effects of cell volume changes were observed; from cell shrinkage in choline chloride to its swelling in KCl [91]. Only the naturally slow conductive chloride anion intrusion to the cell could limit the hemolysis, the swelling of the cell, and its lysis [147]. Additionally, it was shown that Vacidin triggered the H^+/K^+ exchange and caused small changes in RBCs membrane potential. Although the intracellular pH in the cells decreased, the H^+ could rapidly return to the external medium to aim to balance the pH [146][148]. The tests on lipid vesicles indicated that the carboxyl group at C18 in the structure characterized the type of induced permeability by polyene macrolides. The results additionally prove the viability of the pore formation model application in the MOA of AHMs.

The characteristics of the channels are determined by the structure and stability of these molecular complexes within the membrane, which can transition between various states. As mentioned previously regarding the MOA of AmB - "open states" refer to the associated molecules of antibiotic and sterol, forming a channel with high ionic conductance, while "closed states" are assigned to the dissociated molecules of antibiotic and sterol or their association in non-conducting structures. Moreover, an open channel state is established when the sterol and polyene macrolide form the complex. Following the classical pore formation model, the channel's ionophoric properties are assigned to internal ionic permeability, as well as the duration of the open state. Presuming that polyene macrolide-sterol complexes form channels, the interaction of this 'partnership' emerges as a primary determinant of their effectiveness and, ultimately, their selectivity for membranes containing particular sterol [149].

Research [148] conducted on blood cells has provided valuable insights into the action of AHMs, demonstrating that protonophoric activity is important in the case of hemolysis. Antibiotics present in the Aureofacin complex, Vacidin, and Gedamycin, induce membrane permeability to sodium ions, potassium ions, and protons, exhibiting high hemolytic activity. The further results provided by Cybulska and others on lymphoma B cell line, A20 [148] indicated that in Na^+ -rich media, AHMs form ion channels, leading to the flow of sodium and protons along the concentration gradient. Mammalian cell membranes contain proteins responsible for ion transport into and out of the cell, including the sodium-proton antiporter. Therefore, the increased influx of sodium ions into the cell induced by AHMs can be balanced by the Na^+/H^+ exchanger, where sodium ions are exchanged for protons. Moreover, it was proved that Vacidin, itself, is also involved in H^+ flux. Interestingly, in Na^+ -rich media, Vacidin preferably induces the exchange of K^+ for Na^+ over the exchange of K^+ for H^+ .

It was shown [147] that aromatic and nonaromatic polyene macrolides differed in ionic selectivity, membrane permeability, and structure in aromatic side chains (in the case of AHMs). AHM's channels are concentration-dependent, for example, the higher the concentration of Vacidin, the higher proton permeability in cells. The channel selectivity in AHMs depends on the presence of a free carboxyl group, as its substitution enhanced the potassium selectivity, permeability, and consequently lowered the hemolytic activity. AmB formed concentration-independent channels. A similar substitution would not change the properties of nonaromatic

polyene macrolides. Moreover, the selectivity of Cl^- and monovalent cations is different for the specific antibiotic and for Vacidin, it was very strong, while for AmB it was weak [147].

1.4.5. The role of the aromatic side chain

The role of the side chain in the interaction of AHMs with sterols in the lipid membrane is significant, although not well understood. Based on Cybulska et al. results of studies [25], it can be concluded that the alkyl-aromatic group has an impact on antifungal activity, with approximately a two- to three-fold higher antifungal activity for AHMs compared to non-aromatic heptaene macrolides. Furthermore, the aromatic residue's role in the biological activity, which differs between aromatic and nonaromatic antibiotics, can indicate its significant meaning in membrane permeabilization to K^+ and hemolysis [147]. Based on computer simulations, it has been determined that the side chain can exist in three different conformations: extended or straight ($\phi 180^\circ$), arranged perpendicular to the macrolactone ring, termed as bent ($\phi 90^\circ$), and completely folded ($\phi 0^\circ$), see Figure 17 [90].

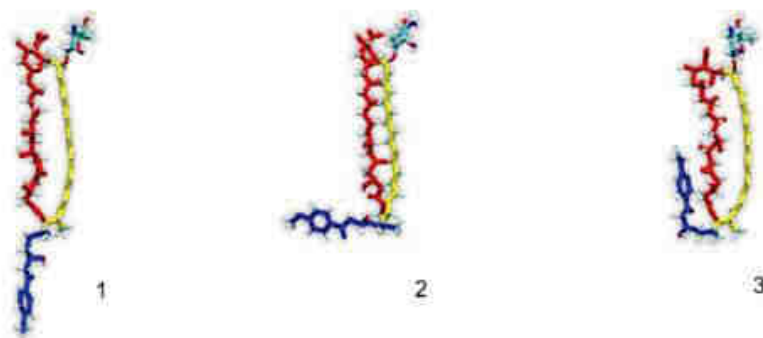


Figure 17. Proposed structures of the side chain for each orientation: 1) straight, 2) bent, 3) completely folded based on [150]

The extended form ($\phi 180^\circ$), is primarily characteristic of Candididin D, but it has also been observed in the case of Vacidin and Gedamycin (Figure 18). For components of the Aureofacin complex, a fully coiled structure of the side chain has also been observed.

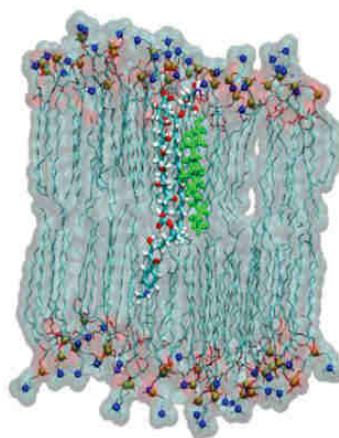


Figure 18. The simulation system of the Vacidin monomer with ergosterol in DPPC based on [150]. For clarity, water molecules and inorganic ions have been omitted.

It is worth noting that there are two main differences in the side chain of studied AHMs (Vacidin, Gedamycin, and Candicidin D), see Figure 19:

- the presence of a methyl group at carbon C40 in Candicidin D (compared to the Aureofacin complex)
- the methyl group attached to the nitrogen of the aromatic group in Gedamycin (compared to Vacidin)

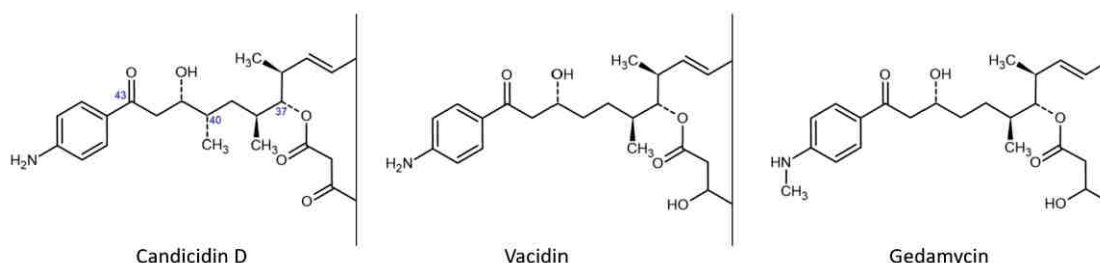


Figure 19. Alkyl-aromatic side chains attached to the macrolide ring (presented partially) of Candicidin D, Vacidin, and Gedamycin. The numbers of several carbon atoms were added in the Candicidin D side chain

The results obtained by Borzyszkowska-Bukowska et al. [120] indicated reduced mobility of the side chain due to the presence of an additional -CH_3 group at C40 of the Candicidin D molecule. The CH_3 group likely acts as a steric hindrance, inducing an extended "tail" conformation ($\theta \approx 180^\circ$) in the lipid bilayer. Additionally, hydrophobic interactions contribute to the stabilization of this conformation. The lack of methyl group at carbon C40 of Vacidin significantly increases the mobility of its side chain. For Gedamycin, it can be seen that the additional methyl group in the aromatic part of the side chain is more hydrophobic than for Vacidin and Candicidin D, suggesting its possible better stabilization in the membrane. In general, the side chain of AHMs enhances the lipophilicity of the molecules (compared to the non-aromatic heptaene macrolides). Such property significantly augments the ability of the side chain to locate near the second lipid layer and interact with membrane components. It probably serves as a molecular "anchor" in the lipid bilayer for the polyene macrolide. The role of the aromatic side chain is believed to facilitate more efficient penetration of the antibiotic molecule into the membrane through hydrophobic interactions, faster formation of channel structure, and improved stabilization. This may contribute to noticeably higher antifungal activity observed *in vitro* studies [90].

1.5. Light-induced isomerization of AHMs

To perform the photochemical reaction, a crucial parameter is the proper light source, as its emission spectrum should be very close to the desired absorption spectrum. Mercury Lamps, fluorescent tubes, halogen lamps, and light-emitting diodes are essential light "suppliers" in organic photochemistry. The latter have been developed recently. Light-emitting diodes can provide UV light with stable intensities (below 500 mW per unit) down to 360 nm or 250 nm (for shorter wavelengths with an intensity below 10 mW) and narrower spectral bands. Moreover, they have a longer lifetime and almost entirely no heating time [151]. Of course, sunlight can also

be used as a light source; however, the full light spectrum may affect the compound, leading to its degradation.

One of the results of photochemical transformation is isomerization. This phenomenon is widely observed in nature, for example, in compounds from the carotenoid group (e.g., β -carotene) [152] and polyphenols (e.g., resveratrol) [153]. The light-induced reaction entails a configurational change around a bond with restricted rotation. It mainly involves double bonds, altering their geometry mostly from *trans* to *cis* isomers [154]. In the case of alkenes, an excited electron moves from the highest to the lowest energy level, causing the double bond's disruption. This allows the remaining sigma bond to rotate freely and the subsequent re-pairing can change the geometry of the "native" alkene, providing both isomers. If the light exposure is sustained for an adequate period, a photostationary state⁷ is achieved [151]. The ratio of obtained isoforms depends on the substrate's ability to absorb light at a specific wavelength, as well as on the probability of the excited state favoring the formation of one isomer over the other [151]. Additionally, the effectiveness of photoconversion is limited by the narrow-band absorption spectrum of "photoswitches" as most of them undergo conversion while exposed to the UV or UV-Vis light [155][156].

1.5.1.Light-induced isomerization of AHM

Our research team initially discovered that the obtained pure complex of Candidicin is unstable in solution under daylight conditions [118]. During the structural identification of this complex [33] with the use of liquid chromatography-mass spectrometry (LC-MS), additional structures with molecular weights identical to the native AHMs but differing in UV-Vis spectra were observed (Figure 20). The obtained spectra suggested a probable change in the chromophore's geometry to an Amphotericin-like *all-trans* form, based on the shape and range of the spectra corresponding to this antibiotic. These unknown compounds were isolated and structural studies were conducted using two-dimensional NMR (2D NMR) methods. It was then confirmed that these additional structures corresponded to *all-trans* isomers of the antibiotics in the Candidicin complex.

It was demonstrated that photoisomerization of the Candidicin chromophore occurred at positions 26Z and 28Z. Still, it was uncertain whether a similar *cis-trans* bond position change at 28Z, 30Z (as in the components of the Aureofacin complex) would also undergo this reaction [149]. It is important to note that isolating 100% pure *all-trans* forms is highly challenging due to the complex nature of AHMs and the doubled amount of components resulting from photoisomerization reactions (see example, Figure 20).

⁷ equilibrium under constant light exposure

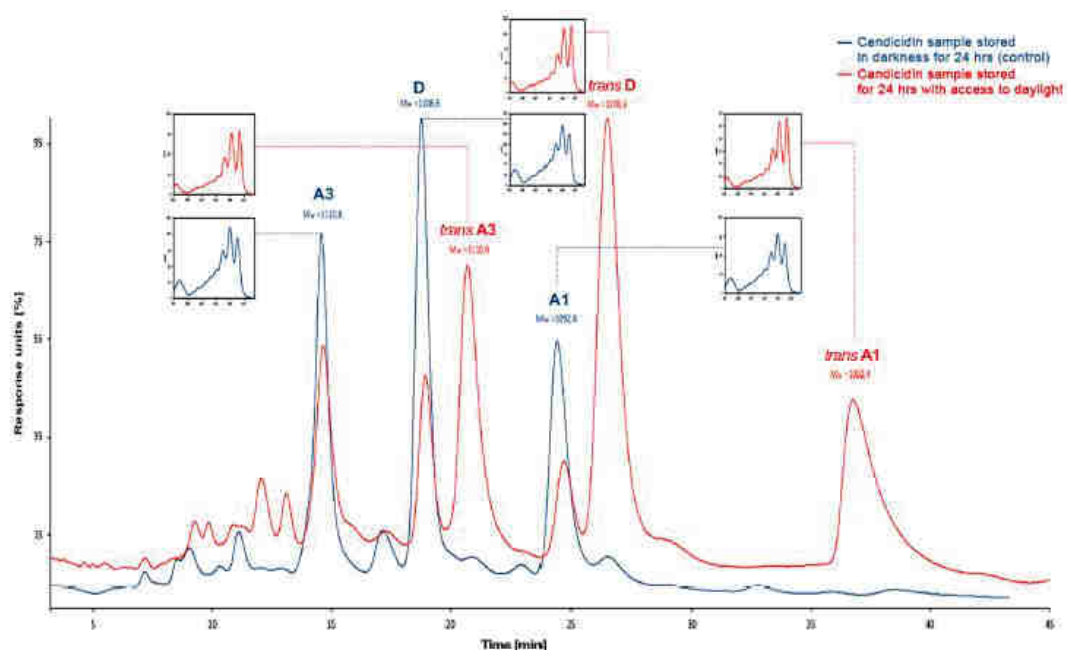


Figure 20. Chromatogram HPLC-DAD of Candicidin complex as an example of the light-induced isomerization influence on the amounts of the components in the complex before (*cis-trans* chromophore, blue line) and after photoisomerization (*all-trans* chromophore, red line) [33]

This complexity likely contributed to the discrepancies observed in the amounts of Candicidin or Levorin components, which were previously isolated using glass, transparent Craig apparatus in the last century. Consequently, conducting biological studies is difficult and additionally, requires working with limited light exposure for unstable *cis-trans* forms of antibiotics. On the contrary, it has been demonstrated that the *all-trans* Candicidin complex is stable [33][145]. The macrolide ring of these photoisomers is “longer”, more straight, and likely has a less mobile polyol fragment. Additionally, exposure to sunlight and wavelengths around 254 nm resulted in a huge amount of degradation products and reduced process efficiency. Subsequently, when the experimental wavelength for light-induced isomerization was determined to be 365 nm, significantly fewer degradation products were observed. The scheme of the reaction occurring with Candicidin D is shown in Figure 21 [33]. Figure 21 shows the geometrical change of Candicidin D chromophore from the native structure (*cis-trans*) to its *all-trans* isomer through photoisomerization.

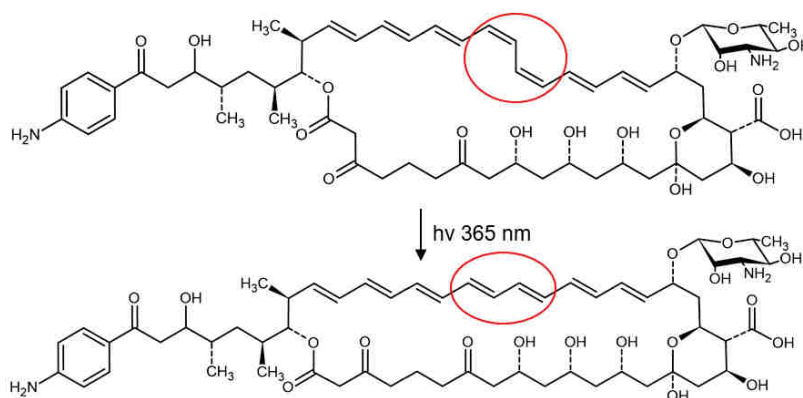


Figure 21. Scheme of the photochemical isomerization of Candicidin D. The geometrical changes were marked in red circles [33]

2. RESEARCH OBJECTIVE AND DESCRIPTION OF THE RESEARCH PROBLEM

In 2018, our research team observed that Candicidin D, a representative of the AHMs group, underwent a photochemical isomerization reaction, resulting in a change in the antibiotics' chromophore geometry from the native *cis-trans* structure to an *all-trans* [33]. This alteration elongates the polyene part, making the entire macrolactone ring more rigid/less labile, and as a result, AHMs become somewhat "similar" to AmB (*all-trans* form).

As presented in section 1.3., the mechanism of action of heptaene macrolides mainly relies on their affinity for binding to sterols in the membrane, with a higher affinity for ergosterol (in fungal cells) than for cholesterol (in human cells). However, this affinity does not provide sufficient selective toxicity of these compounds. The only antibiotic that is distinct within HMs is AmB, whose selective toxicity is relatively acceptable. It is used as a drug of the last choice. According to promising literature data [25], AHMs exhibit greater antifungal activity than AmB. Nevertheless, studies on human red blood cells have revealed that Vacidin and Gedamycin - both components of the Aureofacin complex - are more toxic than AmB, while Candicidin D, the main antibiotic of the Candicidin complex, is slightly less toxic. Therefore, considering that, the pore-forming model suggests that macrolide heptaenes interact with sterols through their polyene region, the following questions arise:

- Would modifying AHMs to resemble AmB (by straightening the chromophore) affect the toxicity of these compounds to humans?
- Would the *all-trans* chromophore geometry improve the interaction with ergosterol, and enhance the antifungal activity?
- Would straightening the chromophore enhance its interaction with ergosterol over cholesterol while also reducing the toxicity of aromatic heptaene macrolides to human cells?

In reference to these questions, my doctoral studies aimed to verify if altering **the chromophore geometry from *cis-trans* to *all-trans* would decrease the membrane damaging effect of AHMs on mammalian cells, while maintaining or improving their antifungal activity**. Therefore, my doctoral dissertation was divided into three parts;

a) isolation of the aromatic analogues of Amphotericin B (AHMs);

- purifying of the specified AHM complexes - Aureofacin and Candicidin, produced in the Department of Pharmaceutical Technology and Biochemistry,
- designing and optimizing the isolation process of the native (*cis-trans*) AHMs (Candicidin D, Gedamycin, Vacidin) from their complexes with the use of preparative chromatography techniques such as Centrifugal Partition Chromatography (CPC) and High-Performance Liquid Chromatography (prep-HPLC),
- obtaining a sufficient quantity of *cis-trans* antibiotics at a high purity level from their complexes,
- conducting the photoisomerization process to obtain *all-trans* isomers of AHMs,
- obtaining the appropriate quantity of *all-trans* antibiotics at a high purity level,

- identifying and determining the purity of isolated components with the usage of UV-Vis spectrophotometry and LC-MS technique,
- b) determination of their biological properties;
- determining the antifungal activity of *all-trans* AHMs in comparison to *cis-trans* AHMs and AmB, using the minimal inhibitory concentration (MIC) assay against fungal species from the genus *Candida* (*Candida albicans*, *Candida glabrata*, *Candida krusei*, *Candida parapsilosis*, *Candida dubliniensis*, *Candida guilliermondii*, *Candida rugosa*, *Candida famata*) and *Saccharomyces cerevisiae* in RPMI 1640 and BDS media,
 - determining the hemolytic effect of *all-trans* AHMs and its comparison to *cis-trans* AHMs and AmB on human red blood cells (RBCs),
 - determining the cytotoxic effect of *all-trans* AHMs and its comparison to *cis-trans* AHMs and AmB on human cell lines (MRC-5, HaCaT, HEK 293, HeLa, HEP G2, A549), using MTT and WST-1 assays conducted partially in collaboration with the University of Geneva,
- c) investigation of their molecular organization in the membrane;
- tracking the behavior of AHMs in a biological membrane model – giant unilamellar vesicles (GUVs) with and without the sterol content (cholesterol or ergosterol) – using fluorescence lifetime imaging microscopy (FLIM). This part of the research was conducted in collaboration with the research group at Maria Curie-Skłodowska University in Lublin.

3. MATERIALS AND METHODS

3.1. Materials

3.1.1. Heptaene macrolide preparations

Table 7. Properties of crude heptaene macrolide preparations used in the studies.

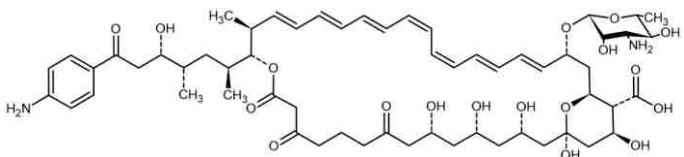
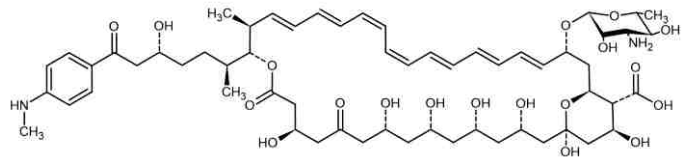
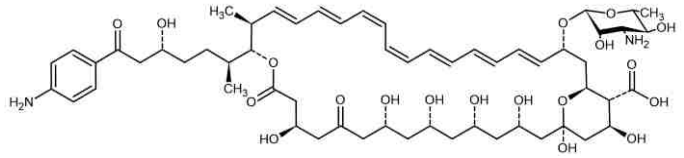
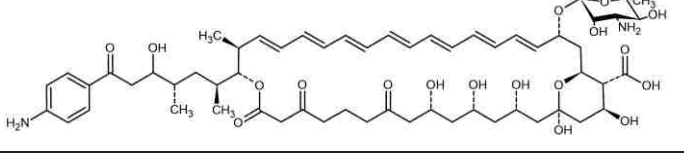
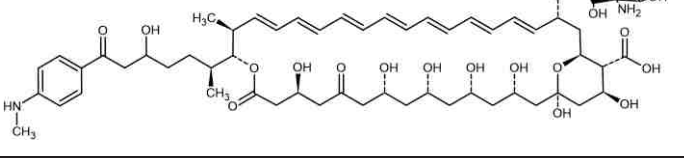
Complex	Description	Purity (%)*
Aureofacin	Complex of Gedamycin and Vacidin produced by <i>Streptomyces aureofaciens</i> . Isolated as a crude preparation at the Department of Pharmaceutical Technology & Biochemistry many decades ago and stored at -18 °C.	23
Candidicin	Complex of Candidicin A1, Candidicin A2, and Candidicin A3 produced by <i>Streptomyces griseus</i> IMRU 3570. Isolated as a crude preparation at the Department of Pharmaceutical Technology & Biochemistry many decades ago and stored at -18 °C.	21

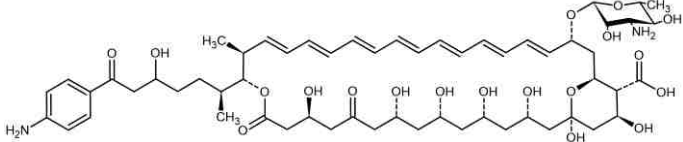
* Content of polyene macrolide compounds in crude preparation.

Determined as $E^{1cm,1\%}_{\text{sample}} / E^{1cm,1\%}_{\text{reference}} \times 100\%$ measured at 378 nm for 0.01 mg/mL solution in DMSO/MeOH 1:99 v/v mixture (3.2.1)

3.1.2. Isolated heptaene macrolides

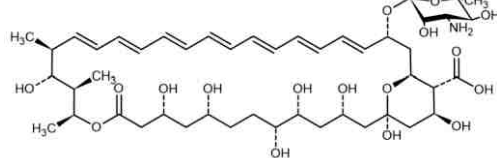
Table 8. Structures and purities of isolated heptaene macrolide antibiotics used in the studies.

Compound	Stereostructure	Purity* (%)
<i>cis-trans</i> Candidicin D		85
<i>cis-trans</i> Gedamycin		86
<i>cis-trans</i> Vacidin		88
<i>all-trans</i> Candidicin D		82
<i>all-trans</i> Gedamycin		88

Compound	Stereostructure	Purity* (%)
<i>all-trans</i> Vacidin		88

*Based on the results of HPLC-DAD-ESIMS analysis

Table 9. Structure and purity of reference heptaene macrolide used in the studies.

Compound	Structure	Manufacturer/Purity
Amphotericin B		Sigma-Aldrich/ ≥ 80%

3.1.3.Reagents and buffer preparations

Table 10. Reagents.

Reagent	Manufacturer	Purity [%]
1mM Ethylenediaminetetraacetic acid (EDTA)	Sigma Aldrich	≥ 99.9%
3-(4,5-dimethylthiazol-2-yl)-2,5-diphenyl-2H-tetrazolium bromide (MTT)	Sigma-Aldrich	≥ 97.0%
3-(N-Morpholino) propanesulfonic acid (MOPS)	Sigma-Aldrich	Not applicable
4-[3-(4-Iodophenyl)-2-(4-nitrophenyl)-2H-5-tetrazolio]-1,3-benzene disulfonate (Water Soluble Tetrazolium 1, WST-1)	Sigma-Aldrich	Not applicable
7-aminoactinomycin D	Thermo Fisher	≥ 97.0%
Acetic acid	POCH	≥ 98.5%
Acetone	POCH	≥ 99.9%
Acetonitrile	POCH	≥ 99.9%
Acetonitrile	Sigma-Aldrich LC-MS Grade	≥ 99.9%
Ammonium acetate (powder)	Sigma-Aldrich	≥ 99.9%
Bactopecton (powder)	OXOID	Not applicable
Boric acid (powder)	Sigma-Aldrich	≥ 99.9%
1-Butanol	POCH	≥ 99.9%
Chloroform	POCH	≥ 98.5%
Dichloromethane	POCH	≥ 99.5%
Diethyl ether	POCH	≥ 99.5%
Dimethylsulfoxide	POCH	≥ 99.7%
EDTA disodium salt dihydrate	Sigma-Aldrich	≥ 99.0%
Ethyl acetate	POCH	≥ 99.8%
Glucose	Sigma-Aldrich	≥99.5%
Hexane	Sigma-Aldrich	≥ 99%
Methanol	POCH	≥ 99.8%
Phosphate buffered saline (solution)	Sigma-Aldrich	Not applicable
Potassium chloride	Sigma-Aldrich	≥99.0%
Propidium iodide	Sigma-Aldrich	≥94.0%
RPML-1640 medium (powder)	Sigma Aldrich	Not applicable
Sabouraud agar medium (powder)	Graso Biotech	Not applicable

Reagent	Manufacturer	Purity [%]
Sodium bicarbonate	Sigma-Aldrich	≥99.7%
Sodium chloride	Sigma-Aldrich	≥99%
Sodium hydroxide	Sigma-Aldrich	≥97.0%
Triton X-100	BioChemika	Not applicable
Trypsin	Sigma-Aldrich	Not applicable
Ultrapure water	In house	≥ 99.9%
Fetal bovine serum	Sigma-Aldrich	Not applicable
L-glutamine	Corning	≥ 99.0%
Penicillin	Sigma-Aldrich	Not applicable
Streptomycin	Sigma-Aldrich	Not applicable

Table 11. Buffer and salt solutions.

Solution	Preparation description
5.5 mM Ammonium acetate buffer, pH = 4.5	0.424 g of ammonium acetate dissolved in 1000mL of ultrapure water and adjusted with acetate acid to pH=4.5
Borate buffer pH=8.2 or pH=8.6	3.09 g of KCl and 3.73 g of boric acid dissolved in 500 mL of ultrapure water. pH adjusted with 0.1M NaOH to pH=8.2 or 8.6 and filled up to 1000 mL.
0.5% EDTA pH=5.1/8.6	5.54 g of EDTA disodium salt dihydrate dissolved in 994.5 g of ultrapure water and adjusted with 40% NaOH to pH 5.1/8.6
0.9% NaCl	4.5g of NaCl dissolved in 500 mL of ultrapure water
0.1M Sodium bicarbonate	3.36g of sodium bicarbonate dissolved in 400 mL of ultrapure water
0.1M NaOH	0.8g of NaOH dissolved in 200mL of ultrapure water
40% NaOH	66g of NaOH dissolved in 100 mL of ultrapure water

3.1.4.Culture media

Table 12. Solid medium for yeast cultivation.

Medium	Preparation description
Sabouraud agar medium	6.5 g of Sabouraud agar dissolved in 100 mL of ultrapure water and autoclaved.

Table 13. Liquid media for yeast cultivation.

Medium	Preparation description
RPMI 1640 ⁸	5.2 g of RPMI 1640 solid medium, 9 g glucose, and 17.5 g MOPS dissolved in 500 ml of pure water and adjusted with NaOH to pH=7.0. The solution was filtered through 0.45 µm PES filter under sterile conditions.
BDS ⁹	5 g of Bactopepton, 10 g of glucose, and 2.5 g of sodium chloride dissolved in 500ml of pure water.

Table 14. Media used for cultivation of mammalian cells.

Medium	Manufacturer	Comment
RPMI 1640	Corning	Additionally supplemented with 10% of fetal bovine serum (final concentration 10%),
DMEM	Corning	
F-12	Corning	

⁸RPMI 1640 was used also with modification; without MOPS or with pH=5.2, pH=5.6

⁹ BDS was used also with modifications; 5g of NaCl (1%) or 1.25g NaCl (0.25%), pH=7.0

Medium	Manufacturer	Comment
MEM	Corning	L-glutamine (final concentration 2 mM), penicillin (62.6 µg/mL), and streptomycin (40 µg/mL)
EMEM	Corning	

3.1.5. Human cell lines

Table 15. Human cell lines used in the studies.

Cell line	Source	Meaning	Cell culture medium	Conditions of cell culture
MRC-5	ATCC	human normal lung fibroblasts cell line	EMEM	5% CO ₂ , 37°C
HEK293		human embryonic kidney cell line (immortalized)	DMEM	10% CO ₂ , 37°C
Hep G2		human liver cancer cell line	MEM	5% CO ₂ , 37°C
HaCaT		human keratinocytes cell line (immortalized)	RPMI 1640	5% CO ₂ , 37°C
A549		human non-small cell lung cancer cell line	RPMI 1640/F-12	5% CO ₂ , 37°C
HeLa		human cervical cancer cell line	MEM	5% CO ₂ , 37°C

3.1.6. Microorganisms

Table 16. Yeast strains.

Yeast strain
<i>Candida albicans</i> ATCC 10231
<i>Candida albicans</i> ATCC SC 5314
<i>Candida glabrata</i> DSM 11226
<i>Candida krusei</i> DSM 6128
<i>Candida parapsilosis</i> DSM 5784
<i>Candida dubliniensis</i> CBS 7987
<i>Candida guilliermondii</i> DSM 11947
<i>Candida famata</i> DSM 3428
<i>Candida rugosa</i> DSM 2031
<i>Saccharomyces cerevisiae</i> ATCC 9763

3.1.7. Laboratory equipment

Table 17. Equipment used in doctoral research

Equipment	Producent
ACCQPREP HP125 UV-VIS	Teledyne ISCO
Analytical balance AS 310.R2	Radwag
ASYS UVM 340 microplate spectrophotometer	Biochrom
Autoclave	Classic Prestige Medical
Binder C8 160	Avantor
Centrifuge 5424 R	Eppendorf

Equipment	Producent
Centrifuge 5819 R	Eppendorf
Centrifuge FRONTIER ^{TM5714}	OHAUS
Confocal Laser Scanning Microscopy LSM 800 with Airyscan Detector	ZEISS
CPC-250-DAD (Gilson)	Gilson
GENESYS 20 spectrophotometer	Thermo Scientific
HPLC-DAD system	Shimadzu
HPLC-MS Triple Quad LC/MS (Agilent) ¹⁰	Agilent
Incubator	INFORS HT Ecotron
Magnetic stirrer	LME-1
MicroTime MT200	Picoquant
Milli-Q IQ 7003/7005/7010/7015 Ultrapure and Pure Lab Water Purification System	Merck
Miniorbital shaker SSM1	Stuart
NovoCyte, NovoSampler Pro	Agilent
pH-meter	Mettler Toledo
Primovert Microscope	Zeiss
Rotary evaporator	Heidolph
Scanning multiwell spectrophotometer (ELISA reader)	BioTek
SPECORD 200 PLUS Double-beam	Analytic Jena
Ultrasonic bath RK 510	Bandelin electronic GmbH & Co.KG
Vacuum desiccator	ROHS
Victor ³ V 1420 Multilabel Counter	Perkin Elmer
Vortex TTS 2	Yellow ^{line}
Z2 Coulter Particle Count and Size Analyzer	Beckman Coulter

3.1.8. Softwares

Table 18. Software

Software
SymPhoTime 64 v. 2.3 software (Picoquant)
FlowJo TM Software

3.2. Methods

3.2.1. Determination of purity of antibiotic complexes

The purity of the antibiotic complexes, i.e. content of heptaene macrolide compounds in the crude preparations, was determined by a spectroscopic method, as the $E^{1\%}_{1\text{cm}}$ parameter of sample solutions, measured at 378 nm, in relation to $E^{1\%}_{1\text{cm}}$ of the reference of standard. Samples of a crude complex were dissolved in DMSO at 1 mg/mL and next diluted with MeOH to the final concentration of 0.01 mg/mL. The mixture of DMSO and MeOH at 1:99 v/v was used as the negative (0%) control, while the 0.01 mg/mL solution of antibiotic was used as the positive (100%) control. Determinations were performed in triplicates. Conditions for the determination of purity following [40] are shown in Table 19.

¹⁰ The equipment was purchased thanks to the generosity of the Foster Foundation and Prof. Ryszard Andruszkiewicz

Table 19. Conditions for determination of purity.

Equipment	Settings of the instrument method	
	Fixed parameter	Values
Spectrophotometer UV-Vis (Analytik Jena, SPECORD 200 PLUS Double-beam)	Range wavelength [nm]	250 – 450
	Temperature [°C]	25
	Speed [nm/s]	10
	Collected point [nm]	0.2

3.2.2. Preliminary isolation of heptaene macrolide complexes from crude preparations

Sample of the crude preparation (10g) was dissolved in 30 mL of DMSO. After 30 minutes, a mixture of BuOH, MeOH, and ultrapure water (10:1:2, v/v/v, final volume of 1L) was added. The air was removed from the solution using argon, and the mixture was stirred for 1 hour at room temperature. The insoluble precipitate (sludge-waste) was removed by filtration through the filter paper in a Buchner funnel under vacuum conditions. The filtrate was transferred to a separatory funnel, followed by the addition of 1L of 0.5% EDTA solution (pH 5.1). Argon was used to remove the air from the separatory funnel. The mixture was then thoroughly shaken and stored in a light-protected environment.

After 30 minutes, when phase equilibrium was achieved, the lower aqueous layer was discarded. The upper organic layer remaining in the separatory funnel was extracted with 1 L of 0.5% EDTA (pH=8.6). After phase equilibrium was established, the lower layer was discarded. The organic layer was subjected to liquid-liquid extraction with ultrapure water (1L) without air access. The final solution was stored in a separatory funnel overnight in the dark to allow it to reach the state of equilibrium. The scheme of this procedure is shown in Figure 22.

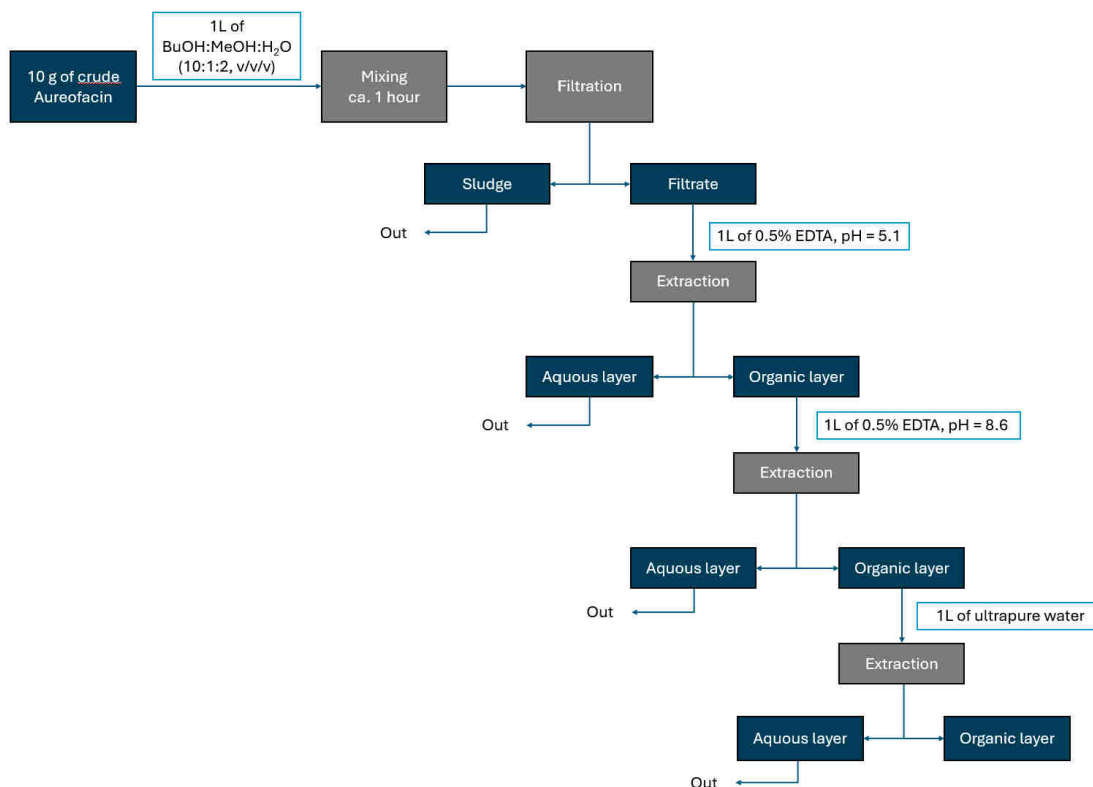


Figure 22. Scheme of part 1 of Aureofacin complex preliminary purification

After the equilibrium was reached, the aqueous phase was discarded. The organic layer was then subjected to evaporation under controlled conditions (temperature = 36°C, 100 rpm/min, 25 mbar) until the volume was reduced to approximately 15 mL, resulting in a concentrated antibiotic suspension in butanol. Water was added during the evaporation to facilitate butanol removal at 36°C in the form of the butanol-water azeotrope. Partial precipitation of the antibiotics from the solution was observed and the suspension was next placed on ice to facilitate complete precipitation. The fully precipitated antibiotic mixture was subsequently washed with 25 mL of acetone, followed by two additional washes with 25 mL of diethyl ether. The precipitate was then dried by purging with nitrogen (or argon) gas and transferred to a vacuum desiccator for 24 hours to remove any remaining solvent. A schematic representation of this second part of the purification process is shown in Figure 23.

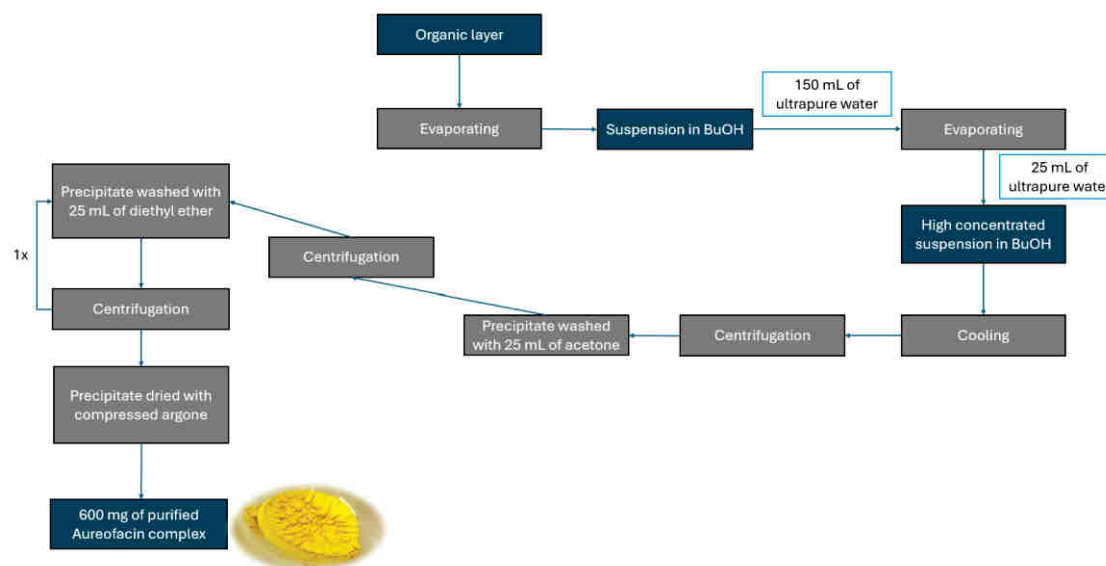


Figure 23. Scheme of part 2 of Aureofacin complex preliminary purification – part 2, presented figure shows purified complex; the gray field is assigned to the analysis performance, the blue field is assigned to the material, 1x – one time

3.2.3. Biphasic solvent system selection (shake-flask test) for the CPC purification process

Based on the literature data the solvent systems were selected. These solvent systems and their volume ratio are presented in Table 20.

Table 20. The volume ratio of the tested solvent systems.

Solvent number	Solvent system	Volume ratio
1	CHCl ₃ : MeOH : borate buffer (pH=8.2)	4 : 4 : 3
2	CHCl ₃ : MeOH : borate buffer (pH=8.6)	4 : 4 : 3
3	CHCl ₃ : MeOH : ammonium acetate buffer (pH=4.5)	4 : 4 : 3
4	CHCl ₃ : MeOH : H ₂ O	4 : 4 : 3
5	CH ₂ Cl ₂ : MeOH : H ₂ O	5 : 4 : 2
6	AcOEt : BuOH : EtOH : H ₂ O	15 : 5 : 3 : 25
7	Hexane : AcOEt : MeOH : H ₂ O	6 : 5 : 6 : 5

For the experiment, the Aureofacin complex was used to represent the AHMs group. The first selective step to find the proper solvent system within the mentioned in Table 20, involved

using the UV-Vis spectrophotometry method (Analyticjena, SPECORD 200 PLUS Double-beam). The indicated solvent systems (Table 20) were prepared in small separatory funnels (no. 1) and allowed to reach equilibrium. Once equilibrium was achieved, 6 mL of the lower and upper phases were transferred to a separate separatory funnel (no. 2). Additionally, 1 mg of Aureofacin was dissolved in a mixture containing 1 mL of each phase in a small flask (no. 3). This solution was mixed thoroughly and transferred to the separatory funnel (no. 2), which contained equal volumes of both phases. The mixture was shaken and left undisturbed for a few minutes to allow the phases to reach equilibrium. Afterward, 1 mL of each phase (heavier and lighter) was filtered through a 0.22 μ m Nylon membrane into a cuvette for spectrophotometric analysis. The pure phases (heavier or lighter) were used as reference samples in the UV-Vis method for accurate measurements.

Next, K_D of the Aureofacin complex was initially determined based on the UV-Vis spectrum at wavelength $\lambda=378$ nm. The results were calculated based on the absorbance parameter and equation 1.4.3.1. Further, two solvent systems, the most promising, CHCl_3 : MeOH: borate buffer (pH=8.2), CHCl_3 : MeOH: ammonium acetate buffer (pH=4.5) were verified on the HPLC-DAD system (Shimadzu). Samples of the Aureofacin complex dissolved in a specified solvent system were prepared according to the above procedure, but in the final stage, 1 mL of each phase (upper and lower) was filtered through 0.22 μ m Nylon filter into the HPLC vials and analyzed according to the method described in section 3.2.5. For the HPLC method, the K_D values of the individual antibiotics were calculated by dividing the area under the peaks assigned to Vacidin or Gedamycin in the stationary phase by their area in the mobile phase (equation 1.4.3.1). Additionally, the coefficient α (separation factor) was determined according to equation 3.2.3.1 to quantitatively represent the separation of the antibiotics in the liquid system:

$$\alpha = \frac{K_D(\text{Gedamycin})}{K_D(\text{Vacidin})} \text{ (equation 3.2.3.1)}$$

Where,

K_D (Gedamycin) – K_D value obtained for Gedamycin calculated according to equation 1.4.3.1

K_D (Vacidin) – K_D value obtained for Vacidin calculated according to equation 1.4.3.1

3.2.4. Isolation of the antibiotics by CPC-DAD technique

The selected solvent system from section 3.2.3., CHCl_3 : MeOH: borate buffer (4: 4: 3, v/ v/ v, pH=8.2) was prepared in separatory funnels. The preparation of the borate buffer was based on Clark and Lubs' receipt [157]. After the achievement of the equilibrium state, two phases (lighter and heavier) were separated into the bottles. One of them served as a stationary phase (with a higher density) and the second as a mobile phase (with a lower density).

After the selection of a suitable solvent system, the next step concerned the analysis parameters settings such as rotor speed, volumetric flow [ω], mode of action (ASC/ DSC/ Dual Mode), sample concentration [c], and injection volume [v_i]. The parameters of the separation method were set at the beginning (according to Tables 21, 22) and after applying the eluents to proper channels, the analysis was run using a Gilson apparatus CPC-250.

Table 21. Equipment - settings of the instrument method.

Equipment	Settings of the instrument method	
	Fixed parameter	Values
Centrifugal Partition Chromatography system (Gilson CPC-250)	Column	Rotor 250 ml
	Range wavelength [nm]	Ch1= 220-500 nm, Ch2= 378 nm, Ch3= 407 nm, Ch4= 254 nm
	Injection volume [mL]	10
	Mode	ASC
	Type of elution	isocratic
	Temperature [°C]	Not monitored, room temperature
	Solvent system: CHCl ₃ : MeOH: borate buffer (pH=8.2), 4:4:3, v/v/v	

Table 22. Elution program.

Stage of the analysis	Settings
Initiation	ω = 30 mL/min, μ = 500 rpm/min, t=12 min, 100% stationary phase
Column equilibrium	ω = 5 mL/min, μ = 800 rpm/min,, t=16 min, 100% mobile phase
Elution	ω = 5 mL/min, μ = 800 rpm/min, t=100 min, 100% mobile phase
Extrusion	ω = 30 mL/min, μ = 500 rpm/min, t=12 min, 100% stationary phase

In the meantime, the purified complex was prepared for the isolation process. 80 mg of the antibiotic was dissolved in 1 mL of DMSO. Then, the stationary and mobile phases of the solvent system were added to the sample in a ratio 2: 8 (v/v), respectively to obtain a final volume of 10 mL. The solution was mixed and filtered through a 0.45 μ m Nylon filter. After achieving the column equilibrium stage, the prepared sample was injected (10mL) into the CPC column. Based on the obtained chromatogram, the fractions (14 mL each) of the specific antibiotic were collected.

In the next step, the obtained solution was concentrated in a vacuum rotary evaporator (36°C, 150 rpm/min, 25 mbar). After removing chloroform and partially methanol from the mixture, 100 mL of butanol was added. The mixture was evaporated again to remove the methanol. Subsequently, 3 extractions with 80 mL of ultrapure water were performed. Then, it was evaporated again until a highly concentrated suspension of the isolated antibiotic in butanol was obtained. Further, the suspension was chilled on ice for 5 min and centrifuged (5 min, 2300 rpm/min). Butanol was separated from the precipitate and removed. The precipitate was washed with diethyl ether and centrifuged (5 min, 2300 rpm/min) twice. The antibiotic was dried with nitrogen and put in the desiccator under reduced pressure for 24 hours.

3.2.5. Initial determination of purity by HPLC-DAD technique (analytical scale)

The implementation of the HPLC-DAD method on an analytical scale was used for qualitative analysis after each stage of the preparative techniques and for determining the degree of the antibiotic's photoisomerization. The reference sample (purified complexes) and tested samples of isolated antibiotics after CPC and prep-HPLC were diluted to the concentration of 2 mg/mL in the solution of DMSO and MeOH in a volume ratio of 1:3 v/v, then filtered through 0.22 μ m Nylon filter directly into inserts placed in the HPLC vials. The analysis parameters were selected by me and our research team. Moreover, the flow rate of the mobile phase was also

optimized as 1 mL/min and the temperature as 25 °C. The parameters of the analysis were set according to Table 23.

Table 23. Equipment- settings of the instrument method.

Equipment	Settings of the instrument method	
	Fixed parameter	Values
HPLC-DAD system (Shimadzu)	Range wavelength [nm]	200 - 600
	Column	Luna 100Å C18 (150 mm × 4.6 mm, 5 µm)
	Flow [mL/min]	1
	Injection volume [µL]	20
	Temperature [°C]	25
	Elution	Isocratic
	Mobile phase: 38% ACN, 62% ammonium acetate (5.5 mM, pH=4.5), v/v	

3.2.6. Isolation of the antibiotics using Preparative HPLC

Based on the fixed parameters of HPLC analysis on the analytical scale (section 3.2.5.), the parameters were recalculated for the semipreparative scale and implemented in the next isolation method – preparative HPLC. This method was mainly used to isolate the *cis-trans* Candicidin D after the CPC isolation process (section 3.2.4.) and *all-trans* AHM after photoisomerization (section 3.2.7.). The isolated antibiotics were diluted to a concentration of approximately 4 mg/mL in a solution of DMSO, MeOH, and ammonium acetate (5.5 mmol, pH=4.5) (1:4:5; v/v/v). Then, such prepared samples were filtered through a 0.22 µm Nylon filter and injected (2.5 mL) into the column. The parameters of the analysis are presented in Table 24.

Table 24. Equipment- settings of the instrument method.

Equipment	Settings of the instrument method	
	Fixed parameter	Values
Preparative High-Performance Liquid Chromatography System (Teledyne ISCO apparatus ACCQPREP HP125 UV-VIS)	Column	LiChrospher 100 RP-18e (250 x 25 mm, 10 µm)
	Range wavelength [nm]	220-600
	Flow [mL/min]	29.5
	Injection volume [mL]	2.5
	Temperature [°C]	Not monitored, room temperature
	Elution	Isocratic
	Mobile phase: 38% ACN, 62% ammonium acetate (5.5 mmol, pH=4.5), v/v	

This procedure was repeated 8-12 times for each antibiotic to obtain its appropriate amount for further analysis. The column had to be flushed with two column volumes of 95% methanol in ultrapure water (v/v) after each isolation process. Collected fractions were concentrated in a vacuum rotary evaporator (36°C, 150 rpm/min, 25 mbar). After removing acetonitrile, the pH of the solution was adjusted to 6.5 with NaHCO₃, and 100 mL of butanol was added. The mixture was evaporated again to remove the residues of acetonitrile. Subsequently, 3 extractions with 80 mL of ultrapure water were performed. Then, it was evaporated again until a highly concentrated suspension of the isolated antibiotic in BuOH was obtained. Further, the suspension was chilled on ice for 5 min and centrifuged (5 min, 2300 rpm/min). Butanol was separated from the precipitate and removed. The precipitate was washed with diethyl ether and

centrifuged (5 min, 2300 rpm/min) twice. The antibiotic was dried with nitrogen and put in the desiccator under reduced pressure for 24 hours.

3.2.7. Photoisomerization of aromatic heptaene macrolides

To perform the light-induced isomerization, the isolated antibiotics (ca. 80 mg) were dissolved in 1 mL of DMSO. The obtained solution was slowly added to 1 L of 95% methanol in ultrapure water (v/v) with continuous stirring. The solution was stirred for approximately 5 min and then transferred to a vessel with a large bottom surface area (diameter = 20 cm). Subsequently, it was subjected to UV irradiation at a maximum wavelength of 365 nm. Argon was let above the surface of the liquid. Then, under such prepared conditions, the antibiotic solution was stirred slowly using a magnetic stirrer for approximately 4 hours. The progress of the photoisomerization reaction was monitored using the HPLC-DAD method described in section 3.2.5. The scheme of photoisomerization based on Candicidin D is presented in Figure 21.

Upon completion of the reaction, the solution was concentrated with the vacuum rotary evaporator (36°C, 200 rpm/min, 25 mbar) to the final volume of approximately 25 mL. The suspension of the antibiotic was cooled, and after adding 25 mL of acetone, the suspension was centrifuged (5 min, 2500 rpm/min). Next, the supernatant was removed and the solid product was flushed with 25 mL of diethyl ether once. Further, it was centrifuged again (5 min, 2500 rpm/min), and the supernatant was removed. The solid product was dried with argon and left in the vacuum desiccator for 24 hours.

3.2.8. Final identification and purity determination of the isolated antibiotics using LC-DAD-ESI-MS in positive ion mode

For LC-DAD-ESI-MS chromatographic process isolated *cis-trans* and *all-trans* AHMs were diluted to the concentration of 2 mg/mL in DMSO and MeOH (1:3, v/v), filtered through a 0.22 µm Nylon filter to HPLC vials, and analyzed in LC-DAD-ESI-MS system. The analysis parameters were selected by me and our research team. The parameters, and settings fixed in the instrument are presented in Table 25.

Table 25. Equipment - settings of the instrument method.

Equipment	Settings of the instrument method	
	Fixed parameter	Values
HPLC-MS Triple Quad LC/MS (Agilent)	Column	Luna 100 C18 (150 mm × 4.6 mm, 5 µm)
	Wavelength range [nm]	220-600
	Flow [mL/min]	1
	Injection volume [µL]	20
	Electrospray	Positive; gas temperature 300°C and flow 5 L/min, sheath gas heater 250°C and flow 11 L/min, nebulizer 45 psi, capillary voltage of 3500 V
	MS scanning range [m/z]	1000-1200
	Frag [V]	135

Equipment	Settings of the instrument method	
	Fixed parameter	Values
	Temperature [°C]	Not monitored, room temperature
	Mobile phase: 38% ACN, 62% ammonium acetate (5.5 mmol, pH=4.5), v/v	

3.2.9. Determination of antifungal *in vitro* activity

The minimal inhibitory concentration (MIC) values were determined to assess and compare the antifungal activity of isolated antibiotics. The assay was performed according to the Clinical and Laboratory Standards Institute (CLSI) standard methodology [158] with some modifications. The evaluation of the antifungal potential of all compounds was performed in two different liquid media: in RPMI 1640 medium and also in BDS medium prepared according to Cybulska et al. [25]. The yeast cells for inoculum preparation were cultivated (37°C, 24h) on Sabouraud agar medium. Inoculum suspensions were prepared by taking one loop of pure culture from an agar plate into sterile water, adjusting optical density to 0.1 at 660 nm wavelength, and further diluting 50-fold with RPMI 1640 medium or BDS medium, resulting in a cell density of approximately 2×10^4 CFU/mL.

Antibiotics were dissolved in DMSO to the stock solution concentration of 0.64 mg/mL (for RPMI 1640 medium) and 0.04 mg/mL (for BDS medium). Then, the serial two-fold dilutions of antibiotics in a specified medium were prepared in a 96-well plate. The last two columns were destined for positive and negative control samples. In the final step, the diluted fungal culture was added to a specified medium (in the volume ratio 1:1). The final concentration range of all antibiotics in the case of RPMI 1640 medium was 0.03 - 16 µg/mL and 0.0015 - 1 µg/mL for BDS medium. The microplates were incubated (37°C, 24h) under limited access to the light. The inhibition of fungal growth was determined by measuring the absorbance of cell density at wavelength $\lambda = 660$ nm using a microplate reader (Victor³V). The lowest concentration of the antibiotic with no visible yeast growth was taken as the MIC value.

3.2.10. Determination of hemolytic activity

The hemolysis test was performed on human red blood cells (RBCs), which were kindly provided by the Regional Center for Blood Donation and Blood Treatment in Gdansk. The hemolytic activity determination was carried out according to the procedure developed by Ślisz [159] with slight modifications. Firstly, antibiotics were diluted in DMSO to obtain the following concentrations: 50 µg/mL, 100 µg/mL, 125 µg/mL, 250 µg/mL, 500 µg/mL, and 1000 µg/mL. The *cis-trans* isomers were kept with limited access to light. During the work with human erythrocytes, it was necessary to keep reagents and samples on ice. Human red blood cells were suspended in a saline solution to achieve a cell density of 2×10^7 cells/mL. The experiment required the preparation of four control samples as follows;

- 0.9% NaCl solution – blank, negative control (0% lysis)
- RBCs suspension in 0.9% NaCl - control of saline influence on RBCs

- RBCs suspension in 0.1% Triton - positive control (100% lysis)
- RBCs suspension in 1% DMSO – control of DMSO influence on RBCs

Cis-trans antibiotics and AmB diluted in DMSO were added to the red blood cell suspension to obtain the final concentrations in the eppendorfs; 0.5 µg/mL, 1.0 µg/mL, 1.5 µg/mL, 2.5 µg/mL, 5.0 µg/mL, 10.0 µg/mL, and 20.0 µg/mL. For the *all-trans* antibiotics, the final concentrations obtained in the eppendorfs were; 2.0 µg/mL, 3.0 µg/mL, 5.0 µg/mL, 10.0 µg/mL, 15.0 µg/mL, 20.0 µg/mL, and 40.0 µg/mL. Subsequently, samples were gently vortexed and incubated in a heating block at 37°C for 30 min. Then, samples were centrifuged at low temperatures (1700 x g, 5 min, 4°C ± 1 °C) and the concentration of hemoglobin in the supernatant was determined by measuring the absorbance at wavelength $\lambda = 540$ nm in a plate reader (ASYS UVM 340). 100% of hemolysis was determined based on the standard curve prepared for serial dilution of Triton-X100. Each assay was repeated at least twice. Moreover, samples were prepared in three replicates.

The level of hemolysis in a suspension of 2×10^7 cells/mL in isotonic sodium chloride, treated with varying concentrations of antibiotics, was measured after a 30-minute incubation at 37°C. Following low-speed centrifugation, the hemoglobin concentration in the supernatant was used to evaluate the degree of hemolysis. The EH_{50} is the interpolated concentration of the compound, for which the A_{540} value is exactly 50% of the A_{540} value measured for the positive control sample (0.1% Triton X-100). The EH_{50} values for each compound were calculated according to the equation 3.2.10.1, presented below:

$$EH_{50} (\%) = \frac{A_{540}^{sample} - A_{540}^{DMSO}}{A_{540}^{0.1\% \text{ Triton X-100}} - A_{540}^{0.9\% \text{ NaCl}}} \times 100$$

(equation 3.2.10.1)

Where,

A_{540}^{sample} – the absorbance of hemoglobin contained in the supernatant after centrifugation of erythrocytes suspension treated with antibiotic measured at 540 nm

A_{540}^{DMSO} - the absorbance of hemoglobin contained in the supernatant after centrifugation of erythrocytes suspension treated with 1% DMSO measured at 540 nm

$A_{540}^{0.1\% \text{ Triton X-100}}$ - the absorbance of hemoglobin contained in the supernatant after centrifugation of erythrocytes suspension treated with 0.1% Triton X-100 measured at 540 nm, positive control

$A_{540}^{0.9\% \text{ NaCl}}$ - the absorbance of hemoglobin contained in the supernatant after centrifugation of non-treated erythrocytes suspension measured at 540 nm, negative control

3.2.11. Calculation of selective toxicity index (STI_{HEM})

The results obtained from MIC_{90} of *C.albicans* and hemolysis assay served to calculate selective toxicity index (STI_{HEM}) according to the equation:

$$STI_{HEM} = \frac{EH_{50}}{MIC_{90}} \text{ (equation 3.2.11.1)}$$

3.2.12. Determination of cytotoxic activity

The cytotoxicity assay was partially performed in cooperation with Prof Norbert Lange from the University of Geneva and partially at the Gdańsk University of Technology. The methods used at both universities differed slightly. The WST-1 compound was used at the University of Geneva and MTT assay at the Gdańsk University of Technology. The tested cell lines are presented in Table 15.

On the first day of the experiment, the cells were seeded into a 96-well plate at a volume of 100 μ L per well; MRC-5 cell line - 16000 cells/well, HEK293 cell line - 5000 cells/well, HEPG2 - 10000 cells/well, HaCaT cell line - 4000 cells/well, A549 cell line - 5000 cells/well, HeLa cell line - 20 000 cells/well. The penultimate column was left cell-free (and antibiotic-free) as a control for culture medium sterility. The last column was designated as a cell growth control, containing cells without the addition of antibiotics. These two controls were assigned as blank, consisting of medium with 1% DMSO (without cells) and negative control, consisting of cells treated with 1% DMSO. The plate was incubated for 24 hours at 37°C.

The next day, antibiotics were diluted in DMSO by serial dilution method to obtain stock concentrations ranging from 1.95 μ g/mL to 500 μ g/mL. These stock solutions were further diluted in culture medium to achieve final concentrations of 0.04 μ g/mL, 0.08 μ g/mL, 0.16 μ g/mL, 0.31 μ g/mL, 0.63 μ g/mL, 1.25 μ g/mL, 2.5 μ g/mL, 5 μ g/mL, and 10 μ g/mL (excluding the MRC-5 cell line). The subsequent analysis proceeded in two different ways depending on the specific method used (see below).

a) MTT assay

Antibiotics diluted in culture medium (1:1, v/v) were added to the 96-well plate containing the pre-seeded cells to achieve final concentrations in wells of 0.02 μ g/mL, 0.04 μ g/mL, 0.08 μ g/mL, 0.16 μ g/mL, 0.31 μ g/mL, 0.63 μ g/mL, 1.25 μ g/mL, 2.5 μ g/mL, and 5 μ g/mL. The prepared plate was incubated for 24 hours at 37°C. The DMSO concentration in each well was standardized to 1% for all cell lines except for MRC-5, where it was set to 0.5%. For the MRC-5 cell line, the test performed with the content of 1% DMSO caused the death of all the cells.

On the third day, 20 μ L of MTT (4 mg/mL) solution was added to each well, followed by incubation for 2 hours (3 hours for MRC-5 cell line) at 37 °C. Metabolically active cells reduced MTT to the colored product, formazan crystals. To assess cell viability, the culture medium was carefully aspirated, leaving formazan crystals intact, and the plate was air-dried. Subsequently, 100 μ L of DMSO was added to each well to solubilize the formazan, and the plate was agitated for 30 min to ensure complete dissolution. The amount of formazan formed, which correlates with the number of viable cells, resulted in a more intense coloration of the DMSO solution. Absorbance was then measured at 540 nm using a spectrophotometer (ASYS, UVM 340).

b) WST-1 assay

The culture medium was removed from a 96-well plate containing adherent cells, and the wells were washed twice with PBS (100 μ L). Subsequently, antibiotic solutions at

the previously prepared concentrations, diluted in culture medium, were added to each well in a volume of 100 μ L. For controls, 100 μ L of culture medium without antibiotics was added to the last two columns of the plate, designated for medium sterility and cell growth controls. The plate was then incubated for 24 hours at 37°C.

On the third day, 10 μ L of WST-1 solution was added to each well, and the plate was incubated for an additional 2 hours. WST-1 is cleaved by the metabolically active cells into a water-soluble formazan form. The intensity of the resulting color is proportional to the amount of formazan produced, which directly correlates with the number of viable cells and the corresponding increase in absorbance. After incubation, absorbance was measured using a scanning multiwell spectrophotometer (ELISA reader, Bio Tek) at a wavelength of 450 nm (formazan absorbance) with a reference wavelength of 690 nm.

c) Calculations

For the WST-1 assay, the sample absorbance at $\lambda=450$ nm was subtracted from $\lambda=690$ nm (giving Abs_{sample}). Besides, the calculation for both methods was the same according to the equation below:

$$\text{Viability [\%]} = \frac{Abs_{sample} - Abs_B}{Abs_{DMSO} - Abs_B} \times 100\% \text{ (equation 3.2.12.1)}$$

where,

Abs_{sample} - absorbance of the viable cells treated with the antibiotic, measured at 540 nm (MTT method) or at 450 nm and 690 nm (WST-1 method)

Abs_B - absorbance of the cell-free medium measured at 540 nm (MTT method) or at 450 nm and 690 nm (WST-1 method)

Abs_{DMSO} - absorbance of the viable cells treated with 0.5 - 1% DMSO, measured at 540 nm (MTT method) or at 450 nm and 690 nm (WST-1 method)

3.2.13. Imaging cell morphology using Confocal Microscopy

The morphology of MRC-5 cells non-treated and treated with antibiotics at IC_{50} and IC_{90} concentrations was inspected by confocal microscopy. The pattern of the sample preparation was similar to that one performed for the MTT assay (section 3.2.12.a). On the third day, the culture medium was carefully aspirated and PBS was added to each well. Then, 7-AAD¹¹ and Hoechst 33342¹² were added to the wells to achieve a final concentration of 10 μ g/mL and 1 μ g/mL, respectively. Further, it was incubated for 10 min. After the incubation, the images of the MRC-5 cells were captured using confocal microscopy (Confocal Laser Scanning Microscopy, ZEISS).

¹¹ 7-AAD is a red fluorescent DNA-binding dye that is impermeant to cell membranes, and as such, it is generally excluded from viable cells [179]

¹² Hoechst 33342 is a cell-permeant nuclear counterstain that binds specifically to double-stranded DNA and emits blue fluorescence [180]

3.2.14. Calculation of selective toxicity index (STI_{CYT})

The results obtained from MIC₉₀ of *C. albicans* and cytotoxicity assay served to calculate the selective toxicity index of the tested antibiotics (STI_{CYT}) according to the equation:

$$STI_{C_{YT}} = \frac{IC_{50}}{MIC_{90}} \text{ (equation 3.2.14.1)}$$

3.2.15. Determination of cell viability by flow cytometry

HEK293 cells were seeded in a 24-well microplate (30,000 cells/well) in a volume of 400 µL per well and placed in an incubator (37°C, 10% CO₂) for 24 hours. Amphotericin B, *all-trans* Vacidin, and *all-trans* Gedamycin were used for the tests. The antibiotics diluted in DMSO and medium (DMEM), were added to each well at a volume of 100 µL, achieving the following final concentrations: 3.46 µg/mL (Amphotericin B), 1 mg/mL, and 37.2 µg/mL (*all-trans* Vacidin), and 0.6 µg/mL (*all-trans* Gedamycin). The concentration of DMSO in the final medium volume was 1%. The chosen final concentrations were equivalent to the EH₅₀ for AmB and

all-trans Vacidin (37.2 µg/mL), as well as the IC₅₀ for *all-trans* Gedamycin and *all-trans* Vacidin (1 mg/mL). Untreated cells were used as a control in the experiment.

Next, propidium iodide was added to the final concentration of 2 µg/mL in each well. The microplates were incubated for 30 minutes. During the experiment, it was observed that the cells partially detached from the bottom of the wells immediately after the addition of antibiotics, therefore the medium after incubation was transferred to the falcon tube. Subsequently, the plate with cells (without medium) was washed with 300 µL PBS containing 1 mM EDTA to remove any remaining medium, and the entire contents were transferred to the same falcon tube. Cells were detached from the plate by adding 200 µL trypsin (0.05%) and further incubation (5 min). The detached cells in trypsin were transferred to the same falcon tube. The wells were washed again with 300 µL PBS (without EDTA), and the content was transferred to the falcon tube. The prepared falcon tubes for each antibiotic were centrifuged (4°C, 1000 rpm/min). The supernatant was removed, and 200 µL PBS was added to the pellet. The contents of the falcon tubes were then transferred to a 96-well plate, and cell viability was analyzed using at λ=675 nm in a flow cytometry system (NovoCyte and NovoSampler Pro, Agilent).

3.2.16. Investigation of the antibiotic behavior in the lipid bilayer using FLIM

Lipid vesicles were made of 1,2-dimyristoyl-sn-glycero-3-phosphocholine (DMPC) lipids (M_{DMPC}= 677,9 g/mol) with (or without) the addition of sterols (cholesterol or ergosterol). DMPC was diluted in CHCl₃: MeOH mixture (2:1, v/v) to the concentration of 20 mg/mL. Subsequently, DMPC lipids, antibiotics, and sterols (if needed) were mixed to achieve a final solution volume of 100 µL, containing 0.5 mol%¹³ of the antibiotic and 30 mol% of the indicated sterol. 50 µL of the prepared mixture was applied in layers on the interior part of one platinum plate and the next 50 µL on another platinum plate. The distance of the plates was fixed to 2-3 mm.

¹³ mol% - molar concentration (molarity), the percentage of moles' number of a solute (antibiotic / sterol) calculated from the numbers of DMPC moles in a solution

This system was placed in the cuvette filled with the PBS solution (pH=7.4). Electrodes were connected to a sinusoidal voltage with a peak-to-peak value of 3 V and a frequency of 10 Hz for 2 hours. Electroformation was conducted above the temperature of the main phase transition of the phospholipids at 26°C (for DMPC it is 24 °C). Afterward, the content of the cuvette was transferred to the 2 mL vial. Then, the instrument was calibrated and the instrumental correction factor (G) of the detector's sensitivity to the polarization direction of the recorded light was determined in a separate measurement on air. Approximately 50 µL of the solution was placed on the microscope slide placed on an objective lens with the addition of silicon oil-immersed objective.

The lipid vesicles containing the specified antibiotic were found under the confocal fluorescence microscope (Picoquant MicroTime MT200), and then analyzed with the application of SymPhoTime 64 v. 2.3 software (Picoquant GmbH). GUVs were scanned in cross-section within the focal plane of a confocal fluorescence microscope enabling determination of the antibiotic's fluorescence. The characteristics of the equipment and the fixed parameters are presented in Table 26.

Table 26. Equipment and fixed parameters.

Equipment	Settings of the instrument method	
	Fixed parameter	Values
Picoquant MicroTime MT200 (Picoquant MicroTime 200 main module, Olympus IX71 confocal microscope; picosecond diode-pumped solid-state lasers (~1 mW): 405 nm, EXCELITAS photon counting detectors (350 ps resolution)	Channels wavelength (pulsed laser) [nm]	405
	Repetition frequency [MHz]	10
	Laser [au]	123 (1,968 µW)
	Confocal pinhole (diameter) [µm]	50
	Resolution time [ps]	16
	Dwell time [ms]	0.4

Obtained fluorescence intensities were used to calculate the anisotropy (r) according to the equation 3.2.16.1:

$$r = \frac{F_{\parallel} - GF_{\perp}}{F_{\parallel} + 2GF_{\perp}} \text{ (equation 3.2.16.1)}$$

Where,

F_{\parallel} - fluorescence intensity polarized in parallel to the polarization of the excitation light

F_{\perp} - fluorescence intensity polarized perpendicularly to the polarization of the excitation light

G -instrumental correction factor of the detector's sensitivity to the polarization direction of the recorded light, determined before each experiment

The r value is in the range between 0.0 to 0.4. The fluorescence anisotropy values were analyzed and determined with the application of SymPhoTime 64 v. 2.3 software (Picoquant GmbH, Germany). Additionally, the fluorescence anisotropy values determined as the angle between the direction of antibiotic transition dipole and the axis normal to the plane of the lipid bilayer (see Figure 24) were calculated based on equation 3.2.16.2:

$$\frac{F_Z}{F_Y} = \frac{1}{2} \tan^2 \alpha \text{ (equation 3.2.16.2)}$$

Where,

α – orientation angle [°]

F_Y , F_Z - fluorescence signals recorded from two sides of membrane fragments spanned by the axes Y and Z, see Figure 25

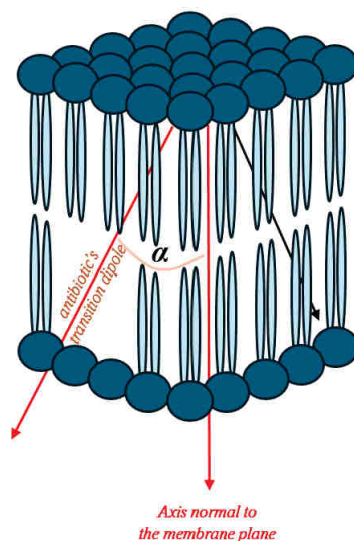


Figure 24. A simplified model of the Gedamycin molecule orientation with respect to the lipid bilayer

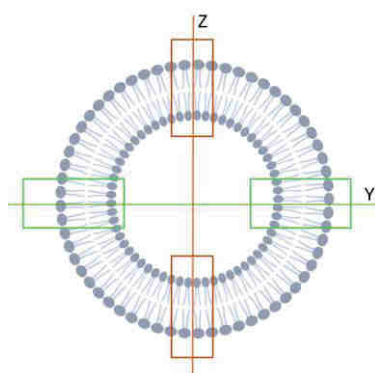


Figure 25. The membrane sides of which the fluorescence signals were recorded (green rectangle- one side, orange rectangle- another side)

Fluorescence signals were collected from the symmetric fragments of the imaged liposome membrane, located on both sides of the Y and Z axes. Taking into account the deviation standards of the obtained average orientation angle, the U-Mann Whitney test was used. The hypothesis being tested was as follows: the distributions of both populations are the same. The obtained orientation angles of the experimental systems were arranged in order from smallest to largest. Next, ranks were assigned to these ordered values and summed for each population (S_1 , S_2). The coincidence of the average orientation angle was assessed according to equations 3.2.16.3, 3.2.16.4:

$$U_1 = n_1 \times n_2 + \frac{n_1(n_1+1)}{2} - S_1 \text{ (equation 3.2.16.3)}$$

$$U_2 = n_1 \times n_2 + \frac{n_2(n_2+1)}{2} - S_2 \text{ (equation 3.2.16.4)}$$

Where,

U_1, U_2 – the value of U-Mann Whitney test

n_1, n_2 - the number of GUVs tested in the two selected experimental systems

S_1, S_2 - the sum of ranks assigned to the orientation angles obtained in the two selected experimental systems

The obtained U_1, U_2 were compared, and the lowest value was compared to $U_{critical} (\alpha=0.05)$ [160] and interpreted as follows:

- If $U > U_{critical}$ - there is no basis for rejecting the hypothesis
- If $U \leq U_{critical}$ - the hypothesis is rejected

4. RESULTS AND DISCUSSION

The subject of the research, the results of which are described in this dissertation, have been the aromatic analogues of Amphotericin B, namely aromatic heptaene (or polyene) macrolides (AHMs), Candicidin D, Gedamycin, and Vacidin. The former is a major component of the Candicidin complex and the two latter constitute the Aureofacin complex, which exhibits slightly higher antifungal activity than the Candicidin D [145]. Major antibiotics derived from these complexes have *cis-trans* bonds in different positions in chromophores (in the positions 26Z, 28Z for the Candicidin complex and 28Z, 30Z for the Aureofacin complex).

The scheme presenting an outline of the research concept is shown in Figure 26.

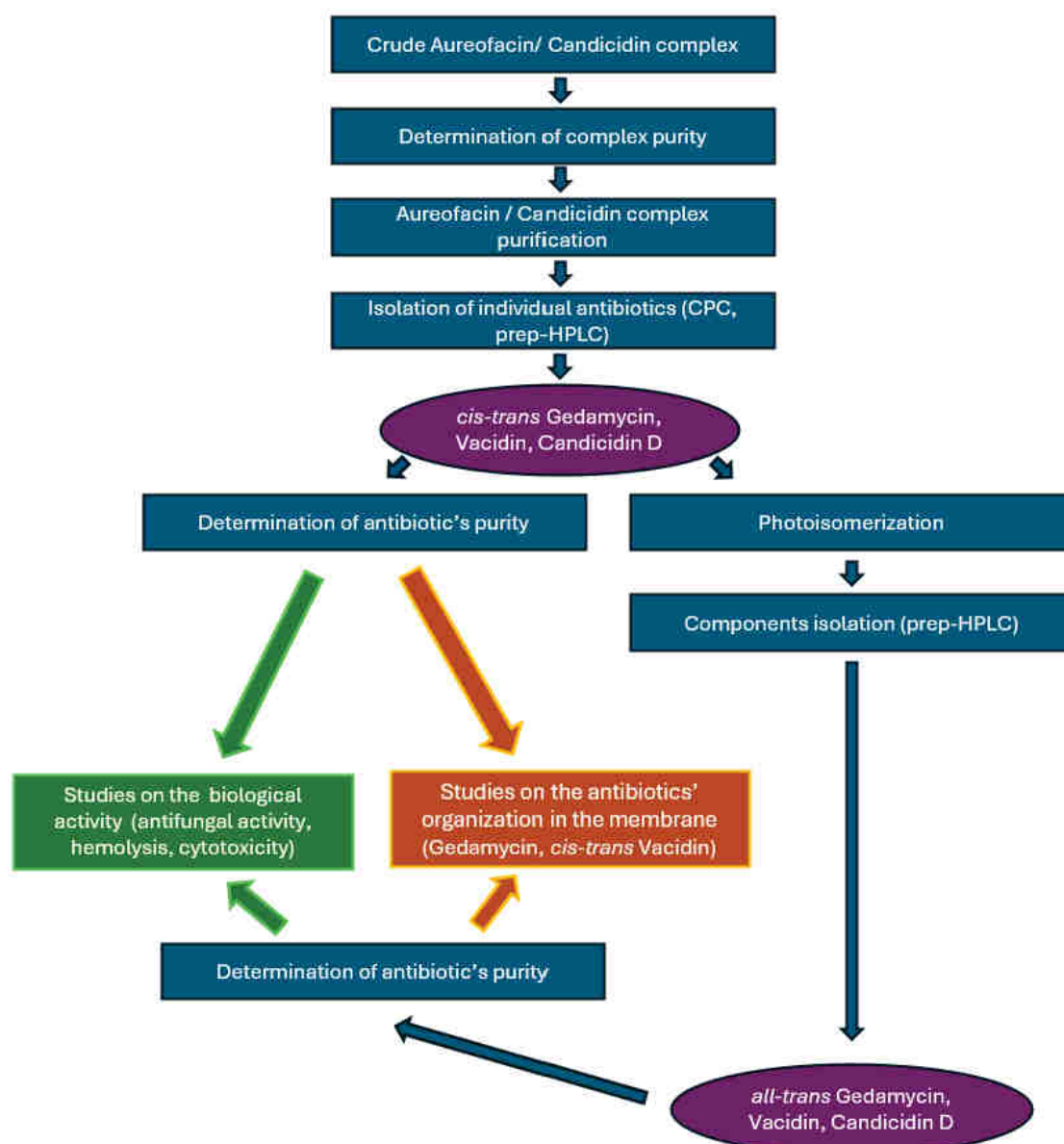


Figure 26. Scheme of the research; blue color – steps of antibiotics' isolation, purple color - isolated antibiotics, green color – step of biological studies, orange color – step of biophysical studies. CPC – centrifugal partition chromatography, prep-HPLC – preparative High-Performance Liquid Chromatography

4.1. Selection of starting materials and determination of complex purity

AHMs are not commercially available, except for the Candididin complex of low purity [161]. Moreover, there was no access to high-efficiency *Streptomyces* spp. strains producing Candididin or Aureofacin complexes. On the other hand, crude preparations of Candididin and Aureofacin complexes isolated from the fermentation broth at the Department of Pharmaceutical Technology and Biochemistry in the seventies of XXth century, stored at -18°C in tightly closed vessels made of brown glass, have been available as a starting material for my research.

In the first preparatory step of my research, an analysis of the long-term stored 10 batches of crude preparations of Candididin and Aureofacin complexes, aimed at selecting those with the highest content of AHMs, was performed. Samples of these materials were subjected to UV-Vis analysis, as described in section 3.2.1. The UV-Vis spectra of the selected crude preparations taken in the 250-450 nm region are presented in Figure 27 and the results of the complex purity determination of these specimens are shown in Table 27.

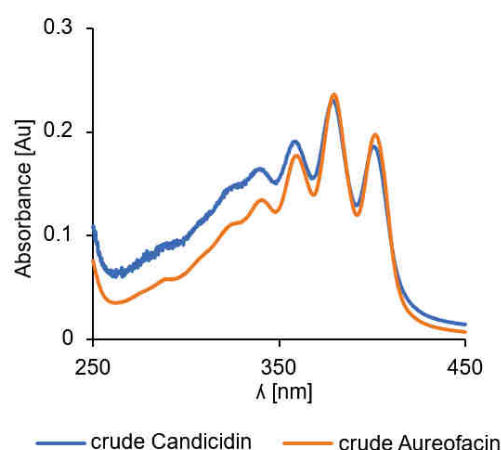


Figure 27. UV-Vis spectra of the chosen crude Aureofacin and Candididin complexes (samples of 0.01 mg/mL in MeOH)

Table 27. Results of the complex purity determination for the selected preparations of AHMs.

Sample name	λ_{\max} [nm]	Absorbance [Au]	Purity [%]
Crude Aureofacin	378	0.23	23
Crude Candididin	378	0.21	21

The UV-Vis spectra of the Aureofacin and Candididin complexes (Figure 27) contained three absorbance maxima: $\lambda_1 = 360$ nm, $\lambda_2 = 378$ nm, and $\lambda_3 = 401$ nm, corresponding to the chromophore (seven conjugated double bonds) of AHMs, in a good agreement with previously reported data [27][40][114]. The highest absorbance intensity was observed at λ_2 , i.e. at the local maximum characteristic for the *cis-trans* AHMs [114], and this wavelength was selected as the reference for assessing the purity of the complexes. The absorbance obtained for the selected Aureofacin and Candididin preparations was 0.23 Au and 0.21 Au, respectively (Table 27). Based on the extinction coefficient method ($E^{1\%}_{1\text{cm}}$) and the known sample concentration equal to 0.01 mg/mL, the purity of the selected preparations was 23% for crude Aureofacin complex and 21% for crude Candididin complex. For other specimens, their purities were below 20%. Absorbance in the 250-350 nm spectral region is attributed to the presence

of degraded chromophore products [27], as well as residual materials from the fermentation process. As shown in Figure 27, the level of impurities was higher in the Candicidin complex compared to the Aureofacin complex.

Although the selected preparations exhibited the highest purity among the specimens analyzed, their purity level was insufficient for the efficient isolation of pure antibiotics directly from these preparations of complexes. In consequence, a further step of purification of the selected preparations was required.

4.2. Preliminary purification of the selected complexes

Conditions for preliminary purification of heptaene complex from the crude preparations (section 3.2.2.) were based on the literature procedures [162] with own modifications. Since it is known that the degradation of AHMs is catalyzed by some metal cations (e.g. iron, copper, chromium, cobalt, nickel, and manganese) and on the other hand, calcium, and magnesium can form complexes with the antibiotic, making them challenging to remove during isolation and contributing to increased ash content in the final product found in the fermentation broth [162], the EDTA solution was used. This approach aimed to remove residual metal ions from the Aureofacin and Candicidin crude complexes. Acetone, which is fully miscible with water and does not dissolve the antibiotics, was employed to remove any water residues (if present in the suspension) as well as butanol remains. Then, diethyl ether was used to remove any low-polarity compounds, as antibiotics are not soluble in this solvent. The verification of the implemented purification process was assessed by the determination of the purity using the UV-Vis method. Examples of the obtained results are presented below (Figure 28, Table 28).

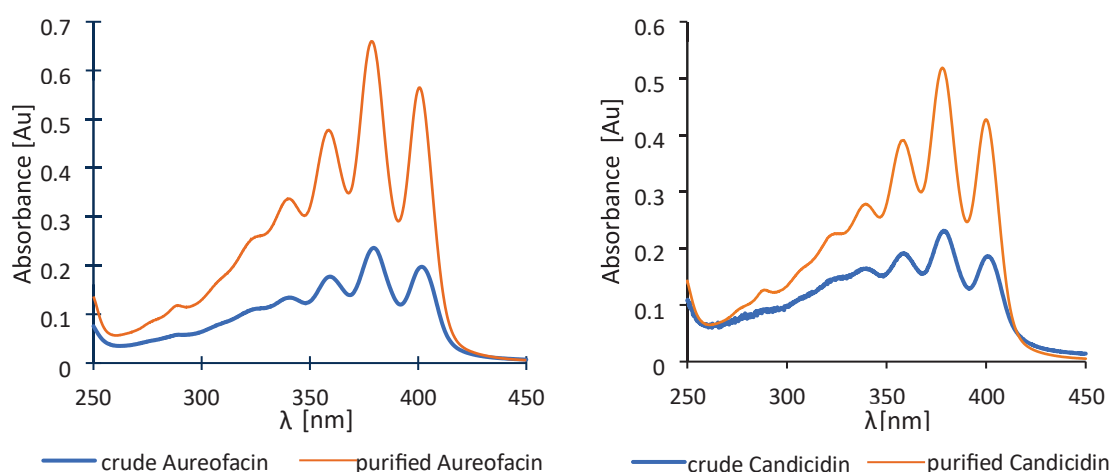


Figure 28. UV-Vis spectrum of crude and purified Aureofacin (left) and Candicidin (right) complexes at concentrations of 0.01mg/mL in MeOH

Table 28. The comparison of crude and purified Aureofacin – purification process summary.

Sample name	λ_{\max} [nm]	Absorbance [Au]	$E^{1\%}_{1\text{cm}}$ (Purity) [%]	Mass [g]	Process efficiency [%]
Crude Aureofacin	378	0.23	23	10.0	17
Purified Aureofacin		0.67	67	0.6	
Crude Candicidin	378	0.21	21	10.0	14
Purified Candicidin		0.51	51	0.6	

Based on the obtained absorbance values, it can be concluded that the purity of the purified complexes increased approximately two- to threefold compared to the "crude" preparations. The purification process applied (liquid-liquid extraction) not only increased the AHMs content in the preparation but also reduced the presence of degradation products, as indicated by the spectrum in the 350-300 range, especially for the Candicidin complex. From 10 g of the Aureofacin and Candicidin crude complexes (with 23% purity, corresponding to 2.3 g of the pure AHM antibiotics within the Aureofacin complex; and 21% purity, corresponding to 2.1 g of the pure AHM antibiotics within the Candicidin complex, respectively), 0.6 g of each preparation was obtained at the end of the process (with ca. 67% purity, yielding 0.4 g of the pure AHMs within the Aureofacin complex; and ca. 51% purity, yielding 0.3 g of the pure AHMs within the Candicidin complex, respectively). This indicates that the process efficiency (expressed as the antibiotic content in the fresh preparation recovered from the original preparation) was 17% for Aureofacin and 14% for Candicidin (Table 28). Although the process had low efficiency, such purification was essential to ensure better isolation of the individual AHM antibiotics at a higher purity level.

Composition of the both purified complexes was analyzed by HPLC-DAD under conditions described in 3.2.5 The results of these analyses are shown in Figures 29 and 30,

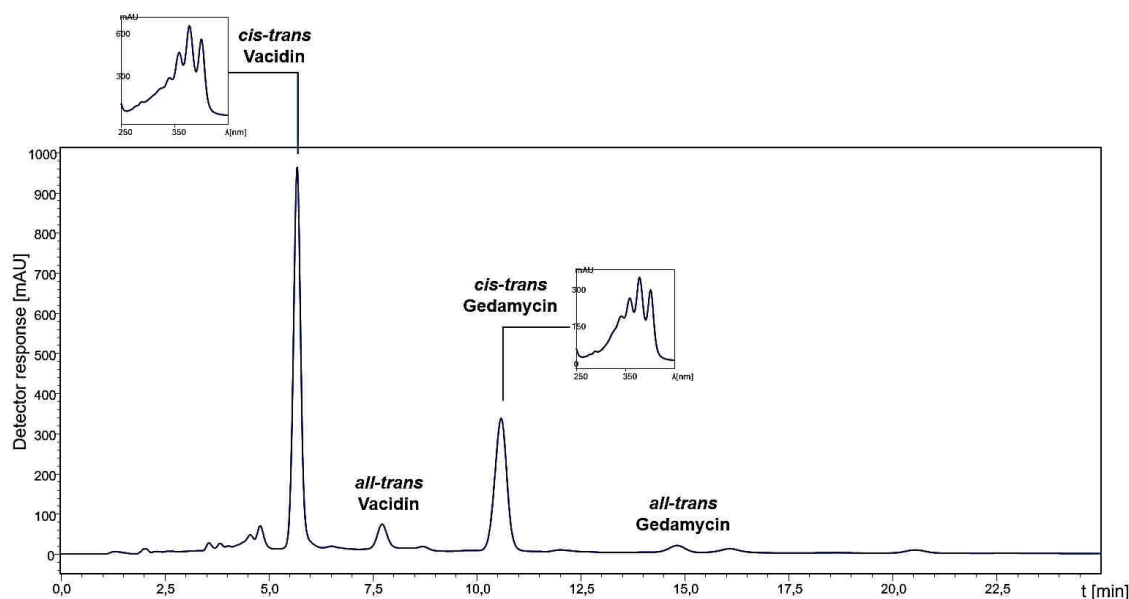


Figure 29. HPLC –DAD chromatogram of the purified Aureofacin complex.
Conditions: column: Luna 100 Å C18 (150 mm × 4.6 mm, 5 µm); mobile phase: 38% ACN/ 62% ammonium acetate (5.5 mmol, pH=4.5), v/v; ω=1 mL/min; c= 2 mg/mL, v_i = 20 µL, RT, λ=378 nm.

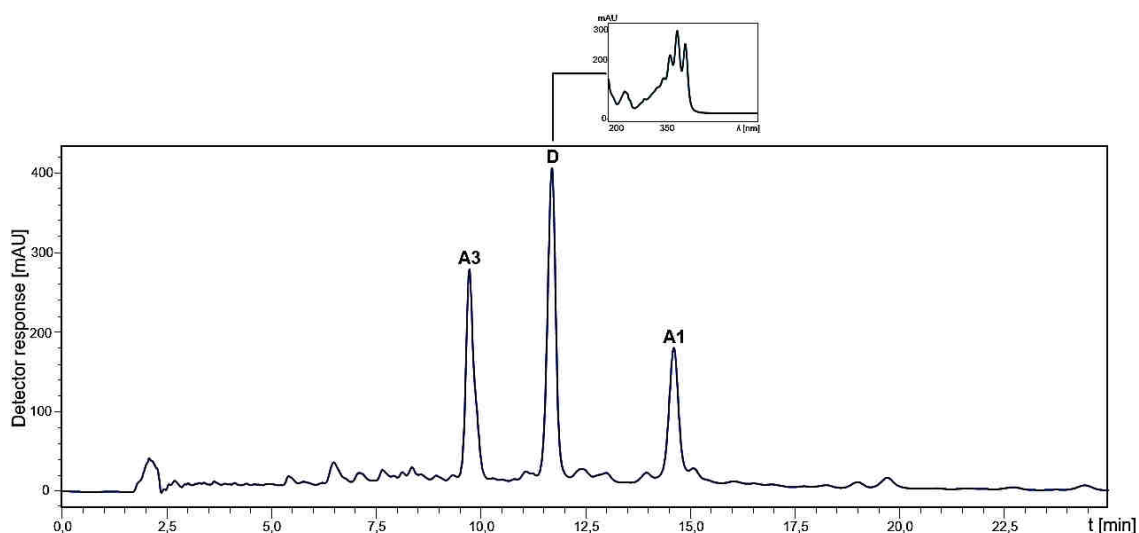


Figure 30. HPLC –DAD chromatogram of the purified Candidicin complex.
 Conditions: column: Luna 100 Å C18 (150 mm × 4.6 mm, 5 µm); mobile phase: 38% ACN/
 62% ammonium acetate (5.5 mmol, pH=4.5), v/v; ω=1 mL/min; c= 2 mg/mL, v_i = 20 µL, RT, λ=378 nm

Unequivocal assignment of peaks in HPLC-DAD chromatograms was possible due to the previous identification of components of both complexes by 2D NMR and LC-MS analysis [118][145]. The elution order observed in both complexes corresponds to the polarity of the compounds. In the case of separation of components of the Aureofacin complex, Vacidin (*N-p*-aminoacetophenone group in the side chain) eluted first, followed by Gedamycin (*N*-methyl-*p*-aminoacetophenone group in the side chain). Notably, the purified Aureofacin complex contained minor amounts of *all-trans* versions of both antibiotics. In the case of analysis of components of the Candidicin complex; Candidicin A3, containing the –OH group at C3 eluted first, followed by Candidicin D, containing =O at C3, and finally Candidicin A1, lacking -OH groups at C9 and C11.

Furthermore, the available patents primarily concern the isolation and purification of the AHM complexes rather than the isolation of their individual compounds. There is a notable absence of patents and publications concerning the isolation of pure aromatic heptaene macrolides, despite the antibiotic potential and growing interest in this group of compounds (as evidenced by recent publications). The isolation of AHMs proved sufficiently challenging that the Italian company SPA-Societa Prodotti Antibiotici S.p.A. adopted biotechnological strategies to modify the production strain, targeting the production of specific antibiotics and enhancing the activity of the resulting derivatives [163]. This underscores the challenges associated with the isolation of high-purity antibiotics from AHM complexes.

4.3. Separation and isolation of individual AHMs from complexes by CPC

The next step, after the preliminary purification process, was the separation and isolation of the components of the Aureofacin complex (Vacidin, Gedamycin), and the isolation of the major component of the Candidicin complex (Candidicin D). Due to the irreversible adsorption of AHMs onto the chromatographic column bed, preparative HPLC was deemed unsuitable for this purpose. Therefore, it was decided to use the Centrifugal Partition Chromatography.

The Aureofacin complex contains fewer components, and therefore, it is easier to separate than the Candididin complex. Aureofacin was selected as the model for these studies.

4.3.1. Selection of the biphasic solvent system (shake-flask test)

The crucial step for the CPC isolation process is selection of an appropriate biphasic solvent system. The shake flask method is commonly used for this purpose. It allows for the rapid testing of many potential systems on a small scale, without the need for special equipment or time. The composition and proportions of the mentioned solvent systems play a critical role in the separation of compound mixtures in CPC. Solvents and their mutual proportions must be carefully selected to form a biphasic system of immiscible liquids, corresponding to the stationary and mobile phases. Once introduced into the CPC rotor, these phases create a chromatographic column where the separation of the target substances occurs. Based on the literature data, as well as considering the structure and properties of heptaene macrolides, it was decided to verify the distribution of the antibiotics between the two phases in the following solvent systems:

- CHCl_3 : MeOH: H_2O (4:4:3, v/v/v),
- CH_2Cl_2 : MeOH: H_2O (4:4:3, v/v/v),
- CHCl_3 : MeOH: borate buffer (pH=8.2) (4:4:3, v/v/v),
- CHCl_3 : MeOH: borate buffer (pH=8.6) (4:4:3, v/v/v),
- CHCl_3 : MeOH: ammonium acetate buffer (pH=4.5) (4:4:3, v/v/v),
- AcOEt: BuOH: EtOH: H_2O (15:5:3:25, v/v/v/v),
- hexane: AcOEt: MeOH: H_2O (6:5:6:5, v/v/v/v).

The CHCl_3 : MeOH: H_2O solvent system was particularly interesting as it was used to purify the derivatives of polyene macrolides by the Counter-Current Chromatography (CCC) technique [164]. Assuming that this solvent would be the most suitable for the AHMs separation and isolation by CPC, it would simplify the post-chromatographic purification process, as ultrapure water would be used instead of buffers. Furthermore, Lightbown et al. [165] reported the use of CHCl_3 : MeOH: borate buffer (pH=8.2) system for the separation of Candididin in a coil planet centrifuge, which also is based on the liquid-liquid extraction. The presence of salts in this solvent system could decrease its emulsification ability. Furthermore, the pH influence on the antibiotic distribution in the solvent system was tested with the use of two solvent systems: CHCl_3 : MeOH: borate buffer (pH=8.6) and CHCl_3 : MeOH: ammonium acetate buffer (pH=4.5). The other solvent system selected for testing was CH_2Cl_2 : MeOH: H_2O . The dichloromethane serves as a suitable substitute for chloroform, due to its comparable polarity and solvent strength. The density of dichloromethane is 1.33 g/cm^3 , while chloroform's density is 1.48 g/cm^3 . It can be expected that a solvent system containing chloroform would generate high internal pressure within the apparatus, whereas the lighter dichloromethane might help reduce it. Considering that the compound may show relatively good solubility in aqueous alcohols such as butanol (BuOH) and ethanol (EtOH), the AcOEt: BuOH: EtOH: H_2O system was also employed in this study. Finally the hexane: AcOEt: MeOH: H_2O (HEMWat system) was tested. HEMWat is one of the most commonly used in the CPC chromatographic systems and does not require prior

preparation of the two-phase system (as it occurs within the new commercially available apparatus). The specified proportions of HEMWat components enable the formation of a solvent system with medium polarity, which could be useful for the separation of amphoteric compounds such as heptaene macrolides.

The UV-Vis method was employed as a preliminary assessment to identify the most appropriate solvent system for the CPC isolation process. This approach facilitated the rapid selection of an optimal biphasic solvent system. It is important to note, that the determined K_D values indicate the resultant of the partition coefficient of the two antibiotics, Gedamycin and Vacidin. The obtained values were calculated based on the absorbance parameter (at $\lambda=378$ nm) according to equation 3.2.3.1. and the results are presented in Table 29.

Table 29. The calculated K_D values of Gedamycin and Vacidin in solvent systems tested for CPC analysis

Solvent number	Solvent system	Volume ratio (v/v/v)	K_D
1	CHCl ₃ : MeOH: borate buffer (pH=8.2)	4 : 4 : 3	0.54
2	CHCl ₃ : MeOH: borate buffer (pH=8.6)	4 : 4 : 3	0.26
3	CHCl ₃ : MeOH: ammonium acetate buffer (pH=4.5)	4 : 4 : 3	0.98
4	CHCl ₃ : MeOH: H ₂ O	4 : 4 : 3	0.77
5	CH ₂ Cl ₂ : MeOH: H ₂ O	5 : 4 : 2	3.54
6	AcOEt: BuOH: EtOH : H ₂ O	30 : 10 : 6 : 50	0.23
7	hexane: AcOEt: MeOH: H ₂ O	6 : 5 : 6 : 5	-

For the HEMWat solvent system, K_D could not be determined due to the lack of the antibiotics' affinity to the upper phase (it was not detected by UV-Vis analysis), so the solvent system No. 7 was rejected. Since the solvent system affording the K_D value greater than 2 is unsuitable for separation, as it indicates that a given compound has a higher affinity for the stationary phase, remaining there much longer, the No. 5 system (CH₂Cl₂: MeOH: H₂O) was also eliminated. For $K_D > 2$, the peaks may become more broadened, occasionally reaching a height that is challenging to detect and can be obscured by baseline noise. In addition, the analysis time is considerably extended. Conversely, the compounds with a K_D value lower than 0.5, which exhibit a higher affinity for the mobile phase, are rapidly eluted from the column, nearly coinciding with the dead volume time. Due to this diminished interaction with the stationary phase, the likelihood of separation of these compounds is minimal, as they elute along with the leading edge. Therefore, solvent systems No. 2 and 6 were considered unsuitable. The K_D value for the solvent system No. 4 (CHCl₃: MeOH: H₂O) was 0.77 (within the appropriate range), however, the system could not be considered for further analysis due to its ability to form emulsions (observed during the shake flask test), leading to the long equilibration time of the two phases, caused probably by the absence of salt in the system. The most promising solvent systems among the all tested were No. 1 (CHCl₃: MeOH : borate buffer, pH=8.2; $K_D=0.54$), and No. 3 (CHCl₃: MeOH : ammonium acetate buffer, pH=4.5: $K_D=0.98$).

The suitability of the pre-selected solvent systems in isolating components of the Aureofacin complex was further evaluated by determining the separatory factor (α) between Vacidin and Gedamycin using the HPLC-DAD method (according to method described in section

3.2.5). As a result, the K_D values for both antibiotics were determined. The partition coefficient values and separation factors were calculated according to the equations 1.4.3.1 and 3.2.3.1, respectively. The obtained values are presented in Table 30.

Table 30. The K_D values for Gedamycin and Vacidin in selected biphasic solvent systems and related selectivity for Gedamycin and Vacidin.

Solvent system	Volume ratio (v/v/v)	K_D Vacidin	K_D Gedamycin	α
No. 1 CHCl ₃ : MeOH: borate buffer (pH=8.2)	4 : 4 : 3	0.27	0.86	3.14
No. 3 CHCl ₃ : MeOH: ammonium acetate buffer (pH=4.5)	4 : 4 : 3	0.75	1.80	2.41

Based on the obtained results presented in Table 30, the separatory factor of the solvent system was more favorable for the No. 1 system, in comparison with the No. 3 system. Although the K_D value for Vacidin is less than 0.5, the α factor plays a more significant role here, as the antibiotics are strongly separated. Therefore, it was concluded that the most suitable solvent system among all tested was CHCl₃: MeOH: borate buffer (pH=8.2), and it was used in further studies aimed at developing a procedure for the isolation of Gedamycin and Vacidin using the CPC technique.

4.4. Isolation of the antibiotics by preparative CPC with DAD detection

Based on the results of the optimization described in section 4.3.1. a biphasic solvent system – CHCl₃: MeOH: borate buffer (pH=8.2, 4:4:3; v/v/v) was selected for application in CPC separation of AHMs. This system formed two phases with the following qualitative composition:

- the stationary phase (lower phase) mainly consisted of chloroform and methanol,
- the mobile phase (upper phase) mainly consisted of borate buffer and methanol.

In addition to selecting the solvent system for the CPC isolation process, further optimization of process parameters was performed:

a) Rotation speed

Various rotation speeds were tested, ranging from 500 rpm/min to 2000 rpm/min. The use of low rotation speed did not ensure sufficient phase separation, while rotation speeds at 2000 rpm/min caused a rapid increase in pressure to levels at which the CPC system could no longer function, due to the significant differences in the densities of the lower and upper phases. Consequently, despite going against general principles, it was decided to use a rotation speed of 800 rpm/min, which allowed for the best separation of the antibiotic complex components.

- The ascending and descending modes were compared. It was found that the ascending mode generated much more stable chromatographic conditions, with the antibiotics eluting in a relatively short time.

c) Eluent flow rate

The volumetric flow rates of the eluent were tested in the 4 – 10 mL/min range and the optimal value was set at 5 mL/min. Above this established flow rate, a significant loss of the stationary

phase from the column was observed, along with increased emulsification, which was accompanied by a sharp rise in column pressure. A flow rate lower than 4 mL/min was not considered due to the excessively long duration of the chromatographic process.

d) Injection volume

Due to the limited solubility of the compounds in organic solvents and the low solubility in the selected solvent system, a column overloading of concentration type was not conducted. In CPC, sample preparation typically involves using a solvent system after reaching equilibrium, with the mixture of the upper and lower phases adjusted to the experimental volume ratio. For the CPC optimization process, a mixture of the upper and lower phases in an 8:2 volume ratio was added to the antibiotic dissolved in DMSO (160 mg/mL). DMSO was used due to the aforementioned low solubility of heptaene macrolides in the chosen solvent system. This allowed the maximum concentration to be achieved - 8 mg/mL - which remained well below the concentration column overload threshold. Therefore, only volumetric overloading was investigated by testing various sample injection volumes, ranging from 1 mL to 10 mL. Optimization of the injection volume was constrained by the available maximum loop volume of 10 mL. Given the preparative nature of the study, an injection volume of 10 mL did not result in any loss of chromatographic quality (peaks of the Aureofacin complex's components remained baseline-resolved). This was especially important since the technique is preparative, and the goal of this separation step was to isolate the maximum amount of the antibiotic. Additionally, it should be noted that further increases in injection volume would result in a broad injection band migrating through the column, ultimately reducing chromatographic selectivity. Therefore, based on the obtained chromatographic results, the 10 mL injection volume (disregarding the loop volume limitation) was deemed optimal.

The implementation of a borate buffer in the solvent system led to the presence of salt in the sample which required removal. Therefore, an additional step of extraction with ultrapure water was implemented after the CPC isolation process. The representative examples of chromatograms obtained in the isolation of components of the complexes using CPC under optimized conditions are presented in Figure 31 for the Aureofacin complex and in Figure 34 for the Candicidin complex. The content of the fractions collected after both CPC separations was verified using the HPLC-DAD method under conditions described in 3.2.5.

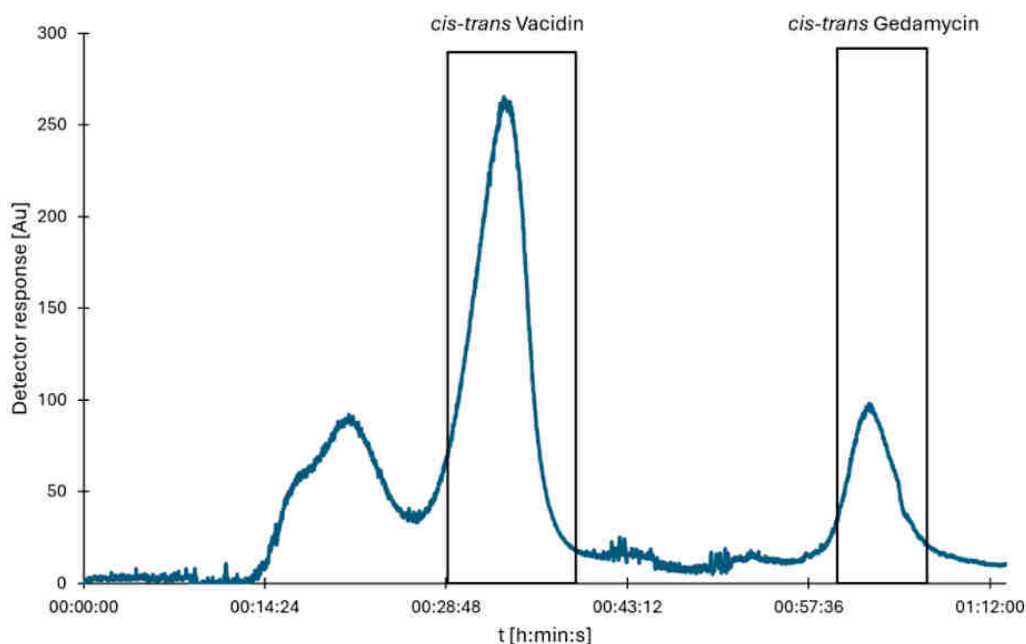


Figure 31. CPC-DAD chromatogram of separation of components of the purified Aureofacin complex. Black rectangles refer to the collected fractions containing *cis-trans* Vacidin and *cis-trans* Gedamycin, respectively. Conditions: CPC rotor 250 ml, biphasic solvent system: CHCl_3 : MeOH: borate buffer (pH=8.2, 4:4:3, v/v/v), ASC mode, 800 rpm/min, ω = 5 mL/min, c = 8 mg/mL, v_i = 10 mL, RT, λ = 378 nm

In the chromatogram shown in Figure 31, the peak corresponding to *cis-trans* Vacidin was observed within a retention time range of 28 min to 40 min (collected fractions between 28-40 min), while the peak corresponding to *cis-trans* Gedamycin eluted between 57 to 70 min (collected fractions between 58-66 min). The smallest peaks eluted between 14 and 25 min were identified as corresponding to degradation products, as confirmed by HPLC combined with DAD-ESI-MS. The peaks corresponding to Vacidin and Gedamycin were well separated, symmetric and their shapes closely resemble a Gaussian distribution. There was little doubt that the chromatographic conditions for this separation process ensured high resolution and selectivity. The HPLC-DAD chromatograms of Vacidin and Gedamycin collected fractions are presented in Figures 32, 33.

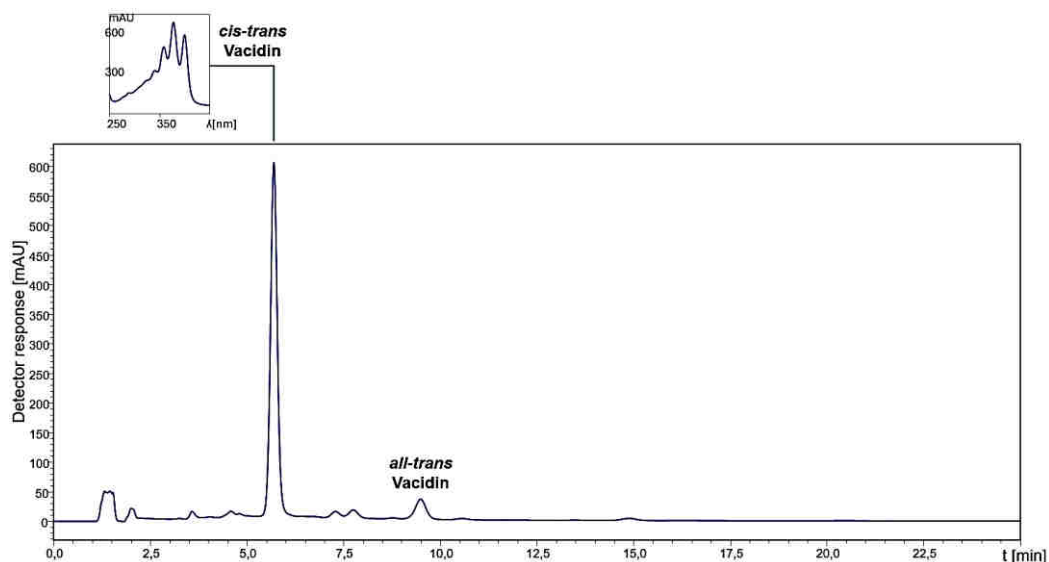


Figure 32. HPLC-DAD chromatogram of fractions 28-40 min (Vacidin) from CPC separation of Aureofacin purified complex (Figure 31).

Conditions: column: Luna 100 Å C18 (150 mm × 4.6 mm, 5 μm); mobile phase: 38% ACN/ 62% ammonium acetate (5.5 mmol, pH=4.5), v/v; ω=1 mL/min; c= 2 mg/mL, v_i = 20 μL, RT, λ=378 nm

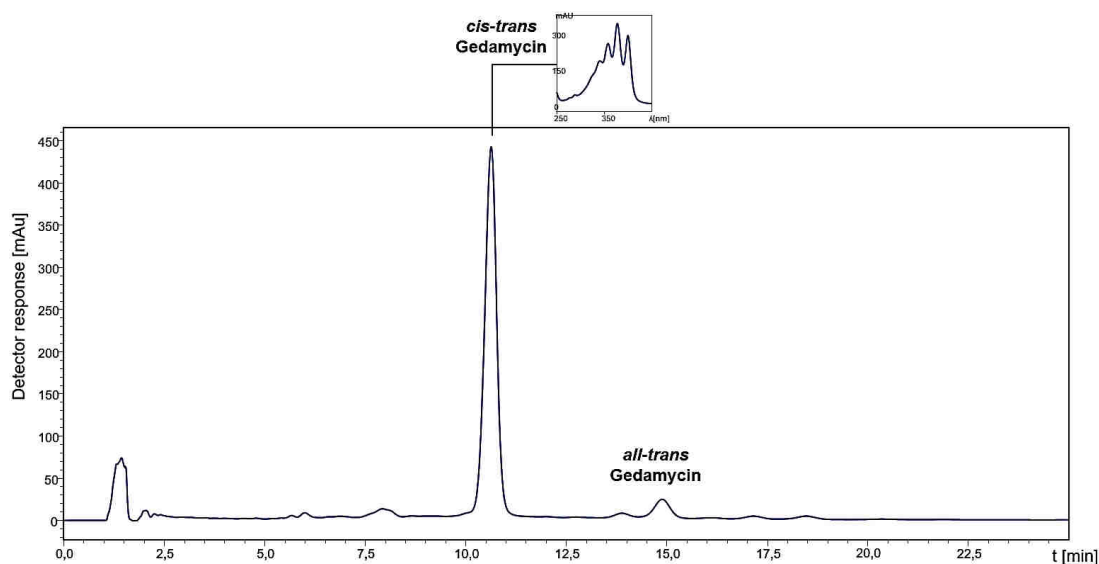


Figure 33. HPLC-DAD chromatogram of fractions 57-70 min (Gedamycin) from CPC separation of Aureofacin purified complex (Figure 31).

Conditions: column: Luna 100 Å C18 (150 mm × 4.6 mm, 5 μm); mobile phase: 38% ACN/ 62% ammonium acetate (5.5 mmol, pH=4.5), v/v; ω=1 mL/min; c= 2 mg/mL, v_i = 20 μL, RT, λ=378 nm

The CPC separation of Aureofacin complex components was repeated eight times with high reproducibility to collect larger amounts of constitutive AHMs. Fractions of approximately 12 mL each were pooled (480 mL in total for Vacidin and 320 mL in total for Gedamycin), desalted with ultrapure water, and concentrated by solvent evaporation under reduced pressure, to obtain solid antibiotics, namely ~80 mg of *cis-trans* Vacidin and ~45 mg of *cis-trans* Gedamycin. The determined content of Vacidin and Gedamycin in collected fractions using the CPC technique was approximately 87%, 86% respectively.

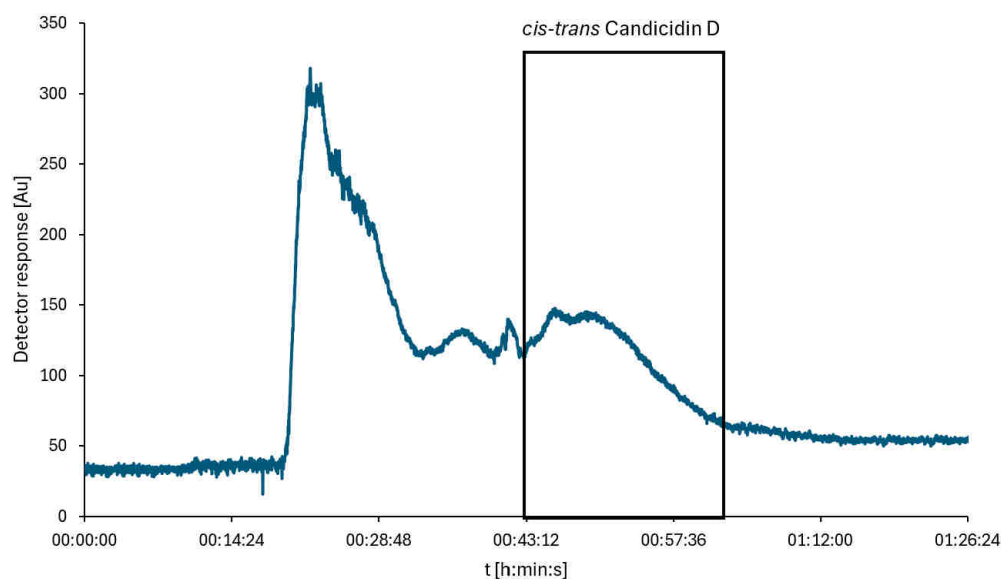


Figure 34. CPC-DAD chromatogram of separation of components of the Candidicin complex. Black rectangle refers to the collected fractions containing *cis-trans* Candidicin D. Conditions: CPC rotor 250 ml, biphasic solvent system: CHCl_3 : MeOH: borate buffer (pH=8.2, 4:4:3, v/v/v), ASC mode, 800 rpm/min, ω = 5 mL/min, c = 8 mg/mL, v_i = 10 mL, RT, λ =378 nm

The CPC-operating conditions set for the isolation of Vacidin and Gedamycin, when applied for the isolation of components of the Candidicin complex, appeared less effective, as substantial peak overlapping was observed (Figure 34). However, the content of Candidicin D in fractions collected between 43 and 60 min (peak in a black rectangle) was substantially enriched compared to that in the purified complex (Figure 30) - some amounts of Candidicin A1 and Candidicin A3 were still present.

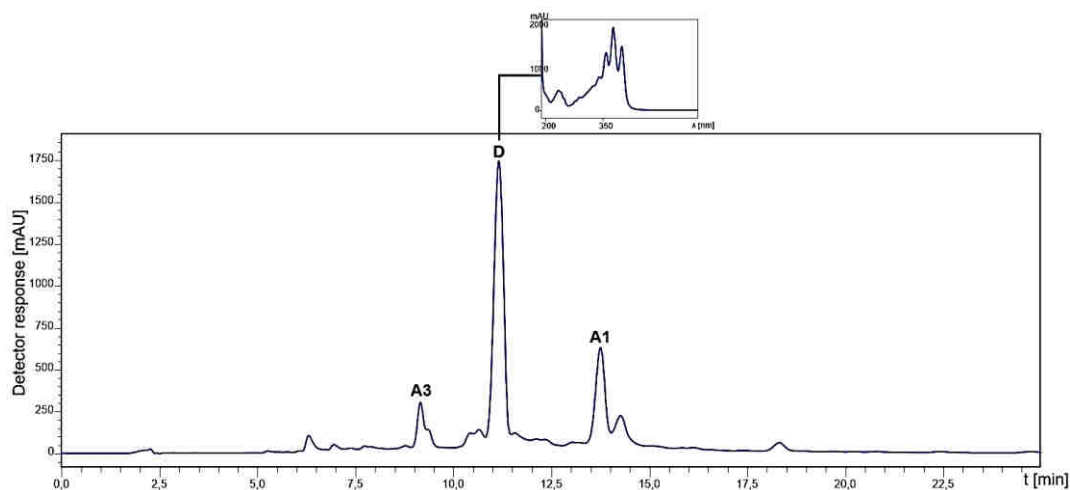


Figure 35. HPLC-DAD chromatogram of 43-60 min (Candidicin D) from CPC separation of Candidicin purified complex (Figure 34)

Conditions: column: Luna 100 Å C18 (150 mm × 4.6 mm, 5 μ m); mobile phase: 38% ACN/ 62% ammonium acetate (5.5 mmol, pH=4.5), v/v; ω =1 mL/min; c = 2 mg/mL, v_i = 20 μ L, RT, λ =378nm

Before the CPC isolation process the content of the antibiotics in pure Candidicin complex was as follows: Candidicin A1 – 21%, Candidicin D – 30%, Candidicin A3 – 28% (Figure 30). The determined content of Candidicin D in fractions between 43-60 min after CPC separation was approximately 45% but two other antibiotics remained in the sample in significant quantities, namely Candidicin A1 – 19 % and Candidicin A3 – 25 % (Figure 35). Therefore,

fractions between 43-60 min were collected for further separation and purification by prep-HPLC. The purification process was repeated eight times. Fractions of approximately 12 mL each were pooled (680 mL in total for Candicidin D), desalted with ultrapure water, and concentrated by solvent evaporation under reduced pressure, to obtain solid antibiotics, ~60 mg of *cis-trans* Candicidin D collected fractions.

It seems that the observed substantial difference in efficiencies of separation of components of Aureofacin and Candicidin complexes could be related to the structural properties of the constitutive antibiotics. Gedamycin and Vacidin (Aureofacin complex) differ in the structure of the alkyl-aromatic side chain, possibly generating differential polarity of both molecules. Very subtle structural differences between Candicidin A1, Candicidin D, and Candicidin A3 concern their polyol fragments, little if affecting the polarity of these molecules. Several attempts made to improve the efficiency of CPC separation of Candicidin complex components were not successful.

The parameters of CPC separation with the chosen solvent system were a bit different from the conventional methodology for isolation using the CPC technique. Particularly, the process was conducted at 800 rpm/min, *i.e.* the rotor speed felt outside the typical range of 850-2300 rpm/min [166]. According to available literature data [167], at higher rotational speeds, the number of theoretical plates increases, which should improve separation efficiency. However, in the case of my studies, separation efficiency decreased with increasing the rotor speed above 800 rpm/min (data not shown). This discrepancy could be due to significant differences in the densities of the upper and lower phases, which at higher rotational speed may impede the flow of the mobile phase through the stationary phase, reduce the stability of the biphasic solvent system, and promote emulsification. Additionally, the CPC system is not equipped with temperature control, and during rotor operation the temperature increases, especially at higher rotor speeds, leading to a decrease in the viscosity of the liquid phases in the solvent system. This may disturb the equilibrium between the phases in the rotor and may lead to solvents emulsification [144]. The parameters set for the CPC-operated isolation process allowed for two injections per sequence. Attempting a third injection resulted in a marked decrease in chromatographic resolution, preventing effective fraction collection. As noted in the literature [144], it seems understandable due to the gradual loss of the stationary phase from the CPC column and lower separation efficiency.

To briefly summarize this step, the following conclusions are presented: the chromatographic conditions of CPC analysis enabled the successful isolation of almost pure *cis-trans* Gedamycin and *cis-trans* Vacidin, but for the isolation of pure *cis-trans* Candicidin D, further separation by prep-HPLC was needed. The methods of purification proposed to date, for example in patents, were primarily designed for the purification of complexes. As a result of the conducted research, an original method for purifying AHMs using the CPC technique was developed - such a solution has not been previously proposed in the literature. Furthermore, there are no available literature reports of AHMs isolation with the use of modern isolation techniques that are successfully applied for the purification of natural compounds. The only known

documentation by me is a patent describing the isolation of Vacidin and Gedamycin using a column packed with styrene macroporous anti-phase adsorption resin. However, this method requires the consumption of large quantities of chemical solvents. Additionally, the adsorptive resin undergoes gradual degradation, necessitating replacement or replenishment of the material over time, which incurs additional costs. My doctoral studies represent the first application of CPC for the isolation of components from AHM complexes. It can be said that this study is paving the way in this area.

4.5. Isolation of *cis-trans* Candididin D using preparative HPLC

Isolation of *cis-trans* Candididin D from the fractions collected between 43 – 60 min after CPC required the use of an additional technique, namely prep-HPLC-DAD. Based on the principles of a proper scaling-up, the conditions of separation applied for HPLC-DAD (analytical scale) of AHMs were transferred to the preparative scale, taking into account the internal diameter of the preparative column and appropriately scaling both the injection volume and the volumetric flow rate of the eluent. These were set to the flow rate of 29.5 mL/min and an injection volume of 2.5 mL. Since the LiChrospher column used for prep-HPLC was longer (250 mm) than the analytical column, it was expected that the retention times obtained for the preparative column could be longer than those in HPLC-DAD.

Fractions collected between 43- 60 min after CPC separation were pooled, desalted with ultrapure water, and concentrated by solvent evaporation under reduced pressure, to obtain solid antibiotics. Subsequently, the sample was prepared according to section 3.2.6., and injected into the prep-HPLC column. The exemplary chromatogram of prep-HPLC-DAD separation is depicted in Figure 36.

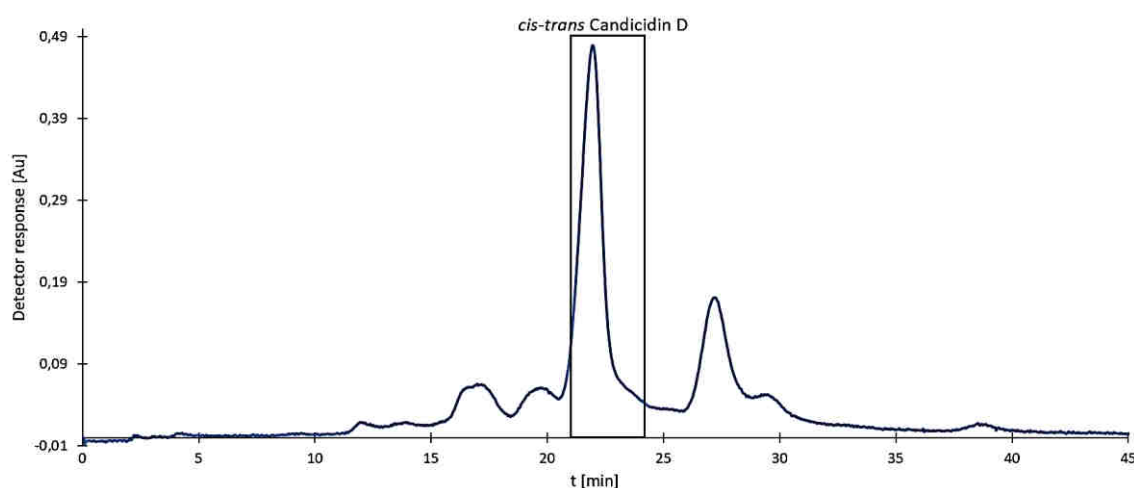


Figure 36. Preparative HPLC - DAD chromatogram of Candididin D sample after CPC. Collected fractions corresponding to Candididin D after CPC are marked by black rectangle.

Conditions: column: Merck, LiChrospher, RP-18 (250 mm x 25 mm, 10 μ m); mobile phase: 38% ACN/ 62% ammonium acetate (5.5 mmol, pH=4.5), v/v; ω = 29.5 mL/min; c=4 mg/mL, sample dissolved in following solvent system DMSO: MeOH: ammonium acetate (5.5 mmol, pH=4.5) (1:4:5, v/v/v), v_i =2.5 mL, RT, λ =378 nm

As the chromatogram obtained (Figure 36) demonstrates, *cis-trans* Candididin D eluted at a retention time between 20.6 and 24.4 minutes. To isolate the antibiotic in its purest form,

fractions (5 mL each) corresponding to the retention time range of 20.9 to 22.9 minutes, as indicated by the black rectangle, were collected. 354 mL of collected fractions, equal to an approximate total loading of 60 mg of the antibiotic onto the column (around 6 runs) were required to obtain 5 mg of the antibiotic. The retention times were consistent across multiple runs, however, the column cleaning (with MeOH:H₂O, 95:5, v/v) had to be implemented before each isolation process. The purification process had to be repeated around 7 times. Finally, ~35 mg of *cis-trans* Candididin D with a purity of 85% was obtained (measured by HPLC-DAD).

My studies on preparative HPLC separation revealed that components of the Aureofacin and Candididin complexes similarly exhibited strong and irreversible adsorption to the chromatographic stationary phase in HPLC columns (silica gel - normal phase, modified silica with C18 - reversed phase). This phenomenon posed challenges during the preparative separation processes, particularly when a series of antibiotic complex separations were run. Decreased chromatographic resolution and peak broadening, leading to peak overlapping were observed. This was likely due to a reduction in the number of theoretical plates caused by persistent adsorption of the antibiotics, which blocked parts of the chromatographic bed. To cope with these issues, a regular column regeneration procedures were necessary. The regeneration process involved the use of a high-elution-strength solution (95% methanol) to increase the solubility of the remaining antibiotics. In 95% methanol, AHMs remained relatively soluble, while, they are not good soluble in ACN, used as a component of eluent of prep-HPLC procedure. During the antibiotic isolation on the prep-HPLC column, issues related to column overloading, both in terms of concentration and volume, were encountered. The implemented complex concentration (4 mg/mL) and injection volume (2.5 mL), set for a RP-18 column (250 mm x 25 mm, 10 µm) operation, corresponded to a single load of 10 mg of the complex per run, which is significantly lower than the typical sample load used for separation on reversed-phase prep-HPLC columns of these dimensions and pore diameters. Despite the limited capacity of the solvent system, Candididin D of high purity was successfully isolated, providing material of good quality for further studies.

4.6. Photoisomerization of AHMs and isolation of *all-trans* isomers

The previous studies performed at the Department of Pharmaceutical Technology and Biochemistry resulted in the discovery of a phenomenon of light-induced photoisomerization of *cis-trans* Candididin D into its *all-trans* isomer [33]. The assumption seemed justified that the same conversion could be possible for Vacidin and Gedamycin. Therefore, after the successful isolation of pure *cis-trans* AHMs, an attempt of their photoisomerization was made. The process was optimized by evaluating the light source, including a UV lamp (254 nm and 365 nm) and a xenon lamp (with filter of 380 nm). The solvent composition required for the photoisomerization process was also selected, with MeOH:H₂O (95:5, v/v) providing relatively good solubility for the antibiotics. Additionally, the optimal antibiotic exposure time for the light was determined.

The solutions of antibiotics in MeOH: H₂O (95:5, v/v) mixture, were exposed to the light of the long-wavelength UV-Vis lamp ($\lambda=365$ nm) for ~4 h. The progress of the photoisomerization process was verified using a UV-Vis spectrophotometer and HPLC-DAD. All three antibiotics underwent the photoisomerization process, which was manifested by changes in the UV-Vis spectrum and retention time. After completion of the photoisomerization process, the solvents were evaporated under reduced pressure as described in section 3.2.7. The identity of the obtained products was verified using UV-Vis spectroscopy and HPLC-DAD analysis according to section 3.2.5. The UV-Vis spectra results, based on the Vacidin *cis-trans* and *all-trans* isomers, are presented in Figure 37.

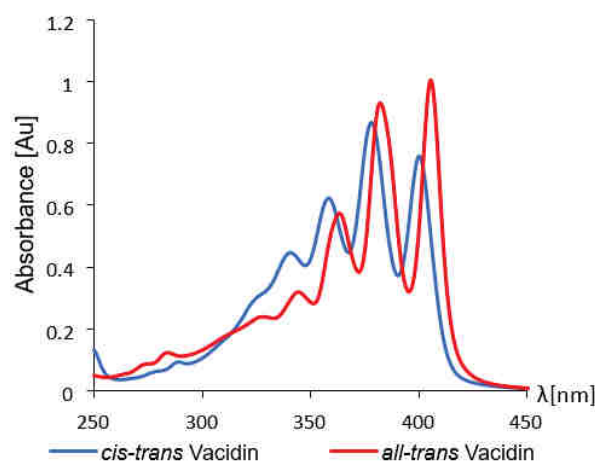


Figure 37. The UV-Vis spectrum of *cis-trans* and *all-trans* Vacidin at concentration 0.01 mg/mL in MeOH

UV-Vis spectra of the native *cis-trans* AHMs are characterized by three absorption maxima at $\lambda_1 = 360$ nm, $\lambda_2 = 378$ nm, and $\lambda_3 = 401$ nm, reflecting the system of seven conjugated double bonds. The intensity of the absorption band at λ_3 is lower than that at λ_2 . According to the literature, such relative intensities suggest the presence of internal Z double bonds [119]. The UV-Vis spectra of the AHMs photoisomers obtained in my research showed bathochromic shifts, with absorption maxima at $\lambda_1^* = 364$ nm, $\lambda_2^* = 384$ nm, and $\lambda_3^* = 407$ nm. Additionally, the relative intensities of λ_2^* and λ_3^* were reversed compared to the native compounds (λ_2 and λ_3). Such features of the UV-Vis spectrum were previously identified as characteristic of an *all-trans* heptaenic chromophore, similar to that found in AmB [168] and confirmed in studies on photoisomerization of Candicidin D by 2D NMR [33]. Structures of the obtained *all-trans* isomers of Vacidin and Gedamycin were also elucidated and the geometry of their chromophores was confirmed [145]. Results of HPLC-DAD analysis are shown in Figures 38-40.

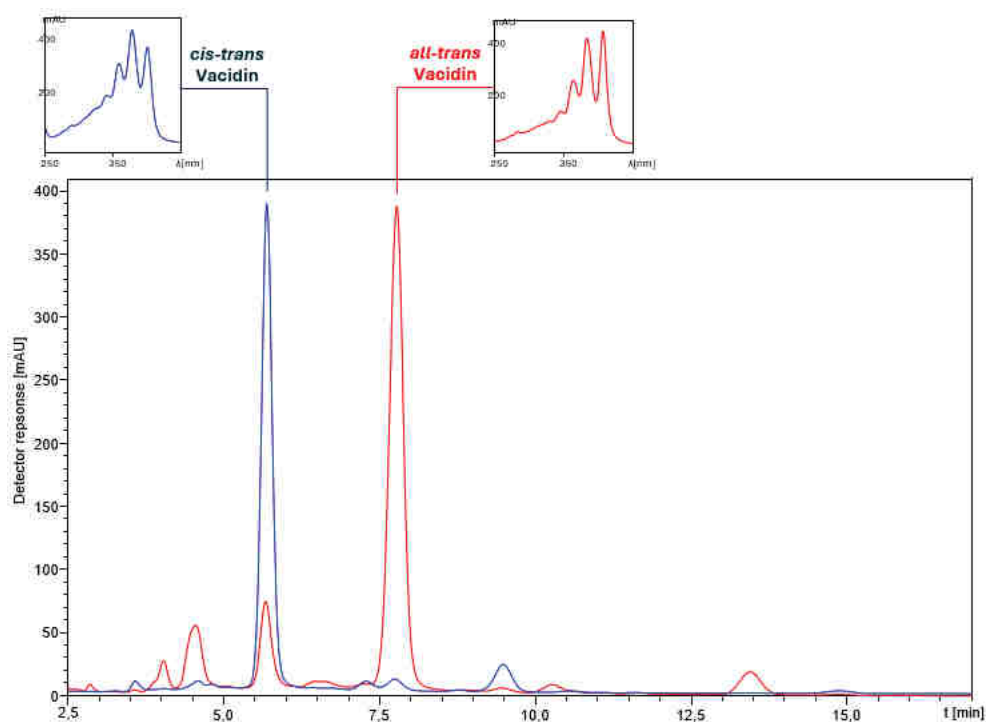


Figure 38. The overlay of HPLC-DAD chromatograms of *cis-trans* Vacidin sample (blue line), and *all-trans* Vacidin sample (red line).

Chromatographic conditions: column Luna 100 Å C18(2), (150 mm × 4.6 mm, 5 μm) ; mobile phase composition: 38% acetonitrile/ 62% ammonium acetate buffer (5.5 mmol, pH = 4.5) v/v; ω=1 mL/min; v_i = 20 μL, c= 2 mg/mL, λ=378 nm, RT

Figure 38 presents the overlay of chromatograms for two Vacidin isomers: *cis-trans* (blue line) and *all-trans* (red line). The *cis-trans* substrate eluted at 5.6 min and the *all-trans* product at 7.7 min.

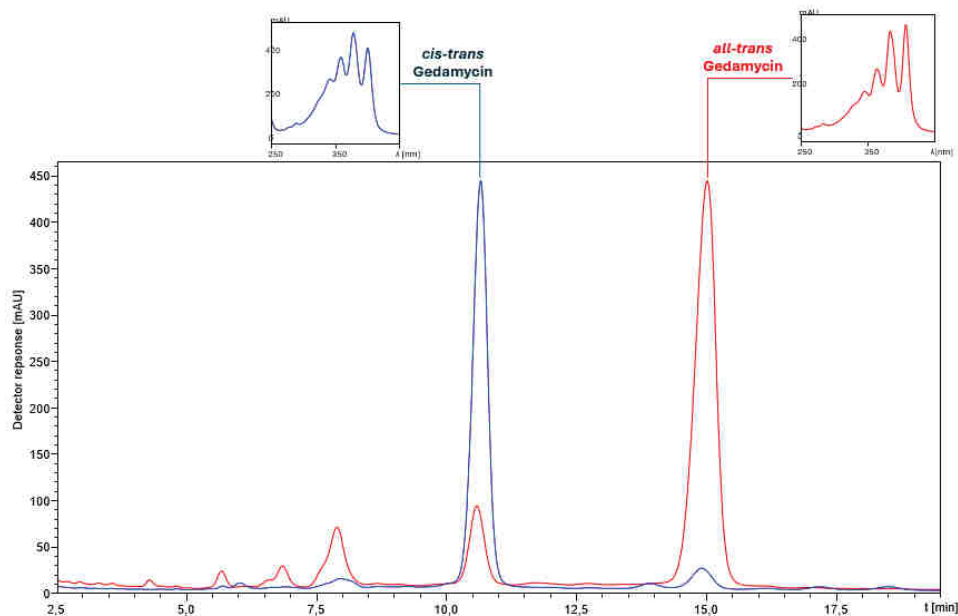


Figure 39. The overlay of HPLC-DAD chromatograms of *cis-trans* Gedamycin sample (blue line), *all-trans* Gedamycin sample (red line).

Chromatographic conditions: column Luna 100 Å C18(2), (150 mm × 4.6 mm, 5 μm) ; mobile phase composition: 38% acetonitrile/ 62% ammonium acetate buffer (5.5 mmol, pH = 4.5) v/v; ω =1 mL/min; v_i = 20 μL, c=2 mg/mL, λ=378 nm, RT

Figure 39 shows the overlay of chromatograms for two Gedamycin isomers: *cis-trans* (depicted by the blue trace) and *all-trans* (depicted by the red trace). The isomers eluted at distinct retention times: *cis-trans* at 10.3 min. and *all-trans* at 14.9 min.

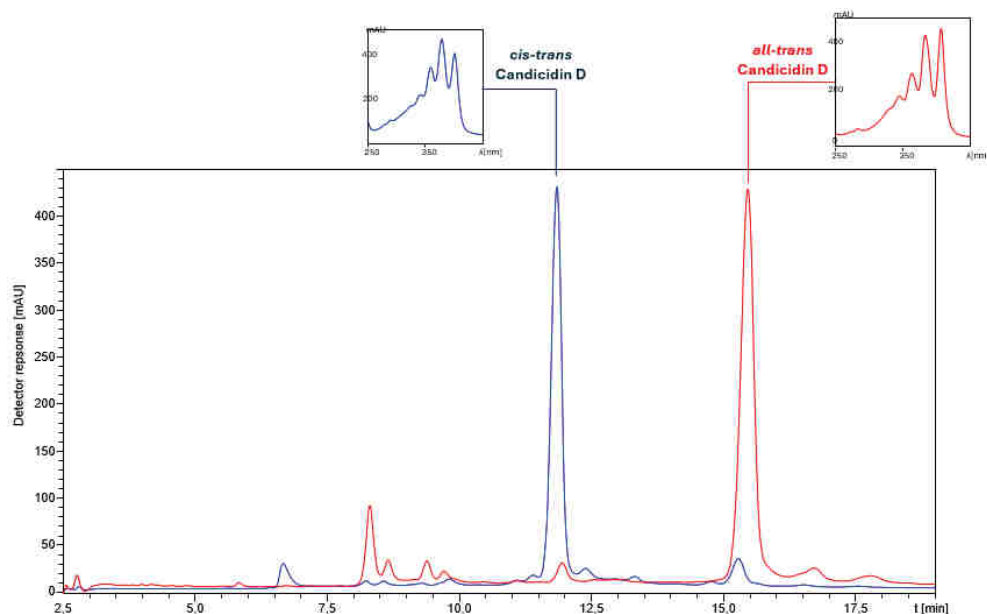


Figure 40. The overlay of HPLC-DAD chromatograms of *cis-trans* Candidicin D sample (blue line), *all-trans* Candidicin D sample (red line).
Chromatographic conditions: column Luna 100 Å C18(2), (150 mm × 4.6 mm, 5 µm) ; mobile phase composition: 38% acetonitrile/ 62% ammonium acetate buffer (5.5 mmol, pH = 4.5) v/v; ω = 1 mL/min; v_i = 20 µL, c = 2 mg/mL, λ = 378 nm, RT

Figure 40 illustrates the overlay of chromatograms for two isomers of Candidicin D: *cis-trans* (represented by the blue trace) and *all-trans* (represented by the red trace). The isomers eluted at distinct retention times, *cis-trans* at 11.8 min. and *all-trans* at 15.4 min.

The UV-Vis spectra obtained from the HPLC-DAD chromatograms provided confirmatory evidence for the photoisomerization reaction and enabled differentiation between the native form of an antibiotic (maximum absorbance at λ = 378 nm) and its isomer with altered chromophore geometry, *all-trans* (maximum absorbance at λ = 407 nm).

The final yields of photoisomerization were in the 49% – 55% range, as 32 mg of *all-trans* Candidicin D were formed from the 65 mg load of *cis-trans* Candidicin D, 27 mg of *all-trans* Gedamycin, from 50 mg the *cis-trans* isomer and 66 mg of *all-trans* Vacidin from 120 mg of *cis-trans* Vacidin. Conditions of the photoisomerization process were optimized to minimize the formation of degradation products. Photoisomerization also produces other stable products, such as those with retention times of 8 min in the HPLC-DAD chromatogram for Gedamycin sample (see Figure 39) and 4.5 min in the HPLC-DAD chromatogram for Vacidin sample (see Figure 38) as well as 8 min in the HPLC-DAD chromatogram for Candidicin D sample (see Figure 40). However, due to their low quantities, they were beyond the scope of potential structural studies.

To conclude, during this process, two *Z* double bonds in the chromophores were converted into the *E* form, and in consequence, a bathochromic shift in the UV spectrum was observed. It can be thus concluded, that the photoisomerization of AHMs occurs independently

of the positions of the *cis* double bonds in the polyene fragment. There are no known AHMs with Z-bonds in positions other than 26, 28 (Candicidin), and 28, 30 (Vacidin). Therefore, it is expected that photoisomerization of the other AHMs would occur in a similar manner, e.g., for Trichomycin, which also contains a *cis-trans* chromophore [169]. Furthermore, the results of our studies have demonstrated that the light-induced transformations of Candicidin D [33], Vacidin, and Gedamycin (this work) lead to yielding stable isomers.

Based on the conducted experiments, it can be concluded that photoisomerization for Vacidin and Gedamycin proceeds according to a simplified scheme. The schemes of photoisomerization reaction from native Vacidin and Gedamycin to their *all-trans* isomers are presented in Figures 41-42.

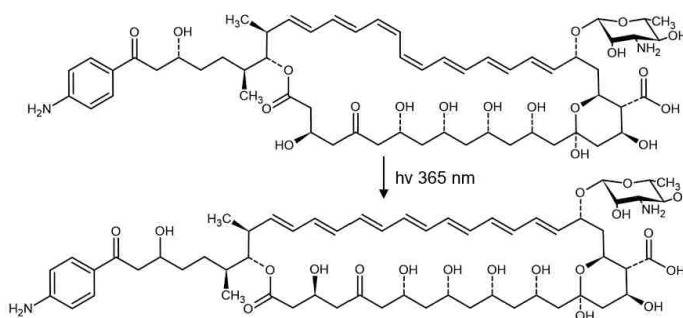


Figure 41. The scheme of the photoisomerization of *cis-trans* Vacidin to *all-trans* Vacidin

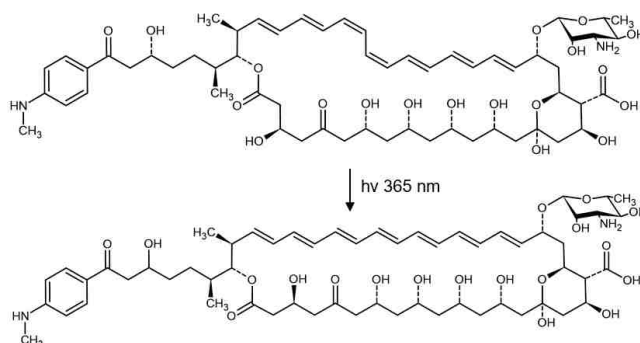


Figure 42. The scheme of the photoisomerization of *cis-trans* Gedamycin to *all-trans* Gedamycin

4.6.1. Isolation of *all-trans* AHMs by preparative HPLC

The post-reaction mixtures contained also some unidentified products of degradation. Therefore, due to the heterogeneity of the post-reaction mixtures, an additional isolation step using prep-HPLC was required.

The isolation procedure for the *all-trans* isomers was identical to that employed for *cis-trans* Candicidin D (section 3.2.6.), only the monitored detector wavelength was 407 nm as it corresponds to the highest absorbance maximum for *all-trans* antibiotics. Chromatograms of the prep-HPLC-DAD separations of components of the post-reaction mixtures are presented in Figures 43-45. The fractions were given in minutes, and the volume of the collected fractions was calculated based on the applied flow rate (29.5 mL/min).

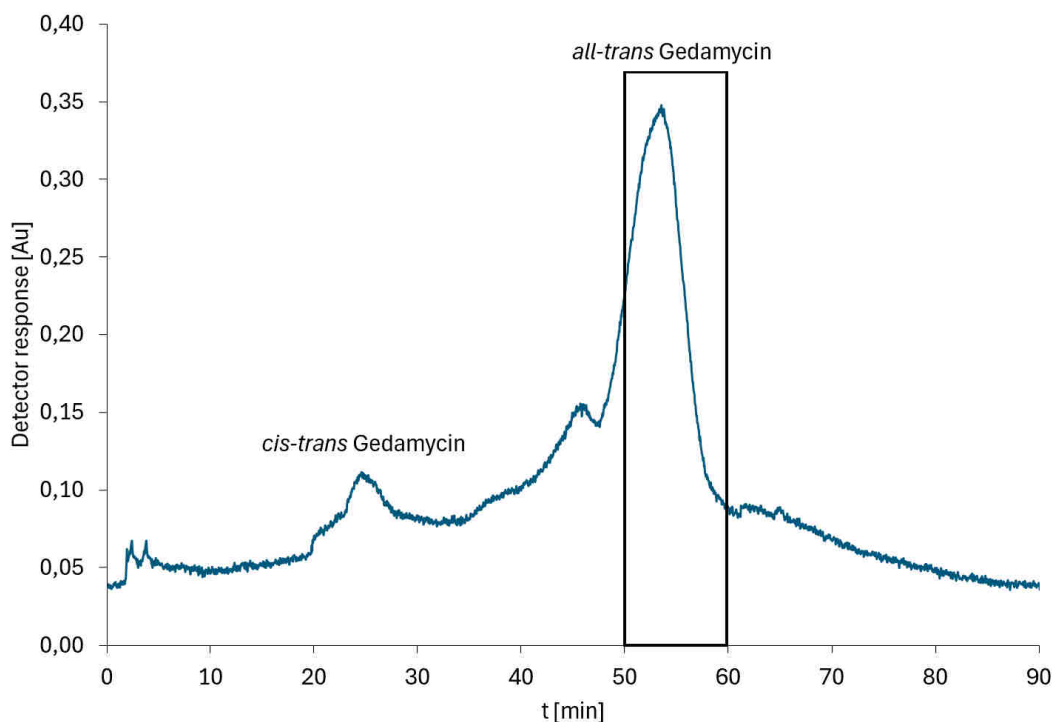


Figure 43. Chromatogram of the prep-HPLC-DAD separation of components of the post-reaction mixture after photoisomerization of *cis-trans* Gedamycin. *All-trans* Gedamycin collected fractions marked by black rectangle

Conditions: Column: Merck, LiChrospher, RP-18 (250 mm x 25 mm, 10 μ m); mobile phase: 38% ACN/ 62% ammonium acetate (5.5 mmol, pH=4.5), v/v; ω = 29.5 mL/min; c=4 mg/mL dissolved in the following solvent system DMSO: MeOH: ammonium acetate (5.5 mmol, pH=4.5) (1:4:5, v/v/v), v_i =2.5 mL, RT, λ =407 nm

As shown in Figure 43, two major components, namely the isoforms of Gedamycin were present in the mixture. *Cis-trans* Gedamycin eluted at 20-30 min. and its *all-trans* isomer at 48-60 min. Fractions between 50 - 60 min (black rectangle) were collected and pooled. 885 mL of collected fractions, equal to an approximate total loading of 30 mg of the antibiotic onto the column (around 3 runs) were required to obtain 3 mg of the *all-trans* Gedamycin. The final purity of the obtained *all-trans* Gedamycin preparation was 88%, as assessed by HPLC-DAD.

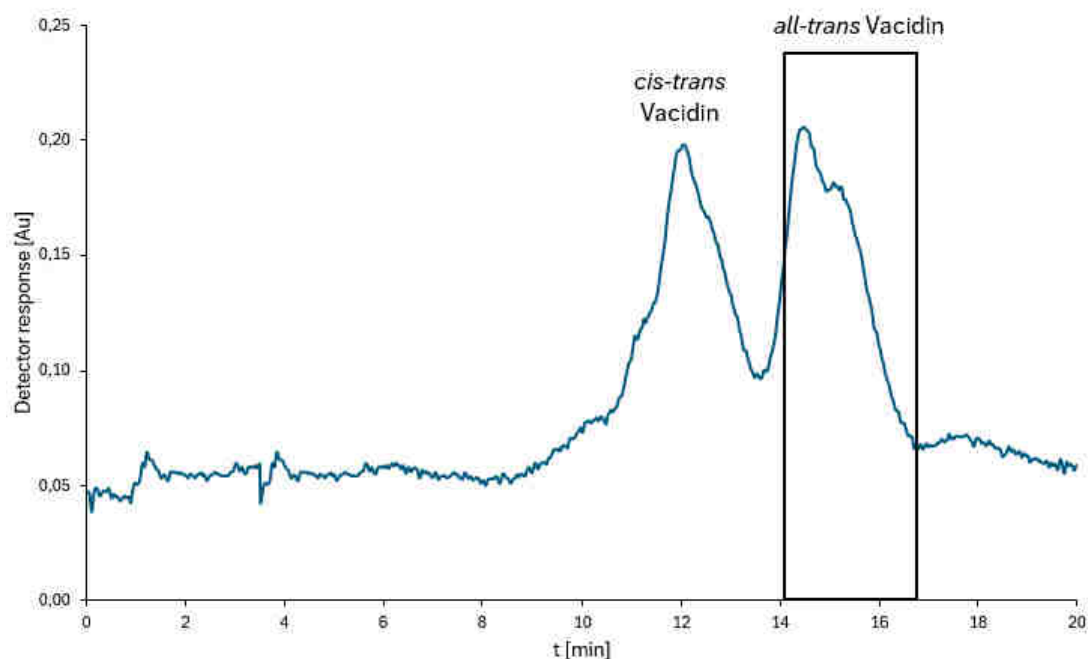


Figure 44. Chromatogram of the prep-HPLC-DAD separation of components of the post-reaction mixture after photoisomerization of *cis-trans* Vacidin. *All-trans* Vacidin collected fractions marked by black rectangle.

Conditions: column: Merck, LiChrospher, RP-18 (250 mm x 25 mm, 10 μ m); mobile phase: 38% ACN/ 62% ammonium acetate (5.5 mmol, pH=4.5), v/v; ω = 29.5 mL/min; c=4 mg/mL dissolved in the following solvent system DMSO: MeOH: ammonium acetate (5.5 mmol, pH=4.5) (1:4:5, v/v/v), v_i =2.5 mL, RT, λ =407 nm

As shown in Figure 44, two major components, namely the isoforms of Vacidin were present in the mixture. *Cis-trans* Vacidin eluted at 10-13.5 min and its *all-trans* isomer at 13.6-16.5 min. Fractions between 14.1-16.5 min (black rectangle) were collected and pooled. 566 mL of collected fractions, equal to an approximate total loading of 80 mg of the antibiotic onto the column (around 8 runs) were required to obtain 6 mg of the *all-trans* Vacidin. The final purity result of *all-trans* Vacidin was 88%.

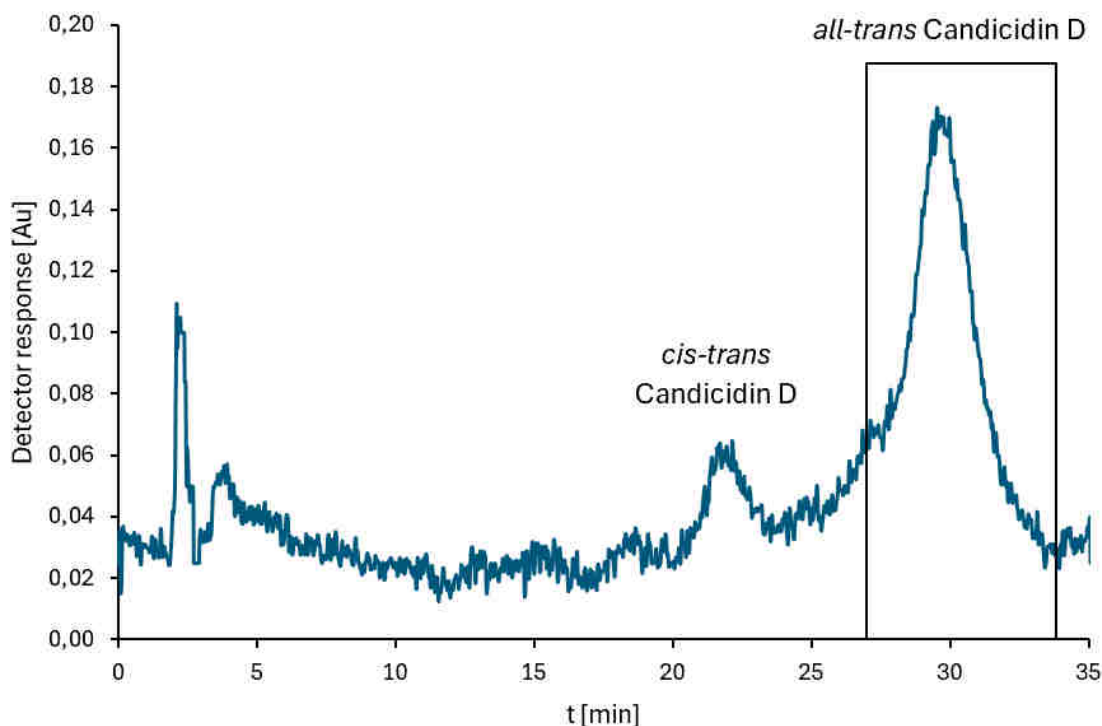


Figure 45. Chromatogram of the prep-HPLC-DAD separation of components of the post-reaction mixture after photoisomerization of *cis-trans* Candididin D. *All-trans* Candididin D collected fractions marked by black rectangle.

Conditions: column: Merck, LiChrospher, RP-18 (250 mm x 25 mm, 10 μ m); mobile phase: 38% ACN/ 62% ammonium acetate (5.5 mmol, pH=4.5), v/v; ω = 29.5 mL/min; c=4 mg/mL dissolved in the following solvent system DMSO: MeOH: ammonium acetate (5.5 mmol, pH=4.5) (1:4:5, v/v/v), v_i =2.5 mL, RT, λ =407 nm

As shown in Figure 45, two major components, namely the isoforms of Candididin D were present in the mixture. *Cis-trans* Candididin D eluted at 20-23 min and its *all-trans* isomer at 24.5-34.5 min. Fractions between 27-34 min (black rectangle) were collected and pooled. 1239 mL of collected fractions, equal to an approximate total loading of 60 mg of the antibiotic onto the column (around 6 runs) were required to obtain 6 mg of the antibiotic *all-trans* Candididin D with 82% purity.

The low efficiency of the process is due to the low solubility of the separated compounds in most organic solvents, e.g. in ACN, which is used in the selected solvent system. In addition, since the process is performed in reverse-phase mode, a non-organic solvent/water-based solution must be used to achieve the desired elution strength and effective separation. However, this reduces the solubility of the target compounds, as they are not water-soluble, and maintaining a stable pH of 4.5 does not resolve this phenomenon.

4.7. Final identification and purity determination of the isolated *cis-trans* and *all-trans* AHMs

The method using the LC system combined with DAD-ESIMS served for the determination of final confirmation of the purity of the obtained compounds. Samples' quality and quantity before and after the light-induced isomerization were determined. The HPLC-DAD-ESI-

MS chromatograms of isolated *cis-trans* and *all-trans* antibiotics are presented in Figures 46- 51.

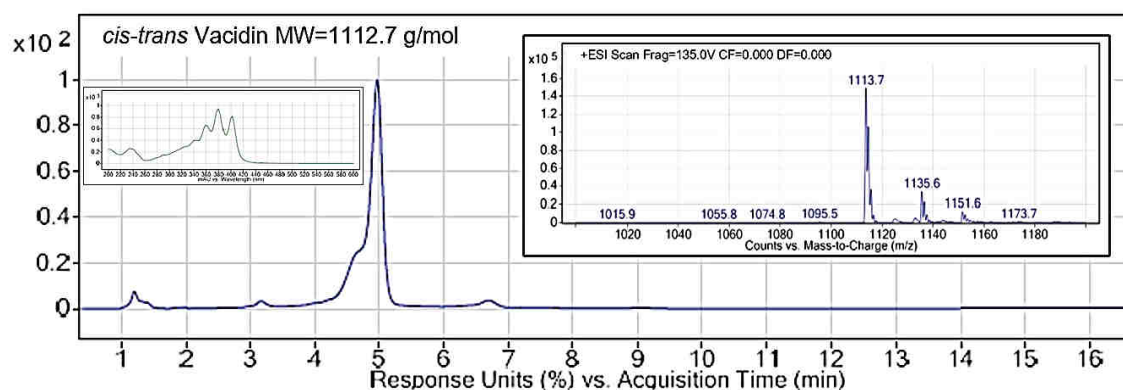


Figure 46. The superimposed HPLC-DAD-ESI-MS chromatogram of *cis-trans* Vacidin. Mass spectrum recorded in positive electrospray ionization mode.

Chromatographic conditions: column Luna 100 Å C18(2), (150 mm × 4.6 mm, 5 μm); mobile phase composition: 38% acetonitrile/ 62% ammonium acetate buffer (5.5 mmol, pH = 4.5), v/v; ω=1 mL/min; v_i = 20 μL, c= 2 mg/mL, λ=378 nm, RT

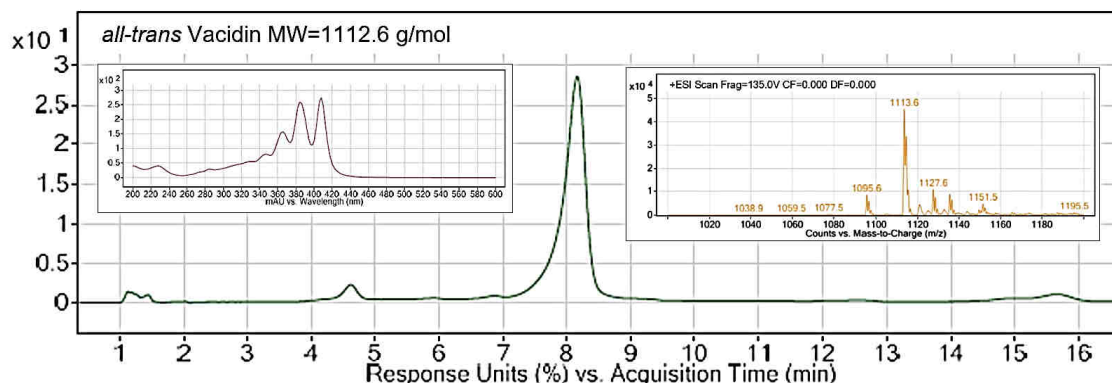


Figure 47. The superimposed HPLC-DAD-ESI-MS chromatogram of *all-trans* Vacidin. Mass spectrum recorded in positive electrospray ionization mode.

Chromatographic conditions: column Luna 100 Å C18(2), (150 mm × 4.6 mm, 5 μm); mobile phase composition: 38% acetonitrile/ 62% ammonium acetate buffer (5.5 mmol, pH = 4.5), v/v; ω=1 mL/min; v_i = 20 μL, c= 2 mg/mL, λ=407 nm, RT

Figures 46- 47 present the chromatograms of two Vacidin isomers: *cis-trans* and *all-trans*, respectively. LC-MS analysis allowed to confirm the molecular masses of the isolated antibiotics as 1112.7 g/mol in both cases, indicating the isolation of isomers of “the same” compound. The elution occurred at distinct retention times: 4.9 min for *cis-trans* isomer and 8.2 min for its *all-trans* counterpart. The UV-Vis spectra provided confirmatory evidence of the photoisomerization reaction and enabled differentiation between the native form of the antibiotic (maximum absorbance at λ = 378 nm) and the isomer with altered chromophore geometry, *all-trans* (maximum absorbance at λ = 407 nm).

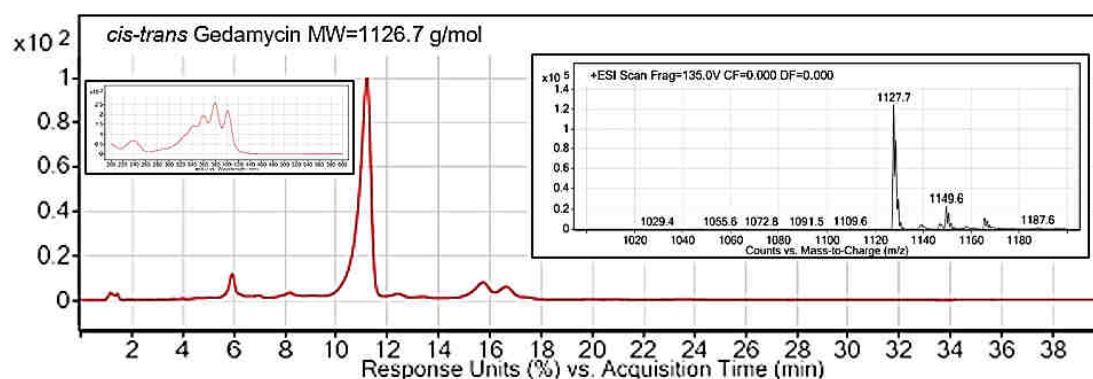


Figure 48. The superimposed HPLC-DAD-ESI-MS chromatogram of *cis-trans* Gedamycin. Mass spectrum recorded in positive electrospray ionization mode.

Chromatographic conditions: column Luna 100 Å C18(2), (150 mm × 4.6 mm, 5 μm); mobile phase composition: 38% acetonitrile/ 62% ammonium acetate buffer (5.5 mmol, pH = 4.5), v/v; ω=1 mL/min; v_i = 20 μL, c= 2 mg/mL, λ=378 nm, RT

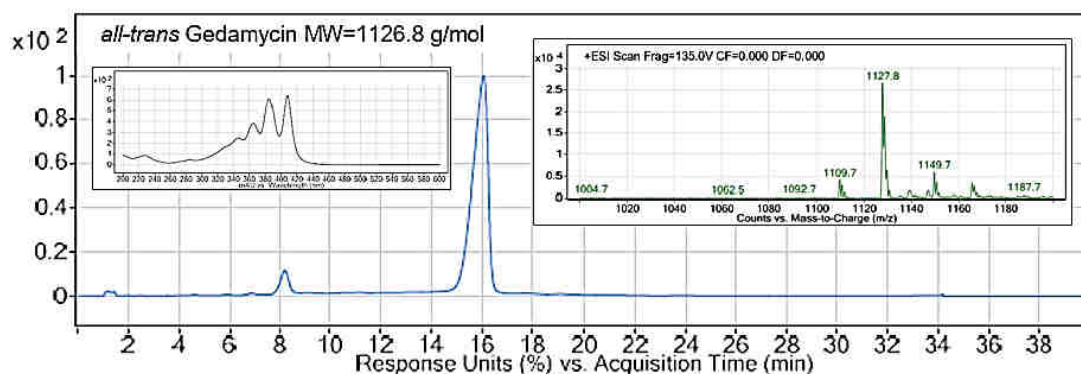


Figure 49. The HPLC-DAD-ESI-MS chromatogram of *all-trans* Gedamycin. Mass spectrum recorded in positive electrospray ionization mode.

Chromatographic conditions: column Luna 100 Å C18(2), (150 mm × 4.6 mm, 5 μm); mobile phase composition: 38% acetonitrile/ 62% ammonium acetate buffer (5.5 mmol, pH = 4.5), v/v; ω = 1 mL/min; v_i = 20 μL, c=2 mg/mL, λ=407 nm, RT

Figures 48-49 show the chromatograms of two Gedamycin isomers: *cis-trans* and *all-trans*, respectively. LC-MS analysis confirmed that both isomers had identical molecular masses of 1126.7 g/mol, indicating they represented the same compound. Moreover, the isomers eluted at distinct retention times: 11.7 for *cis-trans* and 16.0 minutes for *all-trans*. UV-Vis spectra confirmed the photoisomerization process, allowing differentiation between the native form of the antibiotic (λ_{max} = 378 nm) and the isomer with modified chromophore geometry, *all-trans* (λ_{max} = 407 nm).

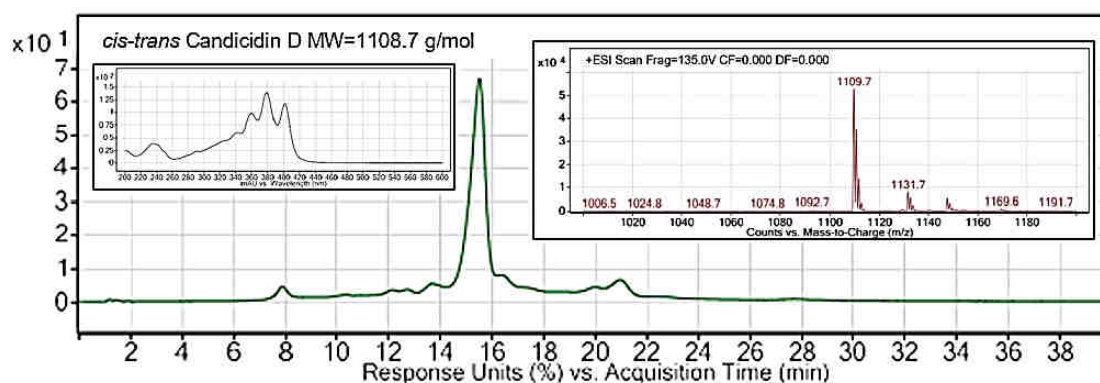


Figure 50. The HPLC-DAD-ESI-MS chromatogram of *cis-trans* Candicidin D. Mass spectrum recorded in positive electrospray ionization mode.

Chromatographic conditions: column Luna 100 Å C18(2), (150 mm × 4.6 mm, 5 μm) ; mobile phase composition: 38% acetonitrile/ 62% ammonium acetate buffer (5.5 mmol, pH = 4.5), v/v; ω =1 mL/min; v_i = 20 μL, c= 2 mg/mL, λ=378 nm, RT

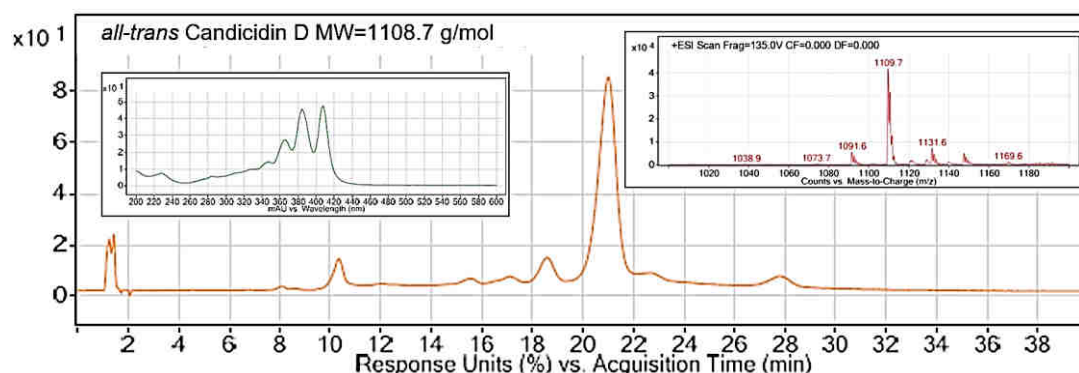


Figure 51. The HPLC-DAD-ESI-MS chromatogram of *all-trans* Candicidin D. Mass spectrum recorded in positive electrospray ionization mode

Chromatographic conditions: column Luna 100 Å C18(2), (150 mm × 4.6 mm, 5 μm) ;mobile phase composition: 38% acetonitrile/ 62% ammonium acetate buffer (5.5 mmol, pH = 4.5), v/v; ω =1 mL/min; v_i = 20 μL, c= 2 mg/mL, λ=407 nm, RT

Figures 50- 51 illustrate the chromatograms of two isomers of Candicidin D: *cis-trans* and *all-trans*. LC-MS analysis confirmed that both isomers possessed identical molecular masses of 1108.7 g/mol, signifying the isolation of the same isomer. The isomers eluted at different retention times 15.6 min. for *cis-trans* and 21.2 min for *all-trans*. The UV-Vis spectral analysis corroborated the occurrence of the photoisomerization process, distinguishing the native form of the antibiotic (λ_{max} = 378 nm) from the isomer with altered chromophore geometry, *all-trans* (λ_{max} = 407 nm).

The values of m/z for molecular ions $[M+H]^+$ of tested antibiotics are summarized μpin Table 31.

Table 31. The m/z values of the molecular ions $[M + H]^+$ obtained for the analyzed antibiotics.

Antibiotic	$m/z [M + H]^+$	
	<i>Cis-trans</i>	<i>All-trans</i>
Gedamycin	1127.7	1127.8
Vacidin	1113.7	1113.6
Candicidin D	1109.7	1109.7

In ESI+ the m/z of pseudomolecular ion $[M + H]^+$ differ from the molecular weight of the compound by 1, suggesting the additional proton presence in the structure due to the protonation of the tested molecule. Therefore, for both isomers of each antibiotic - Gedamycin, Vacidin, and Candicidin D, the molecular masses, which are the same for both isomers of the antibiotic, are equal to 1126.7 g/mol, 1112.7 g/mol, and 1108.7 g/mol, respectively. The HPLC-DAD-ESI-MS analysis revealed the identity of the *cis-trans* and *all-trans* forms of antibiotics – Vacidin, Gedamycin, and Candicidin D. Obviously, an identity of molecular masses and UV-Vis spectra were not definitive evidence for the structural identity of examined compounds, but their structures were confirmed in [33][145] by 2D NMR, and above data are in full agreement with the LC-MS data accompanying the 2D NMR.

Furthermore, based on the HPLC chromatograms (Figures 46- 51), the purity of isolated antibiotics in obtained preparation after CPC and prep-HPLC separation processes was determined, and the results are presented in Table 32.

Table 32. Obtained purity results of isolated antibiotics in the preparations after CPC and prep-HPLC separation process.

Antibiotic	Antibiotic purity [%]
<i>cis-trans</i> Vacidin	87
<i>cis-trans</i> Gedamycin	86
<i>cis-trans</i> Candicidin D	85
<i>all-trans</i> Vacidin	88
<i>all-trans</i> Gedamycin	88
<i>all-trans</i> Candicidin D	82

The results presented in Table 32 show that the *cis-trans* and *all-trans* AHMs were isolated at a high level of purity, which ranges between 82-88%. To sum up, the analyses of HPLC-DAD-ESI-MS confirmed the identity of the isolated compounds and allowed to establish their purity degree. It was possible to isolate *cis-trans* Vacidin, *cis-trans* Gedamycin, *cis-trans* Candicidin D and *all-trans* Vacidin, *all-trans* Gedamycin, and *all-trans* Candicidin D at a high purity level.

Completing this stage allowed me to start the next part of the doctoral project i.e. determination of the biological activity of the obtained antibiotics and their behavior in the lipid bilayers.

4.8. Biological activity studies

The isolated *cis-trans* and *all-trans* isomers of Gedamycin, Vacidin, and Candicidin D were the subject of my further studies aimed at the determination of their biological properties, including antifungal *in vitro* activity, hemolytic activity, and cytotoxicity against mammalian cells. The non-aromatic heptaene antibiotic Amphotericin B was included as a reference compound in these studies.

4.8.1. Determination of antifungal activity (MIC assay)

Antifungal *in vitro* activity of isolated AHMs in comparison with AmB was studied against the fungal strains presented in Table 16 by a serial dilution microplate method. Values of MIC₉₀ is defined as a minimal concentration of an antifungal agent tested causing 90% growth inhibition. Determination was performed in two growth media, namely RPMI 1640 and BDS. The composition of the former simulates the composition of low molecular weight compounds pool found in human plasma and for this reason, is recommended by CLSI for determination of antifungal activity. In my studies, the determination of MIC in this medium was performed strictly under conditions described in CLSI protocol [158]. The BDS medium was used in the previous studies on the properties of AHMs [25].

The activity of the antibiotics was assessed in RPMI 1640 medium over a concentration range from 0.03 µg/mL to 16 µg/mL and in the BDS at a concentration range of 0.0015 µg/mL – 1 µg/mL. The results obtained are shown in Tables 33 and 34.

Table 33. MIC values of Gedamycin, Vacidin, and Candicidin D isomers and Amphotericin B (AmB) against human pathogenic yeasts of *Candida* genus and *S. cerevisiae* determined in RPMI 1640 medium under condition recommended by CLSI.

	MIC (µg/mL)						
	Candicidin D		Gedamycin		Vacidin		AmB
	<i>cis-trans</i>	<i>all-trans</i>	<i>cis-trans</i>	<i>all-trans</i>	<i>cis-trans</i>	<i>all-trans</i>	
<i>C. albicans</i> ATCC 10231	0.25	0.5	0.25	1.0	0.25	0.5	0.25
<i>C. glabrata</i> DSM II 226	0.5	0.5	0.125	0.5	0.125	0.25	1.0
<i>C. krusei</i> DSM 6128	0.25	0.25	0.125	0.5	0.5	0.5	0.5
<i>C. parapsilosis</i> DSM 5784	0.25	0.06	0.06	0.125	0.25	0.125	0.5
<i>C. dubliniensis</i> CBS 7987	0.25	0.125	0.125	0.5	0.25	0.25	0.25
<i>C. guilliermondii</i> DSM 11947	1.0	0.5	0.5	0.5	1.0	1.0	0.25
<i>C. famata</i> DSM 3428	1.0	1.0	1.0	1.0	1.0	1.0	1.0
<i>C. rugosa</i> DSM 2031	1.0	1.0	1.0	1.0	1.0	1.0	2.0
<i>S. cerevisiae</i> ATCC 9763	0.5	0.25	0.125	0.5	0.125	0.25	0.5

Table 34. MIC values of Gedamycin, Vacidin, and Candicidin D isomers and Amphotericin B (AmB) against human pathogenic yeasts of *Candida* genus and *S. cerevisiae* determined in BDS medium.

	MIC (µg/mL)						
	Candicidin D		Gedamycin		Vacidin		AmB
	<i>cis-trans</i>	<i>all-trans</i>	<i>cis-trans</i>	<i>all-trans</i>	<i>cis-trans</i>	<i>all-trans</i>	
<i>C. albicans</i> ATCC 10231	0.003	0.003	0.002	0.006	0.002	0.003	0.06
<i>C. glabrata</i> DSM II 226	0.006	0.003	0.002	0.006	0.002	0.006	0.25
<i>C. krusei</i> DSM 6128	0.006	0.003	0.002	0.006	0.003	0.003	0.25
<i>C. parapsilosis</i> DSM 5784	0.01	0.006	0.003	0.006	0.006	0.006	0.125
<i>C. dubliniensis</i> CBS 7987	0.002	0.002	0.001	0.006	0.002	0.002	0.06
<i>C. guilliermondii</i> DSM 11947	0.03	0.03	0.006	0.03	0.01	0.01	0.125
<i>C. famata</i> DSM 3428	0.01	0.03	0.01	0.05	0.01	0.05	0.25
<i>C. rugosa</i> DSM 2031	0.03	0.03	0.03	0.05	0.03	0.03	0.125
<i>S. cerevisiae</i> ATCC 9763	0.006	0.006	0.002	0.001	0.003	0.003	0.06

The MIC values of AmB and AHMs in RPMI 1640 medium ranged between 0.06 µg/mL and 2 µg/mL. In general, the activity of AHMs in this medium was comparable to that of AmB, although in most cases the MIC values of AHMs were slightly (2-4 fold) lower than that of AmB. *C. famata* and *C. rugosa* were somewhat less susceptible to all tested antibiotics than other species. Differences in MIC values between respective *cis-trans* and *all-trans* isomers of a given AHM were maximally 4-fold. *All-trans* Candicidin D was equally or slightly more active than *cis-trans* Candicidin D (except for *C. albicans*). *All-trans* Gedamycin and *all-trans* Vacidin were generally equally or slightly less active than their *cis-trans* isomers.

The MIC values determined in the BDS medium, ranging between 0.001 µg/mL to 0.25 µg/mL, were generally lower than those determined in RPMI 1640. In the case of AmB, this difference was relatively small (2-4-fold) but the activity of AHMs was higher by about two orders of magnitude. Both isomers of Candicidin D were equally active or a slightly higher activity was observed for the *all-trans* isomer, except for *C. famata*. Conversely, the *all-trans* isomers of Gedamycin and Vacidin generally exhibited lower activity compared to their *cis-trans* counterparts, yet they remained more active than AmB.

The MIC values determined in my studies in BDS medium were consistent with the literature data [25][119]. Obviously, in the case of aromatic AHMs, the *in vitro* activity data presented in the cited literature were determined for their native forms, *i.e.* the *cis-trans* isomers. The MIC₉₀ values of AmB determined in RPMI 1640 medium were also in good agreement with previous reports (Table 35). On the other hand, the antifungal *in vitro* activity of AHMs has never been determined in RPMI 1640 medium before, so any comparison with previous data is not possible. Nevertheless, since RPMI 1640 is the medium recommended as a standard for the determination of *in vitro* growth inhibitory activity of antifungals, a comparison of AHMs' activity

in this medium seems to provide more reliable results in terms of predicting possible *in vivo* activity of these compounds.

Table 35. Comparison of AmB MIC₉₀ values determined against four representatives of *Candida* spp. In RPMI 1640 medium under CLSI-recommended conditions.

AmB MIC ₉₀ [µg/mL]			
Fungal strain	This work	Other works	References
<i>C. albicans</i>	0.25	≤1 0.25-1 0.5	[170] [64] [171]
<i>C. glabrata</i>	1.0	≤1 0.25-2 1.0 -2.0	[170] [64] [171]
<i>C. krusei</i>	0.5	0.75-2 2 0.5-1.0	[170] [64] [171]
<i>C. parapsilosis</i>	0.5	≤1 1 0.5-2	[170] [64] [171]

A significant difference in the antifungal activity of macrolide heptaenes was observed when tested in the used media. To verify the influence of the media content on the obtained results, there were performed the experiments with its modification; BDS pH=7.0, BDS with 0.25% NaCl or 1% NaCl, RPMI 1640 without MOPS, RPMI pH=5.2 and pH=5.6. The results are presented in Tables 36, 37.

Table 36. MIC values of Gedamycin, Vacidin, and Candicidin D isomers and Amphotericin B (AmB) against *C. albicans* SC 5314 determined in BDS medium and its modification.

Compound	isomer	BDS	BDS pH=7.0	BDS with 0.25% NaCl	BDS with 1% NaCl
AmB	-	0.063	>0.125	0.063	0.031
Candicidin	<i>cis-trans</i>	0.008	0.016	0.016	0.008
	<i>all-trans</i>	0.004	0.008	0.008	0.004
Vacidin	<i>cis-trans</i>	0.008	0.016	0.008	0.008
	<i>all-trans</i>	0.016	0.031	0.016	0.016
Gedamycin	<i>cis-trans</i>	0.002	0.008	0.004	0.002
	<i>all-trans</i>	0.004	0.008	0.004	0.004

Table 37. MIC values of Gedamycin, Vacidin, and Candicidin D isomers and Amphotericin B (AmB) against *C. albicans* SC 5314 determined in RPMI 1640 medium and its modification.

Compound	isomer	RPMI 1640	RPMI 1640 without MOPS	RPMI 1640 pH=5.2	RPMI 1640 pH=5.6
AmB	-	0.5	0.5	1	0.5
Candicidin	<i>cis-trans</i>	1	1	1	1
	<i>all-trans</i>	1	1	1	1
Vacidin	<i>cis-trans</i>	0.5	0.5	0.5	0.5
	<i>all-trans</i>	1	1	2	1
Gedamycin	<i>cis-trans</i>	0.5	0.25	0.5	0.5
	<i>all-trans</i>	0.5	0.25	0.5	0.5

The obtained MIC values are comparable within the medium with implemented modifications (pH and salt concentration - Tables 36, 37) and could not give the exact answer for the observed MIC difference in the used media. It was also found that activity in RPMI 1640

medium without MOPS, a compound that stabilizes the pH of the medium during yeast cell growth, was exactly the same as in the case of the medium with stabilized pH (supplemented with this compound). These observations confirm that multiple factors can contribute to the observed important differences in the antifungal potential of the investigated antibiotics in BDS and RPMI 1640 media. So far we were not able to identify the reason (component/components of RPMI 1640) - it could be assumed that multiple factors contribute to it.

4.8.2. Determination of hemolytic activity

A hemolysis test was conducted on human red blood cells provided by the Regional Center for Blood Donation and Blood Treatment in Gdansk. Hemolytic activity was assessed using the procedure detailed in section 3.2.10., and the results were calculated according to equation 3.2.10.1. The determined parameter was EH_{50} , i.e. concentration of a given antibiotic at which 50% lysis of RBCs is observed. The values obtained are shown in Table 38.

Table 38. The hemolytic activity of the analyzed compounds, determined as EH_{50} values. The maximal final concentration of analyzed compounds was 50 $\mu\text{g/mL}$. AmB – Amphotericin B.

EH_{50} [$\mu\text{g/mL}$]		
Compound	<i>cis-trans</i> isomer [$\mu\text{g/mL}$]	<i>all-trans</i> isomer [$\mu\text{g/mL}$]
Candididin D	7.53 ± 0.82	16.67 ± 1.40
Vacidin	0.66 ± 0.09	37.32 ± 0.02
Gedamycin	1.28 ± 0.68	>50
AmB	3.46 ± 0.15	

The results obtained in my study align with the literature data available for native, i.e. *cis-trans* AHMs and AmB (Table 39).

Table 39. Comparison of EH_{50} data of *cis-trans* AHMs and AmB. AHMs – aromatic heptaene macrolides, AmB- Amphotericin B.

Antibiotic	EH_{50} [$\mu\text{g/mL}$]		References
	This work	Literature result [$\mu\text{g/ml}$]	
<i>Cis-trans</i> Candididin D	7.53	2	[25]
<i>Cis-trans</i> Gedamycin	1.28	0.4	
<i>Cis-trans</i> Vacidin	0.66	0.2	
AmB	3.46	1.6	[172]
		3.16	

Data presented in Table 38 indicates that the *all-trans* AHMs and *cis-trans* Candididin D exhibited lower hemolytic activity than Amphotericin B, while the *cis-trans* isomers of Vacidin and Gedamycin demonstrated higher hemotoxicity. In general, the *all-trans* AHMs were less hemolytic than their *cis-trans* isomers. This difference was small for isomers of Candididin D, and much more remarkable for Vacidin isomers, whereas *all-trans* Gedamycin was not hemolytic at all.

The hemolytic activity of *all-trans* isomers of AHMs was determined for the first time. According to the assumptions of this doctoral thesis, the straightening of the chromophore of *cis-trans* isomers due to the photoisomerization to their *all-trans* counterparts rigidifies the macrolide ring (i.e., lowers its conformational freedom), making AHMs “more similar” to AmB. This was confirmed in 2D-NMR studies conducted by our research team [33][131].

It is possible that the change in the chromophore geometry of AHMs molecules significantly disturbs their interactions with cholesterol in the membrane while having very little stimulating effect on interactions with ergosterol, which presumably might result in reduced hemotoxicity of *all-trans* AHMs. This assumption was partially supported by the results of molecular modeling of binary AHM/sterol complexes [120].

Structurally, *all-trans* AHMs and AmB differ in the presence of a side chain and a polyol fragment. The research conducted as part of this doctoral work sheds new light on the previously accepted assumption that the side chain plays a significant role in the activity of these compounds. It has been demonstrated that, despite the presence of the side chain, the hemolytic activity is lower for *all-trans* antibiotics in comparison to AmB. However, it cannot be completely ruled out that the side chain influences the mechanism of action of AHMs. The presence of the *p*-aminoacetophenone moiety in the structure of AHMs may serve as a molecular "anchor" for the compound within the membrane. The aromatic side chain presumably could facilitate the rapid formation of two-barrel channel structures, enhance their stabilization, and promote more effective penetration of the antibiotic molecule into the membrane through hydrophobic interactions. This could explain the observed differences in hemolytic activity in *in vitro* studies.

4.8.3. Calculation of selective toxicity indexes values of AHMs isomers and AmB (STI_{HEM})

Determination of MIC_{90} and EH_{50} values for AHMs allowed calculation of their selective toxicity indexes (STI_{HEM}). STI_{HEM} was calculated as the $EH_{50}:MIC_{90}$ ratio, where MIC_{90} was the value determined against *C. albicans* in RPMI 1640 or BDS medium. The results are presented in Tables 40 and 41.

Table 40. Selective toxicity indexes (STI_{HEM}) of *cis-trans* Candididin D, *cis-trans* Gedamycin, *cis-trans* Vacidin, their *all-trans* isomers, and Amphotericin B (AmB). $STI_{HEM} = EH_{50}/MIC_{90}$ against *C. albicans* in RPMI 1640 medium.

Compound	<i>cis-trans</i> Candididin D	<i>all-trans</i> Candididin D	<i>cis-trans</i> Gedamycin	<i>all-trans</i> Gedamycin	<i>cis-trans</i> Vacidin	<i>all-trans</i> Vacidin	AmB
STI_{HEM}	30.12	33.34	5.12	>50	2.64	75	13.84

Table 41. Selective toxicity indexes (STI_{HEM}) of *cis-trans* Candididin D, *cis-trans* Gedamycin, *cis-trans* Vacidin, their *all-trans* isomers, and Amphotericin B (AmB). $STI_{HEM} = EH_{50}/MIC_{90}$ against *C. albicans* in BDS medium.

Compound	<i>cis-trans</i> Candididin D	<i>all-trans</i> Candididin D	<i>cis-trans</i> Gedamycin	<i>all-trans</i> Gedamycin	<i>cis-trans</i> Vacidin	<i>all-trans</i> Vacidin	AmB
STI_{HEM}	2510	5557	640	>8333	330	12440	57

The STI_{HEM} parameters of *all-trans* isomers calculated with MIC_{90} values determined in RPMI 1640 medium were consistently higher than those of the *cis-trans* compounds. The difference between STI_{HEM} of both Candididin D isomers was relatively small, while a significant difference was found for *cis-trans* and *all-trans* Gedamycin and Vacidin. Amphotericin B appeared more selective than *cis-trans* Vacidin and Gedamycin but less selective than *cis-trans* Candididin D. The *all-trans* isomers of AHMs were more selective than AmB.

The STI_{HEM} calculated with MIC_{90} values determined in BDS medium was slightly higher (about 4-fold) for AmB but much higher for AHMs isomers. The latter is an obvious consequence

of much lower MIC values. Due to the inability to determine the hemolytic activity of *all-trans* Gedamycin, the adopted calculation was based on the highest used concentration (50 µg/mL), thus the result was termed as “>50”. Notably, the *all-trans* isoforms of the Gedamycin and Vacidin, demonstrated the highest STI_{HEM} values among the tested compounds, exceeding 8333 and 12440, respectively.

Parameters of antifungal activity and hemotoxicity of *all-trans* isomers of AHMs have been determined for the first time in this study. The previously published data on Candicidin D, Vacidin, and Gedamycin [25] concerned compounds present in Aureofacin or Candicidin complexes, *i.e.* the *cis-trans* isomers. It is noteworthy, therefore, that the MIC₉₀ values determined in BDS medium and EH₅₀ data for *cis-trans* AHMs in my study are generally in good agreement with respective parameters determined 41 years ago. Nevertheless, the determination of antifungal *in vitro* activity in RPMI 1640 medium provides data that are considered more useful for predicting *in vivo* antifungal activity of a given antibiotic than those obtained in artificial, rich media like BDS. In consequence, the STI_{HEM} parameters presented in Table 40 seem more reliable than those shown in Table 41. Based on these data, the *all-trans* isomer of Gedamycin with antifungal *in vitro* activity in RPMI 1640 medium comparable to that of AmB and EH₅₀ > 50 µg/mL, seemed to be a promising candidate for a novel antifungal drug.

4.8.4. Determination of mammalian *in vitro* cytotoxicity

The STI_{HEM} index is a generally accepted parameter characterizing *in vitro* selective toxicity of antifungal drug candidates. The high values of this parameter and low hemolytic activity of *all-trans* isomers of AHMs, especially of Gedamycin, were promising in the context of antifungal therapy. However, *in vitro* mammalian cytotoxicity of a given drug candidate should be tested against several human cell lines for a more complete picture of this phenomenon. In my study, six cell lines were used for this purpose, three normal and three of the cancer type. The normal cell lines included immortalized human keratinocytes (HaCaT), immortalized human kidney embryonic cells (HEK 293), and human normal lung fibroblasts (MRC-5). The latter is a diploid cell culture, commonly used during vaccine manufacturing [173]. MRC-5 cell line is made up of fibroblasts originally isolated from the lung tissue of a 14-week-old aborted Caucasian male fetus. The set of cancer cell lines consisted of HeLa cells (human cervical cancer cell line), Hep G2 cells (human liver cancer cell line), and A549 cells (human non-small cell lung cancer cell line). The cytotoxicity assays were performed according to the methodology presented in section 3.2.12.

Results were calculated according to equation 3.2.12.1 to determine the concentration of the antibiotic at which 50% of cells are killed (IC₅₀). IC₅₀ are the interpolated concentrations of the compound, for which the optical density value (Abs_{sample}) is exactly 50% of the optical density of the negative control sample (cells treated DMSO, Abs_{NC}) value. The results are presented in Table 42.

Table 42. Cytotoxic activity of AHMs and AmB determined as IC₅₀ (µg/mL). The maximal final concentration of analyzed compounds was 5 µg/ml. AHMs – aromatic heptaene macrolides, AmB – Amphotericin B.

IC ₅₀ (µg/mL)							
Cell line	Candididin D		Gedamycin		Vacidin		AmB
	<i>cis-trans</i>	<i>all-trans</i>	<i>cis-trans</i>	<i>all-trans</i>	<i>cis-trans</i>	<i>all-trans</i>	
MRC-5 (EMEM)	0.65 ± 0.13	0.82 ± 0.12	0.08 ± 0.01	0.25 ± 0.01	0.13 ± 0.02	0.58 ± 0.06	>5.00
HEK 293 (DMEM, MTT)	0.22 ± 0.01	0.80 ± 0.07	0.13 ± 0.01	0.44 ± 0.07	0.09 ± 0.01	0.60 ± 0.02	>5.00
HaCaT (RPMI, MTT)	0.43 ± 0.22	1.02 ± 0.15	0.09 ± 0.02	0.66 ± 0.18	0.25 ± 0.09	0.75 ± 0.25	>5.00
Hep G2 (DMEM, MTT)	0.34 ± 0.02	0.96 ± 0.01	0.08 ± 0.03	0.55 ± 0.03	0.08 ± 0.01	0.57 ± 0.06	>5.00
HeLa (MEM, WST-1)	0.08 ± 0.02	0.45 ± 0.04	0.08 ± 0.02	1.20 ± 0.09	0.08 ± 0.03	0.74 ± 0.12	>5.00
A549 (DMEM, MTT)	0.30 ± 0.04	0.95 ± 0.03	0.08 ± 0.01	0.42 ± 0.02	0.19 ± 0.06	0.64 ± 0.03	>5.00

Surprisingly enough, the all AHMs tested appeared highly toxic against all cell lines. Their IC₅₀ values were in the 0.08 – 1.20 µg/mL range, whereas for reference AmB, no cytotoxicity was observed up to 5 µg/mL. In this respect, it is worth mentioning that in the previous study of Borowski et al. [174], AmB demonstrated cytotoxicity against Hep G2 cell with IC₅₀ = 5.4 µg/mL. In my study, the *all-trans* AHMs exhibited slightly lower but still very high cytotoxicity compared to their *cis-trans* isomers. Among the AHMs tested, *cis-trans* Gedamycin showed the highest cytotoxicity (with the exception of HeLa cells). Conversely, *cis-trans* Candididin D exhibited the lowest cytotoxic activity within the native group of aromatic heptaene macrolides. The HeLa cell line was slightly less sensitive to *all-trans* Gedamycin. The HaCaT cell line was less sensitive to *all-trans* Vacidin compared to the other AHMs antibiotics. *All-trans* Candididin D was the least toxic AHM for most of the tested cell lines.

Obtained results showed that the *all-trans* antibiotics exhibit a lower cytotoxic effect than their *cis-trans* isomers. *Cis-trans* Gedamycin was the most toxic among the tested compounds (except HEK 293 – *cis-trans* Vacidin). On the other hand, *cis-trans* Candididin D exhibited the lowest cytotoxic activity in the native group of AHMs. The HeLa cell line was somewhat less sensitive to *all-trans* Gedamycin as well as the HaCaT cell line to *all-trans* Vacidin than to the other antibiotics from the AHMs group. *All-trans* Candididin D is less toxic, among the aromatic heptaene macrolides, for most tested cell lines.

The cytotoxicity comparison between the isomers revealed that the difference was least pronounced for *cis-trans* and *all-trans* Candididin D, with a maximal 5-fold variation. However, for *cis-trans* and *all-trans* Gedamycin, as well as *cis-trans* and *all-trans* Vacidin, the differences in cytotoxicity were significantly more marked. In the case of Gedamycin, the fold change ranged

from 3- to 14-fold and from 4- to 28-fold. Among the isolated *all-trans* compounds, *all-trans* Gedamycin exhibited the highest cytotoxicity across the tested cell lines, except the HeLa cell line, when compared to the other antibiotics.

4.8.5. Calculation of selective toxicity indexes values of AHMs isomers and AmB (STI_{CYT})

Similarly to the hemolysis assay, the STI_{CYT} values were calculated as the IC₅₀/MIC₉₀ ratio. The results are shown in Table 43.

Table 43. Selective toxicity indexes (STI_{CYT}) of AHMs and Amphotericin B (AmB). STI_{CYT} = IC₅₀/MIC₉₀ against *C. albicans* in RPMI medium.

STI _{CYT}		Candididin D		Gedamycin		Vacidin		AmB
IC ₅₀	MIC ₉₀	<i>cis-trans</i>	<i>all-trans</i>	<i>cis-trans</i>	<i>all-trans</i>	<i>cis-trans</i>	<i>all-trans</i>	
MRC-5 (EMEM)	<i>C. albicans</i> (RPMI-1640)	2.60	1.64	0.20	0.25	0.52	1.16	>20.0
HEK 293 (DMEM, MTT)		0.88	1.60	0.52	0.44	0.36	1.20	>20.0
HaCaT (RPMI, MTT)		1.72	2.04	0.36	0.66	1.00	1.50	>20.0
HEP G2 (DMEM, MTT)		1.36	1.92	0.32	0.55	0.32	1.14	>20.0
HeLa (MEM, WST-1)		0.32	0.90	0.32	1.20	0.32	1.48	>20.0
A549 (DMEM, MTT)		1.20	1.90	0.32	0.42	0.76	1.28	>20.0

Table 43 presents the selective toxicity index (STI_{CYT}) data for both isomers of AHMs against fungal cells of the *C. albicans* genus tested in RPMI 1640 medium, as well as various human cell lines. The *all-trans* isomers of AHMs exhibited slightly higher STI_{CYT} compared to the *cis-trans* isomers (except Candididin D and Gedamycin which showed lower STI_{CYT} values of *cis-trans* for MRC-5 and HEK 293 cell lines, respectively). This trend suggests a potential difference in selective toxicity between the isomer types, highlighting the slightly more favorable profile of *all-trans* isomers in most cases.

The STI_{CYT} values for AHMs showed general consistency across the tested human cell lines, with a few notable deviations; in the MRC-5 cell line treated with *cis-trans* Candididin D, in the HaCaT cell line treated with *cis-trans* Vacidin, in the HEK 293 cell line treated with *cis-trans* Candididin D, and in the HeLa cell line treated with both isomers of Candididin D and *all-trans* Gedamycin. Among the antibiotics studied, the *cis-trans* isomers of Vacidin and Gedamycin exhibited particularly low STI_{CYT}. For AmB, an STI_{CYT} value exceeding 20 was recorded, as no IC₅₀ was obtained within the tested concentration range (up to 5 µg/mL).

Generally, the STI_{CYT} indexes of all AHMs tested were much lower than the STI_{HEM} indexes for the same compounds. It can therefore be concluded that AHMs are weakly hemotoxic, or not hemotoxic at all (as in the case of *all-trans* Gedamycin), but exhibit high cytotoxicity against several human cell lines. This finding significantly limits the possibility of treating AHMs

as antifungal drug candidates. On the other hand, the apparent contradiction between the lack of hemotoxicity and strong cytotoxicity is an intriguing phenomenon from a scientific perspective and it is worth further investigation. RBCs are very different from most other human cells, as they lack a nucleus and other internal organelles, making them more like “sacs filled with hemoglobin” than regular cells. One may thus speculate that the high cytotoxicity of AHMs against cells other than RBCs may be due to their possible interactions with intracellular components, but evidence for that is not available.

The substantial cytotoxicity of AHMs was unexpected, in light of the confirmed low hemotoxicity of these compounds, especially the *all-trans* isomers of Vacidin and Gedamycin. Wanting more data that could help understand the basis of this phenomenon, it was decided to monitor possible morphological changes that cells undergo when treated with AHMs using confocal microscopy. The MRC-5 cell line model was used to visualize the cells treated with antibiotics at concentrations of IC₅₀ and IC₉₀. The visualization was performed on non-treated cells (control) and treated with both isomers of Gedamycin. The images obtained are presented in Figures 52- 54.

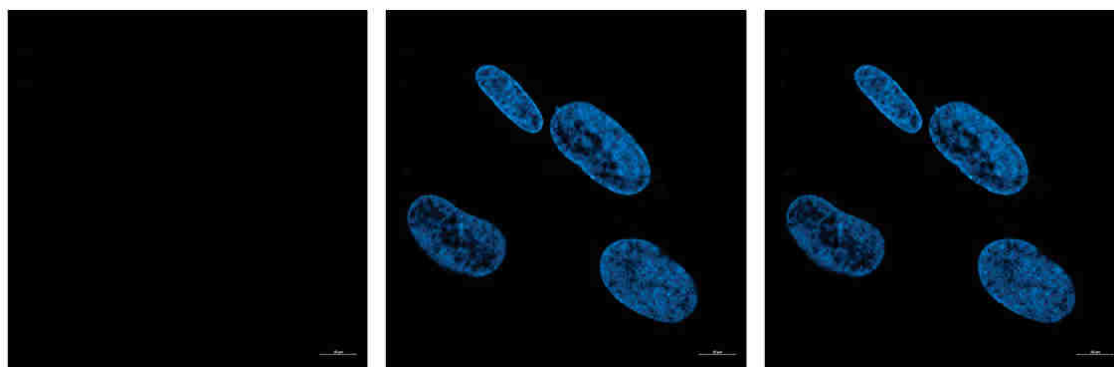


Figure 52. The image of control MRC-5 cells after 24h incubation. Dead cells were stained with 7-AAD- left, nuclei were stained blue with Hoechst 33342- middle, the merged images- right. The bar in the lower right corner corresponds to 10 μm

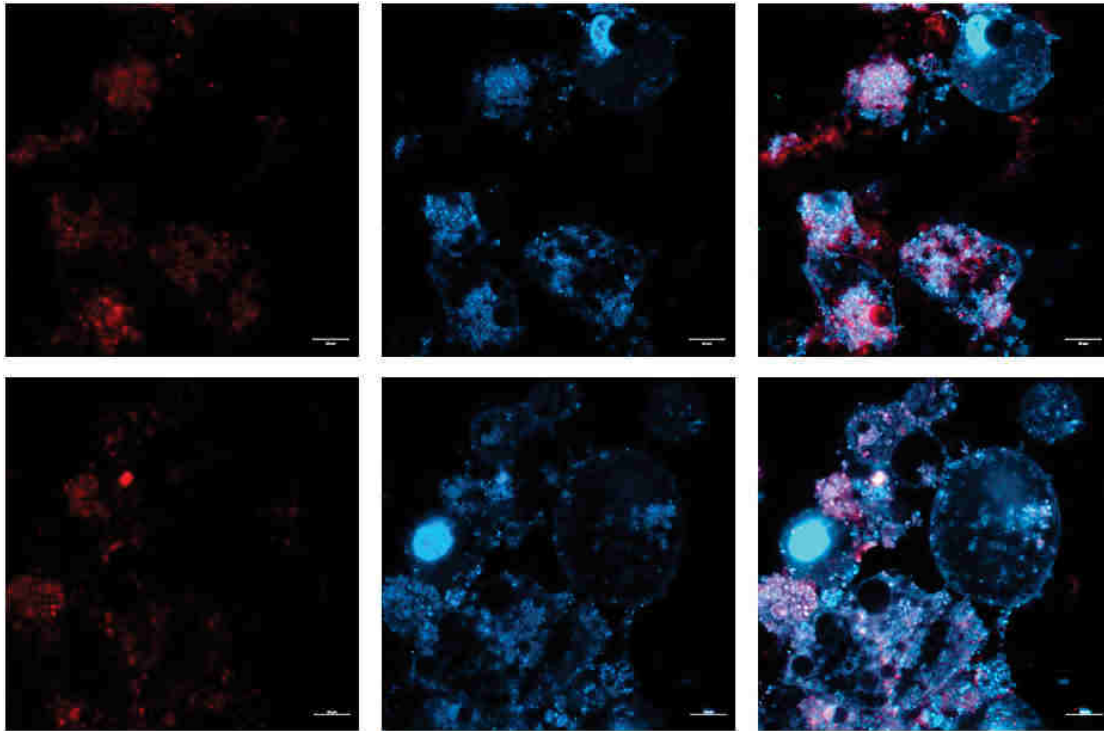


Figure 53. The images of MRC-5 cells treated with *cis-trans* Gedamycin at concentrations of IC_{50} (up) and IC_{90} (down) after 24 h. Dead cells were stained red with 7-AAD- left, nuclei were stained blue with Hoechst 33342- middle, the merged images- right, image scale - 10 μ m

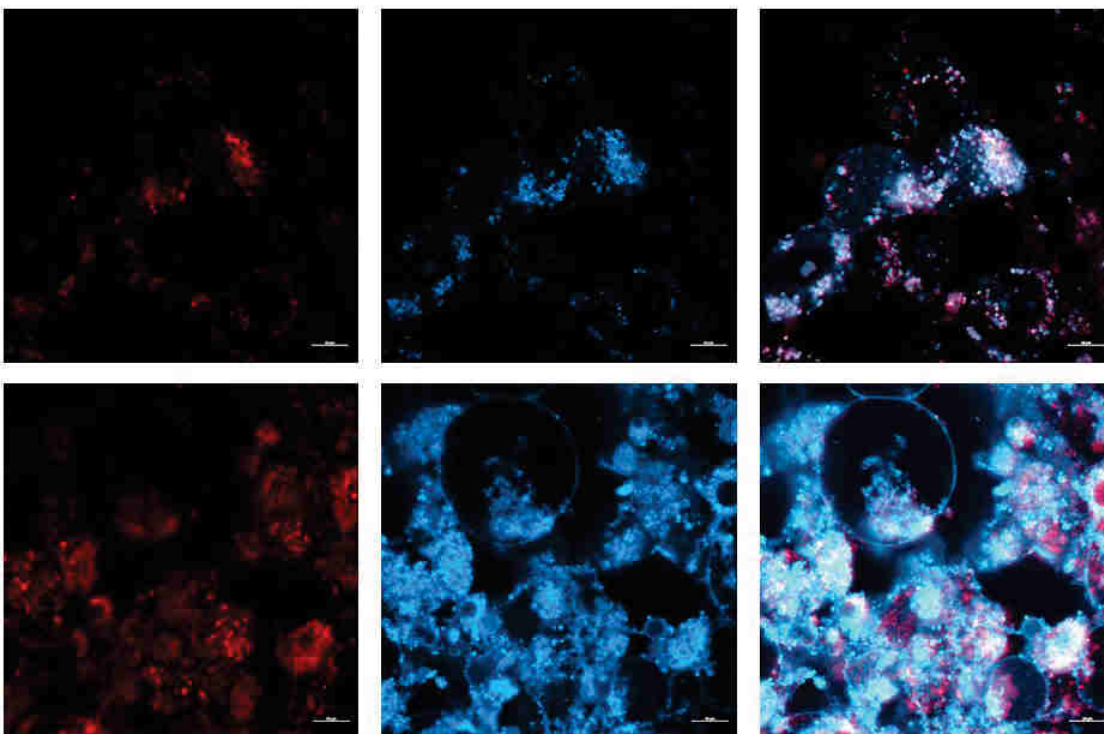


Figure 54. The images of MRC-5 cells treated with *all-trans* Gedamycin at concentrations of IC_{50} (up) and IC_{90} (down) after 24 h. Dead cells were stained red with 7-AAD- left; nuclei were stained blue with Hoechst 33342- middle, the merged images- right, image scale - 10 μ m

The confocal microscopy allowed to visualize the cytotoxic effect of *cis-trans* and *all-trans* AHMs (with Gedamycin serving as a representative of the AHMs group, Figures 52-54).

This effect was compared to the image of the non-treated cells (Figure 52). Untreated cells (Figure 52) maintained an unchanged morphology. In this image of untreated cells, there was an absence of the 7-AAD signal, which indicates dead cells (red color). In contrast, the nuclei of cells treated with antibiotics (Figure 53- 54) were apparently fragmented and the strong 7-AAD signal (visible red color) indicated cell death. The presented images of cells treated with concentrations corresponding to IC₅₀ and IC₉₀ appeared similar, showing some cells in the process of dying while the other were already dead. The more intense red staining in the images may indicate a higher number of dead cells captured by the microscope.

The imaging results confirm that cells treated with the tested AHMs at concentrations corresponding to IC₅₀ and IC₉₀ undergo destruction, which verifies the cytotoxicity of these compounds. However, the molecular basis of this effect is unknown, particularly whether it is due to membrane damage or another mechanism induced by the action of AHMs.

4.8.6.Determination of cell viability by flow cytometry

This study aimed to provide insights into the interpretation of results from toxicity assays, specifically hemolysis and cytotoxicity tests. To achieve this, experimental conditions similar to those in the cytotoxicity test (excluding the final MTT step) were applied, but the incubation period was limited to 30 minutes to align with the duration of erythrocyte incubation in the hemolysis assay. The concentration of antibiotics used in the experiment reflected the concentration of the EH₅₀ of *all-trans* Vacidin (37.2 µg/mL) and Amphotericin B (3.46 µg/mL) and the concentration of IC₉₀ of *all-trans* Vacidin (1.0 µg/mL) and *all-trans* Gedamycin (0.6 µg/mL). The obtained results were processed in the FlowJo program and are presented in Figure 55 and Table 44.

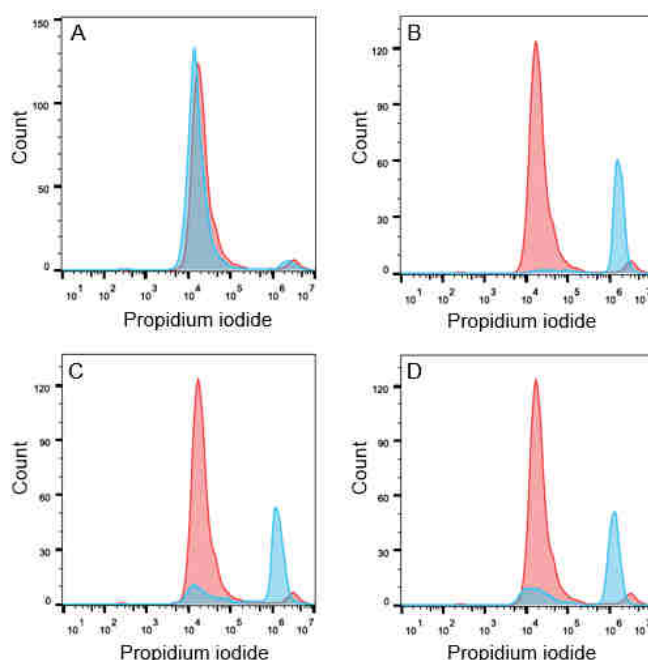


Figure 55. Overlay of flow cytometry histograms corresponding to HEK 293 cell line stained with propidium iodide in two conditions: without exposure to antibiotic (control, red color) and treated with specified antibiotic (blue color); A - Amphotericin B (3.46 µg/mL), B - *all-trans* Vacidin (37.2 µg/mL), C - *all-trans* Vacidin (1.0 µg/mL), D - *all-trans* Gedamycin (0.6 µg/mL)

The results presented in Figure 55 depict the number of HEK 293 cells in relation to the fluorescence intensity of cells stained with propidium iodide ($\lambda = 675$ nm). The red color represented the control cells not exposed to the antibiotic, while the blue color indicated the antibiotic-treated cells. In each of the observed distributions of HEK 293 cells treated with antibiotics, two populations of cells are visible: the first with fluorescence intensity of stained cells around 10^4 - 10^5 , corresponding to live cells, and the second with fluorescence intensity of stained cells around 10^6 - 10^7 , representing cell with damaged membrane, considered as dead cells. After 30 minutes of incubation, following antibiotic treatment, the experiment yielded the percentage of live and dead cells, as indicated in Table 44.

Table 44. The percentage of live and dead HEK 293 cells obtained as a result of cells' exposure to antibiotics. The control group, consisting of cells not treated with any antibiotic, was also included. AmB- Amphotericin B, n=3.

Antibiotic	Antibiotic concentration [µg/mL]	Live cells [%]	Dead cells [%]
Control	-	91.4	8.6
AmB	3.46	95.6	4.4
<i>all-trans</i> Vacidin	1.0	38.4	61.7
	37.2	10.2	89.8
<i>all-trans</i> Gedamycin	0.60	31.4	68.6

After 30 min of cells' treatment with AHMs at given concentrations, a quantitative analysis revealed a marked rise in necrotic cell count, along with a reduction in the number of viable cells compared to the control. The results obtained (Table 44) indicate that AmB at the concentration equivalent to EH_{50} did not affect cell viability after 30 minutes of incubation. In contrast, the concentration equal to EH_{50} of *all-trans* Vacidin (37.2 µg/mL) drastically damaged the cells, leading to their death—practically all cells were dead (89.9%). Concentrations corresponding to IC_{90} of *all-trans* Vacidin (1.0 µg/mL) and *all-trans* Gedamycin (0.6 µg/mL) also significantly impacted cell mortality, with rates of 61.7% and 68.6%, respectively.

Confocal microscopy and cytometry confirmed the destruction of cells treated with AHMs at concentrations corresponding to IC_{50} and IC_{90} . Specifically, cytometry results, in which cells were stained with propidium iodide, confirm membrane damage. It remains unclear why membrane destruction occurs in HEK 293 cells but not in RBCs. Answering this question requires further research.

4.9. Investigation of the antibiotic behavior in the lipid bilayer using FLIM

The further step of my research concentrated on the studies on the molecular organization of AHMs within a single lipid bilayer in the form of a giant unilamellar vesicle (GUV) using fluorescence lifetime imaging microscopy (FLIM). The antibiotics chosen for this experiment included both isomers of Gedamycin (*all-trans* isomer, which did not exhibit toxicity in hemolytic assay, and *cis-trans* isomer for comparative analysis). Additionally, *cis-trans* Vacidin was used to assess how structural variations influence antibiotic orientation within the Aureofacin complex. Giant unilamellar vesicles with and without sterols (cholesterol or ergosterol) were employed as the biological membrane models. This part of my doctoral studies was performed under

the supervision of R. Luchowski from Maria Curie-Skłodowska University in Lublin. For the aromatic heptaene macrolides, this experiment was performed for the first time.

The experiment is based on the fluorescence¹⁴ phenomenon. The main parameter measured during this study was fluorescence anisotropy, which allows for determining the molecules' orientation using their natural fluorescence. Fluorescence anisotropy refers to the phenomenon where the intensity of light emitted by a fluorophore varies depending on the axis of polarization, see Figure 56.

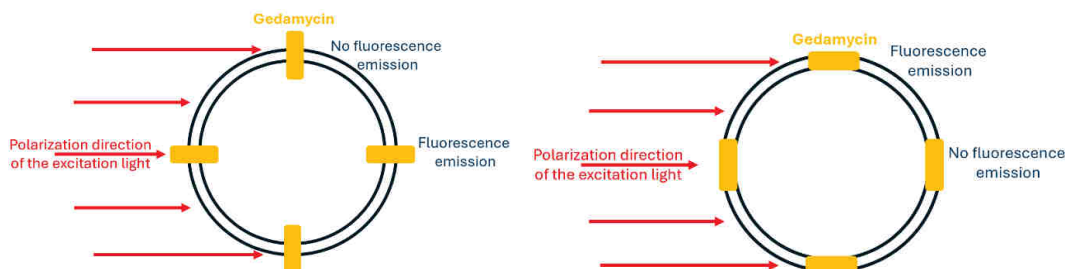


Figure 56. A simplified diagram of the photoselection phenomenon based on the example of two possible arrangements of Gedamycin (yellow) in the lipid bilayer; Gedamycin located perpendicularly to the membrane plane (left) and Gedamycin located parallelly to the membrane plane (right)

The polyene macrolide molecule contains a chromophore (so-called fluorophore) that is excited by linearly polarized light. When it comes back to its ground state the intensity of the emitted light is measured through two detectors, placed perpendicular and parallel to the incident light. At the molecular level, the rotation of the fluorophore's transition dipole affects the fluorescence anisotropy. For aromatic polyene macrolides, the fluorophore's transition dipole is aligned with the chromophore of the molecule, and thus with the entire macrolactone ring due to its rigid structure. Therefore, the position of the fluorophore within the bilayer can be considered as the position of the entire macrolactone ring within the membrane. Figure 56 presents the simplified model of the photoselection in the GUV model. When the antibiotic molecule (its moment of transition dipole) is oriented in the same direction (parallel) as the incidence of the excited polarized light, the fluorescence is emitted and can be detected. If the antibiotic molecule is oriented perpendicularly to the incidence of the excited polarized light the fluorescence is not emitted. In effect, the fluorescence could not be observed.

GUVs model was formed by the electroformation technique. GUVs are widely recognized as effective model systems for exploring membrane structure and dynamics. Electroformation (electroswelling) of GUVs entails influencing the natural swelling of lipids (particularly dry lipid bilayer located on the electrode in the performed experiment) in an aqueous solution by applying an external electric field.

A similar study previously conducted by researchers from Maria Curie-Skłodowska University in Lublin [175][176] provided fascinating details of the behavior of AmB within the lipid membrane. To this date, for AHMs such a study has never been performed. Therefore, it could provide invaluable insight into their organization in the membrane and facilitate elucidation of their probable mechanism of action. Consequently, to conduct the experiment, a series of

¹⁴ Fluorescence - a phenomenon involving the emission of light returning from the excited state of an electron to its original ground state [181]

GUVs were prepared in three versions: 1) DMPC without sterols, in order to highlight the role of sterols in antibiotic's orientation within the membrane; 2) DMPC with cholesterol and 3) DMPC with ergosterol. All three versions were tested independently in the presence of three antibiotics: *cis-trans* Vacidin, *cis-trans* Gedamycin, and *all-trans* Gedamycin, yielding 9 measurement systems in total. The bilayers containing cholesterol served as a model of the human cell membrane (i.e., erythrocytes), while those with ergosterol served as the model of the fungal cells. It is important to note that one is aware that this model is far from a perfect imitation of a real cell membrane. It lacks transport proteins and other components that impact major biophysical properties of a cell membrane, such as thickness and fluidity. Nevertheless, such models may still provide very useful data. To accurately reflect the lipid composition of a cell membrane, a sterol concentration of 30% was employed. The obtained images are shown in Figures 57- 59 and the calculated results (according to the equation 3.2.16.1., 3.2.16.2) are presented in Tables 45, 46. The r value is in the range between 0.0 to 0.4.

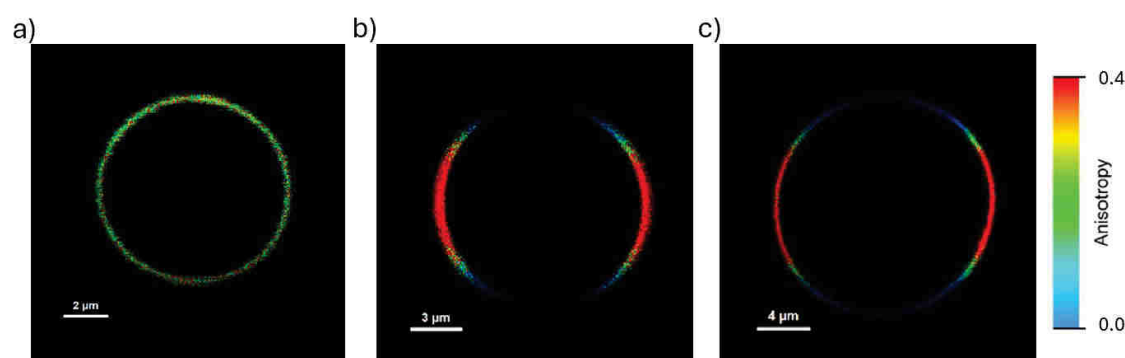


Figure 57. The results of microscopic imaging of lipid bilayer (DMPC) vesicle a) containing 0.5 mol% *cis-trans* Vacidin; b) 0.5 mol% *cis-trans* Vacidin A and 30 mol% cholesterol; c) 0.5 mol% *cis-trans* Vacidin and 30 mol% ergosterol, respectively

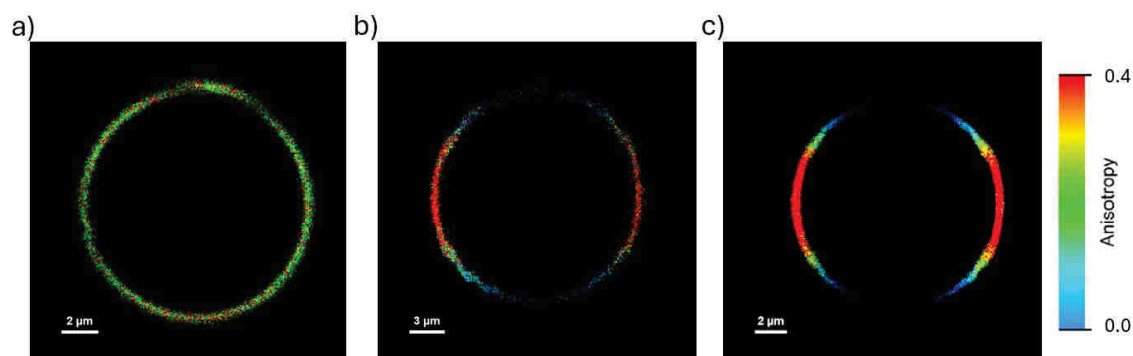


Figure 58. The results of microscopic imaging of lipid bilayer (DMPC) vesicle a) containing 0.5 mol% *cis-trans* Gedamycin; b) 0.5 mol% *cis-trans* Gedamycin and 30 mol% cholesterol; c) 0.5 mol% *cis-trans* Gedamycin and 30 mol% ergosterol, respectively

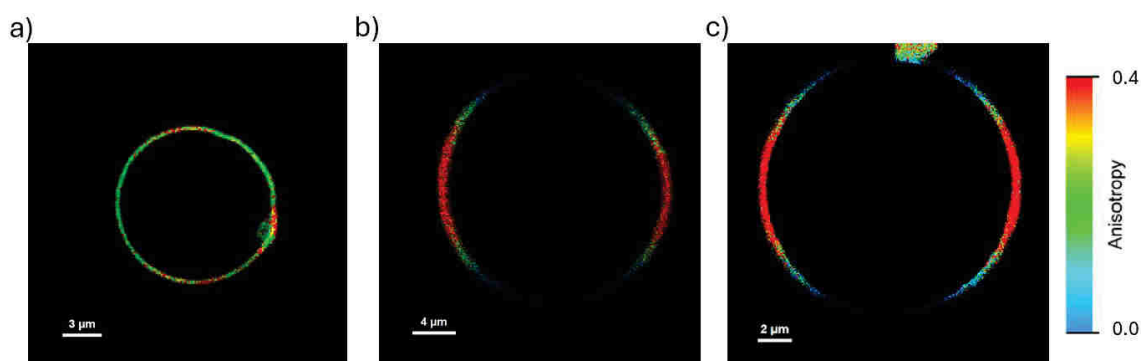


Figure 59. The results of microscopic imaging of lipid bilayer (DMPC) vesicle a) containing 0.5 mol% *all-trans* Gedamycin; b) 0.5 mol% *all-trans* Gedamycin and 30 mol% cholesterol; c) 0.5 mol% *all-trans* Gedamycin and 30 mol% ergosterol, respectively

The fluorescence of the tested antibiotics allowed to obtain the images of single GUVs with incorporated *cis-trans* and *all-trans* Gedamycin into the lipid membrane. The images of *cis-trans* and *all-trans* Gedamycin incorporated into GUVs composed of DMPC and DMPC with the addition of cholesterol or ergosterol are presented in Figures 58 and 59, respectively. Based on the photoselection, highly supported by the fluorescence anisotropy distribution, it can be concluded that in a liposome membrane composed of pure phospholipids, the antibiotic molecules did not exhibit any preferential orientation. Its alignment distribution was homogenous – antibiotics could adopt all possible orientations with respect to the membrane plane, from parallel to perpendicular, as evidenced by the mostly uniform green color of the vesicle. Conversely, in a lipid membrane containing a fraction of sterols, elevated fluorescence anisotropy values, depicted in red, were observed in specific membrane fragments on the left and right sides of the GUVs. In turn, the upper and lower regions of the lipid bilayer exhibited substantially lower anisotropy values, represented by the barely visible blue color. This indicates that the addition of sterols induces particular orientation of the antibiotic molecules within the membrane. The fluorescence anisotropy distribution in the GUV suggests a perpendicular orientation of the antibiotic fluorophore with respect to the membrane plane; in other words, the antibiotic molecules are aligned parallel to the lipids comprising the lipid bilayer.

Additionally, the fluorescence anisotropy values determined as the angle between the direction of antibiotic transition dipole and the axis normal to the plane of the lipid bilayer were calculated based on equation 3.2.16.1, 3.2.16.2. The calculated results of the orientation angle are presented in Tables 45, 46.

Table 45. *Cis-trans* and *all-trans* Gedamycin orientation angle α with respect to the axis normal to the plane of the lipid bilayer. n – the number of experimental systems taken into the calculation.

Membrane composition	Orientation angle α [°]	
	<i>cis-trans</i> Gedamycin	<i>all-trans</i> Gedamycin
DMPC	54.0 ± 3.6 (n=5)	56.4 ± 0.2 (n=5)
DMPC ergosterol	44.3 ± 3.0 (n=5)	39.4 ± 3.8 (n=4)
DMPC cholesterol	43.9 ± 6.0 (n=6)	36.8 ± 3.3 (n=9)

Table 46. *Cis-trans* Vacidin orientation angle α with respect to the axis normal to the plane of the lipid bilayer. n – the number of experimental systems taken into the calculation.

Membrane composition	Orientation angle α [°]
	<i>Cis- trans</i> Vacidin
DMPC	54.6 \pm 2.8 (n=6)
DMPC ergosterol	26.4 \pm 3.4 (n=11)
DMPC cholesterol	32.9 \pm 2.9 (n=9)

The results presented in Table 45 show that the transition dipoles of *cis-trans* and *all-trans* Gedamycin incorporated into the membrane of the vesicle without sterol formed angles of 54.0° and 56.4°, respectively with respect to the axis normal to the lipid bilayer plane. These calculated values are practically equal to the magic angle (54.7°), indicating either that the antibiotic was oriented at this angle (making it unlikely) or that the antibiotic did not have any orientation (it had a homogenous distribution of orientation) in the tested experimental system. In the absence of sterols in the lipid vesicle, both isomers of Gedamycin did not exhibit any preferable orientation, which contrasted with their behavior in sterol-containing lipid membranes. The average orientation angles of *cis-trans* Gedamycin in the presence of ergosterol and cholesterol were 44.3° and 43.9°, respectively, and for *all-trans* Gedamycin, they were 39.4° and 36.8°, respectively. *Cis-trans* Gedamycin formed similar orientation angles in the presence of ergosterol or cholesterol, with values approximately 5°- 7° greater than those of *all-trans* Gedamycin observed in identical experimental conditions. However, considering the standard deviations, the formed angles by both isomers in both tested sterol environments could coincide. To verify this dependency, the U-Mann Whitney test was performed (according to the equation 3.2.16.3, 3.2.16.4). The results are presented in Table 47.

Table 47. The verification of the hypothesis that the orientation angles (table 45) belong to the same population (coincide) by the U-Mann Whitney test. Results present the Gedamycin incorporated into GUVs with or without sterols (cholesterol, ergosterol); TG- *all-trans* Gedamycin, CG – *cis-trans* Gedamycin. $U_{critical}$ is taken from Critical values of the Mann-Whitney U table, $\alpha=0.05$ [160]

Tested systems comparison (no.)	Experimental system	Number of GUVs (n ₁ ,n ₂)	Sum of ranks	U-Mann Whitney result	$U_{critical}$ (0.05)	Do the obtained orientation angles belong to the same population?
1	TG	5	35	3	2	Yes
	CG	5	20	18		
2	TG-cholesterol	9	53.5	41.5	10	No
	CG-cholesterol	6	66.5	6		
3	TG-ergosterol	4	13	15.5	1	No
	CG-ergosterol	5	32	1		
4	TG-cholesterol	9	55	22	4	Yes
	TG-ergosterol	4	36	8.5		
5	CG-cholesterol	6	36	13	3	Yes
	CG-ergosterol	5	30	9		

U-Mann Whitney test allowed to determine whether the obtained orientation angles belong to the same population (coincide) or if they are significantly different from each other. The lowest obtained U values of tested systems comparison no. 1, 4, and 5 were higher than

$U_{critical}$. It means that the determined orientation angles belong to the same population within the compared systems. Therefore, it can be concluded that the average orientation angles are the same between both isomers of Gedamycin in GUVs without incorporated sterols, and between the same isomer of antibiotic in the presence of different sterols (cholesterol or ergosterol). However, for the tested systems comparison, no. 2 and 3 the obtained U values were below or equal to the $U_{critical}$. Such results suggest, that differences between these populations may represent distinct groups, potentially reflecting different orientation angles of *cis-trans* and *all-trans* Gedamycin in the membrane containing sterols (cholesterol or ergosterol).

The orientation angles obtained, along with the fluorescence anisotropy images of both isomers of Gedamycin (Figures 58bc and 59bc), revealed a predominantly vertical orientation of the antibiotics within the lipid bilayer. The fluorescence anisotropy results (Table 45) demonstrated that the straightening of the chromophore in the *cis-trans* Gedamycin led to a decrease in the orientation angle of the antibiotic's transition dipole relative to the normal axis of the lipid bilayer, indicating a more vertical alignment within the membrane. Similarly, the average orientation angle of *cis-trans* Vacidin (Table 46, Figure 57) in pure lipid (without sterol) was comparable to the magic angle observed for Gedamycin, suggesting a lack of preferential orientation in the membrane. Notably, the average orientation angles indicated that *cis-trans* Vacidin exhibited a more vertical alignment in the membrane containing ergosterol compared to that containing cholesterol. The orientation angles in the presence of sterols were particularly noteworthy, as the measured values were significantly lower than those for Gedamycin. The difference in orientation angles between the two *cis-trans* antibiotics (Vacidin, Gedamycin) was approximately 18° in the ergosterol-containing membrane and around 11° in the cholesterol-containing membrane.

The examined AHMs did not exhibit any specific orientation in vesicles lacking sterols. In contrast, the observed vertical orientation of the antibiotic molecules within the membrane of sterol-containing vesicles, seems to favor the ion channel formation model over the sterol sponge model, as a part of the mechanism of action of these compounds. According to the principles of FLIM, if the antibiotic molecule "lies down" on the cell membrane, *i.e.* is oriented parallel to the direction of incident linearly polarized light, then in the obtained GUV images, the top and bottom of the vesicle should exhibit highest fluorescence anisotropy. Such a picture would suggest a mechanism consistent with the sterol sponge theory. This type of correlation was not observed in the anisotropy images obtained for AHMs. However, based on the results presented in this dissertation, the sterol-sponge mechanism could not be completely ruled out as a possible mode of AHMs action.

Previously, the FLIM studies with AmB were performed by researchers from the University of Maria Curie-Skłodowska in Lublin and Gdańsk University of Technology. The results obtained are shown in Figure 60 [176].

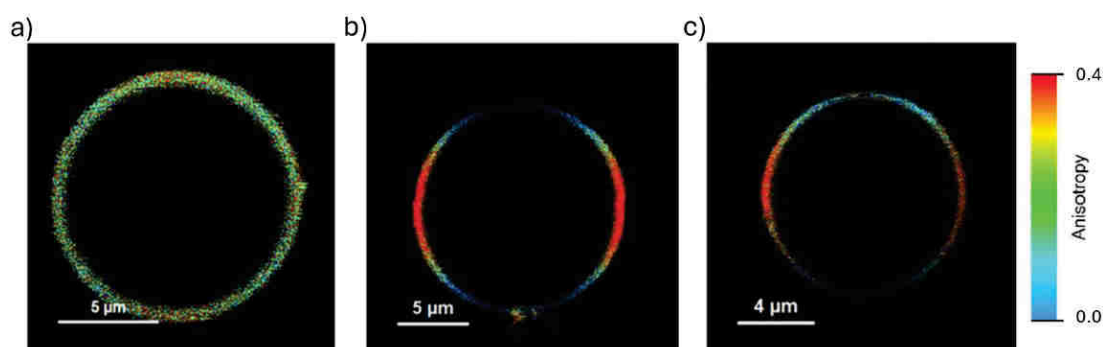


Figure 60. The results of microscopic imaging of DMPC vesicle containing a) 0.5 %M AmB, b) 0.5 %M AmB and 30mol% cholesterol, c) 0.5 %M AmB with 30%mol ergosterol respectively [176]

The results obtained for AmB to some extent supported the findings of biological studies. Conversely, this principle could not be applied to Gedamycin and Vacidin in a straightforward manner, where, despite their purported higher affinity for ergosterol, the STI results did not appear to directly result from differences in their affinity for cholesterol versus ergosterol. It is important to acknowledge, however, that FLIM studies were conducted using artificial lipid membranes. Furthermore, in my work, the average orientation angles of both Gedamycin isomers and *cis-trans* Vacidin in the membranes were calculated based on FLIM studies (Tables 45, 46).

The change in chromophore geometry from *cis-trans* to *all-trans* not only alters the rigidity of the molecule but likely also affects the dipole transition moment of the chromophore. Since FLIM measures the latter, it can be stated that there is a difference between the dipole transition moment of *cis-trans* and *all-trans* isomers of the same antibiotic in a given membrane. Assuming that the dipole transition moment for the *all-trans* isomers does not differ fundamentally from that of their *cis-trans* counterparts, one could conclude that the notably smaller values of the orientation angles measured for the *all-trans* isomers indeed indicate that the *all-trans* AHM molecules adopt a more vertical orientation within the membranes. Such orientation may promote stronger interactions with sterols and perhaps the formation of more stable channels. In the case of Gedamycin, the presence of the N-methyl-*p*-aminoacetophenone group (more lipophilic than N-*p*-aminoacetophenone) significantly increases the possibility of interaction with the second lipid layer. It may have either a stabilizing or destabilizing effect on the antibiotic aggregation, depending on the dynamic properties of the membrane. It is worth noting that the alkyl-aromatic side chain can be engaged in π -electronic interactions with sterols in the second layer, provided it is not folded. Additionally, in artificially created DMPC vesicles, the antibiotic is long enough to potentially fully penetrate the second layer of the lipid bilayer, in contrast to AmB, which lacks the alkyl-aromatic group. It is worth noting that researchers from Maria Curie-Skłodowska University in Lublin attempted to determine the average orientation of the alkyl-aromatic residue within the membrane, applying the same principles used for the heptaene chromophore. However, it was found that the wavelength of the light emitted by the side chain during fluorescence corresponded to one of the absorption maxima of the chromophore, and was consequently fully absorbed by the antibiotic molecule itself. As a result, fluorescence anisotropy measurements for the side chain could not be obtained.

In the end, FLIM results did not conclusively indicate the role of the alkyl-aromatic side chain of aromatic heptaene macrolides in terms of their biological activity. Yet, the differences in angles between *cis-trans* Vacidin and *cis-trans* Gedamycin may be related to the differences in the side chain structures, i.e., the lack (Vacidin) or presence (Gedamycin) of N-methyl moiety. The experiments for both antibiotics were conducted under the same conditions. According to computational simulations, Vacidin, with a less lipophilic side chain, may fold more readily toward the hydrophilic part of the molecule. In contrast, Gedamycin's side chain is likely more frequently extended, allowing it to anchor within the opposite leaf of the lipid bilayer [120]. Therefore, for both Gedamycin isomers, the side chain, which may contribute to the antibiotic's vertical orientation, could mitigate angle differences independently of sterol presence. Conversely, in the case of Vacidin, the differences between different membranes are more noticeable due to the less frequent extension of the alkyl-aromatic moiety.

Both *in vitro* biological studies and biophysical investigations suggested that the side chain might play an important role in the mechanism of AHM action. Additionally, this hypothesis is supported by the computational simulations [120]. However, the supposed vertical orientation of Gedamycin was not fully consistent with the observed biological activity of AHMs. Therefore, one has to conclude that the molecular foundation of the biological activity of AHMs is a multifaceted phenomenon, an interplay of numerous factors, both biological and biophysical, and therefore requires further extensive studies.

5. SUMMARY AND FINAL CONCLUSIONS

The subject of the presented doctoral dissertation was research concerning the isolation and characterization of the biological properties of aromatic heptaene macrolides, as well as the investigation of their behavior in the model of biological membranes. Vacidin and Gedamycin complexes, components of the Aureofacin complex, and Candicidin D, the component of the Candicidin complex were tested as representatives of the AHMs group. AHMs were subjected to the photoisomerization process, which resulted in the change of their chromophore geometry from native *cis-trans* to *all-trans*. The most important results of my studies are presented below;

- Development of an effective method for isolating highly purified AHMs (82–89%) that are part of the antibiotic complexes; Aureofacin (Vacidin, Gedamycin) and Candicidin (Candicidin D),
- First-time application of CPC in the AHMs purification process
- Demonstration that Vacidin and Gedamycin undergo *cis-trans* to *all-trans* photoisomerization under conditions analogous to those previously developed for Candicidin D,
- Demonstration of a significant difference in *in vitro* antifungal activity of AHMs determined in BDS medium versus RPMI-1640 medium (importantly lower activity was observed in RPMI medium),
- Demonstration of a significant decrease in hemotoxicity of Vacidin and especially Gedamycin as a result of *cis-trans* to *all-trans* photoisomerization,
- Demonstration of high cytotoxicity of all AHMs against mammalian cells from six different human cell lines, generally exceeding the cytotoxicity of AmB,
- Demonstration that *all-trans* AHMs adopt a more ordered and perpendicular orientation relative to the plane of the membrane in lipid vesicles containing sterols, compared to their *cis-trans* counterparts using FILM.

The conducted research allowed to determine the following conclusions:

- Preparative CPC and HPLC techniques can be utilized for obtaining pure aromatic polyene antibiotics,
- Upon exposure to light radiation of an appropriate wavelength, *cis-trans* AHMs undergo photoisomerization to *all-trans* AHMs,
- The obtained *cis-trans* and *all-trans* AHM isomers exhibit antifungal activity comparable to AmB (in RPMI 1640 medium),
- The *all-trans* isomers demonstrate lower hemolytic activity compared to the *cis-trans* isomers and AmB,
- Both the *cis-trans* isomers and the photoisomerization products show very high cytotoxic activity, significantly exceeding that of AmB,
- High cytotoxicity significantly limits the potential use of AHMs in clinical practice,

- The examined AHMs and AmB do not exhibit a specific orientation in vesicles lacking sterols, in contrast to sterol-containing vesicles, where a vertical orientation of the antibiotic within the membrane is observed,
- A diminution in the orientation angle of the antibiotic in the membrane was observed between native (*cis-trans*) AHMs and their *all-trans* counterparts,
- The obtained results support the theory suggesting that polyene macrolides localize within the membrane and form pores.

SCIENTIFIC ACHIEVEMENTS

ARTICLES PUBLISHED IN SCIENTIFIC JOURNALS

1. Szczepblewski, P.; **Górska, J.**; Andrałójć, W.; Janke, P.; Wąsik, K.; Laskowski, T. Iso-Partricin, an Aromatic Analogue of Amphotericin B: How Shining Light on Old Drugs Might Help Create New Ones. *Antibiotics*, 2021, 10, 1102. <https://doi.org/10.3390/antibiotics10091102> – second author
2. Borzyszkowska-Bukowska, J. & **Górska, J.**; Szczepblewski, P.; Laskowski, T.; Gabriel, I.; Jurasz, J.; Kozłowska-Tylingo, K.; Szweda, P.; Milewski, S. Quest for the Molecular Basis of Improved Selective Toxicity of *All-Trans* Isomers of Aromatic Heptaene Macrolide Antifungal Antibiotics. *Int. J. Mol. Sci.*, 2021, 22, 10108. <https://doi.org/10.3390/ijms221810108>; Julia Borzyszkowska-Bukowska & **Justyna Górska** - first authors
3. Szczepblewski P., Wróblewski M., Borzyszkowska-Bukowska J., Bairamova T., **Górska J.**, Laskowski T., Samulewicz A., Kosno M., Sobiech Ł., Polit JT., Kukula-Koch W. The role of centrifugal partition chromatography in the removal of β -asarone from *Acorus calamus* essential oil. *Sci Rep.*, 2022 Dec 23;12(1):22217, <https://10.1038/s41598-022-26726-6>
4. Nowak, M., Skwarecki, A., Pilch, J., **Górska, J.**, Szweda, P., Milewska, M., & Milewski, S. Fatty acids as molecular carriers in cleavable antifungal conjugates. *EJMECH*, 252, 2023, 115293. <https://doi.org/10.1016/j.ejmech.2023.115293>
5. Patent application; Szczepblewski, P., **Górska, J.**, Kukula-Koch, W., Borzyszkowska-Bukowska, J., Laskowski, T., Sposób otrzymywania partrycyny A oraz partrycyna A otrzymana tym sposobem, application number: P.448765
6. Patent application; Szczepblewski, P., **Górska, J.**, Kukula-Koch, W., Borzyszkowska-Bukowska, J., Laskowski, T., Sposób otrzymywania partrycyny B oraz partrycyna B otrzymana tym sposobem, application number: P.448766

SCIENTIFIC CONFERENCES

1. **Górska J.**, Szczepblewski P., Kozłowska-Tylingo K.
14-16.09.2023 XI Konwersatorium Chemii Medycznej w Lublinie, PTCHM, Lublin,
Poster presentation: 'Rapid method for purity determination of AHM antibiotic complexes'
2. Szczepblewski P., **Górska J.**, Borzyszkowska-Bukowska J., Laskowski T., Gabriel I., Milewski S., Szweda P.
14-16.09.2023 XI Konwersatorium Chemii Medycznej w Lublinie, PTCHM, Lublin,
Poster presentation: 'Aromatic heptaenes seen in a new light: aromatic analogues of amphotericin B with improved selective toxicity'

3. Stefaniak J., **Górska J.**, Maciejewska N., Skwarecki A., Milewska M.
27-30.06.2023 23rd Tetrahedron Symposium, Goteborg, Szwecja
Poster presentation: 'Organic synthesis of novel hydroxamate siderophore and enzymatic inhibitor direct conjugates'

4. Szczeblewski P., **Górska J.**, Borzyszkowska-Bukowska J., Laskowski T., Polit J., Kukuła-Koch W.
27-28.10.2022 VI All-Ukrainian Scientific and Practical Conference with International Participation - Chemistry of Natural Compounds,
Poster presentation: 'The distribution of β -asarone in Acorus calamus oil samples and a rapid method of its removal'

5. **Górska J.**, Szczeblewski P., Szweda P.
09-14.07.2022 The Biochemistry Global Summit, Lisbon, the 25th IUBMB Congress, the 46th FEBS Congress, and the 15th PABMB Congress
Poster presentation: 'Aromatic heptaene macrolides as an initial "golden shot" towards systemic mycoses'

6. **Górska J.**, Szczeblewski P., Laskowski T.
03-05.09.2021 X Konwersatorium Chemii Medycznej w Lublinie, PTCHM, Lublin
Oral presentation: 'Aromatic analogues of amphotericin B. How to isolate these promising agents for antifungal therapy?'

PARTICIPATION IN PROJECTS

1. Argentum Triggering Research Grants Program, IDUB
Project title: Aromatic heptaenes seen in a new light: N-substituted aromatic analogues of amphotericin B with improved selective toxicity
grant holder: Paweł Szczeblewski, PhD, DSc

2. Opus 20 project
Project title: Cleavable molecular nanocarrier: antimetabolite conjugates of antimicrobial activity
grant holder: Sławomir Milewski PhD, DSc

3. Opus 19 project
Project title: Derivatives of aromatic polyene macrolides of improved selective toxicity
grant holder: Sławomir Milewski PhD, DSc

BIBLIOGRAPHY

- [1] C. Firacative, "Invasive fungal disease in humans: are we aware of the real impact?," *Mem Inst Oswaldo Cruz*, vol. 115, 2020, doi: 10.1590/0074-02760200430.
- [2] D. W. Denning, "Global incidence and mortality of severe fungal disease," *Lancet Infect Dis*, 2024, doi: 10.1016/S1473-3099(23)00692-8.
- [3] WHO, "World Health Organization. WHO publish fungal priority pathogens list.," <https://www.who.int/publications/i/item/9789240060241>.
- [4] WHO, "World Health Organization. WHO fungal priority pathogens list to guide research, development and public health action.," <https://www.who.int/publications/i/item/9789240060241>.
- [5] D. Neofytos, C. Garcia-Vidal, F. Lamothe, C. Lichtenstern, A. Perrella, and J. J. Vehreschild, "Invasive aspergillosis in solid organ transplant patients: diagnosis, prophylaxis, treatment, and assessment of response," *BMC Infect Dis*, vol. 21, p. 296, 2021, doi: 10.1186/s12879-021-05958-3.
- [6] P. G. Pappas, M. S. Lionakis, M. C. Arendrup, L. Ostrosky-Zeichner, and B. J. Kullberg, "Invasive candidiasis," *Nat Rev Dis Primers*, vol. 4, p. 18026, 2018, doi: 10.1038/nrdp.2018.26.
- [7] I. Mareković, S. Pleško, V. Rezo Vranješ, Z. Herljević, T. Kuliš, and M. Jandrlić, "Epidemiology of Candidemia: Three-Year Results from a Croatian Tertiary Care Hospital," *J Fungi*, vol. 7, p. 267, 2021, doi: 10.3390/jof7040267.
- [8] A. L. Mora Carpio and A. Climaco, "Candidemia," *StatPearls*, 2024.
- [9] Y. Qiao, Z. Tao, F. Hao, Y. Huang, H. Sun, and P. Guo, "Epidemiological Characteristics, Antifungal Susceptibility, Risk Factors, and Outcomes of Candida Bloodstream Infection: A Ten-Year Surveillance in a Teaching Hospital in China," *Infect Drug Resist*, vol. 16, pp. 4769–4778, 2023, doi: 10.2147/IDR.S411283.
- [10] W. Zhang, X. Song, H. Wu, and R. Zheng, "Epidemiology, species distribution, and predictive factors for mortality of candidemia in adult surgical patients," *BMC Infect Dis*, vol. 20, p. 506, 2020, doi: 10.1186/s12879-020-05238-6.
- [11] I. Das, P. Nightingale, M. Patel, and P. Jumaa, "Epidemiology, clinical characteristics, and outcome of candidemia: experience in a tertiary referral center in the UK," *Int J Infect Dis*, vol. 15, pp. e759–e763, 2011, doi: 10.1016/j.ijid.2011.06.006.
- [12] M. Puig-Asensio et al., "Epidemiology and predictive factors for early and late mortality in Candida bloodstream infections: a population-based surveillance in Spain," *Clin Microbiol Infect*, vol. 20, no. 4, pp. O245–O254, 2014, doi: 10.1111/1469-0691.12380.
- [13] A. Korula et al., "Invasive fungal infection following chemotherapy for acute myeloid leukaemia—Experience from a developing country," *Mycoses*, vol. 60, pp. 686–691, 2017, doi: 10.1111/myc.12646.
- [14] M. Ciotti et al., "COVID-19 Outbreak: An Overview," *Chemotherapy*, vol. 64, pp. 215–223, 2019, doi: 10.1159/000507423.

- [15] WHO, "World Health Organization. WHO Coronavirus (COVID-19) Dashboard," <https://covid19.who.int/> (accessed on 03 March 2024).
- [16] X. Zhu et al., "Co-infection with respiratory pathogens among COVID-2019 cases," *Virus Res*, vol. 285, p. 198005, 2020, doi: 10.1016/j.virusres.2020.198005.
- [17] J. A. W. Gold et al., "Increased Hospitalizations Involving Fungal Infections during COVID-19 Pandemic, United States, January 2020–December 2021," *Emerg Infect Dis*, vol. 29, 2023, doi: 10.3201/eid2907.221771.
- [18] M. A. Ghannoum and L. B. Rice, "Antifungal Agents: Mode of Action, Mechanisms of Resistance, and Correlation of These Mechanisms with Bacterial Resistance," *Clin Microbiol Rev*, vol. 12, pp. 501–517, 1999, doi: 10.1128/CMR.12.4.501.
- [19] C. M. Hossain et al., "Antifungals and Drug Resistance," *Encyclopedia*, vol. 2, pp. 1722–1737, Oct. 2022, doi: 10.3390/encyclopedia2040118.
- [20] J. Houšť, J. Spížek, and V. Havlíček, "Antifungal Drugs," *Metabolites*, vol. 10, p. 106, 2020, doi: 10.3390/metabo10030106.
- [21] K. Saris, J. F. Meis, and A. Voss, "Candida auris," *Curr Opin Infect Dis*, vol. 31, pp. 334–340, 2018, doi: 10.1097/QCO.0000000000000469.
- [22] P. Lakhani, A. Patil, and S. Majumdar, "Challenges in the Polyene- and Azole-Based Pharmacotherapy of Ocular Fungal Infections," *J Ocul Pharmacol Ther.*, vol. 35, pp. 6–22, 2019, doi: 10.1089/jop.2018.0089.
- [23] F. B. Cavassin, J. L. Baú-Carneiro, R. R. Vilas-Boas, and F. Queiroz-Telles, "Sixty years of Amphotericin B: An Overview of the Main Antifungal Agent Used to Treat Invasive Fungal Infections.," *Infect Dis Ther*, vol. 10, pp. 115–147, 2021, doi: 10.1007/s40121-020-00382-7.
- [24] S. Zotchev, "Polyene Macrolide Antibiotics and their Applications in Human Therapy," *Curr Med Chem*, vol. 10, pp. 211–223, 2003, doi: 10.2174/0929867033368448.
- [25] B. Cybulska, T. Ziminski, E. Borowski, and C. M. Gary-Bobo, "The influence of electric charge of aromatic heptaene macrolide antibiotics on their activity on biological and lipidic model membranes.," *Mol Pharmacol*, vol. 24, pp. 270–276, 1983.
- [26] R. Vardanyan and V. Hruby, "Antifungal Drugs," *Synth. Best-Seller Drugs*, pp. 677–686., 2016, doi: 10.1016/B978-0-12-411492-0.00033-X.
- [27] J. M. Hamilton-Miller, "Chemistry and biology of the polyene macrolide antibiotics.," *Bacteriol Rev*, vol. 37, pp. 166–196, 1973.
- [28] J. Bolard, "How do the polyene macrolide antibiotics affect the cellular membrane properties?," *Biochim Biophys Acta.*, vol. 864, pp. 257–304, 1986, doi: 10.1016/0304-4157(86)90002-X.
- [29] K. D. Lenz, K. E. Klosterman, H. Mukundan, and J. Z. Kubicek-Sutherland, "Macrolides: From Toxins to Therapeutics," *Toxins*, vol. 13, p. 347, 2021, doi: 10.3390/toxins13050347.
- [30] T. Haro-Reyes, L. Díaz-Peralta, A. Galván-Hernández, A. Rodríguez-López, L. Rodríguez-Fragoso, and I. Ortega-Blake, "Polyene Antibiotics Physical Chemistry and Their Effect

- on Lipid Membranes; Impacting Biological Processes and Medical Applications.," *Membranes*, vol. 12, 2022, doi: 10.3390/membranes12070681.
- [31] B. Cybulska, E. Borowski, Y. Prigent, and C. M. Gary-Bobo, "Cation permeability induced by two aromatic heptaenes, vacidin A and candicidin D on phospholipid unilamellar vesicles.," *J Antibiot*, vol. 34, pp. 884–891, 1981, doi: 10.7164/antibiotics.34.884.
- [32] V. V. Belakhov, A. V. Garabadzhiu, and T. B. Chistyakova, "Polyene Macrolide Antibiotic Derivatives: Preparation, Overcoming Drug Resistance, and Prospects for Use in Medical Practice (Review)," *Pharm Chem J*, vol. 52, pp. 890–901, 2019, doi: 10.1007/s11094-019-01922-3.
- [33] P. Szczepblewski, T. Laskowski, A. Bałka, E. Borowski, and S. Milewski, "Light-Induced Transformation of the Aromatic Heptaene Antifungal Antibiotic Candicidin D into Its All-Trans Isomer," *J Nat Prod*, vol. 81, pp. 1540–1545, 2018, doi: 10.1021/acs.jnatprod.7b00821.
- [34] C.-M. Liu, L. E. Mcdaniel, and C. P. Schaffner, "Fungimygin, biogenesis of its aromatic moiety," *J Antibiot*, vol. 25, pp. 187–188, 1972, doi: 10.7164/antibiotics.25.187.
- [35] G.-M. Liu, L. E. Mcdaniel, and C. P. Schaffner, "Studies on Candicidin biogenesis," *J Antibiot*, vol. 25, no. 2, pp. 116–121, 1972, doi: 10.7164/antibiotics.25.116.
- [36] C. M. Gary-Bobo, "Polyene - sterol interaction and selective toxicity," *Biochimie*, vol. 71, pp. 37–47, 1989, doi: 10.1016/0300-9084(89)90129-6.
- [37] J. Aparicio, M. Mendes, N. Anton, E. Recio, and J. Martin, "Polyene Macrolide Antibiotic Biosynthesis," *Curr Med Chem*, vol. 11, pp. 1643–1656, 2004, doi: 10.2174/0929867043365044.
- [38] K. Szwarc, "Wybrane aspekty chemii antybiotyków przeciwgrzybowych z grupy wielopierścieniowych makrolidów polienowych," Politechnika Gdańska, Gdańsk, 2016.
- [39] J. F. Martin and L. E. McDaniel, "Production of Polyene Macrolide Antibiotics," *Adv Appl Microbiol.*, vol. 21, pp. 1 - 52, 1977 doi: 10.1016/S0065-2164(08)70037-6.
- [40] K. Szwarc, P. Szczepblewski, P. Sowiński, E. Borowski, and J. Pawlak, "The stereostructure of candicidin D," *J Antibiot*, vol. 68, pp. 504–510, 2015, doi: 10.1038/ja.2015.17.
- [41] J. Szlinder-Richert, B. Cybulska, J. Grzybowska, J. Bolard, and E. Borowski, "Interaction of amphotericin B and its low toxic derivative, N-methyl-N-D-fructosyl amphotericin B methyl ester, with fungal, mammalian and bacterial cells measured by the energy transfer method," *Il Farmaco*, vol. 59, pp. 289–296, Ar. 2004, doi: 10.1016/j.farmac.2003.12.007.
- [42] D. W. Warnock, "Amphotericin B: an introduction.," *J Antimicrob Chemother*, vol. 28, p. 27–38, 1991, doi: 10.1093/jac/28.suppl_b.27.
- [43] J. Dutcher, W. Gold, J. Pagano, and J. Vandeputte, "Amphotericin b, its production, and its salts," Patent no. 2,908,611, 1959
- [44] W. H. Trejo and R. E. Bennett, "*Streptomyces nodosus* sp. n., the amphotericin -producing organism," *J Bacteriol*, vol. 85, pp. 436–439, 1963, doi: 10.1128/jb.85.2.436-439.1963.

- [45] W. P. Jambor, B. A. Steinberg, and L. O. Suydam, "Amphotericins A and B: two new antifungal antibiotics possessing high activity against deep-seated and superficial mycoses.," *Antibiot Annu*, vol. 3, pp. 574–8, 1955.
- [46] J. D. Dutcher, "The Discovery and Development of Amphotericin B," *Dis Chest*, vol. 54, pp. 296–298, 1968, doi: 10.1378/chest.54.Supplement_1.296.
- [47] A. Noor and C. Preuss, "Amphotericin B," 2024
<https://www.ncbi.nlm.nih.gov/books/NBK482327/>.
- [48] H. Carolus, S. Pierson, K. Lagrou, and P. Van Dijck, "Amphotericin B and Other Polyenes-Discovery, Clinical Use, Mode of Action and Drug Resistance.," *J Fungi*, vol. 6,. 2020, doi: 10.3390/jof6040321.
- [49] F. H. O. AL-Khikani, "Amphotericin B from antifungal to antiviral therapy: promising modern therapeutic branch," *Res. Results Pharmacol.*, vol. 6, pp. 57–65, 2020, doi: 10.3897/rrpharmacology.6.53649.
- [50] L. D. Saravolatz, L. Ostrosky-Zeichner, K. A. Marr, J. H. Rex, and S. H. Cohen, "Amphotericin B: Time for a New 'Gold Standard,'" *Clin Infect Dis.*, vol. 37, pp. 415–425, 2003, doi: 10.1086/376634.
- [51] J. J. Torrado, R. Espada, M. P. Ballesteros, and S. Torrado-Santiago, "Amphotericin B Formulations and Drug Targeting," *J Pharm Sci*, vol. 97, pp. 2405–2425, 2008, doi: 10.1002/jps.21179.
- [52] Drugs.com, "Fungizone Prescribing Information," 2024
<https://www.drugs.com/pro/fungizone.html>.
- [53] Wielka Baza ChPL, "Charakterystyka produktu leczniczego," 2012.
- [54] E. Abdollahizad, S. Dadashzadeh, S. Bahri, Z. Abbasian, and E. Rezaee, "Amphotericin B Pharmacokinetics: Inter-strain Differences in Rats Following Intravenous Administration of the Most Commonly Marketed Formulations of the Drug," *Iran J Pharm Res.*, vol. 22, no. 1, 2023, doi: 10.5812/ijpr-134772.
- [55] A. A. Volmer, A. M. Szpilman, and E. M. Carreira, "Synthesis and biological evaluation of amphotericin B derivatives.," *Nat Prod Rep*, vol. 27, pp. 1329–49, 2010, doi: 10.1039/b820743g.
- [56] A. N. Plotnick, "Lipid-based formulations of amphotericin B," *J Am Vet Med Assoc*, vol. 216, pp. 838–841, 2000, doi: 10.2460/javma.2000.216.838.
- [57] K. V. Clemons and D. A. Stevens, "Comparison of Fungizone, Amphotec, AmBisome, and Abelcet for Treatment of Systemic Murine Cryptococcosis," *Antimicrob Agents Chemother*, vol. 42, pp. 899–902, 1998, doi: 10.1128/AAC.42.4.899.
- [58] E. Wasan, T. Mandava, P. Crespo-Moran, A. Nagy, and K. M. Wasan, "Review of Novel Oral Amphotericin B Formulations for the Treatment of Parasitic Infections.," *Pharmaceutics*, vol. 14, p. 2316, 2022, doi: 10.3390/pharmaceutics14112316.
- [59] E. Jones and M. Goldman, "Lipid formulations of amphotericin B," *Cleve Clin J Med*, vol. 65, 1998.

- [60] J. W. Hiemenz and T. J. Walsh, "Lipid Formulations of Amphotericin B: Recent Progress and Future Directions," *Clin. Infect. Dis.*, vol. 22, pp. S133–S144, 1996, doi: 10.1093/clinids/22.Supplement_2.S133.
- [61] M. Saqib et al., "Amphotericin B Loaded Polymeric Nanoparticles for Treatment of Leishmania Infections.," *Nanomaterials*, vol. 10, p. 1152, 2020, doi: 10.3390/nano10061152.
- [62] F. F. Tuon, K. L. Florencio, and J. L. Rocha, "Burden of acute kidney injury in HIV patients under deoxycholate amphotericin B therapy for cryptococcal meningitis and cost-minimization analysis of amphotericin B lipid complex," *Med Mycol*, vol. 57, pp. 265–269, 2019, doi: 10.1093/mmy/myy025.
- [63] K. Kaur, P. Kumar, and P. Kush, "Amphotericin B loaded ethyl cellulose nanoparticles with magnified oral bioavailability for safe and effective treatment of fungal infection," *Biomed Pharmacother.*, vol. 128, p. 110297, 2020, doi: 10.1016/j.biopha.2020.110297.
- [64] D. Ellis, "Amphotericin B: spectrum and resistance.," *J Antimicrob Chemother*, vol. 49, pp. 7–10, 2002, doi: 10.1093/jac/49.suppl_1.7.
- [65] E. M. O'Shaughnessy, C. A. Lyman, and T. J. Walsh, "Amphotericin B: Polyene Resistance Mechanisms," *Antimicrob Drug Resist*, pp. 295–305, 2009 doi: 10.1007/978-1-59745-180-2_25.
- [66] DrugBank, "Amphotericin B," 2024, <https://go.drugbank.com/drugs/DB00681>.
- [67] G. Lovero, O. De Giglio, S. Rutigliano, G. Diella, G. Caggiano, and M. T. Montagna, "In vitro antifungal susceptibilities of Candida species to liposomal amphotericin B, determined using CLSI broth microdilution, and amphotericin B deoxycholate, measured using the Etest," *J Med Microbiol*, vol. 66, pp. 213–216, 2017, doi: 10.1099/jmm.0.000402.
- [68] M. T. Montagna et al., "In vitro activities of amphotericin B deoxycholate and liposomal amphotericin B against 604 clinical yeast isolates," *J Med Microbiol*, vol. 63, pp. 1638–1643, 2014, doi: 10.1099/jmm.0.075507-0.
- [69] L. Ahmady, M. Gothwal, M. M. Mukkoli, and V. K. Bari, "Antifungal drug resistance in Candida: a special emphasis on amphotericin B.," *APMIS*, vol. 132, pp. 291–316, 2024, doi: 10.1111/apm.13389.
- [70] S. Sharma, M. Alfatah, V. K. Bari, Y. Rawal, S. Paul, and K. Ganesan, "Sphingolipid biosynthetic pathway genes FEN1 and SUR4 modulate amphotericin B resistance.," *Antimicrob Agents Chemother*, vol. 58, pp. 2409–14, 2014, doi: 10.1128/AAC.02130-13.
- [71] T. R. Sterling, and W. G. Merz, "Resistance to amphotericin B: emerging clinical and microbiological patterns," *Drug Resist Updat.*, vol. 1, pp. 161–165, 1998, doi: 10.1016/S1368-7646(98)80034-4.
- [72] Jacek Czuby, "Molekularne aspekty aktywności biologicznej amfoterycyny B i jej pochodnych o podwyższonej selektywności – badania z zastosowaniem metod chemii obliczeniowej," Politechnika Gdańska, Gdańsk, 2008.

- [73] D. P. Bonner, R. P. Tewari, M. Solotorovsky, W. Mechlinski, and C. P. Schaffner, "Comparative chemotherapeutic activity of amphotericin B and amphotericin B methyl ester.," *Antimicrob Agents Chemother*, vol. 7, pp. 724–9, 1975, doi: 10.1128/AAC.7.6.724.
- [74] P. Legrand, E. A. Romero, B. E. Cohen, and J. Bolard, "Effects of aggregation and solvent on the toxicity of amphotericin B to human erythrocytes.," *Antimicrob Agents Chemother*, vol. 36, pp. 2518–22, 1992, doi: 10.1128/AAC.36.11.2518.
- [75] J. Barwicz, and P. Tancrede, "The effect of aggregation state of amphotericin-B on its interactions with cholesterol- or ergosterol-containing phosphatidylcholine monolayers," *Chem Phys Lipids*, vol. 85, pp. 145–155, 1997, doi: 10.1016/S0009-3084(96)02652-7.
- [76] R. Espada, S. Valdespina, C. Alfonso, G. Rivas, M. P. Ballesteros, and J. J. Torrado, "Effect of aggregation state on the toxicity of different amphotericin B preparations," *Int J Pharm*, vol. 361, pp. 64–69, 2008, doi: 10.1016/j.ijpharm.2008.05.013.
- [77] J. M. Lestner et al., "Population Pharmacokinetics of Liposomal Amphotericin B in Immunocompromised Children.," *Antimicrob Agents Chemother*, vol. 60, pp. 7340–7346, 2016, doi: 10.1128/AAC.01427-16.
- [78] B. E. Sengel et al., "Efficacy of N-acetylcysteine in preventing amphotericin B induced acute kidney injury," *Marmara Med. J.*, vol. 29, p. 73, 2016, doi: 10.5472/MMJoa.2902.02.
- [79] Y. Abdel-Hafez et al., "Tolerability and epidemiology of nephrotoxicity associated with conventional amphotericin B therapy: a retrospective study in tertiary care centers in Palestine.," *BMC Nephrol*, vol. 23, p. 132, 2022, doi: 10.1186/s12882-022-02770-2.
- [80] J. P. Botero Aguirre, and A. M. Restrepo Hamid, "Amphotericin B deoxycholate versus liposomal amphotericin B: effects on kidney function," *Cochrane Database Syst Rev.*, vol. 2015, p. CD010481, 2015, doi: 10.1002/14651858.CD010481.pub2.
- [81] R. L. Wade, P. Chaudhari, J. L. Natoli, R. J. Taylor, B. H. Nathanson, and D. L. Horn, "Nephrotoxicity and other adverse events among inpatients receiving liposomal amphotericin B or amphotericin B lipid complex.," *Diagn Microbiol Infect Dis*, vol. 76, pp. 361–7, 2013, doi: 10.1016/j.diagmicrobio.2013.04.001.
- [82] A. C. Mesa-Arango, L. Scorzoni, and O. Zaragoza, "It only takes one to do many jobs: Amphotericin B as antifungal and immunomodulatory drug," *Front Microbiol*, vol. 3, p. 286, 2012, doi: 10.3389/fmicb.2012.00286.
- [83] B. De Kruijff and R. A. Demel, "Polyene antibiotic-sterol interactions in membranes of *Acholeplasma laidlawii* cells and lecithin liposomes. III. Molecular structure of the polyene antibiotic-cholesterol complexes," *Biochim Biophys Acta*, vol. 339, pp. 57–70, 1974, doi: 10.1016/0005-2736(74)90332-0.
- [84] L. N. Ermishkin, Kh. M. Kasumov, and V. M. Potzeluyev, "Single ionic channels induced in lipid bilayers by polyene antibiotics amphotericin B and nystatine," *Nature*, vol. 262, pp. 698–699, 1976, doi: 10.1038/262698a0.
- [85] L. Kristanc, B. Božič, Š. Z. Jokhadar, M. S. Dolenc, and G. Gomišček, "The pore-forming action of polyenes: From model membranes to living organisms," *Biochim Biophys Acta*, vol. 1861, pp. 418–430, 2019, doi: 10.1016/j.bbamem.2018.11.006.

- [86] K. C. Gray et al., "Amphotericin primarily kills yeast by simply binding ergosterol," *Proc. Natl. Acad. Sci.*, vol. 109, pp. 2234–2239, 2012, doi: 10.1073/pnas.1117280109.
- [87] B. E. Cohen, "A sequential mechanism for the formation of aqueous channels by amphotericin B in liposomes. The effect of sterols and phospholipid composition," *Biochim Biophys Acta*, vol. 1108, pp. 49–58, 1992, doi: 10.1016/0005-2736(92)90113-Z.
- [88] F. C. Odds, A. J. P. Brown, and N. A. R. Gow, "Antifungal agents: mechanisms of action," *Trends Microbiol*, vol. 11, pp. 272–279, 2003, doi: 10.1016/S0966-842X(03)00117-3.
- [89] D. M. Kamiński, "Recent progress in the study of the interactions of amphotericin B with cholesterol and ergosterol in lipid environments," *Eur Biophys J.*, vol. 43, pp. 453–467, 2014, doi: 10.1007/s00249-014-0983-8.
- [90] J. Borzyszkowska-Bukowska, J. Czub, P. Szczepblewski, and T. Laskowski, "Antibiotic-sterol interactions provide insight into the selectivity of natural aromatic analogues of amphotericin B and their photoisomers," *Sci Rep*, vol. 13, p. 762, 2023, doi: 10.1038/s41598-023-28036-x.
- [91] B. Cybulska, J. Mazerski, E. Borowski, and C. M. Gary-Bobo, "Haemolytic activity of aromatic heptaenes," *Biochem Pharmacol*, vol. 33, pp. 41–46, 1984, doi: 10.1016/0006-2952(84)90368-X.
- [92] S. M. Hammond, P. A. Lambert, and B. N. Kliger, "The Mode of Action of Polyene Antibiotics; Induced Entry of Hydrogen Ions as a Consequence of Polyene Action on the Cell Membrane of *Candida albicans*," *Microbiology*, vol. 81, pp. 331–336, 2000, doi: 10.1099/00221287-81-2-331.
- [93] R. J. Hamill, "Amphotericin B Formulations: A Comparative Review of Efficacy and Toxicity," *Drugs*, vol. 73, pp. 919–934, 2013, doi: 10.1007/s40265-013-0069-4.
- [94] T. M. Anderson et al., "Amphotericin forms an extramembranous and fungicidal sterol sponge," *Nat Chem Biol*, vol. 10, pp. 400–406, 2014, doi: 10.1038/nchembio.1496.
- [95] J. Suchodolski, J. Muraszko, P. Bernat, and A. Krasowska, "A Crucial Role for Ergosterol in Plasma Membrane Composition, Localisation, and Activity of Cdr1p and H⁺-ATPase in *Candida albicans*," *Microorganisms*, vol. 7, p. 378, 2019, doi: 10.3390/microorganisms7100378.
- [96] H. L. Choy, E. A. Gaylord, and T. L. Doering, "Ergosterol distribution controls surface structure formation and fungal pathogenicity," *mBio*, 2023, doi: 10.1128/mbio.01353-23.
- [97] A. Lewandowska et al., "Fungicidal amphotericin B sponges are assemblies of staggered asymmetric homodimers encasing large void volumes," *Nat Struct Mol Biol*, vol. 28, pp. 972–981, 2021, doi: 10.1038/s41594-021-00685-4.
- [98] A. Maji et al., "Tuning sterol extraction kinetics yields a renal-sparing polyene antifungal," *Nature*, vol. 623, pp. 1079–1085, 2023, doi: 10.1038/s41586-023-06710-4.
- [99] Š. Zemljič Jokhadar, B. Božič, L. Kristanc, and G. Gomišček, "Osmotic Effects Induced by Pore-Forming Agent Nystatin: From Lipid Vesicles to the Cell," *PLoS One*, vol. 11, p. e0165098, 2016, doi: 10.1371/journal.pone.0165098.

- [100] B. D. Wolf, and S. C. Hartsel, "Osmotic stress sensitizes sterol-free phospholipid bilayers to the action of Amphotericin B," *Biochim Biophys Acta*, vol. 1238, pp. 156–162, 1995, doi: 10.1016/0005-2736(95)00122-J.
- [101] M. L. Sokol-Anderson, J. Brajtburg, and G. Medoff, "Amphotericin B-Induced Oxidative Damage and Killing of *Candida albicans*," *J Infect Dis*, vol. 154, pp. 76–83, 1986, doi: 10.1093/infdis/154.1.76.
- [102] M. Sokol-Anderson, J. E. Sligh, S. Elberg, J. Brajtburg, G. S. Kobayashi, and G. Medoff, "Role of cell defense against oxidative damage in the resistance of *Candida albicans* to the killing effect of amphotericin B," *Antimicrob Agents Chemother*, vol. 32, pp. 702–705, 1988, doi: 10.1128/AAC.32.5.702.
- [103] F. Sangalli-Leite *et al.*, "Amphotericin B mediates killing in *Cryptococcus neoformans* through the induction of a strong oxidative burst," *Microbes Infect*, vol. 13, pp. 457–467, 2011, doi: 10.1016/j.micinf.2011.01.015.
- [104] J. Brajtburg, S. Elberg, J. Medoff, G. S. Kobayashi, D. Schlessinger, and G. Medoff, "Stimulatory, permeabilizing, and toxic effects of amphotericin B on L cells," *Antimicrob Agents Chemother*, vol. 26, pp. 892–897, 1984, doi: 10.1128/AAC.26.6.892.
- [105] K. Bahmed, R. Bonaly, and J. Coulon, "Relation between cell wall chitin content and susceptibility to amphotericin B in *Kluyveromyces*, *Candida* and *Schizosaccharomyces* species," *Res Microbiol*, vol. 154, pp. 215–222, 2003, doi: 10.1016/S0923-2508(03)00049-4.
- [106] M. I. Angelova *et al.*, "pH sensing by lipids in membranes: The fundamentals of pH-driven migration, polarization and deformations of lipid bilayer assemblies," *Biochim Biophys Acta*, vol. 1860, pp. 2042–2063, 2018, doi: 10.1016/j.bbamem.2018.02.026.
- [107] L. Marklund, R. Henriksson, and K. Grankvist, "Amphotericin B-induced apoptosis and cytotoxicity is prevented by the Na⁺, K⁺, 2Cl⁻-cotransport blocker bumetanide," *Life Sci*, vol. 66, pp. PL319–PL324, 2000, doi: 10.1016/S0024-3205(00)00560-9.
- [108] A. Vertut-Doi, P. Hannaert, and J. Bolard, "The polyene antibiotic amphotericin B inhibits the Na⁺/K⁺ pump of human erythrocytes," *Biochem Biophys Res Commun*, vol. 157, pp. 692–697, 1988, doi: 10.1016/S0006-291X(88)80305-X.
- [109] S. Hartsel, and J. Bolard, "Amphotericin B: new life for an old drug," *Trends Pharmacol Sci*, vol. 17, pp. 445–449, 1996, doi: 10.1016/S0165-6147(96)01012-7.
- [110] K. M. Wasan, and S. M. Cassidy, "Role of Plasma Lipoproteins in Modifying the Biological Activity of Hydrophobic Drugs," *J Pharm Sci*, vol. 87, pp. 411–424, 1998, doi: 10.1021/js970407a.
- [111] A. Vertut-Doi, S. I. Ohnishi, and J. Bolard, "The endocytic process in CHO cells, a toxic pathway of the polyene antibiotic amphotericin B," *Antimicrob Agents Chemother*, vol. 38, pp. 2373–2379, 1994, doi: 10.1128/AAC.38.10.2373.
- [112] C. Faustino, and L. Pinheiro, "Lipid Systems for the Delivery of Amphotericin B in Antifungal Therapy," *Pharmaceutics*, vol. 12, p. 29, 2020, doi: 10.3390/pharmaceutics12010029.

- [113] K. M. Wasan, M. G. Rosenblum, L. Cheung, and G. Lopez-Berestein, "Influence of lipoproteins on renal cytotoxicity and antifungal activity of amphotericin B," *Antimicrob Agents Chemother*, vol. 38, pp. 223–227, 1994, doi: 10.1128/AAC.38.2.223.
- [114] J. Mazerski, J. Bolard, and E. Borowski, "Self-association of some polyene macrolide antibiotics in aqueous media," *Biochim Biophys Acta*, vol. 719, pp. 11–17, 1982, doi: 10.1016/0304-4165(82)90300-2.
- [115] J. Vandeputte, "Borate complex of polyene macrolide antibiotics," Patent no. 3,740,44, 1973
- [116] R. Fernández-García et al., "Self-assembling, supramolecular chemistry and pharmacology of amphotericin B: Poly-aggregates, oligomers and monomers," *J Control Release*, vol. 341, pp. 716–732, 2022, doi: 10.1016/j.jconrel.2021.12.019.
- [117] H. Lechevalier, R. F. Acker, C. T. Corke, C. M. Haenseler, and S. A. Waksman, "Candididin, A New Antifungal Antibiotic," *Mycologia*, vol. 45, pp. 155–171, 1953, doi: 10.1080/00275514.1953.12024259.
- [118] P. Szczeblewski et al., "Analytical studies on ascosin, candididin and levorin multicomponent antifungal antibiotic complexes. The stereostructure of ascosin A2," *Sci Rep*, vol. 7, p. 40158, 2017, doi: 10.1038/srep40158.
- [119] S. A. Waksman, H. A. Lechevalier, and C. P. Schaffner, "Candididin and other polyenic antifungal antibiotics.," *Bull World Health Organ*, vol. 33, pp. 219–26, 1965,
- [120] J. Borzyszkowska-Bukowska, J. Czub, P. Szczeblewski, and T. Laskowski, "Antibiotic-sterol interactions provide insight into the selectivity of natural aromatic analogues of amphotericin B and their photoisomers," *Sci Rep*, vol. 13, p. 762, 2023, doi: 10.1038/s41598-023-28036-x.
- [121] H. W. Gordon, and C. P. Schaffner, "The effect of polyene macrolides on the prostate gland and canine prostatic hyperplasia.," *Proc Natl Acad Sci*, vol. 60, pp. 1201–1208, 1968, doi: 10.1073/pnas.60.4.1201.
- [122] K. M.-E. Jensen, and P. O. Madsen, "Candididin treatment of prostatism: A prospective double-blind placebo-controlled study," *Urol Res*, vol. 11, pp. 7–10, 1983, doi: 10.1007/BF00272701.
- [123] P. O. Madsen, T. Dørflinger, P. C. Frimodt-Møller, and K. M.-E. Jensen, "Candididin in Treatment of Benign Prostatic Hypertrophy," *J. Urol.*, vol. 132, pp. 1235–1238, 1984, doi: 10.1016/S0022-5347(17)50112-3.
- [124] "A new agent for the treatment of candidal vaginitis. Candididin (Candeptin).," *JAMA*, vol. 196, p. 1144, 1966, doi: 10.1001/jama.1966.03100260082023.
- [125] E. Vartiainen, and L. Tervilä, "The Use of Candeptin for Treatment of Moniliasis," *Acta Obstet Gynecol Scand*, vol. 49, pp. 22–24, 1970, doi: 10.3109/00016347009155060.
- [126] R. C. Tweit, R. C. Pandey, Jr. , and K. L. Rinheart, "Characterization of the antifungal and antiprotozoal antibiotic partricin and structural studies on partriciens A and B.," *J Antibiot*, vol. 35, pp. 997–1012, 1982, doi: 10.7164/antibiotics.35.997.

- [127] T. Bruzzese, M. Signorini, F. Ottoni, and P. Emanuele, "Partricin derivatives," Patent no. 5,298,495, 1994
- [128] P. Sowinski, J. Pawlak, E. Borowski, and P. Gariboldi, "ChemInform Abstract: Stereostructure of Gedamycin (I).," *ChemInform*, vol. 26, 1995, doi: 10.1002/chin.199526271.
- [129] P. Sowinski, P. Gariboldi, J. K. Pawlak, and E. Borowski, "The structure of vacidin A, an aromatic heptaene macrolide antibiotic. II. Stereochemistry of the antibiotic.," *J Antibiot*, vol. 42, pp. 1639–1642, 1989, doi: 10.7164/antibiotics.42.1639.
- [130] R. J. McRipley, P. J. Erhard, R. A. Schwind, and R. R. Whitney, "Evaluation of vaginal antifungal formulations *in vivo*," *Postgrad Med J*, vol. 55, pp. 648–652, 1979, doi: 10.1136/pgmj.55.647.648.
- [131] P. Szczepblewski, W. Andrałojć, J. Polit, A. Żabka, K. Winnicki, and T. Laskowski, "Ipertrofan Revisited - The Proposal of the Complete Stereochemistry of Mepartricin A and B," *Molecules*, vol. 26, p. 5533, 2021, doi: 10.3390/molecules26185533.
- [132] M. R. Galmozzi, T. Bruzzese, G. Buffa, and A. Bonabello, "Pharmacokinetics of a New Derivative of Partricin A (SPA-S-753) in Rodents," *Chemotherapy*, vol. 46, pp. 153–159, 2000, doi: 10.1159/000007271.
- [133] H. Kakeya et al., "Efficacy of SPK-843, a Novel Polyene Antifungal, in Comparison with Amphotericin B, Liposomal Amphotericin B, and Micafungin against Murine Pulmonary Aspergillosis," *Antimicrob Agents Chemother*, vol. 52, pp. 1868–1870, 2008, doi: 10.1128/AAC.01369-07.
- [134] Y. Ito, "Golden rules and pitfalls in selecting optimum conditions for high-speed counter-current chromatography," *J Chromatogr A*, vol. 1065, pp. 145–168, 2005, doi: 10.1016/j.chroma.2004.12.044.
- [135] A. Czerwiński et al., "New N-alkyl derivatives of amphotericin B. Synthesis and biological properties.," *J Antibiot*, vol. 44, pp. 979–984, 1991, doi: 10.7164/antibiotics.44.979.
- [136] C. Schaffner, and E. Borowski, "Polyenic compounds and procedures related thereto," Patent no. US3244590A, 1960
- [137] M. Bojczuk, D. Żyżelewicz, and P. Hodurek, "Centrifugal partition chromatography- A review of recent applications and some classic references," *J Sep Sci*, vol. 40, pp. 1597–1609, 2017, doi: 10.1002/jssc.201601221.
- [138] Y. Ito, and R. L. Bowman, "Countercurrent Chromatography: Liquid-Liquid Partition Chromatography without Solid Support," *Science*, vol. 167, pp. 281–283, 1970, doi: 10.1126/science.167.3916.281.
- [139] GILSON, "Introduction To Centrifugal Partition Chromatography," https://www.gilson.com/pub/media/docs/TN215_Gilson_Introduction_CPC.pdf.
- [140] L. Lorántfy et al., "Continuous Industrial-Scale Centrifugal Partition Chromatography with Automatic Solvent System Handling: Concept and Instrumentation," *Org Process Res Dev*, vol. 24, pp. 2676–2688, 2020, doi: 10.1021/acs.oprd.0c00338.

- [141] Y.-P. Chin, W. J. Weber, and T. C. Voice, "Determination of partition coefficients and aqueous solubilities by reverse phase chromatography—II," *Water Res*, vol. 20, pp. 1443–1450, 1986, doi: 10.1016/0043-1354(86)90144-2.
- [142] S. Spinu, A. Ortan, D. Ionescu, and I. Moraru, "Centrifugal Partition Chromatography (CPC) – a novel method of separation and purification of natural products – a short review," *Curr. Trends Nat. Sci*, vol. 9, pp. 06–11, 2020, doi: 10.47068/ctns.2020.v9i18.001.
- [143] J. Brent Friesen, and G. F. Pauli, "G.U.E.S.S.—A Generally Useful Estimate of Solvent Systems for CCC," *J Liq Chromatogr Relat Technol*, vol. 28, pp. 2777–2806, 2005, doi: 10.1080/10826070500225234.
- [144] A. Berthod, "Chapter 1 Fundamentals of countercurrent chromatography," *Compr. Anal. Chem*, vol. 38, pp. 1–20, 2002 doi: 10.1016/S0166-526X(02)80004-6.
- [145] P. Szczepblewski, J. Górka, W. Andrałojć, P. Janke, K. Wąsik, and T. Laskowski, "Iso-Partricin, an Aromatic Analogue of Amphotericin B: How Shining Light on Old Drugs Might Help Create New Ones," *Antibiotics*, vol. 10, p. 1102, 2021, doi: 10.3390/antibiotics10091102.
- [146] B. Cybulska, E. Borowski, and C. M. Gary-Bobo, "Relationship between ionophoric and haemolytic activities of perimycin A and vacidin A, two polyene macrolide antifungal antibiotics," *Biochem Pharmacol*, vol. 38, pp. 1755–1762, 1989, doi: 10.1016/0006-2952(89)90409-7.
- [147] B. Cybulska, J. Bolard, O. Seksek, A. Czerwinski, and E. Borowski, "Identification of the structural elements of amphotericin B and other polyene macrolide antibiotics of the heptene group influencing the ionic selectivity of the permeability pathways formed in the red cell membrane," *Biochim Biophys Acta*, vol. 1240, pp. 167–178, 1995, doi: 10.1016/0005-2736(95)00170-0.
- [148] B. Cybulska, O. Seksek, N. Henry-Toulme, A. Czerwinski, and J. Bolard, "Polyene macrolide antibiotics: Indirect stimulation of the Na⁺/H⁺ exchanger of BALB/c B lymphoid cell line, A20," *Biochem Pharmacol*, vol. 44, pp. 539–545, 1992, doi: 10.1016/0006-2952(92)90447-Q.
- [149] M. Hervé, J. C. Debouzy, E. Borowski, B. Cybulska, and C. M. Gary-Bobo, "The role of the carboxyl and amino groups of polyene macrolides in their interactions with sterols and their selective toxicity. A 31P-NMR study," *Biochim Biophys Acta*, vol. 980, pp. 261–272, 1989, doi: 10.1016/0005-2736(89)90312-X.
- [150] J. Borzyszkowska-Bukowska, "Dynamika molekularna oddziaływań przeciwgrzybowych heptaenów aromatycznych i ich izomerów all-trans ze sterolami w błonach lipidowych," Politechnika Gdańska, Gdańsk, 2022.
- [151] C. G. Bochet, "9.13 Organic Photochemistry," *Compr. Org. Synth. II*, pp. 330–350, 2014, doi: 10.1016/B978-0-08-097742-3.00939-3.
- [152] N. H. Jensen, A. B. Nielsen, and R. Wilbrandt, "Chlorophyll a-sensitized trans-cis photoisomerization of all-trans-β-carotene," *J Am Chem Soc*, vol. 104, pp. 6117–6119, 1982, doi: 10.1021/ja00386a048.

- [153] E. Bernard, P. Britz-McKibbin, and N. Gernigon, "Resveratrol Photoisomerization: An Integrative Guided-Inquiry Experiment," *J Chem Educ*, vol. 84, p. 1159, 2007, doi: 10.1021/ed084p1159.
- [154] N. Fomina, J. Sankaranarayanan, and A. Almutairi, "Photochemical mechanisms of light-triggered release from nanocarriers," *Adv Drug Deliv Rev*, vol. 64, pp. 1005–1020, 2012, doi: 10.1016/j.addr.2012.02.006.
- [155] Z.-Y. Zhang et al., "Solar Azo-Switches for Effective E→Z Photoisomerization by Sunlight," *Angew Chem*, vol.63, p. e2024045282, 2024, doi: 10.1002/ange.202404528.
- [156] L. L. Boyle, R. F. Hudson, and J. D. Wallis, "The relative stability of cis and trans isomers," *J. Mol. Struct*, vol. 341, pp. 141–147, 1995, doi: 10.1016/0166-1280(95)04201-G.
- [157] I. Gajewska, Poradnik Fizykochemiczny: Działy: Ogólny, Fizykochemiczny, Nieorganiczny, Organiczny, Analityczny: Praca Zbiorowa," *Wydawnictwa Naukowo-Techniczne*, vol.2, p. E41, 1974.
- [158] J. H. Rex et al., "Reference Method for Broth Dilution Antifungal Susceptibility Testing of Yeasts; Approved Standard—Third Edition," CLSI, vol.28, 2017.
- [159] M. Ślisz, "Instrumental correction factor of the detector's sensitivity to the polarization direction of the recorded light," Politechnika Gdańska, Gdańsk, 2007.
- [160] "Critical Values for the Wilcoxon/Mann-Whitney Test (U)," <https://chem.pg.edu.pl/documents/175361/28234418/U.pdf>.
- [161] Sigma-Aldrich, "Candididin, ≥50% (HPLC)," <https://www.sigmaaldrich.com/PL/pl/product/sigma/sml2574?srltid=AfmBOoruiphqskIO SkFUgfq1IUQWr5Jx8BIRly0e90Y2pGUJWAZDhOSI>.
- [162] E. Borowski, K. Cichocka, M. Dutkiewicz, and T. Zimiński, "Sposób otrzymywania kandycydyny o zwiększonej trwałości czystości i aktywności biologicznej," Patent no. PL83710B2, 1976
- [163] Prodotti Antibiotici Spa, "New antibiotic," Patent no. GB1357538, 1970
- [164] L. Falkowski et al., "N-glycosyl derivatives of polyene macrolide antibiotics.," *J Antibiot*, vol. 28, pp. 244–245, 1975, doi: 10.7164/antibiotics.28.244.
- [165] J. Lightbown, P. Newland, I. Sutherland, and J. Dymond, "Analysis of candididin and related polyene antibiotics by means of the coil planet centrifuge," *Proc. Anal. Div. Chem. Soc.*, vol. 14, p. 34-37, 1977.
- [166] W. Vetter, M. Müller, M. Englert, and S. Hammann, "Countercurrent Chromatography-When Liquid-Liquid Extraction Meets Chromatography," *Liq-Phase Extr*, pp. 289–325, 2020, doi: 10.1016/B978-0-12-816911-7.00010-4.
- [167] L. Marchal, A. P. Foucault, G. Patissier, J.-M. Rosant, and J. Legrand, "Chapter 5 Centrifugal partition chromatography: an engineering approach," *Compr. Anal. Chem*, vol. 38, pp. 115–157, 2002 doi: 10.1016/S0166-526X(02)80008-3.
- [168] W. Oroshnik and A. D. Mebane, "The Polyene Antifungal Antibiotics," *Fortschr Chem Org Naturst*, vol. 17, pp. 17–79, 1963, doi: 10.1007/978-3-7091-7149-3_2.

- [169] K. Hattori, H. Nakano, M. Seki, and Y. Hirata, "Studies on Trichomycin. IV," *J Antibiot*, vol. 9, pp. 176–181, 1956.
- [170] F. Amran et al., "In vitro antifungal susceptibilities of *Candida* isolates from patients with invasive candidiasis in Kuala Lumpur Hospital, Malaysia," *J Med Microbiol*, vol. 60, pp. 1312–1316, 2011, doi: 10.1099/jmm.0.027631-0.
- [171] A. Tevyashova et al., "Semisynthetic Amides of Amphotericin B and Nystatin A1: A Comparative Study of In Vitro Activity/Toxicity Ratio in Relation to Selectivity to Ergosterol Membranes," *Antibiotics*, vol. 12, p. 151, 2023, doi: 10.3390/antibiotics12010151.
- [172] J. Boros-Majewska, "Aktywność biologiczna i selektywna toksyczność nowej klasy N-podstawionych pochodnych antybiotyku polienowego Nystatyny A1," Politechnika Gdańska, Gdańsk, 2015.
- [173] J. D. Grabenstein, "What the World's religions teach, applied to vaccines and immune globulins," *Vaccine*, vol. 31, pp. 2011–2023, 2013, doi: 10.1016/j.vaccine.2013.02.026.
- [174] E. Borowski et al., "The Substantial Improvement of Amphotericin B Selective Toxicity Upon Modification of Mycosamine with Bulky Substituents," *Med Chem*, vol. 16, pp. 128–139, 2020, doi: 10.2174/1573406415666181203114629.
- [175] W. I. Gruszecki, R. Luchowski, P. Wasko, Z. Gryczynski, and I. Gryczynski, "Molecular Organization of Polyene Antibiotic Amphotericin B Studied by Means of Fluorescence Technique," *Methods Mol Biol*, vol. 875, pp. 57–65, 2012, doi: 10.1007/978-1-61779-806-1_3.
- [176] E. Grela et al., "Mechanism of Binding of Antifungal Antibiotic Amphotericin B to Lipid Membranes: An Insight from Combined Single-Membrane Imaging, Microspectroscopy, and Molecular Dynamics," *Mol Pharm*, vol. 15, pp. 4202–4213, 2018, doi: 10.1021/acs.molpharmaceut.8b00572.
- [177] S. Granja, D. Tavares-Valente, O. Queirós, and F. Baltazar, "Value of pH regulators in the diagnosis, prognosis and treatment of cancer," *Semin Cancer Biol*, vol. 43, pp. 17–34, 2017, doi: 10.1016/j.semcancer.2016.12.003.
- [178] E. T. Castellana and P. S. Cremer, "Solid supported lipid bilayers: From biophysical studies to sensor design," *Surf Sci Rep*, vol. 61, pp. 429–444, 2006, doi: 10.1016/j.surfrep.2006.06.001.
- [179] I. Schmid, W. J. Krall, C. H. Uittenbogaart, J. Braun, and J. V. Giorgi, "Dead cell discrimination with 7-amino-actinomycin D in combination with dual color immunofluorescence in single laser flow cytometry," *Cytometry*, vol. 13, pp. 204–208, 1992, doi: 10.1002/cyto.990130216.
- [180] L. S. Yasui et al., "Using Hoechst 33342 to Target Radioactivity to the Cell Nucleus," *Radiat Res*, vol. 167, pp. 167–175, 2007, doi: 10.1667/RR0584.1.
- [181] J. Lakowicz, "Principles of Fluorescence Spectroscopy," Springer, 2006. doi: 10.1007/978-0-387-46312-4.

LIST OF FIGURES

Figure 1. Percentage share of 163 cases of fungal bloodstream infection in <i>Candida</i> strains (%) based on [9].....	16
Figure 2. Compounds used against systemic mycoses belonging to A) the azole group - on the example of Fluconazole, B) the echinocandin group - on the example of caspofungin, C) 5-fluorocytosine, D) polyene macrolides on the example of Amphotericin B.....	18
Figure 3. The elements of HM structure based on the stereostructure of Amphotericin B.	20
Figure 4. Models of molecular assemblies of AmB: sterol complexes. 1 – pore formation model, 2- half-pore model; 3 – surface adsorption model; 4- sterol sponge model. Based on [48]	26
Figure 5. 3D model of AmB, ergosterol, and cholesterol with the marked non-covalent interaction of AmB-ergosterol complex, modified based on [48]	27
Figure 6. The structural interaction between AmB and ergosterol based on [86].....	28
Figure 7. The scheme of the pore formed in the lipid layer. Based on [85].....	29
Figure 8. Schema of the AmB mechanism of action.	34
Figure 9. The elements of AHM structure based on the stereostructure of Candidicin D. Orange box – alkyl-aromatic side chain; red box – chromophore (seven conjugated double bonds); green box - polar head consisting of hemiketal ring with the carboxylic group, and sugar (mycosamine); blue box – polyol chain consisting of a system of oxygen functions.....	36
Figure 10. The stereostructures of A) Amphotericin B, B) Candidicin D, C) Vacidin, and D) Gedamycin	37
Figure 11. The color comparison of A) long-term stored antibiotic (before purification) and B) pure (freshly purified) antibiotic	38
Figure 12. The absorption spectrum of 3'-N-acetylcandidicin D methyl ester in MeOH [40].....	38
Figure 13. The stereostructures of A) Candidicin A1, B) Candidicin A2 (D), C) Candidicin A3 – own work based on [118]	40
Figure 14. The stereostructures of A) Gedamycin and B) Vacidin – own work based on [126][128][129].....	41
Figure 15. CPC's rotor construction images (up) [139] and schema of the CPC operation principles (down).....	43
Figure 16. K_D determination by the shake-flask test, and the obtained chromatographic elution profile of a mixture with three components [140].....	44
Figure 17. Proposed structures of the side chain for each orientation: 1) straight, 2) bent, 3) completely folded based on [150].....	48
Figure 18. The simulation system of the Vacidin monomer with ergosterol in DPPC based on [150].	48
Figure 19. Alkyl-aromatic side chains attached to the macrolide ring (presented partially) of Candidicin D, Vacidin, and Gedamycin.....	49

Figure 20. Chromatogram HPLC-DAD of Candicidin complex as an example of the light-induced isomerization influence on the amounts of the components in the complex before (<i>cis-trans</i> chromophore, blue line) and after photoisomerization (<i>all-trans</i> chromophore, red line) [33]	51
Figure 21. Scheme of the photochemical isomerization of Candicidin D. The geometrical changes were marked in red circles [33]	51
Figure 22. Scheme of part 1 of Aureofacin complex preliminary purification	59
Figure 23. Scheme of part 2 of Aureofacin complex preliminary purification – part 2, presented figure shows purified complex; the gray field is assigned to the analysis performance, the blue field is assigned to the material, 1x – one time.....	60
Figure 24. A simplified model of the Gedamycin molecule orientation with respect to the lipid bilayer	71
Figure 25. The membrane sides of which the fluorescence signals were recorded.....	71
Figure 26. Scheme of the research; blue color – steps of antibiotics' isolation.....	73
Figure 27. UV-Vis spectra of the chosen crude Aureofacin and Candicidin complexes (samples of 0.01 mg/mL in MeOH).....	74
Figure 28. UV-Vis spectrum of crude and purified Aureofacin (left) and Candicidin (right) complexes at concentrations of 0.01mg/mL in MeOH.....	75
Figure 29. HPLC –DAD chromatogram of the purified Aureofacin complex.	76
Figure 30. HPLC –DAD chromatogram of the purified Candicidin complex.	77
Figure 31. CPC-DAD chromatogram of separation of components of the purified Aureofacin complex.....	82
Figure 32. HPLC-DAD chromatogram of fractions 28-40 min (Vacidin) from CPC separation of Aureofacin purified complex (Figure 31).....	83
Figure 33. HPLC-DAD chromatogram of fractions 57-70 min (Gedamycin) from CPC separation of Aureofacin purified complex (Figure 31).	83
Figure 34. CPC-DAD chromatogram of separation of components of the Candicidin complex. .	84
Figure 35. HPLC-DAD chromatogram of 43-60 min (Candicidin D) from CPC separation of Candicidin purified complex (Figure 34)	84
Figure 36. Preparative HPLC - DAD chromatogram of Candicidin D sample after CPC. Collected fractions corresponding to Candicidin D after CPC are marked by black rectangle.	86
Figure 37. The UV-Vis spectrum of <i>cis-trans</i> and <i>all-trans</i> Vacidin at concentration 0.01 mg/mL in MeOH.....	88
Figure 38. The overlay of HPLC-DAD chromatograms of <i>cis-trans</i> Vacidin sample (blue line), and <i>all-trans</i> Vacidin sample (red line).	89
Figure 39. The overlay of HPLC-DAD chromatograms of <i>cis-trans</i> Gedamycin sample (blue line), <i>all-trans</i> Gedamycin sample (red line).....	89
Figure 40. The overlay of HPLC-DAD chromatograms of <i>cis-trans</i> Candicidin D sample (blue line), <i>all-trans</i> Candicidin D sample (red line).	90
Figure 41. The scheme of the photoisomerization of <i>cis-trans</i> Vacidin to <i>all-trans</i> Vacidin	91

Figure 42. The scheme of the photoisomerization of <i>cis-trans</i> Gedamycin to <i>all-trans</i> Gedamycin	91
Figure 43. Chromatogram of the prep-HPLC-DAD separation of components of the post-reaction mixture after photoisomerization of <i>cis-trans</i> Gedamycin. <i>All-trans</i> Gedamycin collected fractions marked by black rectangle	92
Figure 44. Chromatogram of the prep-HPLC-DAD separation of components of the post-reaction mixture after photoisomerization of <i>cis-trans</i> Vacidin. <i>All-trans</i> Vacidin collected fractions marked by black rectangle.	93
Figure 45. Chromatogram of the prep-HPLC-DAD separation of components of the post-reaction mixture after photoisomerization of <i>cis-trans</i> Candicidin D. <i>All-trans</i> Candicidin D collected fractions marked by black rectangle.	94
Figure 46. The superimposed HPLC-DAD-ESI-MS chromatogram of <i>cis-trans</i> Vacidin. Mass spectrum recorded in positive electrospray ionization mode.	95
Figure 47. The superimposed HPLC-DAD-ESI-MS chromatogram of <i>all-trans</i> Vacidin. Mass spectrum recorded in positive electrospray ionization mode.	95
Figure 48. The superimposed HPLC-DAD-ESI-MS chromatogram of <i>cis-trans</i> Gedamycin. Mass spectrum recorded in positive electrospray ionization mode.	96
Figure 49. The HPLC-DAD-ESI-MS chromatogram of <i>all-trans</i> Gedamycin. Mass spectrum recorded in positive electrospray ionization mode.....	96
Figure 50. The HPLC-DAD-ESI-MS chromatogram of <i>cis-trans</i> Candicidin D. Mass spectrum recorded in positive electrospray ionization mode.....	97
Figure 51. The HPLC-DAD-ESI-MS chromatogram of <i>all-trans</i> Candicidin D. Mass spectrum recorded in positive electrospray ionization mode	97
Figure 52. The image of control MRC-5 cells after 24h incubation.....	107
Figure 53. The images of MRC-5 cells treated with <i>cis-trans</i> Gedamycin at concentrations of IC ₅₀ (up) and IC ₉₀ (down) after 24 h.....	108
Figure 54. The images of MRC-5 cells treated with <i>all-trans</i> Gedamycin at concentrations of IC ₅₀ (up) and IC ₉₀ (down) after 24 h.....	108
Figure 55. Overlay of flow cytometry histograms corresponding to HEK 293 cell line stained with propidium iodide in two conditions: without exposure to antibiotic (control, red color) and treated with specified antibiotic (blue color).....	109
Figure 56. A simplified diagram of the photoselection phenomenon based on the example of two possible arrangements of Gedamycin (yellow) in the lipid bilayer.....	111
Figure 57. The results of microscopic imaging of lipid bilayer (DMPC) vesicle a) containing 0.5 mol% <i>cis-trans</i> Vacidin; b) 0.5 mol% <i>cis-trans</i> Vacidin A and 30 mol% cholesterol; c) 0.5 mol% <i>cis-trans</i> Vacidin and 30 mol% ergosterol, respectively	112
Figure 58. The results of microscopic imaging of lipid bilayer (DMPC) vesicle a) containing 0.5 mol% <i>cis-trans</i> Gedamycin; b) 0.5 mol% <i>cis-trans</i> Gedamycin and 30 mol% cholesterol; c) 0.5 mol% <i>cis-trans</i> Gedamycin and 30 mol% ergosterol, respectively	112

Figure 59. The results of microscopic imaging of lipid bilayer (DMPC) vesicle a) containing 0.5 mol% <i>all-trans</i> Gedamycin; b) 0.5 mol% <i>all-trans</i> Gedamycin and 30 mol% cholesterol; c) 0.5 mol% <i>all-trans</i> Gedamycin and 30 mol% ergosterol, respectively.....	113
Figure 60. The results of microscopic imaging of DMPC vesicle containing a) 0.5 %M AmB, b) 0.5 %M AmB and 30mol% cholesterol, c) 0.5 %M AmB with 30%mol ergosterol respectively [176].....	116

LIST OF TABLES

Table 1. Major risk factors associated with the occurrence of IFDs [1].	17
Table 2. <i>Cis-trans</i> bond location with the position of Z-geometry double bonds which is found in the chromophore of HM (E means E-geometry) – own work based on [38][40]	21
Table 3. Characteristic of LFAB and Fungizone – own work based on [23][59][60].	23
Table 4. Combined antifungal treatment for certain IFDs – own work based on [23]. AmB – Amphotericin B, AIDS - Acquired Immunodeficiency Syndrome,	24
Table 5. The molecular mass and molecular formula of the tested antibiotics in comparison to AmB.	39
Table 6. Characteristic steps of a single run during the CPC chromatographic process.	43
Table 7. Properties of crude heptaene macrolide preparations used in the studies.	54
Table 8. Structures and purities of isolated heptaene macrolide antibiotics used in the studies.	54
Table 9. Structure and purity of reference heptaene macrolide used in the studies.	55
Table 10. Reagents.	55
Table 11. Buffer and salt solutions.	56
Table 12. Solid medium for yeast cultivation.	56
Table 13. Liquid media for yeast cultivation.	56
Table 14. Media used for cultivation of mammalian cells.	56
Table 15. Human cell lines used in the studies.	57
Table 16. Yeast strains.	57
Table 17. Equipment used in doctoral research	57
Table 18. Software	58
Table 19. Conditions for determination of purity.	59
Table 20. The volume ratio of the tested solvent systems.	60
Table 21. Equipment - settings of the instrument method.	62
Table 22. Elution program.	62
Table 23. Equipment- settings of the instrument method.	63
Table 24. Equipment- settings of the instrument method.	63
Table 25. Equipment - settings of the instrument method.	64
Table 26. Equipment and fixed parameters.	70
Table 27. Results of the complex purity determination for the selected preparations of AHMs.	74
Table 28. The comparison of crude and purified Aureofacin – purification process summary.	75
Table 29. The calculated K_D values of Gedamycin and Vacidin in solvent systems tested for CPC analysis	79
Table 30. The K_D values for Gedamycin and Vacidin in selected biphasic solvent systems and related selectivity for Gedamycin and Vacidin.	80
Table 31. The m/z values of the molecular ions $[M + H]^+$ obtained for the analyzed antibiotics.	97
Table 32. Obtained purity results of isolated antibiotics in the preparations after CPC and prep-HPLC separation process.	98

Table 33. MIC values of Gedamycin, Vacidin, and Candicidin D isomers and Amphotericin B (AmB) against human pathogenic yeasts of <i>Candida</i> genus and <i>S. cerevisiae</i> determined in RPMI 1640 medium under condition recommended by CLSI.	99
Table 34. MIC values of Gedamycin, Vacidin, and Candicidin D isomers and Amphotericin B (AmB) against human pathogenic yeasts of <i>Candida</i> genus and <i>S. cerevisiae</i> determined in BDS medium.....	100
Table 35. Comparison of AmB MIC ₉₀ values determined against four representatives of <i>Candida</i> spp. In RPMI 1640 medium under CLSI-recommended conditions.	101
Table 36. MIC values of Gedamycin, Vacidin, and Candicidin D isomers and Amphotericin B (AmB) against <i>C. albicans</i> SC 5314 determined in BDS medium and its modification.	101
Table 37. MIC values of Gedamycin, Vacidin, and Candicidin D isomers and Amphotericin B (AmB) against <i>C. albicans</i> SC 5314 determined in RPMI 1640 medium and its modification.	101
Table 38. The hemolytic activity of the analyzed compounds, determined as EH ₅₀ values.	102
Table 39. Comparison of EH ₅₀ data of <i>cis-trans</i> AHMs and AmB. AHMs – aromatic heptaene macrolides, AmB- Amphotericin B.	102
Table 40. Selective toxicity indexes (STI _{HEM}) of <i>cis-trans</i> Candicidin D, <i>cis-trans</i> Gedamycin, <i>cis-trans</i> Vacidin, their <i>all-trans</i> isomers, and Amphotericin B (AmB).	103
Table 41. Selective toxicity indexes (STI _{HEM}) of <i>cis-trans</i> Candicidin D, <i>cis-trans</i> Gedamycin, <i>cis-trans</i> Vacidin, their <i>all-trans</i> isomers, and Amphotericin B (AmB).	103
Table 42. Cytotoxic activity of AHMs and AmB determined as IC ₅₀ (µg/mL).	105
Table 43. Selective toxicity indexes (STI _{cyt}) of AHMs and Amphotericin B (AmB).	106
Table 44. The percentage of live and dead HEK 293 cells obtained as a result of cells' exposure to antibiotics.	110
Table 45. <i>Cis-trans</i> and <i>all-trans</i> Gedamycin orientation angle α with respect to the axis normal to the plane of the lipid bilayer.	113
Table 46. <i>Cis-trans</i> Vacidin orientation angle α with respect to the axis normal to the plane of the lipid bilayer.	114
Table 47. The verification of the hypothesis that the orientation angles (table 45) belong to the same population (coincide) by the U-Mann Whitney test.	114

LIST OF EQUATIONS

Equation 1.4.3.1.....	44
Equation 3.2.3.1.....	61
Equation 3.2.10.1.....	66
Equation 3.2.11.1.....	66
Equation 3.2.12.1.....	68
Equation 3.2.14.1.....	69
Equation 3.2.16.1.....	70
Equation 3.2.16.2.....	70
Equation 3.2.16.3.....	71
Equation 3.2.16.4.....	71